Electronic Thesis and Dissertation Repository

8-13-2014 12:00 AM

New Ligands for Lanthanides and Transition Metals toward Magnetic Resonance Imaging Contrast Agents

Melissa M. Lewis
The University of Western Ontario

Supervisor
Robert H. E. Hudson
The University of Western Ontario

Follow this and additional works at: https://ir.lib.uwo.ca/etd

Part of the Organic Chemistry Commons

Recommended Citation

New Ligands for Lanthanides and Transition Metals toward Magnetic Resonance
Imaging Contrast Agents

(Thesis format: Integrated Article)

by

Melissa M. <u>Lewis</u>

Graduate Program in Chemistry

A thesis submitted in partial fulfillment
of the requirements for the degree of
Doctor of Philosophy

The School of Graduate and Postdoctoral Studies
The University of Western Ontario
London, Ontario, Canada

Abstract

Magnetic Resonance Imaging (MRI) is a non-invasive technique used in medical imaging with applications in diagnosis, stage determination and monitoring of the progress of disease. Although contrast agents have been used to enhance the image generated by MRI, it still suffers the major shortcoming of low sensitivity. This has led to a thrust to develop contrast agents that improve the sensitivity by relaxation (T_1 and T_2) as well as by chemical exchange saturation transfer (CEST).

To further aid in the development of sensitive MRI contrast agents, the synthesis and evaluation of lanthanide and transition metal complexes was executed. The results are presented herein.

Chapter 2 investigated pH dependent reversible binding on CEST effect and relaxivity in macrocyclic complexes possessing three of the same arms and a lone *p*-nitrophenol arm. Unfortunately, only the Tm^{3+} complex had a small CEST signal. T_1 relaxivity of the Gd^{3+} complex showed high relaxivity at acidic pH and low relaxivity at basic pH.

Chapter 3 discussed the rigidification of the DOTAM structure as a means to promote the formation of the SAP isomer for CEST signal generation. These ligands were rigidified by at least one cyclohexyl group and were found to be very selective toward transition metals over lanthanides. However, none of the complexes investigated generated a CEST signal.

Chapter 4 attempted to examine the amide CEST signal of DOTAM-tetraanilide complexes containing various *para*-substituents that would limit T_2 exchange and increase amide-based pH measurements. Due to the insolubility of the other complexes, only the *p*-H and *p*-OMe complexes were evaluated. The CEST spectrum of the Tm^{3+}-*p*-OMe complex revealed two amide signals. The absence of a bound water molecule in the Tm^{3+} agents allowed for higher signal to noise ratios because of reduced T_1 and T_2 relaxation.

Chapter 5 involved a model study that assessed the electronic effects of *para*-substituents on the amide CEST signal and relaxivity of DO3A-monoanilide complexes. CEST spectra of only the Tm^{3+} complexes could be acquired. The various substituents allowed a CEST effect

to be observed at different pH values. The T_1 relaxivities of the Dy^{3+} and Tm^{3+} complexes were both low, while the Dy^{3+} complexes had much higher T_2 relaxivities as compared to the Tm^{3+}-based ones.

Finally, Chapter 6 highlighted the attempt to synthesize *para*-phosphonate monoanilide analogues of the DOTAM tetraanilide complexes mentioned in Chapter 4, which would be suitable for *in vivo* studies. It is anticipated that the two amide signals seen in the CEST spectrum of the Tm^{3+}-*p*-OMe complex would still persist in the modified complex, thus providing a means of a concentration independent ratiometric analysis of the CEST effect. Due to synthetic challenges, the synthesis of these modified complexes is still ongoing.

Keywords

Magnetic resonance imaging; Chemical exchange saturation transfer (CEST); Paramagnetic chemical exchange saturation transfer (PARACEST); Relaxivity; Rigidified ligands; Semi-rigidified ligands; Transition metals; Lanthanides; Electronic effects

Co-Authorship Statement

This thesis includes material from one previously published manuscript (Chapter 4) and a recently accepted manuscript (Chapter 5). The papers presented were collaborations with the Professor Bartha group of the Robart's Research Institute. Detailed descriptions of the author contributions for Chapters 4 and 5 are listed below.

The material outlined in Chapter 4 was a full paper published as:

Mark Milne, **Melissa Lewis**, Nevin McVicar, Robert Bartha and Robert H. E. Hudson, *"ParaCEST agents that improve amide based pH measurements by eliminating inner sphere water T_2 exchange"* *RSC Adv.*, **2014**, 4, 1666–1674

M. Milne designed the agents. M. Lewis performed 50% of the synthetic protocols and synthesis. Data collection and evaluation of CEST, T_1, T_2 properties was done by Mark Milne. N. McVicar obtained the images. Dr. Boyle acquired and solved the X-Ray data. Writing of the manuscript was done by M. Milne with the exception of the description of images, which was done by N. McVicar and the final submission was prepared by Dr. R.H.E Hudson.

The material outlined in Chapter 5 was accepted as a full paper as:

Melissa M. Lewis, Mark Milne, Robert Bartha and Robert H.E. Hudson, "Dysprosium(III) and Thulium(III) Complexes of DO3A-monoanilides: An Investigation of Electronic Effects on their Relaxometric and Amide-based PARACEST Properties" Accepted *Can. J. Chem.*, **2014**.

M. Milne conceived the initial molecular design and M. Lewis identified the agents to be synthesized. All synthesis, evaluation and initial writing of the manuscript was done by M. Lewis. The final submission was prepared by Dr. R.H.E Hudson.

Acknowledgments

During the past four years, I have been privileged to work and study at this institution, thus interacting with a number of persons and developing lifelong friendships. As such, I would first like to thank God for giving me this tremendous opportunity and for the strength and endurance that was necessary to get to this point of my educational development.

I would like to express my gratitude to my supervisor, Dr. Robert H. E. Hudson for giving me the chance to pursue my doctoral studies in his laboratory. I am indeed grateful for his guidance over these years.

I would also like to thank both past and current members of Dr. Hudson's laboratory for their encouragement and advice, in particular, Dr. Mark Milne, Dr. Mojmir Suchy, Augusto Matarazzo, Rachel Wang, Christie Ettles, Kirby Chicas, McHenry Charles and Dr. Mohamed El-sayed Moustafa.

I would additionally like to thank Dr. Martin J. Stillman, Dr. Patrick O' Donoghue, Dr. Gary S. Shaw, and Dr. Xiao-an Zhang for taking the time to read my thesis.

Lastly and by no means least, I would like to express my deepest love and gratitude to my family for their invaluable love, emotional support, consistent persuasion, encouragement and prayers. So too, I also thank my friends who encouraged me emotionally. You have all helped to make this work possible and I thank God for making you a part of my life.

Table of Contents

List of Tables

List of Figures

Figure 3.4: (a) ORTEP drawing of **3.16** showing naming and numbering scheme. Ellipsoids are at the 50% probability level and hydrogen atoms were drawn with arbitrary radii for

selected angles and bond lengths and (b) side on view of **4.11a** showing eightfold coordination of the Tm^{3+} by the nitrogens of cyclen and the oxygens of the amide pendant groups. φ denotes the trans O–Ln–O bond angle.

List of Schemes

List of Supplemental Information

List of Abbreviations and Symbols

Abbreviations	Definitions
Boc	*tert*-butyloxycarbonyl
CA	Contrast Agent
Calcd	calculated
CEST	Chemical Exchange Saturation Transfer
CPMG	Carr-Purcell-Meiboom-Gill
CT	Computed Tomography
Cyclen	1,4,7,10-tetraazacyclododecane
d	doublet
dd	doublet of doublets
dq	doublet of quartets
DMF	Dimethylformamide
DMSO	Dimethyl sulfoxide
DOTA	1,4,7,10-tetraazacyclododecane
DOTAM	1,4,7,10-tetraazacyclododecane-1,4,7,10-tetraacetamide
DO3AM	2,2',2''-(1,4,7,10-tetraazacyclododecane-1,4,7-triyl)triacetamide
DO3A	1,4,7,10-tetraazacyclododecane-1,4,7-triyl)triacetate
DTPA	diethylenetriaminepentaacetic acid
eq	equivalents
ESI	Electro Spray Ionization
Et	ethyl
EtOAc	ethyl acetate
FCC	Flash column chromatography
gCOSY	Gradient Correlation Spectroscopy
gHMBC	Gradient Heteronuclear Multiple Bond Correlation
gHSQC	Gradient Heteronuclear Single Quantum Coherence
HR-ESI-MS	High Resolution Electro Spray Ionization Mass Spectrometry
HPLC	High Performance Liquid Chromatography

Hz	Hertz
J	coupling constant
m	multiplet
Me	methyl
MeCN	acetonitrile
MeOH	methanol
MRI	Magnetic resonance imaging
MT	Magnetization Transfer
m/z	mass to charge ratio
NMR	Nuclear Magnetic Resonance
Ns	4-nitrobenzenesulfonyl; nosyl
o-	*ortho*
p-	*para*
PARACEST	Paramagnetic Chemical Exchange Saturation Transfer
q	Innersphere water
rf	Radio frequency
rt.	room temperature
s	singlet
SAP	Square antiprismatic
SPION	Super Paramagnetic Iron Oxide Nanoparticle
t	triplet
T_1	Longitudinal relaxation time
T_2	Transverse relaxation time
TFA	Trifluoroacetic acid
TLC	Thin Layer Chromatography
TMS	Tetramethylsilane
Ts	4-methylbenzenesulfonyl ; tosyl
TSAP	Twisted square anitprismatic
UPLC	Ultra Performance Liquid Chromatography
UV	ultra violet
Å	angstrom
γ	Gyromagnetic ratio

δ	Chemical shift
ν	Larmor frequency
τ_m	Bound water lifetime
μ_B	Bohr magneton
μw	microwave
ρ	Density
λ	wavelength

Chapter 1

1   Introduction

1.1   Magnetic Resonance Imaging (MRI)

Magnetic Resonance Imaging (MRI) is a practical tool in diagnostic medicine, used for viewing anatomical images. This non-invasive methodology produces images based on the relaxation rate of water protons that are ubiquitous within the body.[1] Within the clinical setting, a subject is placed in an immobile magnetic field (B_0) which causes the nuclei containing the protons to precess or rotate at a particular frequency. This frequency is dependent on two factors, namely the strength of B_0 and the gyromagnetic ratio (γ) of the nucleus, which in this case is ^{1}H (γ_H = 26.752 X 10^7 rad s^{-1} T^{-1}).[2] The spin energy levels of the nuclei within this static magnetic field will be non-degenerate, thus a Boltzmann distribution of the nuclei will persist. There will be more nuclei occupying the low energy (α) state in which the spins are parallel to B_0, than the high energy (β) state in which the spins are anti-parallel to B_0 (Figure 1.1a).
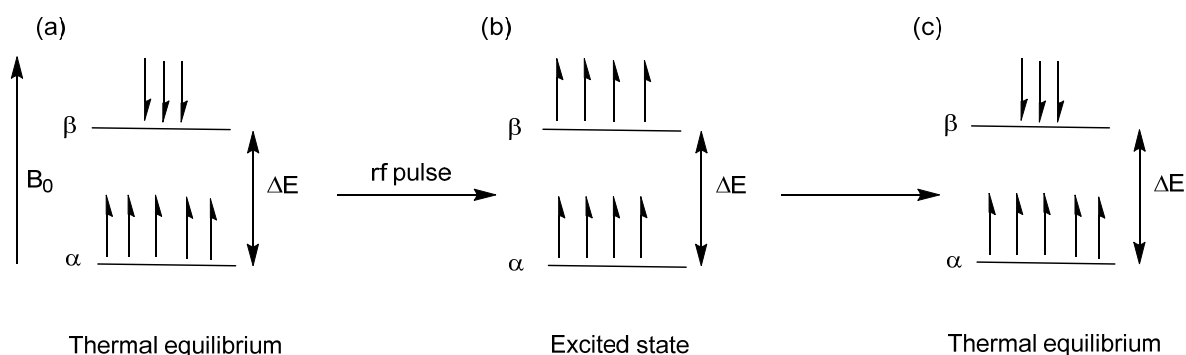
Figure 1.1: Diagram showing the distributions of nuclear spins in a magnetic field, B_o (a) Boltzmann distribution with more spins in lower energy α level than higher energy β level (b) excited state after rf pulse and (c) return to thermal equilibrium.

The nuclei in a state of thermal equilibrium can be re-distributed between the two energy levels by application of a radio-frequency (rf) pulse with the appropriate energy, $\Delta E = h\upsilon$ (where h is Planck's constant and υ is the resonance frequency).[2, 3] In other words, this radiation pulse must occur at the Larmor (resonance) frequency (υ, whereby $\upsilon = \gamma B_0$) of the system.[3] Once the pulse is applied, the distribution of nuclei in the excited state allows equal populations of nuclei between the α and β energy levels (Figure 1.1b).[3] Additionally, the spins of the nuclei will be the same so that phase coherence may be achieved.[3] After some time, the system will return to thermal equilibrium and the Boltzmann distribution will be re-established (Figure 1.1c).

1.2   Relaxation and Relaxivity

The rate at which the system returns to thermal equilibrium after irradiation by 90° rf pulse is termed relaxation, namely T_1 (spin-lattice or longitudinal) and T_2 (spin-spin or transverse) relaxation. Figure 1.2a-c shows the vector diagrams representing these processes. At thermal equilibrium, the net magnetization is in the longitudinal (z) direction ($M_0 = M_z$) and once the rf pulse (B_1) is applied, the magnetization flips into the transverse (xy) plane.[4] This causes a reduction of M_z and an increase in M_{xy}. The magnetization of M_{xy} will precess around the z-axis, thus causing a decrease in M_{xy} and the subsequent return to equilibrium, where $M_0 = M_z$.

The T_1 relaxation rate ($1/T_1$) refers to the rate at which the system returns to Boltzmann distribution while the T_2 relaxation rate ($1/T_2$) refers to the rate at which the system loses phase coherence (Figure 1.2d-e).[4] Associated with T_2 relaxation is T_2* relaxation, resulting from the inhomogeneity of the magnetic field. This effect may cause the magnetization in the xy plane to relax at a much faster rate, than is expected.

$\tau!$

$1/\nu \rightarrow$

Radiofrequency pulse (B_1)

$\vec{B_0}$

z

$\vec{M_0}$

y

x

(a)

z

$\vec{B_1}$

x

y

(b)

$\vec{B_0}$

$\vec{M_z}$

z

y

$\vec{M_{xy}}$

x

(c)

M_z

M_0

$M_0(1-e^{(-t/T1)})$

(d)

t

M_{xy}

M_0

$M_0 e^{(-t/T2)}$

(e)

t
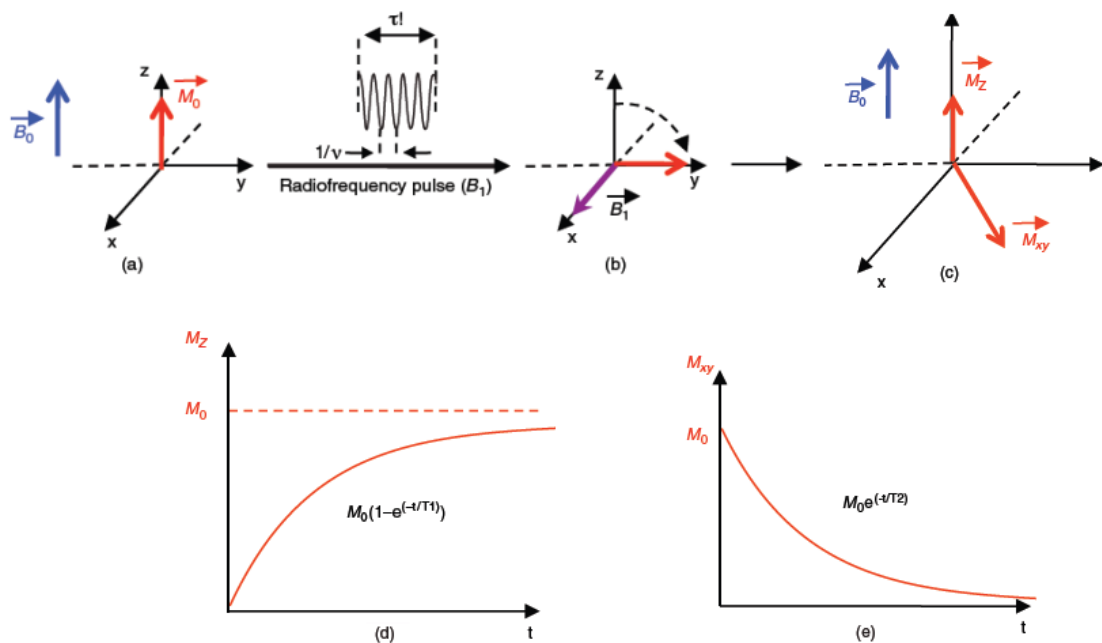
Figure 1.2: Vector diagrams representing (a) net magnetization M_0 at equilibrium when the spins are placed in the external magnetic field B_0 (b) perpendicular RF pulse (B_1) is applied that flips the magnetization into the xy plane (c) magnetization returning to equilibrium (d) T_1 relaxation (return to equilibrium in the z plane) and (e) T_2 relaxation (return to equilibrium in the xy plane). Adapted from Ref. 4 with permission of John Wiley and Sons.

Contrast agents can be used to alter both the T_1 or T_2 relaxation times of water protons and subsequently, the rates of relaxation. The designation of the type of relaxation agent depends on a percentage basis by which that particular rate is altered.[5] Contrast agents that increase the longitudanal relaxation rate in tissue faster than they do the transverse rate, are classified as T_1 contrast agents.[5] These agents enhance the MRI image generated by increasing the signal intensity, thus they are also known as positive contrast agents. Conversely, T_2 contrast agents are known as negative contrast agents because they reduce the signal intensity of the tissue, whilst increasing the transverse relaxation rate.[5]

MRI contrast agents are normally small, metal-containing macrocyclic or linear chelates. The metals used may be paramagnetic, superparamagnetic or ferromagnetic in trait.

Ferromagnetic agents contain iron oxide particles and are T_2 shortening while paramagnetic agents containing gadolinium (Gd^{3+}) are T_1 shortening.[5] Contrast agents containing Gd^{3+} (Figure 1.3) are the most widely used contrast agents within the clinical setting, based on their approval by regulatory health agencies. Nevertheless, there have been other agents based on manganese and iron that have been also approved for use in similar settings (Figure 1.3).
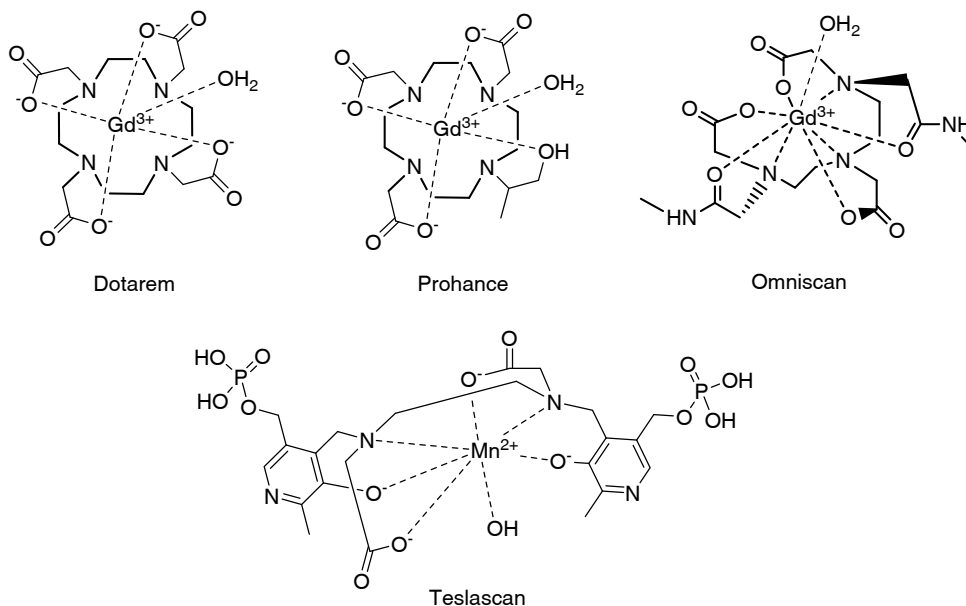
Figure 1.3: Chemical structures of examples of MRI contrast agents.

Gadolinium is a lanthanide and its efficiency as a paramagnetic metal in T_1 contrast agents is derived from the seven unpaired electrons it possesses in its 4f-orbitals. The ground state of Gd^{3+} is symmetric, in that, each electron occupies an f-orbital, resulting in long electronic relaxation times.[1] Direct contact between the water molecule(s) bound to Gd^{3+} and its unpaired electrons (dipole-dipole interaction) results in transference of the electronic magnetization.[6] This in turn, reduces the relaxation time of the water molecule bound to the metal center.[6]

Relaxivity refers to the change in the relaxation rate of water protons per millimolar of contrast agent used, as shown in equation 1.1[5]:

$$r_{1,2} = \frac{[(1/T_{1,2})_{obs} - (1/T_{1,2})_W]}{[CA]} \qquad \text{equation 1.1}$$

where, $r_{1,2}$ is the relaxivity, based on $1/T_1$ or $1/T_2$, respectively and [CA] is the concentration of contrast agent. The subscript "obs" refers to the rate with the CA present while "W" refers to the rate with pure water.

Relaxivity can be classified into two main categories: inner-sphere and outer sphere. Inner-sphere coordination refers to the water molecule bound directly to the metal.[5] This water molecule can be influenced by the inner-sphere relaxation that in turn is dependent on several factors. Firstly, it is possible to increase the relaxivity due to inner sphere coordination by increasing the number of water molecules (*q*) that are bound to the metal, as represented by equation 1.2[5]:

$$r_1^{IS} = \frac{q/[H_2O]}{(T_{1m} + \tau_m)} \qquad \text{equation 1.2}$$

where $[H_2O]$ is the concentration of water in mM, T_{1m} is the T_1 of the inner-sphere water and τ_m is the residency time of that inner-sphere water molecule.[5]

Secondly, the water molecules are also influenced by the the electronic properties of the metal within the chelate, as was discussed earlier. Thirdly, is the rate of water exchange. A requirement for an effective relaxivity agent is fast exchange of the bound water molecule with the bulk water. However, there is a balance at which this rate should occur; too fast and the water molecule does not bind to the metal long enough to be relaxed and too slow means that the effect of relaxation is ineffectively transmitted to the bulk water.[5]

Fourthly, the rotational diffusion of the complex must be well thought-out. Smaller molecules have shorter correlations times due to rotation (τ_R) and larger molecules have longer τ_R, thus the latter is more efficient at promoting the desired relaxation.[5] Lastly, it

may be possible to increase the relaxivity by decreasing the distance between the metal and the bound water proton.[5]

These factors also help govern T_{1m} and are taken into account by the equations of paramagnetic relaxation theory derived by Solomon, Bloembergen and Morgan and can be used to predict high relaxivities of contrast agents.[7-11] Further details about those equations are outside the scope of this thesis and it is the author's belief that the content within this thesis does not warrant further discussion of those equations for comprehension of the remainder of the material.

Second sphere coordination pertains to the protons of the hydrating water molecules of the complex and its contribution to relaxivity depends on the temperature and the external magnetic field.[5] Closely related to second sphere relaxivity (and sometimes difficult to differentiate) is that of outer-sphere relaxivity, which pertains to the water molecules that diffuse near the metal center. It is important to note that the size of the second sphere (and outer sphere) contribution to the overall relaxivity is very challenging to predict.[5] A summary of the afore-mentioned parameters that influences relaxivity is presented in Figure 1.4.[5]
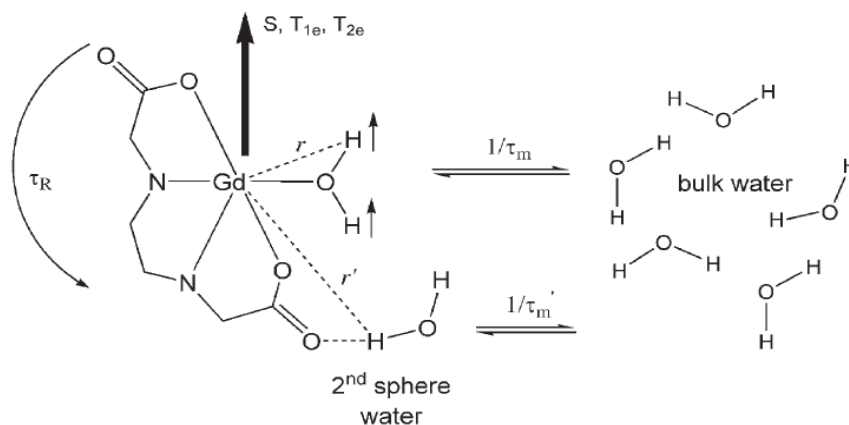
Figure 1.4: Molecular considerations that influence relaxivity. Reprinted from Ref. 5 with permission of The Royal Society of Chemistry.

The T_1 agents currently in use are excellent as blood pool or extracellular T_1 agents but they have limited success as responsive agents *in vivo*. The T_1 change *in vivo* is non-

linearly dependent on concentration. This phenomenon is due to several reasons such as the inconsistent distribution of the contrast agent within the biological system, the pulse sequences used to generate the signal as well as protein binding and differences in viscosity.[5] Additionally, these contrast agents are never completely silent. This drawback means that a signal is generated even if water cannot access the metal center, thus making it difficult to tell whether the change is due to relaxivity or concentration.[12] The detection of the agent is a function of the environment and is directly proportional to concentration, which is usually unknown *in vivo*.[13]

Omniscan (Figure 1.3), which is a Gd^{3+}-DTPA complex has a stability constant of 22.46, while Dotarem and Prohance have stability constants of 24.7 and 23.8, respectively at $25^{o}C$.[14] The higher stability constants for Dotarem and Prohance is attributed to the macrocyclic effect, wherein the stability of a macrocyclic metal complex is higher than that of a complex formed from the analogous monodentate ligands.[14] While these agents generally have an excellent safety profile, patients that have less than perfect kidney function may develop nephrogenic systemic fibrosis, after taking gadolinium based agents. If the kidneys are unable to properly filter waste from the blood, the contrast agent will spend a longer time in the body and is likely to undergo transmetalation with endogenous ions such as Zn^{2+}, Cu^{2+} and Ca^{2+}. The uncomplexed Gd^{3+} aqua ion is very toxic, with an LD_{50} of 0.1-0.2 mmol kg^{-1} in small animals.[14] The toxicity is due to the similarity to Ca^{2+} in size, coordination number and Lewis acidity.

These disadvantages have led to the need for more effective contrast agents that will be both sensitive to physiological changes whilst maintaining the contrast enhancement.

1.3 Chemical Exchange Saturation Transfer (CEST)

A more recent alternative to T_1 contrast proposed by Ward *et al*., termed Chemical Exchange Saturation Transfer (CEST), has been fundamental in the discovery of new contrast agents.[15] Earlier experiments referred to this as Saturation Transfer (ST) or Magnetization Transfer (MT). CEST involves exchange between protons of solutes and

bulk water, while MT occurs between semi-solid macromolecules and bulk water.[15, 16] The contrast generated by MT can arise by either cross-relaxation or a combination of cross-relaxation and chemical exchange.[17-20] CEST agents operate by reducing the water proton signal through a chemical exchange site on an agent. This exchange of protons must occur between two magnetically different environments.[15] Common sites of exchange are -NH (of amines or amides) and -OH (of alcohols).

For a CEST agent to be effective it must meet two criteria. Firstly, the exchange rate (k_{ex}) which is affected by pH, temperature and the ionic environment should be smaller than the chemical shift difference ($\Delta\omega$), that is, $\Delta\omega \gg k_{ex}$.[15] This consequently means that residence proton lifetime, τ_m should be about 10^{-5} - 10^{-2} s, thus translating to the rate falling within the slow to intermediate range. [16, 21]

Secondly, a CEST agent also requires a large $\Delta\omega$ from the bulk water signal. [15] This feature, if met, offers several advantages. If the $\Delta\omega$ is large, then a greater chemical exchange is allowed, provided it remains within the exchange boundary.[14] This should then produce a larger CEST effect. A larger $\Delta\omega$ also allows for specificity of the radiofrequency pulse needed to achieve saturation of the agent without directly affecting other protons.[15, 16] In addition, there is a reduction in the macromolecular MT background effect which always accompanies CEST in tissues. [15]

Figure 1.5 shows a schematic diagram describing the process of CEST. [22] As shown, there are two pools of exchangeable protons but it should be noted that three and four pool models have also been described. [23] Here, pool A represents the exchangeable protons of the bulk water and pool B represents those belonging to the contrast agent. At equilibrium, there is a Boltzmann distribution of the nuclei within both pools. A presaturation pulse is applied at the resonance frequency of the pool B protons, which then causes saturation of said protons and promotion of some nuclei to the higher energy level. This saturation is then transferred by the exchange of nuclei occurs between pool A and pool B. As a result, when the signal is acquired, there is a reduction in the signal due to the bulk water pool A protons. After some time, the nuclei of pool A will return to equilibrium. As can be seen in Figure 1.5, relaxation may be a competing process with

chemical exchange. Hence, the CEST effect will only be seen if the protons of pool B have long relaxation times with respect to their exchange rates.
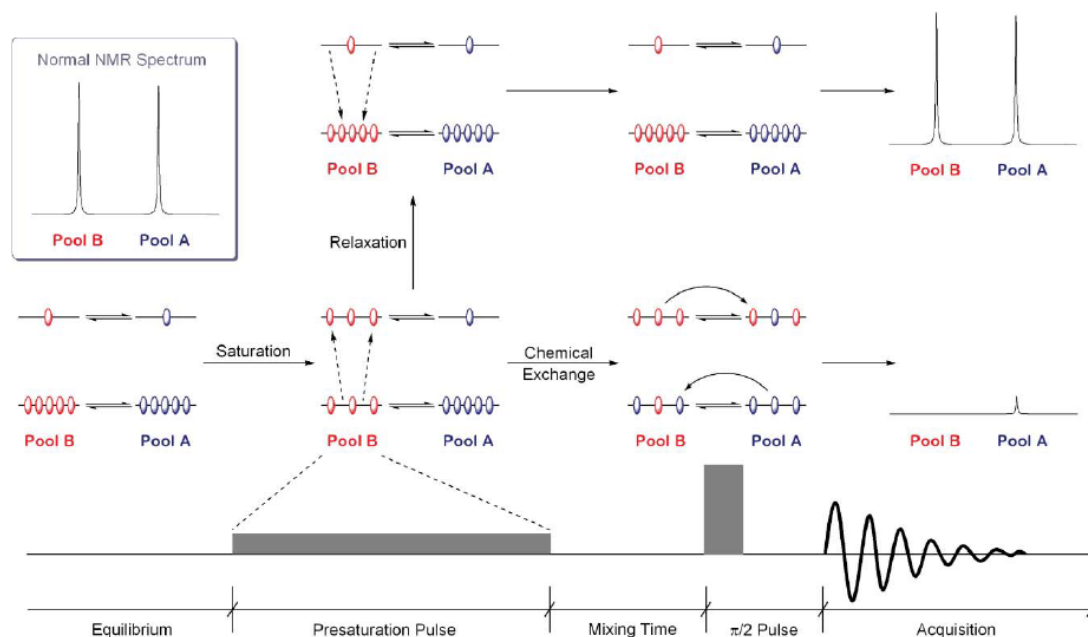
Figure 1.5: A schematic representation of both relaxation and CEST processes. Pool B represents the exchangeable protons of the contrast agent and Pool A represents the bulk water. The distribution of spins in Pool B is altered by application of a presaturation pulse to that pool. Relaxation will dominate dominate when the relaxation rate is faster than the chemical exchange rate and a normal NMR spectrum will be obtained. If chemical exchange is faster, then chemical exchange will cause redistribution of spins in both pools, thereby reducing the bulk magnetization of Pool A. Reprinted from Ref. 22 with permission of The Royal Society of Chemistry.

A CEST spectrum or Z spectrum is generated by selectively saturating a particular proton signal of the contrast agent (M_s) with a radiofrequency pulse, thus generating an image (Figure 1.6).[16] However, another image is needed because the contrast to noise ratio is limited. A similar pulse is applied on the opposite side of the water resonance (M_0), therefore this second image will be without the CEST effect. The images obtained after

each pulse application are subtracted and a CEST image is obtained which shows a darkening or negative contrast due to the contrast agent. The CEST effect is represented as a percent decrease in the total bulk water intensity and is shown in the equation 1.3 [16]:

CEST effect (%) = (1 - M_s/ M_0) x 100   equation 1.3
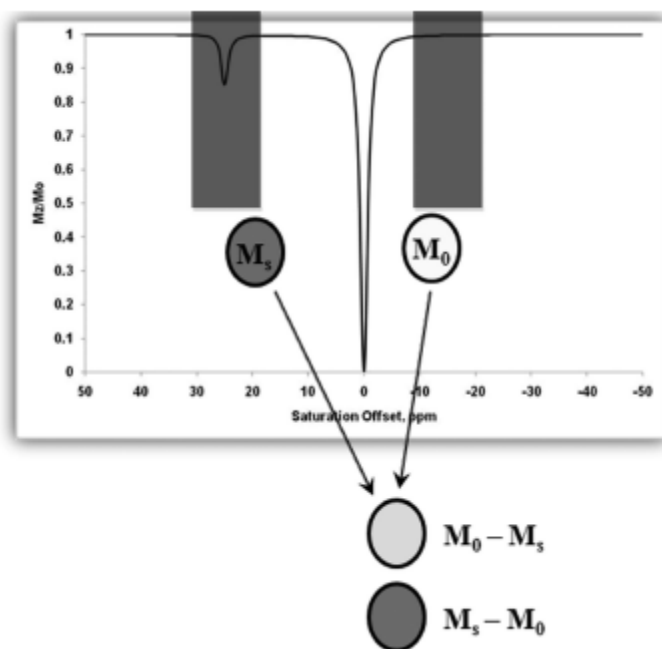
Figure 1.6: A simulated CEST or Z-spectrum for a two-pool exchanging system. Pool A is at 0 ppm and Pool B at 25 ppm. Reprinted from Ref. 16 with permission of The American Chemical Society Publications.

A CEST agent is highly beneficial as compared to other conventional relaxation contrast agents. Firstly, one can turn the contrast effect on and off as desired, either by turning the presaturation pulse off or changing its frequency.[16] Secondly, based on the method of acquisition, there is no need to obtain pre- and post-contrast images, a process necessary to eliminate artifacts due to motion.[24] Although two images are needed for a CEST spectrum, they can be obtained simultaneously. Furthermore, multiple agents with exchangeable protons of different chemical shifts can be designed.[16] Additionally, CEST

contrast has a high contrast to noise ratio that can even be attained at high magnetic fields.[25]

1.4   Diamagnetic Chemical Exchange Saturation Transfer (DIACEST)

The molecules that were initially used to generate a CEST effect were diamagnetic, and thus known as DIACEST agents.[15] DIACEST agents represent one main class of CEST agents (the other will be discussed in the following section). In general, DIACEST agents may take the form of endogenous or exogenous macromolecules and small molecules such as glucosaminoglycans, sugars, amino acids, and heterocyclic compounds (Figure 1.7).
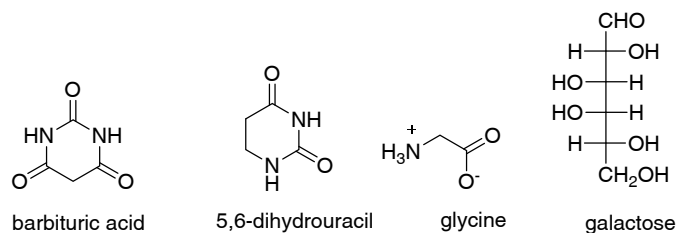
Figure 1.7: Examples of DIACEST agents.

While these agents are sensitive to factors such as pH and temperature, they are faced with a major drawback, that is, the size of their $\Delta\omega$. DIACEST agents have $\Delta\omega < 6$ ppm , therefore the bulk water signal tends to interfere with the signal generated from such agents.[15, 16]

1.5 Paramagnetic Chemical Exchange Saturation Transfer (PARACEST)

1.5.1 Lanthanide-based PARACEST

The principles of CEST have been fundamental in the discovery of other contrast agents known as Paramagnetic CEST (PARACEST) agents.[26-30] PARCACEST agents represent the second main class of CEST agents. These complexes contain paramagnetic metals such as lanthanides. The use of lanthanides as the paramagnetic metal of choice may be based upon the location of the unpaired electrons. In comparison to the paramagnetic 3d-block transition metals that have their unpaired electrons in the d-orbitals, the unpaired electrons of the lanthanides reside in their 4f-orbitals. The 4f-orbitals do not overlap with the orbitals of the ligands, thus the bonding of lanthanides tend to be ionic. Due to their larger size, they may coordinate nine to twelve ligands. However, their coordination geometry is dependent on steric, rather than electronic factors.

The magnetic properties of lanthanides vary along the period since each metal contains a different number of unpaired electrons. As such, each metal possesses a different magnetic moment (measurement of magnetism) and magnetic susceptibility. This latter feature influences the direction and magnitude of the interaction between the external magnetic field and the magnetic moment.[16] The magnetic susceptibility also governs the lanthanide induced shifts (LIS) of the metals.[16] It is this latter property that makes PARACEST agents more advantageous over DIACEST agents: the LIS favourably induces a larger $\Delta\omega$ from the water signal.[16] The larger $\Delta\omega$ allows for a faster exchange rate of the exchangeable protons, which now includes a water molecule that may be bound to the metal. A larger $\Delta\omega$ in conjunction with a faster exchange rate will only hold true if the slow to intermediate exchange condition is maintained.[22] An agent possessing both of these properties permits more spins to be transferred within a particular time frame.[22]
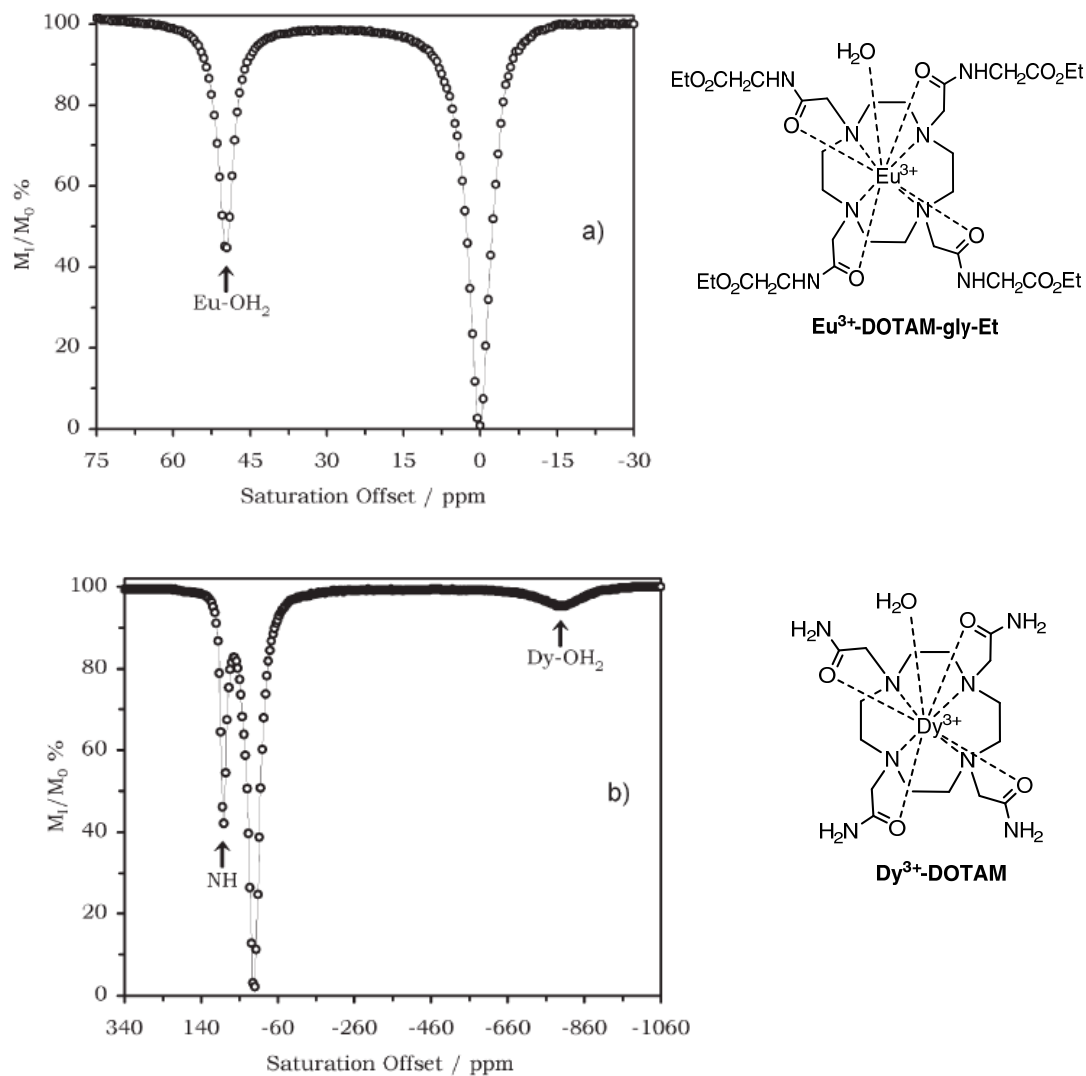
Figure 1.8: (a) CEST spectrum of Eu^{3+}-DOTAM-gly-Et (EuDOTA-4AmCE^{3+}) [63 mM] in aqueous solution at pH 7, rf presaturation applied for 1 s, B$_0$ = 4.7 T, B$_1$ = 16.4 db at 22°C showing bound H$_2$O at 50 ppm and (b) CEST spectrum of DyDOTAM^{3+} at B$_0$ = 9.4 T and at 25°C showing -NH at 80 ppm and bound H$_2$O at -720 ppm. Reprinted from Ref. 22 with permission of The Royal Society of Chemistry.

Contrast agents that are paramagnetic metal complexes and are T_1 shortening have at least one water molecule that is coordinated to the centre of the metal, however, the rate of exchange for such complexes is outside of the slow to intermediate limit which is required for CEST agents.[22] A slower exchange rate has been found for tetraamide derivatives of DOTA (DOTAM) whereby all the acetate arms of DOTA have been replaced by amide arms. The amide arms provide a reduced electron density at the metal center, which in turn leads to the slow exchange of the exchangeable protons.[16] This structure has been rudimentary in the design of subsequent PARACEST agents.[31-34] These DOTAM derivatives are moderately stable and have a high kinetic inertness that has been thought to result from the size of the Ln^{3+} ion and the cavity of the preformed macrocycle.[35]

Of all the lanthanides, europium (Eu^{3+}) has been found to have the slowest rate of water exchange and a low paramagnetic relaxation enhancement.[16] These properties of Eu^{3+} are favourable in the design of PARACEST agents that include the pre-saturation of bound water.[16] An example of such an agent is Eu^{3+}-DOTAM-gly-Et (reported as EuDOTA-4AmCE^{3+}) in which the water exchange rate slowed substantially, thereby allowing for a discrete peak to be observed which had a large $\Delta\omega$ from bulk water (Figure 1.8a).[36] A larger CEST effect may be observed for exchangeable protons such as -NH when compared to water as seen for the Dy^{3+}-DOTAM complex (Figure 1.8b). [22]

1.5.2 Transition metal-based PARACEST

The invention of transition metal CEST (TM-CEST) is a reasonably recent development and as such, the foray into its application is behind that of lanthanide-based PARACEST. The requirements for CEST based on transition metals are similar to that of lanthanide-based PARACEST. These include using a paramagnetic metal, having a slow to intermediate exchange rate and the presence of exchangeable protons. Another similarity with lanthanide-based CEST is the ligand design. An additional consideration for TM-CEST is the number of possible oxidation numbers for the transition metals, which is not as important for lanthanides. Another is in regards to the smaller size of the transition

metals, which causes their coordination number to be six (as compared to nine to twelve for the lanthanides). The transition metals that have been explored thus far for this application include cobalt,[37, 38] nickel[39] and iron[40-44] (Figure 1.9).[45] These metals are biologically relevant and have suitable paramagnetic properties.
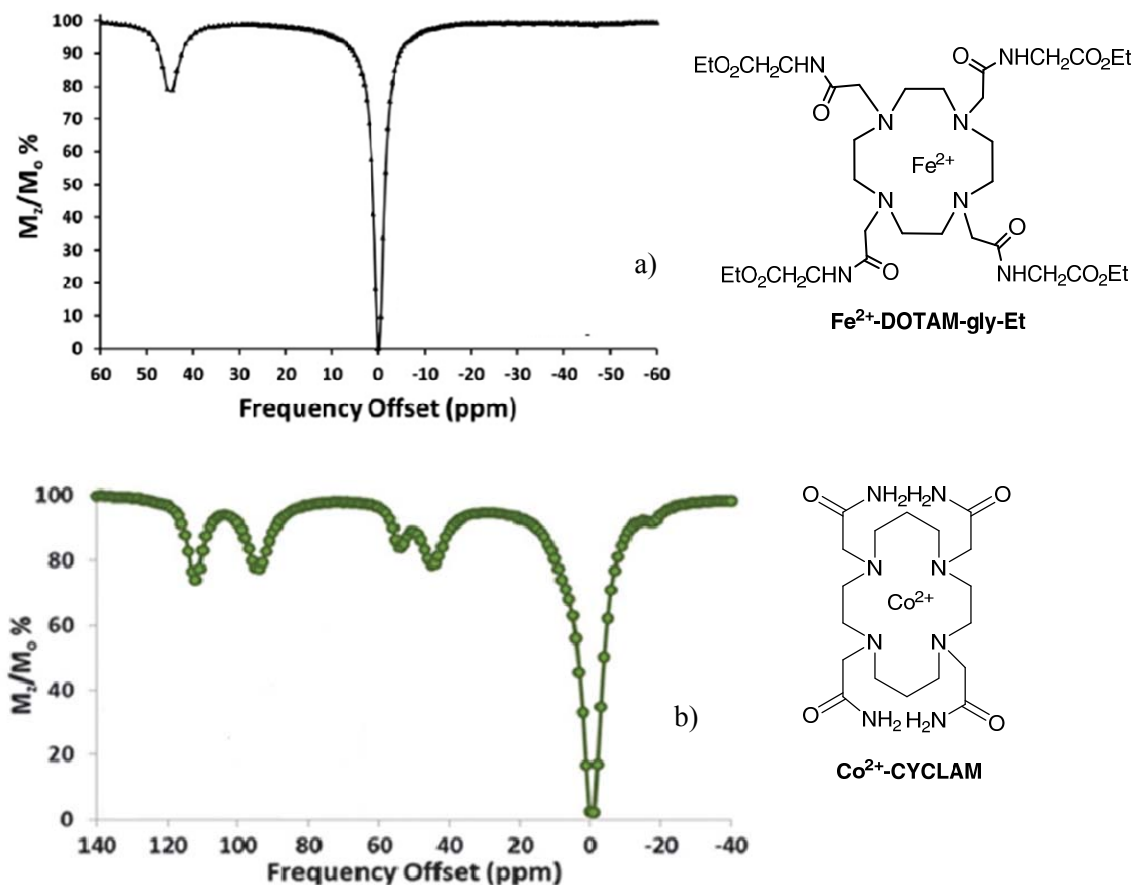
Figure 1.9: Transition metal-based CEST due to amide protons of (a) Fe^{2+}-DOTAM-gly-Et [60mM] at pH 8.6, RF presaturation applied for 4 s, B$_0$ = 500 MHz, B$_1$ = 700 Hz at 25 °C and (b) Co^{2+}-CYCLAM [10 mM] in 100mM NaCl, 20 mM HEPES, pH 7.3-7.4, rf presaturation applied for 2 s, B$_0$ =11.7 T, B$_1$ = 24 µT at 37 °C. Adapted from Ref. 38 and 45 with permission of The Royal Society of Chemistry.

1.5.3 Applications and Challenges of PARACEST agents

Since the reporting of PARACEST began, the associated agents have been shown to be sensitive to varied environments such as pH,[26, 46] temperature[47, 48] and metabolites such as lactate,[49] and glucose[50, 51] (Figure 1.10). A desired feature of responsive PARACEST agents entails having two different types of protons available for chemical exchange. This feature allows a ratiometric analysis of the CEST effect due to each proton, thereby allowing a concentration independent method of assessing these changes. Currently, there are difficulties in designing similar probes using traditional T_1 and T_2 MRI agents of which the local concentration of the agent has to be known.

R = Glycine-Phenylalanine
Temperature sensor

Glucose sensor
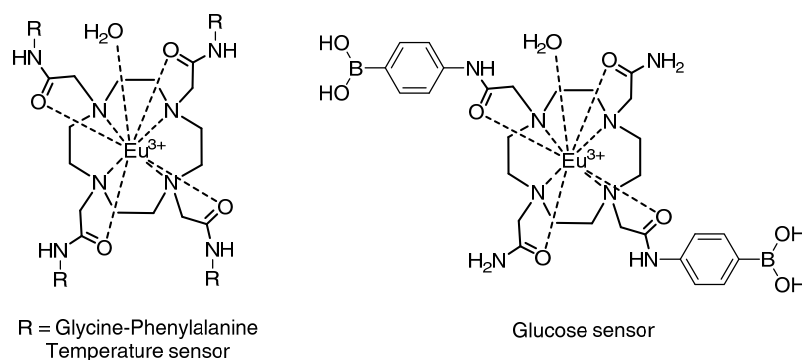
Figure 1.10: Examples of responsive lanathanide-based PARACEST agents.

While there are many advantages to be gained by using PARACEST agents over relaxivity agents, it is important to note that there are limitations that may impede the progress to be made. One of these limitations is the earlier discussed MT effect, which *in vivo*, obstructs the CEST signal as shown in Figure 1.11.[53] This obstruction can be extended to the bound water signal at 50 ppm in Eu^{3+} complexes.[53]

Another limitation of PARACEST agents is that of low sensitivity. However, efforts are currently being made to rectify this impediment. These resolutions include increasing the number of exchangeable protons on the contrast agent, combining the excellent shifting ability of lanthanide complexes with the peculiar characteristics of nanovesicular systems

(NanoCEST) and promoting the formation of non-covalent supramolecular adducts (SupraCEST).[53]
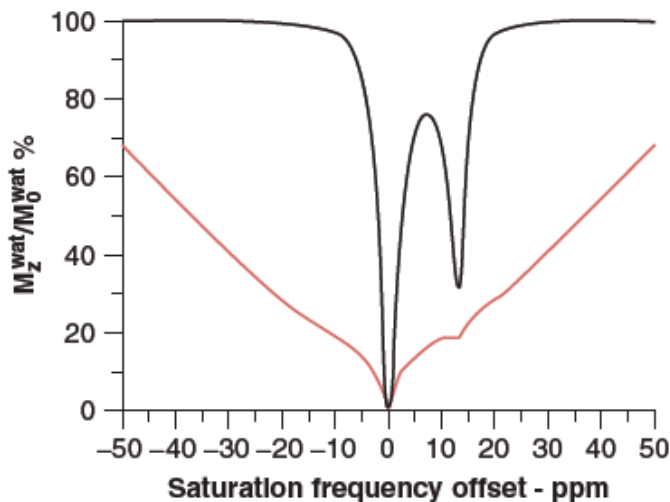
Figure 1.11: Simulated spectra showing comparison between the performance of a CEST system without (black solid curve) and with (red curve) an MTC contribution. Reprinted from Ref. 53 with permission of John Wiley and Sons.

In order to further the optimization of PARACEST agents, it is important to consider the agent, the solvent water, and the instrument settings.[22] Subsequently, τ_m should be short and the concentration of the contrast agent high as possible.[22] Unfortunately, this latter requirement is not favorable and can be compensated for by having a higher number of exchangeable protons present in the compound. In addition, one may increase the pre-saturation power B_1, which allows for an agent undergoing fast exchange to be considered.[22]

The possibilities are endless in regards to the future of PARACEST agents and the considerable knowledge gained about the magnetic properties of PARACEST agents thus far, will be beneficial for further development of these agents. However, these agents will have to be exhaustively evaluated before they can be used in the same context as current

MRI relaxivity agents. The main barrier towards the use of PARACEST agents within a clinical setting is the MT effect of tissues. This issue may be resolved by developing PARACEST agents that produce a CEST signal outside of the range of this effect.

1.6   Scope of Thesis
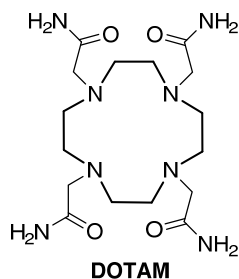
Figure 1.12: Structure of the DOTAM scaffold on which the complexes in the upcoming sections of the thesis are to be based.

In light of the discussion in the prior sections, the focal point of this thesis was to develop and appraise innovative ligands that would incorporate lanthanides and transition metals to be used as MRI contrast agents.   Such metalated complexes would fulfill the requirements of good PARACEST agents, thus serving as promising alternatives to relaxivity agents. These PARACEST agents were predominantly based on the DOTAM scaffold (Figure 1.12), with variations made so as to principally analyze their various CEST properties based on either (or both) the water molecule bound to the metal center as well as the amide proton (s) of the pendant arm (s).

The modifications to be carried out on the DOTAM scaffold may be made on the pendant arms or on the backbone of the macrocyclic ring (or both). Hence, Chapter 2 focused on the synthesis and evaluation of a DOTAM analogue that had one arm replaced with a reversible binding group that would be bound to the metal center in a pH dependent manner. Chapter 3 targeted the preparation and analysis of the DOTAM core structure, which had been rigidified to varying degrees on the backbone of the macrocyclic ring.

Chapter 4 concentrated on the preparation and examination of DOTAM tetraanilines containing varying substituents in the *para*-position of the aniline ring, ideal for electronically tuning the amide protons. As a result of solubility issues with most of the tetraanilide complexes, this led to the synthesis and investigation of *para*-substituted monoanilide complexes which deviated from the DOTAM ligand, as seen in Chapter 5. Chapter 6 details the effort made to make the soluble DOTAM tetraanilides more biocompatible. These efforts involved synthesizing DOTAM tetraanilides that had one of the four aniline rings possess a phosphonate group in the *para*-position.

1.7　References

(1) Werner, E. J.; Datta, A.; Jocher, C. J.; Raymond, K. N. *Angew. Chem. Int. Ed.* **2008,** *47*, 8568-8580.

(2) Bakhmutov, V. I. *Practical NMR Relaxation for Chemists;* John Wiley & Sons, Ltd: West Sussex, England, 2004; pp 1-202.

(3) Britton, M. M. *Chem. Soc. Rev.* **2010,** *39*, 4036-4043.

(4) Doan, B.; Meme, S.; Beloeil, J. General Principles of MRI. In *The Chemistry of Contrast Agents in Medical Magnetic Resonance Imaging,* 2nd Ed.; Merbach, A., Helm, L., Tóth, É. Eds.; John Wiley & Sons, Ltd: West Sussex, England, 2013; pp 1-23.

(5) Caravan, P. *Chem. Soc. Rev.* **2006,** *35*, 512-523.

(6) André, J. P.; Maecke, H. R.; Tóth, É.; Merbach, A. A. *J. Biol. Inorg. Chem.* **1999,** *4*, 341-347.

(7) Bloembergen, N. *J. Chem. Phys.* **1957,** *27*, 572-573.

(8) Bloembergen, N. *Phys. Rev.* **1956,** *104*, 1542-1547.

(9) Bloembergen, N.; Morgan, L. O. *J. Chem. Phys.* **1961,** *34*, 842-850.

(10) Solomon, I. *Phys. Rev.* **1955,** *99*, 559-565.

(11) Solomon, I.; Bloembergen, N. *J. Chem. Phys.* **1956,** *25*, 261-266.

(12) Green, K. N.; Viswanathan, S.; Rojas-Quijano, F. A.; Kovacs, Z.; Sherry, A. D. *Inorg. Chem.* **2011,** *50*, 1648-1655.

(13) Hancu, I.; Dixon, W. T.; Woods, M.; Vinogradov, E.; Sherry, A. D.; Lenkinski, R. E. *Acta Radiologica* **2010,** *51*, 910-923.

(14) Brücher, E.; Tircsó, G.; Baranyai, Z.; Kovács, Z.; Sherry, A. D. Stability and Toxicity of Contrast Agents; In *The Chemistry of Contrast Agents in Medical Magnetic Resonance Imaging,* 2nd Ed.; Merbach, A., Helm, L., Tóth, É. Eds.; John Wiley & Sons, Ltd: 2013;pp 157-208.

(15) Ward, K. M.; Aletras, A. H.; Balaban, R. S. *J. Magn. Reson.* **2000,** *143*, 79-87.

(16) Viswanathan, S.; Kovacs, Z.; Green, K. N.; Ratnakar, S. J.; Sherry, A. D. *Chem. Rev.* **2010,** *110,* 2960-3018.

(17) Wolff, S. D.; Balaban, R. S. *Magn. Reson. Med.* **1989,** *10*, 135-144.

(18) Henkelman, R. M.; Stanisz, G. J.; Graham, S. J. *NMR Biomed.* **2001,** *14*, 57-64.

(19) van Zijl, P. C. M.; Zhou, J.; Mori, N.; Payen, J.; Wilson, D.; Mori, S. *Magn. Reson. Med.* **2003,** *49*, 440-449.

(20) Kingsley, P. B.; Monahan, W. G. *J. Magn. Reson.* **2000,** *143*, 360-375.

(21) Sherry, A. D.; Wu, Y. *Curr. Opin. Chem. Biol.* **2013,** *17*, 167-174.

(22) Woods, M.; Woessner, D. E.; Sherry, A. D. *Chem. Soc. Rev.* **2006,** *35*, 500-511.

(23) Li, A. X.; Hudson, R. H. E.; Barrett, J. W.; Jones, C. K.; Pasternak, S. H.; Bartha, R. *Magn. Reson. Med.* **2008,** *60*, 1197-1206.

(24) Sherry, A.; Woods, M. *Annu. Rev. Biomed. Eng.* **2008,** *10*, 391-411.

(25) Liu, G.; Song, X.; Chan, K. W. Y.; McMahon, M. T. *NMR Biomed.* **2013,** *26*, 810-828.

(26) Aime, S.; Barge, A.; Delli Castelli, D.; Fedeli, F.; Mortillaro, A.; Nielsen, F. U.; Terreno, E. *Magn. Reson. Med.* **2002,** *47*, 639-648.

(27) Zhang, S.; Merritt, M.; Woessner, D. E.; Lenkinski, R. E.; Sherry, A. D. *Acc. Chem. Res.* **2003,** *36*, 783-790.

(28) Zhang, S.; Jiang, X.; Sherry, A. D. *Helv. Chim. Acta.* **2005,** *88*, 923-935.

(29) Yoo, B.; Pagel, M. D. *J. Am. Chem. Soc.* **2006,** *128*, 14032-14033.

(30) Woods, M.; Woessner, D. E.; Zhao, P.; Pasha, A.; Yang, M.; Huang, C.; Vasalitiy, O.; Morrow, J. R.; Sherry, A. D. *J. Am. Chem. Soc.* **2006,** *128*, 10155-10162.

(31) McVicar, N.; Li, A. X.; Suchý, M.; Hudson, R. H. E.; Menon, R. S.; Bartha, R. *Magn. Reson. Med.* **2013,** *70*, 1016-1025.

(32) Wojciechowski, F.; Suchy, M.; Li, A. X.; Azab, H. A.; Bartha, R.; Hudson, R. H. E. *Bioconjugate Chem.* **2007,** *18*, 1625-1636.

(33) Elmehriki, A. A. H.; Milne, M.; Suchý, M.; Bartha, R.; Hudson, R. H. E. *Can. J. Chem.* **2013,** *91*, 211-219.

(34) Suchý, M.; Li, A. X.; Bartha, R.; Hudson, R. H. E. *Bioorg. Med. Chem. Lett.* **2010,** *20*, 5521-5526.

(35) Baranyai, Z.; Bányai, I.; Brücher, E.; Király, R.; Terreno, E. *Eur. J. Inorg. Chem.* **2007,** 3639-3645.

(36) Zhang, S.; Winter, P.; Wu, K.; Sherry, A. D. *J. Am. Chem. Soc.* **2001,** *123*, 1517-1518.

(37) Tsitovich, P. B.; Spernyak, J. A.; Morrow, J. R. *Angew. Chem. Int. Ed.* **2013,** *52*, 13997-14000.

(38) Dorazio, S. J.; Olatunde, A. O.; Spernyak, J. A.; Morrow, J. R. *Chem. Commun.* **2013,** *49*, 10025-10027.

(39) Olatunde, A. O.; Dorazio, S. J.; Spernyak, J. A.; Morrow, J. R. *J. Am. Chem. Soc.* **2012,** *134*, 18503-18505.

(40) Dorazio, S. J.; Morrow, J. R. *Inorg. Chem.* **2012,** *51*, 7448-7450.

(41) Dorazio, S. J.; Tsitovich, P. B.; Siters, K. E.; Spernyak, J. A.; Morrow, J. R. *J. Am. Chem. Soc.* **2011,** *133*, 14154-14156.

(42) Dorazio, S. J.; Morrow, J. R. *Eur. J. Inorg. Chem.* **2012,** *2012*, 2006-2014.

(43) Dorazio, S. J.; Tsitovich, P. B.; Gardina, S. A.; Morrow, J. R. *J. Inorg. Biochem.* **2012,** *117*, 212-219.

(44) Tsitovich, P. B.; Morrow, J. R. *Inorg. Chim. Acta* **2012,** *393*, 3-11.

(45) Dorazio, S.; Olatunde, A.; Tsitovich, P.; Morrow, J. *J. Biol. Inorg. Chem.* **2014,** *19***,** 191-205.

(46) Zhang, S.; Michaudet, L.; Burgess, S.; Sherry, A. D. *Angew. Chem. Int. Ed.* **2002,** *41*, 1919-1921.

(47) Li, A. X.; Wojciechowski, F.; Suchý, M.; Jones, C. K.; Hudson, R. H. E.; Menon, R. S.; Bartha, R. *Magn. Reson. Med.* **2008,** *59*, 374-381.

(48) Stevens, T. K.; Milne, M.; Elmehriki, A. A. H.; Suchý, M.; Bartha, R.; Hudson, R. H. E. *Contrast Media Mol. Imaging* **2013,** *8*, 289-292.

(49) Aime, S.; Delli Castelli, D.; Fedeli, F.; Terreno, E. *J. Am. Chem. Soc.* **2002,** *124*, 9364-9365.

(50) Zhang, S.; Trokowski, R.; Sherry, A. D. *J. Am. Chem. Soc.* **2003,** *125*, 15288-15289.

(51) Ren, J.; Trokowski, R.; Zhang, S.; Malloy, C. R.; Sherry, A. D. *Magn. Reson. Med.* **2008,** *60*, 1047-1055.

(52) Terreno, E.; Castelli, D. D.; Cravotto, G.; Milone, L.; Aime, S. *Invest. Radiol.* **2004,** *39*, 235-243.

(53) Terreno, E.; Castelli, D. D.; Aime, S. Paramagnetic CEST MRI Contrast Agents. In *The Chemistry of Contrast Agents in Medical Magnetic Resonance Imaging,* 2nd Ed.; Merbach, A., Helm, L., Tóth, É. Eds.; John Wiley & Sons, Ltd: 2013; pp 387-425.

Chapter 2

2   Lanthanide DO3AM Complexes with a Reversible Binding Arm

2.1   Introduction

In order to investigate the effect of reversible binding of one arm of the cyclen macrocycle on the CEST effect due to the bound water or amide proton(s), a series of asymmetric DO3AM ligands was designed and synthesized. This design envisioned the ligands possessing three of the same acetamide arms and the fourth arm having a potential donating group further away from the metal center. It was also hypothesized that the lone arm would bind in a pH dependent fashion and thus the ligand would switch between octadentate and heptadentate coordination modes.

Production of a CEST signal requires a slow exchange rate of the exchangeable protons (lifetime, τ_m, of 10^{-5} - 10^{-2} s).[1] This is made possible by the use of amide arms (weak donors) which lower the electron density at the metal center, in comparison to acetate arms.[2] As a result, both the metal bound water protons and the amide protons of the pendant arms exchange slowly with the bulk water in order to meet the electron density requirements of the metal. This slow exchange should still be present when the coordination by the DO3AM ligand is octadentate. The loss of a coordination site to the metal in the heptadentate form may encourage an even slower exchange rate of the amide protons and bound water protons. This is feasible due to the additional reduction in electron density at the metal center. Accordingly, this further reduction may result in an improved CEST signal. Since the electron density requirements of the metal center may be met by the coordination of another water molecule to the metal, resulting in an increase in relaxivity, the relaxometric properties will also be assessed.

In order to achieve the desired heptadentate/octadentate binding modes, a labile ligand with the appropriate pK_a is required. To facilitate this switch in binding, the *para-*

nitrophenol group was chosen as the labile pendant arm and the other three arms were acetamide-glycinate groups. The pK_a of the *para*-nitrophenol group is 7.18 in water [3], which makes it suitable for observing changes in a biological environment. Other *para*-substituted phenols with electron-withdrawing groups such as chloro and cyano have pK_as of 9.38 and 7.8, respectively (in water) [3]. The higher pK_a values for these groups mean that they are less suitable for use within the biologically relevant pH range. As such, the choice of the *para*-nitrophenol for the lone labile arm offers the chance to develop a potential PARACEST pH responsive probe for applications in the detection of cancer cells, which have an acidic pH.[2]
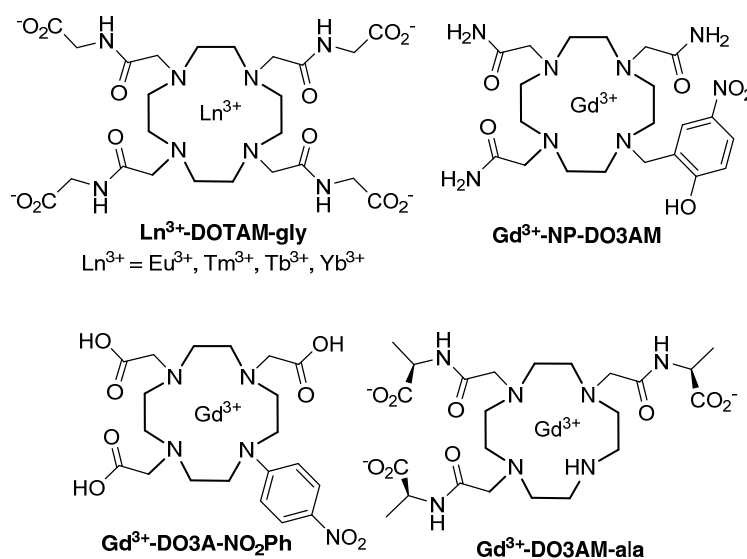
Figure 2.1: Chemical structures of some complexes discussed in this work.

2.2 Results and Discussion

2.2.1 Synthesis

Scheme 2.1 represents the initial attempt to the target nitrophenol-DO3AM-gly (NP-DO3AM-gly) complexes. This route involved trialkylation of cyclen with benzyl (2-chloroacetyl)glycinate **2.1** as previously reported.[3] However, during the synthesis, difficulties such as poor yields were encountered. These yields stemmed from the

incomplete conversion to the desired trialkylated product as well as over-production of the tetraalkylated product.

Several conditions were attempted with the aim of optimizing the yield. These included using varying equivalents of electrophile (1- 5 eq), bases (NaHCO$_3$, Et$_3$N, DIPEA; 0 - 10 eq), solvents (CH$_3$CN, CH$_2$Cl$_2$, CH$_3$Cl), temperatures (-40°C to 80°C) and reaction times (up to 1 week). Additionally, the protecting group of the electrophile was changed to that of the ethyl and *tert*-butyl ester. Regrettably, all these changes were unproductive.

In addition to the synthetic challenges, the purifications were also problematic. For the reason that multiple products formed during the first step of trialkyation, purification by column chromatography was required. The many attempts made to isolate pure trialkylated product were unsuccessful due to the co-elution of both the tri- and tetraalkylated products. Moreover, when HPLC purification using a C$_{18}$ column was attempted, transesterification as well as partial deprotection of the protected ester occurred. This likely happened prior to injection because it was necessary to dissolve the crude reaction mixture in MeOH for sample injection.
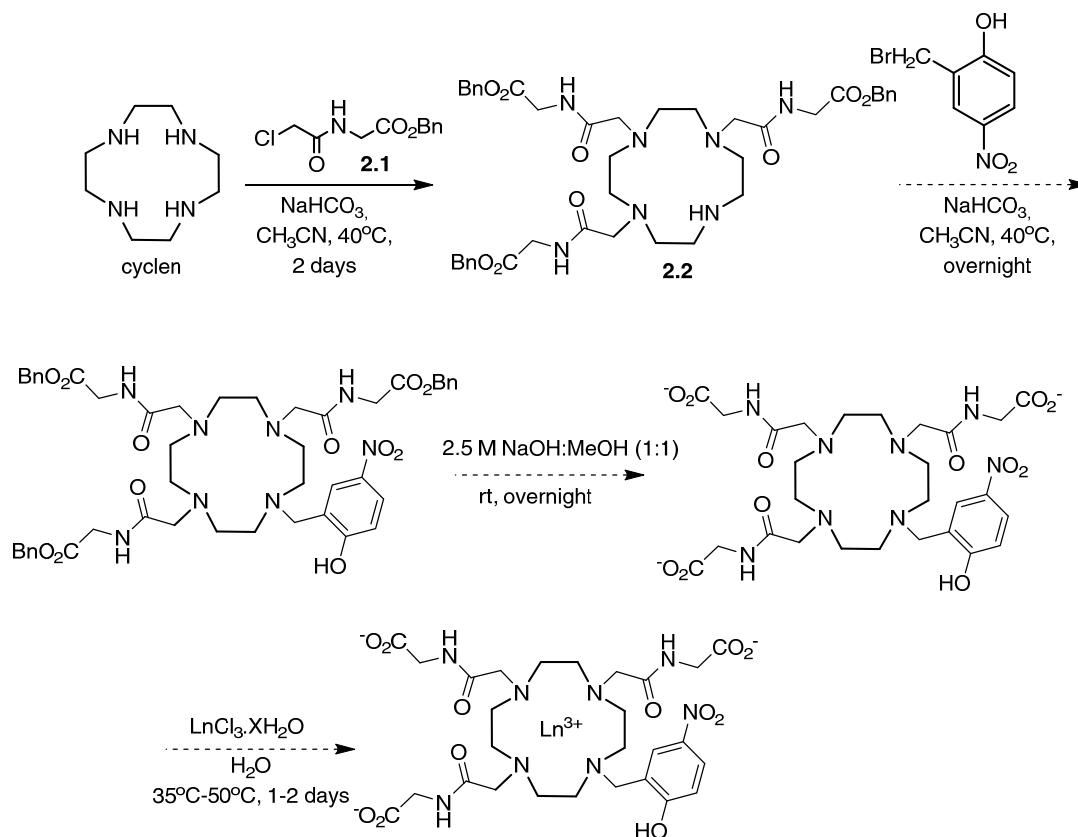
Scheme 2.1: Potential synthetic route towards NP-DO3AM-gly complexes.

Due to the lack of success in what was expected to be a straightforward and easy synthetic pathway to the desired metal complexes, another approach to achieve that objective was attempted. This modification involved a reverse of the initial synthetic steps. As such, a monoalkylation with the electrophile of the lone *p*-nitrophenol arm, followed by trialkylation with the acetamide arms was performed. This sequence of steps worked successfully as seen in Scheme 2.2. Cyclen was first protected using formyl groups as reported to afford tri-formyl cyclen **2.3**.[4] Monoalkylation with 2-hydroxy-5-nitrobenzyl bromide **2.4** and subsequent deprotection of the formyl groups with 2M HCl gave the crude product **2.6**. The crude mixture was precipitated with ether to give the desired monoalkylated cyclen **2.6** in good yield. Compound **2.6** was trialkylated with ethyl (2-chloroacetyl)glycinate **2.7** to afford compound **2.8** in moderate yield after purification by column chromatography. The ester protecting groups were removed by saponification and the crude mixture purified by size-exclusion column chromatography to give the ligand **2.9** in good yield. With ligand **2.9** in hand, metalation with the

lanthanides was done based on literature procedure and this proceeded smoothly. The metalated complexes were purified by size-exclusion column chromatography to give the complexes **2.10 - 2.14** in moderate yields.
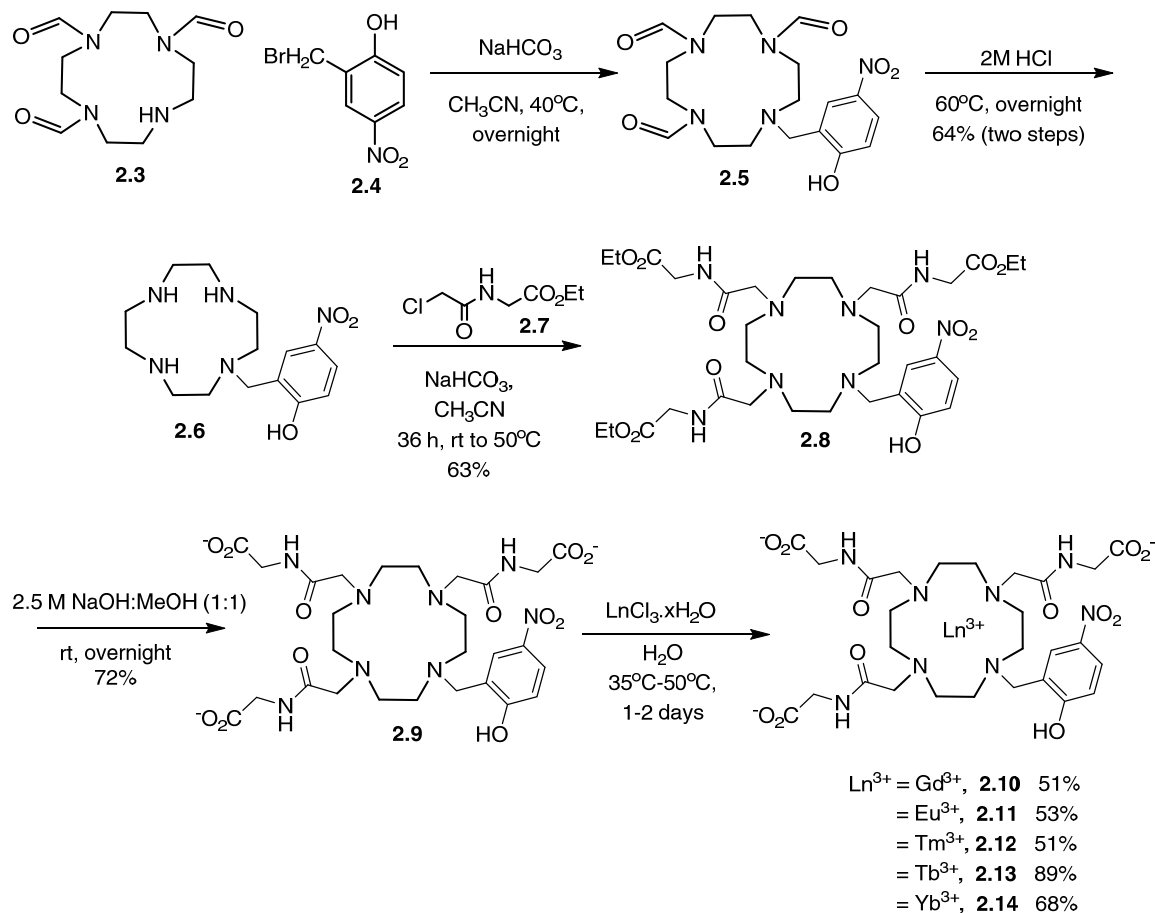
Scheme 2.2: Modified synthetic route towards NP-DO3AM-gly complexes 2.10 – 2.14.

In order to expand the scope of the target ligand and to develop a possible redox responsive CEST agent, we attempted to reduce ligand **2.9** (Scheme 2.3). Several conditions shown in Table 2.1 were attempted but unfortunately, none was successful.
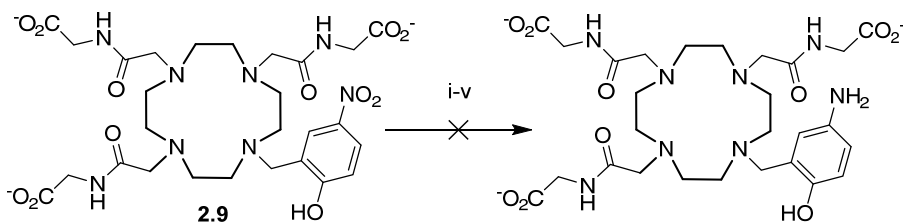
Scheme 2.3: Attempts to reduce the NO$_2$ group of 2.9.

Table 2.1: Conditions attempted for reduction of the NO$_2$ group of 2.9.

Conditions	Results
(i) Pd/C, H$_2$, 2 days	De-benzylation
(ii) Na$_2$S.9H$_2$O, EtOH, rt to 50°C, 2 days	No reaction
(iii) SmI$_2$, H$_2$O, isopropylamine, N$_2$, rt, overnight	De-benzylation
(iv) Zn in conc. HCl, rt to 50°C, 2 days	No reaction
(v) TiCl$_3$ (>12% in HCl), H$_2$O/AcOH (1:1), rt, 10 mins	Decomposition

2.2.2 CEST Evaluation
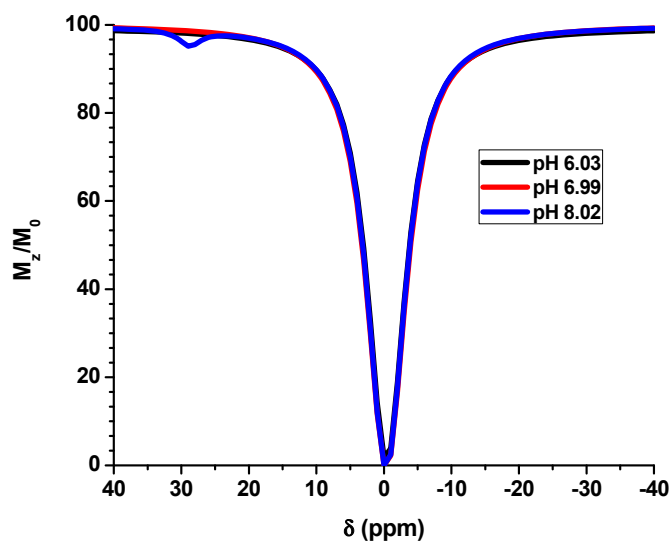
Figure 2.2: CEST spectra of Tb^{3+}-NP-DO3AM-gly 2.13. CEST spectra were acquired at 37°C, with a 15 µT, 2 s presaturation pulse, 10 mM in D$_2$O/H$_2$O (9:1).

CEST experiments for the Eu^{3+}, Tb^{3+}, Tm^{3+} and Yb^{3+} metalated complexes at pH 6, 7 and 8 were carried out in D_2O/H_2O (9:1). Only the Tb^{3+} complex had a CEST signal of 3% at 28 ppm at pH 8 (Figure 2.2). The pH at which the CEST signal occurs prevents the use of this agent as a responsive probe within the biological pH range of 7.35-7.45.

CEST intensity as a function of Ln^{3+} choice

As mentioned in the preceding paragraph, only the Tb^{3+} complex had a CEST signal, albeit a small one. Within the lanthanide series, the size of Tb^{3+} is between Eu^{3+} and Tm^{3+}. As such, the signal seen for the Tb^{3+} complex may be a circumstance of "Goldilocks" fitting. In this situation, the size of Tb^{3+} was ideal for the correct orientation to be achieved by the phenol in order for coordination to the metal center to occur. If the metal is big (Eu^{3+}), there may not be enough space for the phenol to attain the correct orientation for metal coordination. On the other hand, if the metal is small (Tm^{3+}), then the phenol may have more than enough space for proper orientation but then the Tm^{3+} becomes too labile. Considering that the corresponding DOTAM-gly complexes (Figure 2.1) did generate CEST signals,[5] the lack of symmetry within these *p*-nitrophenol complexes may then exacerbate both conditions and thus prevent generation of a CEST signal as was observed for the Eu^{3+}, Tm^{3+} and Yb^{3+} complexes.

CEST intensity as a function of pH for Tb^{3+}-NP-DO3AM-gly **2.13**

The expected trend for CEST signal due to amide protons is an increase in the CEST effect as the pH increases. The rate-determining step for exchange of amide protons is known to be deprotonation under base-catalyzed conditions and protonation under acid-catalyzed conditions.[2] The base-catalyzed exchange occurs at a pH greater than 5.[2] In essence, the CEST effect should increase with increasing pH until a maximum signal is achieved and the exchange rate is no longer favourable (exceeds slow to intermediate exchange) for a CEST effect to occur. Considering that a CEST signal was seen at pH 8 and none at pH 6 and 7 (Figure 2.2), complex **2.13** demonstrated this expected trend of an increase in CEST with increasing pH. One may expect the phenol group to be coordinated to the metal at pH greater than 5. This assumption is based on the results of Gd^{3+}-NP-DO3AM (Figure 2.1) in which the phenol group did not dissociate from the

metal, even at pH values as low as 5.[6] The coordination of the phenolate group at high pH ensured that the electron density requirements of the metal center were met. When this occured, the ligand was octadentate and produced a CEST signal due to the amide protons, as was observed for the Tb^{3+} complex **2.13**.

At pH 6 and 7, lack of an amide CEST signal for the Tb^{3+} complex **2.13** may indicate one of two things. Firstly, the phenol group may in fact be protonated and not be coordinated to the metal center, in which case the ligand was heptadentate. Subsequently, the lowered electron density at the metal center did not lead to a slower exchange as was anticipated, so no CEST signal was observed. Alternatively and more likely is that the phenolate is coordinated to the metal (in octadentate form) but the exchange rate of the amide protons was outside of the slow to intermediate range desired for a CEST signal to be produced. This is likely to be the case for the other complexes **2.11**, **2.12** and **2.14** as well.

Chemical shift (Δω) as a function of ligand design

One of the differences between the CEST results of the Tb^{3+}-DOTAM-gly (Figure 2.1) and the Tb^{3+}-NP-DO3AM-gly **2.13** is the Δω of the observed CEST signals. Previous reports have shown that the symmetric Tb^{3+}-DOTAM-gly complex CEST signal occurs at 61 ppm (pH 7.4).[5] On the other hand, the asymmetric Tb^{3+}-NP-DO3AM-gly complex **2.13** had a more upfield CEST signal at 28 ppm (pH 8.02). This difference in Δω between the complexes was most likely a result of the ligand design, rather than the pH at which the data was acquired. At high pH, the phenol group of **2.13** is expected to be deprotonated and therefore coordinated to the metal center. Hydroxyl groups (and by extension phenols) are weak donors and are not expected to give a strong ligand field.[7] The strength of the ligand field in turn influences the size of the hyperfine shift of the lanthanide.[7] Although Tb^{3+} has a large hyperfine shift,[2] this effect may be over-shadowed by the weak ligand field of the phenol group and subsequently, a small Δω is observed. At pH 6 and 7, this small Δω would violate the criteria for PARACEST agents, leading to the absence of a CEST signal.[7]

2.2.3 Relaxometric Evaluation of Gd^{3+}-NP-DO3AM-gly Complex

Relaxivity studies of the Gd^{3+}-NP-DO3AM-gly complex **2.10** with respect to pH were performed. Complex **2.10** in an aerated solution of water showed an increase in the relaxivity as the pH decreased, with a very sharp increase between pH 5.5 and 6.5 (Figure 2.3a). The r_1 value of 1.5 mM^{-1} s^{-1} at basic pH is lower than that for Gd^{3+}-NP-DO3AM (basic pH: 2.8 mM^{-1} s^{-1}) [6] while at acidic pH, complex **2.10** has an r_1 value of almost 5.3 mM^{-1} s^{-1}. This value is higher than that of Gd^{3+}-NP-DO3AM, which has an r_1 value 3.4 mM^{-1} s^{-1} under similar pH.[6]
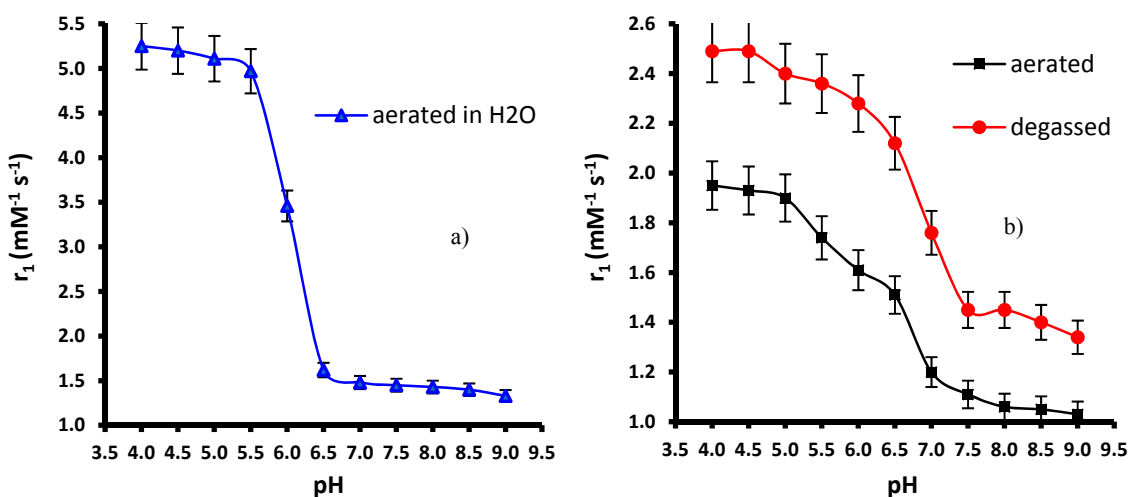
Figure 2.3: Relaxivity profile of 10 mM Gd^{3+}-NP-DO3AM-gly complex 2.10 over pH range 4 to 9, 25°C and 400 MHz in (a) H_2O (aerated) and (b) 10 mM $NaHCO_3$, aerated (■) and H_2O, degassed (●).

This relaxivity enhancement at acidic pH is not limited to complexes with amide side arms. If one compares Gd^{3+}-DO3A-like complexes such as Gd^{3+}-DO3A-NO_2Ph (Figure 2.1), a similar pattern is also seen. For such complexes, the relaxivity is found to be stable between pH 5-8.[8] Below that range, it may increase due to acid-catalyzed demetalation.

Above pH 8, OH^- ions and dissolved CO_2 in the form of carbonate can displace the bound water molecule and cause formation of ternary adducts which leads to a decrease in

relaxivity.[8] In order to determine if carbonate binding did play a role in the relaxometric behavior of **2.10**, a study in aerated bicarbonate solution was similarly done as that reported.[9] Another experiment was done in degassed solution of H_2O and compared to that of the aerated bicarbonate solution. Figure 2.3b shows the relaxivity as a function of pH for the degassed and aerated solutions of the Gd^{3+} complex **2.10** in water and sodium bicarbonate solution, respectively. The trend in the sodium bicarbonate solution was parallel to that previously reported for a Gd^{3+}-DO3AM-ala complex (Figure 2.1).[9] However, since the trend of complex **2.10** in degassed and aerated solutions were similar, this possibly means bicarbonate was also being bound in the degassed solution, even after purging with N_2 for two minutes prior to collecting the data. As previously reported, one should expect the relaxivity in degassed solution to be high and constant over the pH range 2 - 10, indicating two waters coordinating to the metal center.[9] In both solutions of **2.10** at high pH, the carbonate ion will be bound to the metal in a bidentate manner and the metal will have all its coordination sites occupied. As a result, a water molecule would not be coordinated to the metal. Once the pH becomes more acidic, the carbonate ion will no longer bind to the metal and a water molecule may be coordinated instead, leading to an increase in relaxivity.

Increases in relaxivity may also be due to the reduced distance between the metal and bound water protons as well as short correlation times due to rotation but these values are expected to be small for low molecular weight[11] complexes like **2.10**. While the relaxivity enhancement at acidic pH could also be due to demetalation of the ligand, thereby forming $Gd[H_2O]_8{}^{3+}$ ($r_1 = 13$ $mM^{-1}s^{-1}$)[11], the stability constants for Gd^{3+}-DOTAM and Gd^{3+}-DOTAM-gly are 10.05 and 14.54, respectively. [12, 13] These values indicate high stabilities for those complexes and one can infer that the stability for complex **2.10** would be within those values. Additionally, the relaxivity increase at acidic pH may be due to the coordination of two water molecules to the metal center as per the design of the ligand. This would be expected to occur once the phenolate gets protonated at low pH and no longer coordinates to Gd^{3+}. However, in the case of Gd^{3+}-NP-DO3AM, it was observed that the relaxivity enhancement did not correlate with the apparent pK_a of 6.48 for the phenol and an increase in relaxivity was observed at a pH below the phenol pK_a.[6] The pK_a may be influenced by the proximity of the tri-cationic metal and the electron

withdrawing nature of the benzylic amine-like linkage to the ligand. It is not surprising that it is not identical to free *p*-nitrophenol.

The overall relaxivity enhancement of complex **2.10** at acidic pH is likely due to a complex combination of factors such as the increase in prototropic exchange of the phenolic protons and bound water protons [6], as well as the presence of the acetamide-glycinate arms. In the latter case, these arms may form hydrogen bonds with the surrounding water molecules and thereby increase the contribution of outer sphere relaxation to the overall relaxivity.

2.3 Conclusion

The initial route followed towards the synthesis of a series of asymmetric complexes having three acetamide-glycinate arms and a *p*-nitrophenol arm for reversible binding was met with unexpected challenges. However, these were resolved by reversing the order of a few earlier steps in the synthetic scheme and the desired compounds were obtained.

CEST experiments for the Eu^{3+}, Tb^{3+}, Tm^{3+} and Yb^{3+} NP-DO3AM-gly complexes were done at various pH values but only the Tb^{3+} complex showed an amide CEST signal at pH 8. In comparison to the tetraglycinate complexes of the same metals, there was a significant decrease (in the case of Tb^{3+}) as well as elimination of the CEST effect, with respect to the other metals. The lack of a CEST signal for the other complexes as well as at other pH values may be due to a variety of reasons, primarily the faster than ideal exchange rate of the amide protons (and bound water), especially when the ligand is in its heptadentate form. This is in contrast to what was hypothesized based on the reduced electron density at the metal center.

The increase in relaxivity at low pH in both the degassed and aerated solutions of the Gd^{3+} NP-DO3AM-gly complex **2.10** is likely due to a combination of increased prototropic exchange and or outer sphere relaxation, rather than simply an increase in the number of water molecules coordinated to the metal center. This increase in coordinated

water molecules would arise because of dissociation of the protonated phenol group. Sharp increases in relaxivity within the biologically relevant pH range of 5.5 to 7.5 were recorded for these various solutions. This does demonstrate the sensitivity of the phenol group to act as a relaxivity-based pH sensor.

With the information gleaned here, it is now known that amide CEST can be modulated due to reversible binding but may be strongly dependent on the metal center and perhaps type of ligating group involved. Unfortunately, due to the small CEST effect at such high pH, this agent is not suitable as a PARACEST pH responsive probe.

2.4 Supplemental Information

2.4.1 General Experimental

General synthetic details can be found in Appendix 1.

CEST and Relaxivity Experiments

CEST spectra were acquired on a 600 MHz vertical bore NMR spectrometer, using a 15 µT, 2s continuous wave presaturation pulse at offset frequencies ranging from -110 to 110 ppm in steps of 1 ppm at a concentration of 10 mM in D_2O/H_2O (9:1) at pH 6.00 ± 0.03, 7.00 ± 0.03 and 8.00 ± 0.03; 25°C or 37 °C. T_1 relaxation time constant measurements were carried out on a 400 MHz spectrometer with 10 mM of contrast agent in H_2O or in 10 mM $NaHCO_3$ using an inversion recovery sequence (14 inversion times in the range of 0.001 s – 0.3 s) with a minimum $d_1 = 5T_1$ to ensure full recovery, pH 4-9 (±0.03) and 25 °C; degassed with N_2 for 2 mins.

2.4.2 Synthetic Procedures
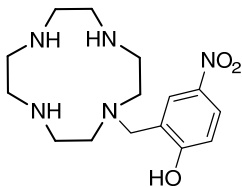
2-((1,4,7,10-tetraazacyclododecan-1-yl)methyl)-4-nitrophenol (2.6)
Tri-formyl cyclen **2.3** (400 mg, 1.56 mmol) and NaHCO$_3$ (262 mg, 3.12 mmol) suspended in CH$_3$CN (15 mL) were stirred for 5 mins at rt upon which 2-hydroxy-5-nitrobenzyl bromide **2.4** (724 mg, 3.12 mmol) in CH$_3$CN (5 mL) was added dropwise. Stirring was continued for 18 h at 40°C. The mixture was concentrated and carried forward to the next step as is. Crude product **2.5** was dissolved in 2M HCl (8 mL). Stirring was continued for 18 h at 60°C. The mixture was concentrated then precipitated with ether. The title compound was obtained as a cream solid (323 mg, 64%). ^{1}H NMR (400 MHz, D$_2$O) δ 8.19-8.15 (2H, m), 7.04 (1H, d, J = 9Hz), 3.72 (2H, s), 3.12 (8H, broad s), 3.06 (4H, broad s), 2.99 (2H, broad s), 2.84 (2H, broad s). ESI-TOF m/z calcd for C$_{15}$H$_{26}$N$_5$O$_3$ (M +H)$^+$, calculated 324.2036, found 324.2035.
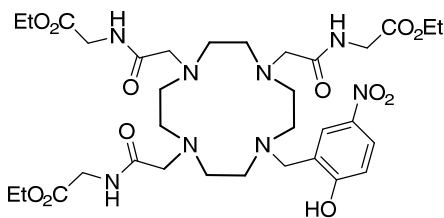
Triethyl 2,2',2''-((2,2',2''-(10-(2-hydroxy-5-nitrobenzyl)-1,4,7,10-tetraazacyclododecane-1,4,7-triyl)tris(acetyl))tris(azanediyl))triacetate (2.8) Starting material **2.6** (250 mg, 0.773 mmol) and NaHCO$_3$ (260 mg, 3.092 mmol) were suspended in CH$_3$CN (8 mL) and stirred for 5 mins at rt upon which ethyl (2-chloroacetyl)glycinate **2.7** (555 mg, 3.092 mmol) dissolved in CH$_3$CN (2 mL) was added dropwise. Stirring was continued for 36 h at 50°C. The mixture was filtered and the filtrate concentrated. The crude was purified by column chromatography (silica gel) by eluting with 0-5% MeOH in CH$_2$Cl$_2$ to give the product. The title compound was obtained as a yellow oil (367 mg, 63%). ^{1}H NMR (400 MHz, CDCl$_3$): δ 8.29-8.17 (3H, m), 8.07-8.04 (1H, dd, J = 9Hz), 7.92 (1H, d, J = 2Hz),

6.49 (1H, s), 4.12 (2H, q, J = 7Hz), 4.05-3.94 (6H, m), 3.81 (4H, broad s), 3.4-2.77 (16H, m), 2.67 (8H, broad s), 1.25 (3H, t, J = 7Hz), 1.15 (6H, t, J = 7Hz). ^{13}C NMR (100 MHz, CDCl$_3$): δ 171.81, 170. 73, 169.64, 126.67, 125.85, 119.48, 117.33, 61.44, 59.72, 58.78, 57.69, 51.28, 49.43, 40.67, 13.93. ESI-TOF m/z calcd for C$_{33}$H$_{53}$N$_8$O$_{12}$ (M+H)$^+$, calculated 753.3783, found 753.3763.
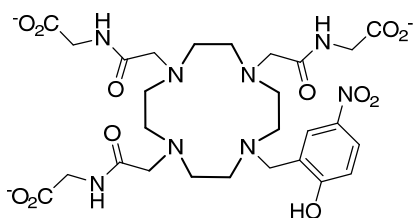
2,2',2''-((2,2',2''-(10-(2-hydroxy-5-nitrobenzyl)-1,4,7,10-tetraazacyclododecane-1,4,7-triyl)tris(acetyl))tris(azanediyl))triacetate (2.9)
Starting material **2.8** (300 mg, 0.399 mmol) was dissolved in 8 mL of 2.5 M NaOH-MeOH (1:1) mixture and stirring continued for 18 h at rt. The mixture was concentrated and brought to pH 6 by addition of 1M HCl. This was again concentrated and purified by twice by size exclusion column chromatography (100% H$_2$O) and the fractions lyophilized to give the product. The title compound was obtained as a yellow solid (192 mg, 72 %).^{1}H NMR (400 MHz, D$_2$O) δ = 8.10 (1H, s), 7.97 (1H, d, J = 9Hz), 6.40 (1H, d), 3.80-3.55 (7H, m), 3.22-2.40 (23H, m). ESI-TOF m/z calcd for C$_{27}$H$_{41}$N$_8$O$_{12}$ (M+H)$^+$, calculated 669.2844, found 669.2822.

General procedure for metalation. Starting material **2.9** was dissolved in H$_2$O (1 mL) then the appropriate lanthanide chloride salts added. The pH was adjusted to 6 and the reaction mixture heated to 35°C - 40°C and left for overnight. The mixture was concentrated, purified by size exclusion chromatography (100% H$_2$O) and the fractions lyophilized.
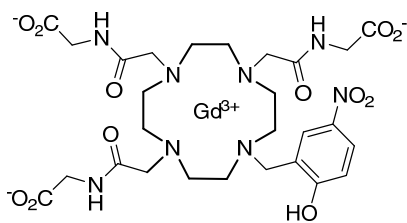
Gadolinium(III) **2,2',2''-((2,2',2''-(10-(2-hydroxy-5-nitrobenzyl)-1,4,7,10-tetraazacyclododecane-1,4,7-triyl)tris(acetyl))tris(azanediyl))triacetate (2.10)** Starting material **2.9** (31 mg, 0.046 mmol) and GdCl$_3$.6H$_2$O (17 mg, 0.046 mmol). The title compound was obtained as a pale yellow solid (19 mg, 51%). ESI-TOF *m/z* calcd for C$_{27}$H$_{38}$ N$_8$O$_{12}$Gd (M-2H)$^+$, calculated 824.1850, found 824.1888.
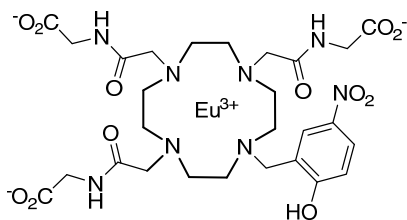
Europium(III) **2,2',2''-((2,2',2''-(10-(2-hydroxy-5-nitrobenzyl)-1,4,7,10-tetraazacyclododecane-1,4,7-triyl)tris(acetyl))tris(azanediyl))triacetate (2.11)** Starting material **2.9** (25 mg, 0.037 mmol) and EuCl$_3$.6H$_2$O (14 mg, 0.037 mmol). The title compound was obtained as a pale yellow solid (16 mg, 53%). ESI-TOF *m/z* calcd for C$_{27}$H$_{38}$ N$_8$O$_{12}$Eu (M-2H)$^+$, calculated 819.1822, found 819.1858.
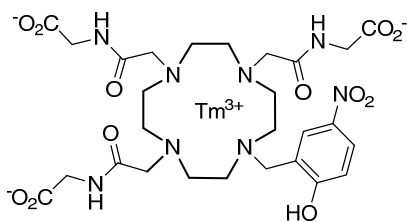
Thulium(III) **2,2',2''-((2,2',2''-(10-(2-hydroxy-5-nitrobenzyl)-1,4,7,10-tetraazacyclododecane-1,4,7-triyl)tris(acetyl))tris(azanediyl))triacetate (2.12)** Starting material **2.9** (30 mg, 0.045 mmol) and TmCl$_3$.7H$_2$O (18 mg, 0.045 mmol). The title compound was obtained as a

pale yellow solid (19 mg, 51%). ESI-TOF *m/z* calcd for $C_{27}H_{38}N_8O_{12}Tm$ (M-2H)$^+$, calculated 835.1951, found 835.1949.
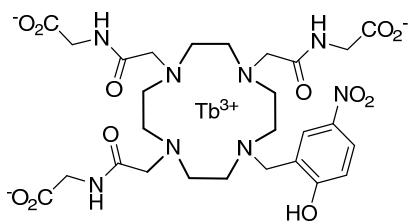
Terbium(III) 2,2',2''-((2,2',2''-(10-(2-hydroxy-5-nitrobenzyl)-1,4,7,10-tetraazacyclododecane-1,4,7-triyl)tris(acetyl))tris(azanediyl))triacetate (2.13) Starting material **2.9** (30 mg, 0.045 mmol) and TbCl$_3$.7H$_2$O (25 mg, 0.068 mmol). The title compound was obtained as a pale yellow solid (33 mg, 89%). ESI-TOF *m/z* calcd for $C_{27}H_{38}N_8O_{12}Tb$ (M-2H)$^+$, calculated 825.1863, found 825.1862.
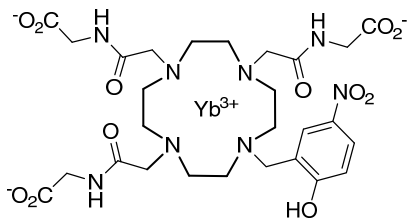
Ytterbium(III) 2,2',2''-((2,2',2''-(10-(2-hydroxy-5-nitrobenzyl)-1,4,7,10-tetraazacyclododecane-1,4,7-triyl)tris(acetyl))tris(azanediyl))triacetate (2.14) Starting material **2.9** (30 mg, 0. 045 mmol) and YbCl$_3$.6H$_2$O (49 mg, 0.127 mmol). The title compound was obtained as a pale yellow solid (72mg, 68 %). ESI-TOF *m/z* calcd for $C_{27}H_{38}N_8O_{12}Yb$ (M-2H)$^+$, calculated 840.1998, found 840.2010.

2.4.3 Spectra

S 2.1: ^{1}H-NMR Spectrum of **2.6**
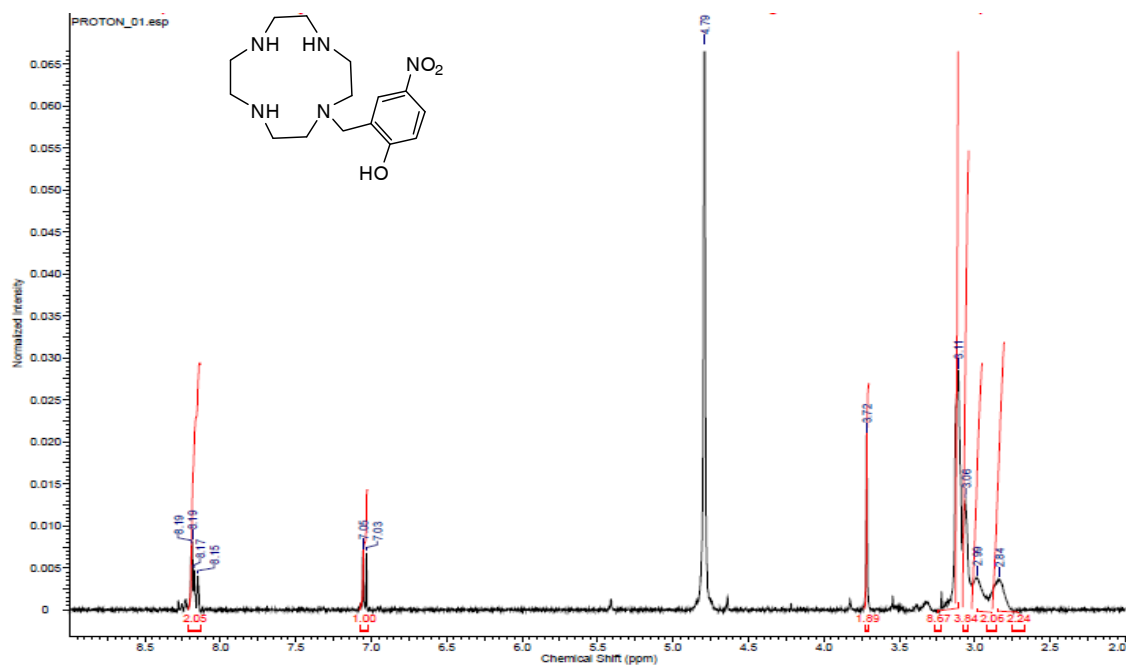
S 2.2: ^{1}H-NMR Spectrum of **2.8**
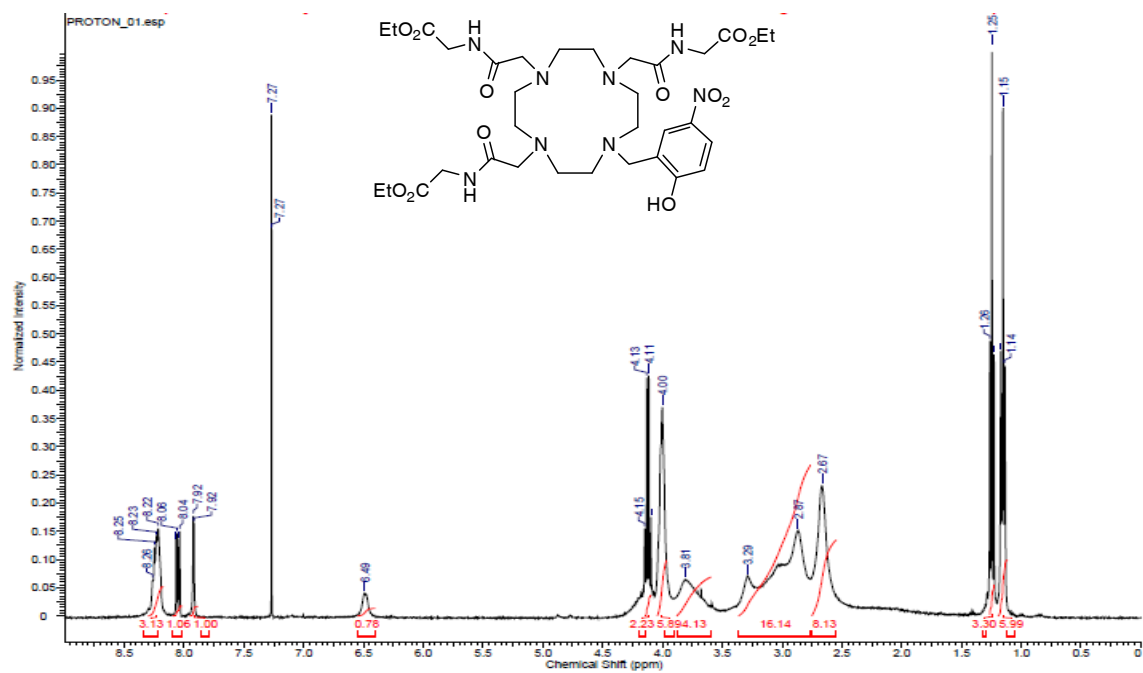
S 2.3: ^{13}C-NMR Spectrum of **2.8**
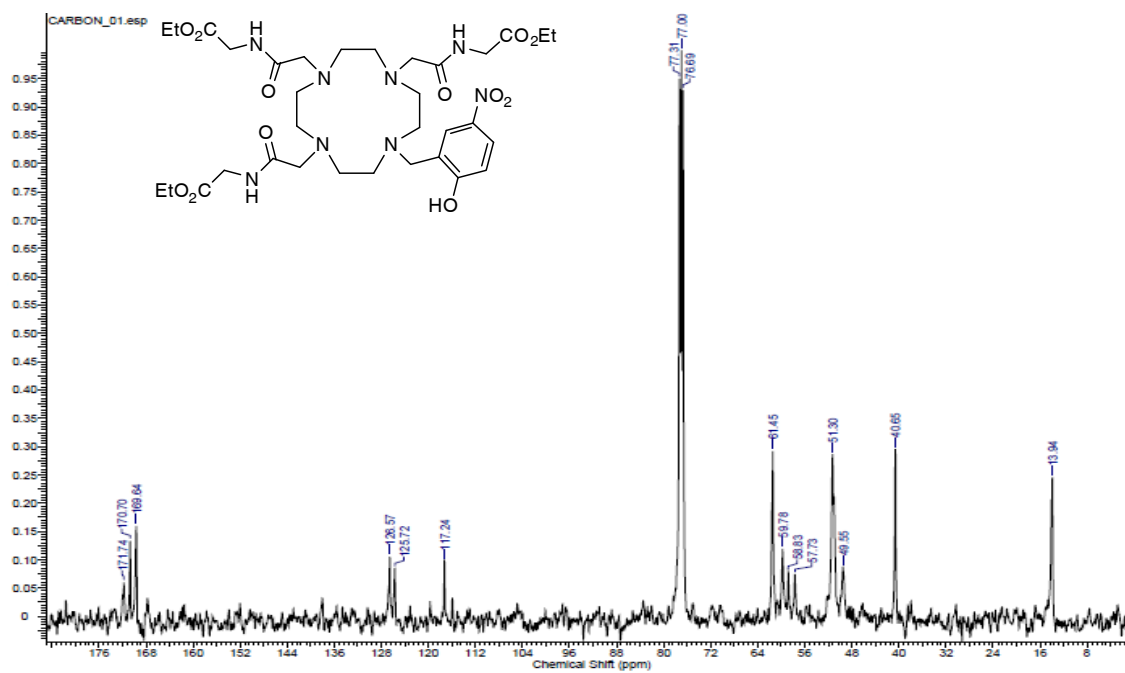
S 2.4: ^{1}H-NMR Spectrum of **2.9**
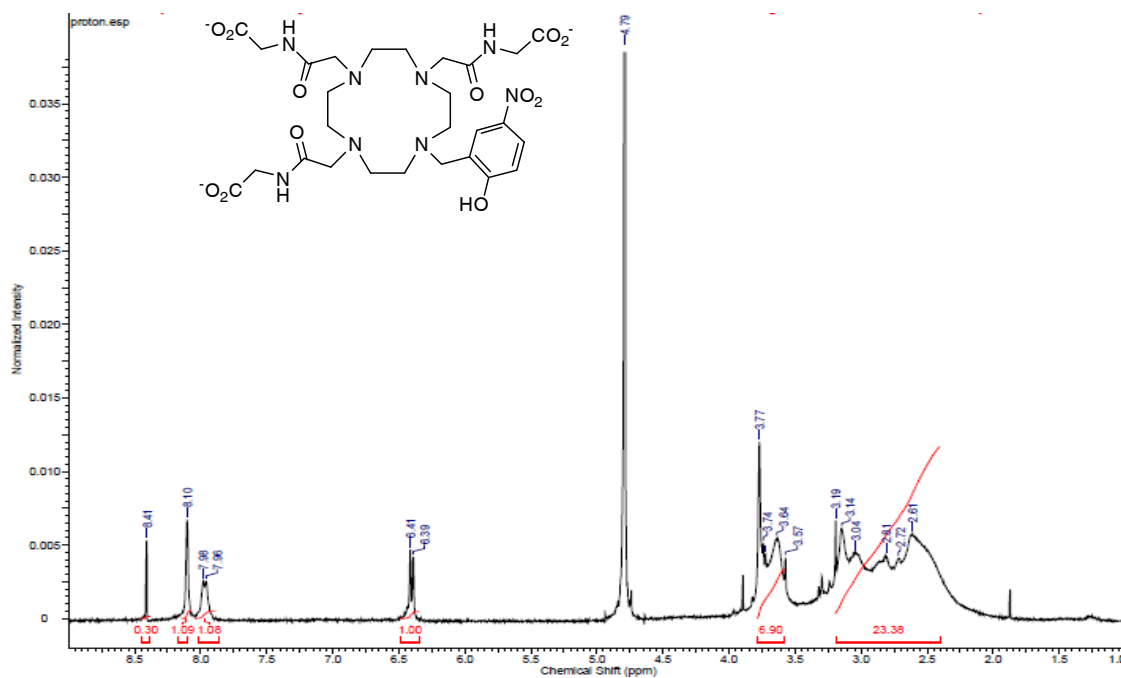
2.5 References

(1) Sherry, A. D.; Wu, Y. *Curr. Opin. Chem. Biol.* **2013,** *17*, 167-174.

(2) Viswanathan, S.; Kovacs, Z.; Green, K. N.; Ratnakar, S. J.; Sherry, A. D. *Chem. Rev.* **2010,** *110*, 2960-3018.

(3) Penhoat, M. *Tetrahedron Lett.* **2013,** *54*, 2571-2574.

(4) Suchy, M.; Hudson, R. H. E. *Eur. J. Org. Chem.* **2008,** *2008*, 4847-4865.

(5) Boldrini, V.; Giovenzana, G. B.; Pagliarin, R.; Palmisano, G.; Sisti, M. *Tetrahedron Lett.* **2000,** *41*, 6527-6530.

(6) Terreno, E.; Castelli, D. D.; Cravotto, G.; Milone, L.; Aime, S. *Invest. Radiol.* **2004,** *39*, 235-243.

(7) Woods, M.; Kiefer, G. E.; Bott, S.; Castillo-Muzquiz, A.; Eshelbrenner, C.; Michaudet, L.; McMillan, K.; Mudigunda, S. D.; Ogrin, D.; Tircso, G.; Zhang, S.; Zhao, P.; Sherry, A. D. *J. Am. Chem. Soc.* **2004,** *126*, 9248-9256.

(8) Woods, M.; Woessner, D. E.; Sherry, A. D. *Chem. Soc. Rev.* **2006,** *35*, 500-511.

(9) Terreno, E.; Boniforte, P.; Botta, M.; Fedeli, F.; Milone, L.; Mortillaro, A.; Aime, S. *Eur. J. Inorg. Chem.* **2003,** *2003*, 3530-3533.

(10) Aime, S.; Barge, A.; Botta, M.; Howard, J.,A.K.; Kataky, R.; Lowe, M.,P.; Moloney, J.,M.; Parker, D.; de Sousa, A.,S. *Chem. Commun.* **1999,** 1047-1048.

(11) Hall, J.; Haner, R.; Aime, S.; Botta, M.; Faulkner, S.; Parker, D.; de Sousa, A.,S. *New J. Chem.* **1998,** *22*, 627-631.

(12) Maumela, H.; Hancock, R. D.; Carlton, L.; Reibenspies, J. H.; Wainwright, K. P. *J. Am. Chem. Soc.* **1995,** *117*, 6698-6707.

(13) Baranyai, Z.; Brücher, E.; Iványi, T.; Király, R.; Lázár, I.; Zékány, L. *Helv. Chim. Acta* **2005,** *88*, 604-617.

Chapter 3

3   Transition Metal Complexes of Semi-rigidified and Fully-Rigidified DOTAM

3.1 Introduction

T_1 contrast agents are more often than not, either small macrocyclic complexes like Gd^{3+}-DOTA, or linear metal complexes such as Gadodiamide (Figure 3.1). The molecular structure of any MRI contrast agent will influence its thermodynamic and kinetic stability, the magnitude of the induced shifts (in the case of PARACEST agents) and even its spectroscopic properties.[1] The acyclic complexes have higher flexibilities, which may facilitate faster water exchange, an important criterion for a good T_1 agent.[1]
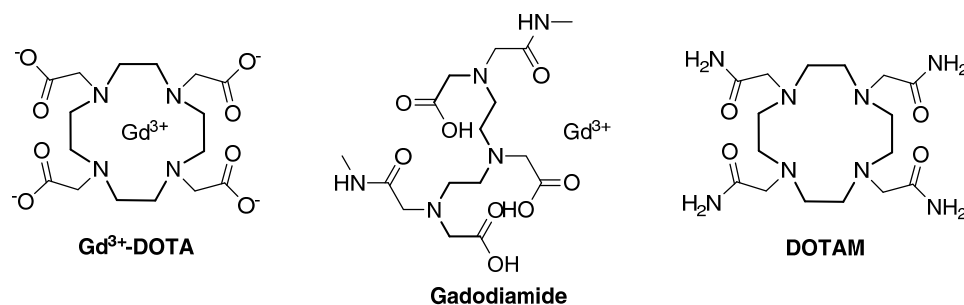
Figure 3.1: Chemical structures of some ligands and complexes discussed in this work.

As previously mentioned in Chapter 1, it is becoming more widespread for PARACEST agents to be designed based on the macrocyclic DOTAM (Figure 3.1). Substituting the acetate arms of DOTA with amide arms provides a reduced electron density at the metal center that in turn leads to the slower exchange of the exchangeable protons of -NH, -OH and a metal bound water. This slow exchange is a requirement for a CEST signal to be produced.[1]

DOTA and its associated structures such as DOTAM, offer higher preorganization, symmetry and rigidity, as compared to conventional acyclic ligands. Once chelation with a metal occurs, these properties subsequently influence the coordination geometries of the macrocycles. DOTA forms very stable lanthanide chelates by adopting either one of two conformations: square anti-prismatic (SAP, more stable) or a twisted square-antiprismatic (TSAP, less stable) (Figure 3.2). The coordination geometry is dictated by the configuration of the substituents on the backbone of the ring as well as the pendant arms. Hence, the two isomers can be differentiated by their respective angles between the N-Ln-N and O-Ln-O planes (α). If the angle α, between the plane of the coordinating nitrogens of the backbone and the oxygens of the pendant arms is about 39°, that indicates the SAP geometry. On the other hand, an α of 25° indicates the TSAP geometry.[2] Larger lanthanide ions (earlier in the period of the periodic table) that are coordinated to DOTA, tend to preferentially form the TSAP isomer while the smaller lanthanides (later in the period), prefer the SAP isomer.[3]

SAP isomer   TSAP isomer
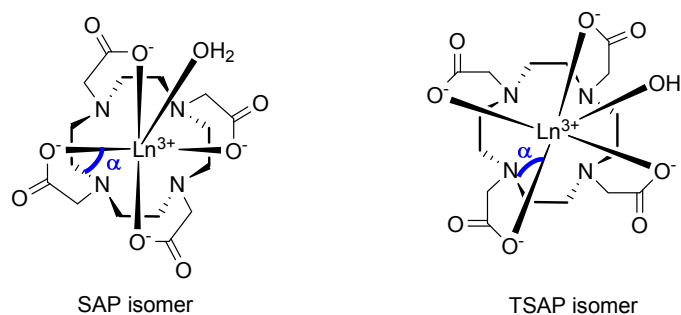
Figure 3.2: Schematic representations of the possible isomeric geometries of Ln^{3+}-DOTA.

It has been shown that the water exchange rate in the SAP isomer of DOTAM is about 50 times slower than that of the TSAP isomer.[3, 4] In the TSAP isomer, the bound water is further away from the metal centre and this facilitates a faster exchange with the surrounding water molecules.[2] It has also been demonstrated that the coordination geometry in DOTAM ligands having bulky amide substituents, normally led to the formation of the SAP isomer.[5] However, the coordination geometry of these types of

complexes was also found be affected by the nature of the solvent.[5] Considering that slow exchange is desired for CEST, using DOTAM ligands that are prone to form the SAP isomer should ideally produce good PARACEST agents.

Potentially, another way to form the SAP isomer over the TSAP isomer is by means of rigidification. Rigidification may be achieved by placing groups on either the backbone of the macrocyclic ring, the alpha position of the pendant arms, or in both positions concurrently. Additionally, rigidification increases the kinetic inertness of the metal complexes.[6] This is likely due to the more compact macrocyclic cage that prevents the nitrogen atoms from being protonated, thus leading to dissociation of the metal from the ligand.[6]

Interest in the modulation of the CEST signal due to the amide proton, directed the research to determine the effect the rigidity of DOTAM-like structures would have on amide CEST generation. This effect has not been studied in detail for DOTAM-like structures. Nonetheless, it has been reported that the TSAP isomer of DOTA and DOTAM ligands, which have been rigidified by one substituent on the backbone of the ring or on each of the pendant arms, have a faster exchange of bound water.[3, 7, 8] It was anticipated that by rigidifying the DOTAM backbone, the preferred SAP conformation for CEST would be "locked in". Taking into account that the amide arms inherently allow for slow exchange of the amide protons, it was hypothesized that an even higher CEST effect should be generated by rigidification of the macrocycle, compared to that due solely to the amide protons.

It was decided, that the structures to be investigated as PARACEST agents would have the DOTAM core structure but be rigidified through substitution of at least one cyclohexyl group on the macrocyclic ring. The cyclohexyl rings should additionally increase the hydrophobicity of the complexes. Hence, for *in vivo* applications, there may be favourable uptake into specific organs of the body.[6] Optimistically, this would provide an opportunity to view these organs by CEST imaging. However, one should bear in the mind that if the agent is too hydrophobic, it might spend a longer time in these organs than is medically safe. Additionally, due to the presence of the amide protons of the

pendant arms, these agents may be pH responsive probes, hopefully within the biologically relevant pH range (pH 7.35-7.45).

3.2 Results and Discussion

3.2.1 Synthesis

Figure 3.3 shows the initial target fully-rigidified **3.1a** and semi-rigidified **3.2a** complexes for this study. The route to achieve these complexes was to follow similar procedures published by Desreux *et al*., with the most important step being a "crab-like" condensation between a bischloroacetamide and a diamine.[9] However, due to the difficulties faced during this crucial step, we modified the target ligands. It is noteworthy to mention, that previous work done on complexes similar to those shown in Figure 3.3, was within the context of conventional T_1 MRI agents and as such had the acetate arms of the DOTA core structure.[9]
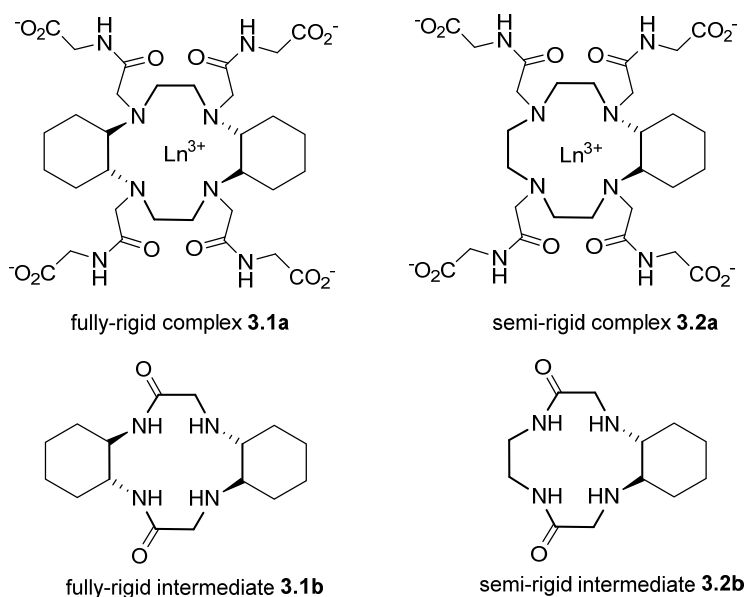
Figure 3.3: Initial target complexes and their intermediate structures.

Synthesis of fully-rigidified complexes
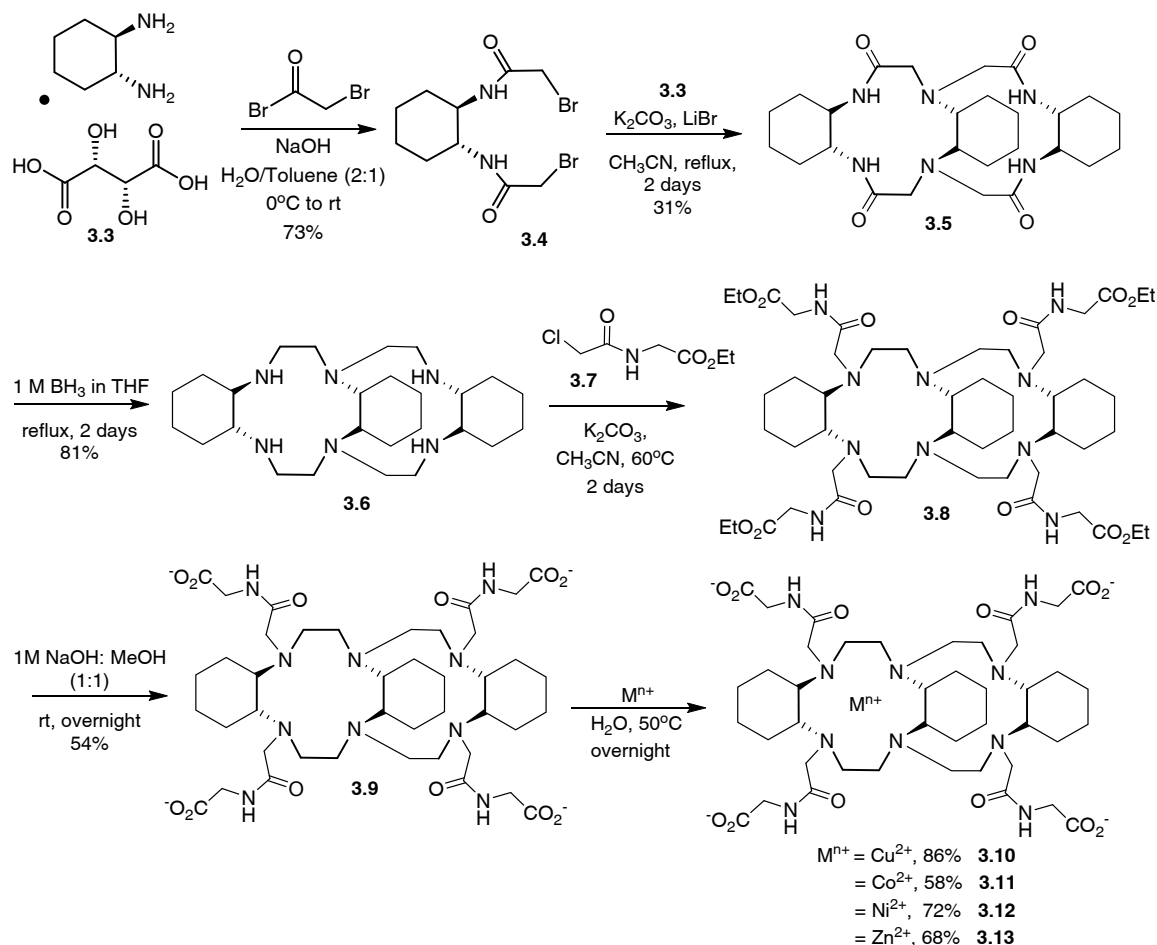
Scheme 3.1: Synthetic route to new target fully-rigidified complexes.

Scheme 3.1 shows the synthetic route taken to achieve the new target fully-rigidified ligand **3.9**. Initially, the free diamine of **3.3** and chloroacetyl chloride was used to form the bischloroacetamide analogue of **3.4** according to literature procedures.[10, 11] However, that product was not isolated in high yield. Several methods were attempted in order to increase the yield of the bischloro analogue of **3.4**. These included varying the solvents (dioxane, CH_2Cl_2, toluene), reaction times (6 - 24 hrs) and temperature (-20°C to rt). Additionally, both organic and inorganic bases were employed and the equivalents of the electrophile chloroacetyl chloride (2.2 - 5 eq) were adjusted. Furthermore, oxalyl chloride

as well as to bromoacteyl bromide were used to increase the strength of the electrophile. Unfortunately, none of these changes improved the yields of the desired bisacetamide.

We opted to use the diamine salt **3.3** that would allow for easier handling. However, it was insoluble in the solvents that were being used for the reaction and this likely had an effect on the low yields that were obtained. As a result, a Schotten-Baumann reaction using two phases of solvents was done following literature procedure.[12] These reaction conditions addressed the solubility issue. Using bromoacteyl bromide as the electrophile, the reaction proceeded very well and the product **3.4** was easily isolated in excellent yield.

Upon obtaining **3.4**, the "crab-like" condensation with the diamine salt **3.3** was performed. The reaction was monitored by UPLC and two products were observed in the chromatogram. One product corresponded to the fully-rigidified intermediate **3.1b** shown in Figure 3.3. The other product was the major one and had a mass with a higher molecular weight. The difference in mass between the two products indicated that the larger molecular weight product had an additional bisacetamide group. The identical reaction reported in the literature [9] made no mention of this larger by-product, although a yield of only 23% was reported for the smaller molecular weight product.

Several things were done in order to improve the yield of **3.1b**. These included varying the type of base and its equivalents (organic and inorganic; 2-10 eq), solvents (CH$_3$CN, anhydrous EtOH, DMF), reaction times (up to 4 days) and temperatures (rt to 80°C). These changes did not improve the yield of the desired product **3.1b**. Using varying equivalents of the bisbromo- or bischloroacetamide electrophile, as well as creating an *in situ* bisiodoacetamide also proved unsuccessful. The templating agent LiBr, was also used according to a procedure by Sharma *et al.*[13] Moderate to excellent yields were reported in the formation of macrocycles, which had been semi-rigidified with a benzene ring. Using templating agents is a well-established strategy for forming macrocycles such as crown ethers.[13]

Due to the afore-mentioned problems, it was decided that the diamine salt **3.3** be protected using TsCl. This protection step was initially challenging, giving low yields

after following reported procedures.[10, 11] It was decided that a Schotten-Baumann reaction, similar to that followed for the synthesizing the bisbromoactemide **3.4**, should be used to improve the yield. This approach was successful giving the ditosylated diamine analogue of **3.3** in excellent yield.

The cyclization reaction between the ditosylated product and **3.4** was attempted. Monitoring the reaction by UPLC showed the desired smaller molecular weight product as the major product, in addition to a by-product with a larger molecular weight. The mass difference between the two products corresponded to an additional ditosylated diamine. Initial attempts at separation and purification of this mixture were unsuccessful due to solubility issues. However, a solvent system of 10-30% acetone in CH_2Cl_2 was attempted and the desired and undesired products were isolated in low yields of roughly equal amounts.

The removal of the Ts protecting groups proved problematic. $LiAlH_4$ is a good reducing agents for amides and can also be used to remove Ts groups. As such, it was hoped that this reagent would allow for a simultaneous reduction and detosylation as demonstrated previously.[14] In this instance, neither reaction worked, with only the starting material being present even after heating to $50^{o}C$ for 2 days. Detosylation was also attempted fruitlessly with 0.1M SmI_2 in THF,[15] heating at $80^{o}C$ in 32% HBr in acetic acid [16] and using a $Ti(O^{i}Pr)_4/Me_3SiCl/Mg$ combination.[17] Refluxing in concentrated H_2SO_4 only partially worked, even after heating up to 5 days at $110^{o}C$. The UPLC chromatogram for that reaction showed a mixture containing starting material as well as partially and fully deprotected compounds. Although the mixture was separated, there were discrepancies observed during characterization of the desired product. The HR-ESI-MS showed the loss of the tosyl groups but the ^{1}H-NMR showed aromatic peaks in the spectrum. Attempts to further purify the compound were unsuccessful.

The difficulty associated with the removal of Ts groups has also been earlier demonstrated.[18] In light of the previous results indicating the need for a protecting group to increase the yield of the initial target intermediate, other protecting groups were investigated. The Ns group was used but the results were the same as that of the Ts

groups during both the cyclization and deprotection steps. The diamine salt **3.3** was protected with Boc groups but no reaction occurred during cyclization with the bisbromoacetamide. It was based on these exhaustive attempts to improve the yield of the initial fully-rigidified intermediate **3.1b**, that we modified our target complexes to those based on compound **3.9** (Scheme 3.1).

Following cyclization of **3.3** and **3.4**, the reaction mixture was purified by column chromatography and product **3.5** was obtained in 31% yield. Reduction of the amide groups of **3.5** was done using 1M BH_3 in THF and the desired compound **3.6** was isolated in good yield. Peralkylation of **3.6** with ethyl (2-chloroacetyl)glycinate **3.7**, followed by saponification, afforded the fully-rigidified ligand **3.9** in a moderate yield of 54% after two steps.

Metalations of ligand **3.9** with lanthanides of varying sizes (Eu^{3+}, Tm^{3+}, Yb^{3+}, Nd^{3+}, Gd^{3+}) were carried out as reported[9] but were unsuccessful. The conditions tried included varying the equivalents of the lanthanide salts, solvents, reaction times and temperatures. It was at this point speculated that the inner cavity of the fully-rigidified ligand **3.9** was too small to accommodate a lanthanide. The ionic radii of the lanthanides range from 1.143 Å for Ce^{3+} to 0.985 Å for Yb^{3+}.[19] It is likely that the chelate cavity is much smaller than this range. Within the context of PARACEST, the metals most commonly used are lanthanides but more recently, there have been reports of transition metals such as cobalt (Co^{2+}),[20, 21] nickel (Ni^{2+})[22] and iron (Fe^{2+}),[23-26] being used to generate CEST due to the amide protons.[27] As such, metalation with some of the smaller transition metals (Fe^{2+}, Co^{2+}, Ni^{2+}, Cu^{2+}, Zn^{2+} and Ga^{3+}) was performed. The metalation of ligand **3.9** was partially successful, giving complexes **3.10 - 3.13** in moderate to good yields. However, no metalation occurred with Fe^{2+} and Ga^{3+}. The ionic radii of these two metals are 0.62 Å and 0.92 Å for Ga^{3+} and Fe^{2+}, respectively. [19] In regards to Co^{2+}, Ni^{2+}, Cu^{2+} and Zn^{2+} that formed complexes, the ionic radii ranged from 0.69 Å for Ni^{2+} to 0.90 Å for both Co^{2+} and Zn^{2+}. It may therefore be inferred that the chelate cavity for the fully-rigidified ligand is greater than 0.62 Å but less than 0.92 Å. The preference of this ligand for transition metals over lanthanides showed the ability of the fully-rigidified ligand to discriminate based on size. This is perhaps due to the very rigid nature of the ligand and the associated

distortion it causes to the cavity. Additionally, the presence of the acetamide-glycinate arms may cause steric crowding which leads to further discrimination against the larger lanthanides. This may be confirmed or disproved by solid state analysis but unfortunately, attempts to grow crystals of the complexes were not successful.

Synthesis of semi-rigidified complexes
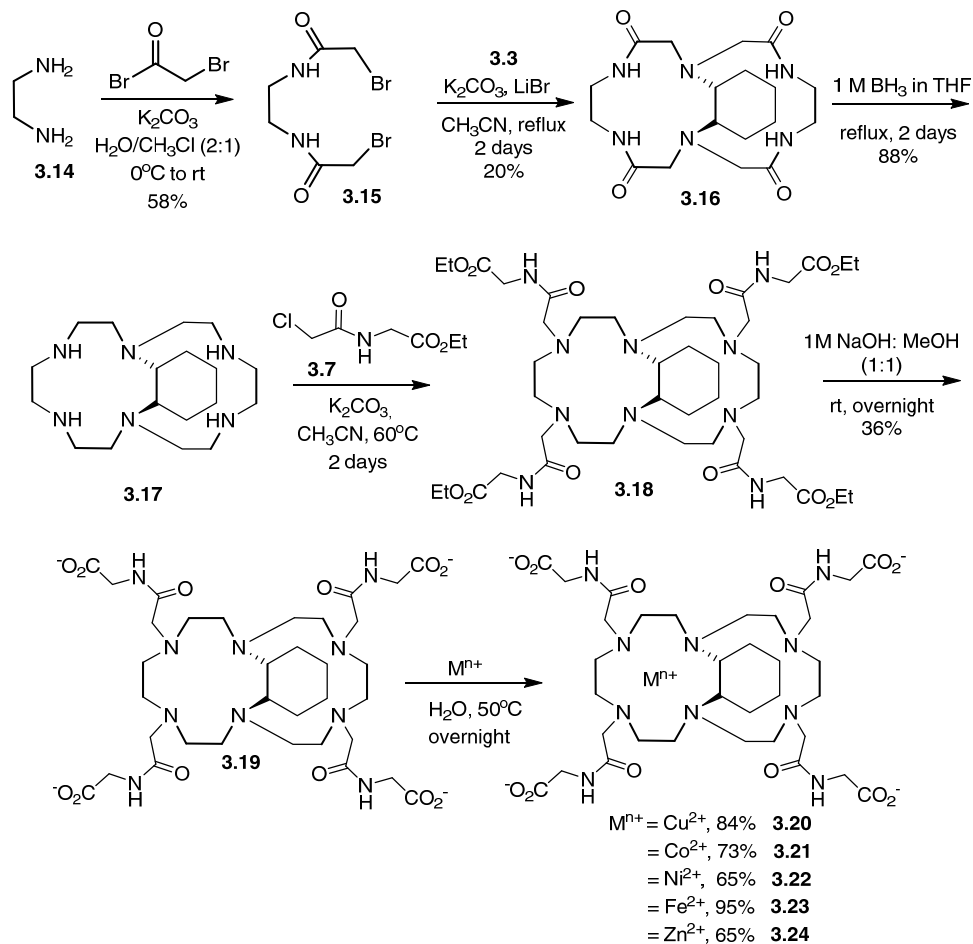
Scheme 3.2: Synthetic route to new target semi-rigidified complexes.

As previously mentioned, the lack of success in the lanthanide metalations of the fully-rigidified ligand **3.9** could be as a result of the very rigid nature of the ligand. For comparison purposes, the synthesis of the semi-rigidified counterpart that contained only one cyclohexyl ring was subsequently attempted. A similar synthetic pathway to that of

the fully-rigidified complex was followed starting with the bisbromoacetamide formation of ethylenediamine (Scheme 3.2). It was hoped that the reduction in rigidity would also lead to the formation of complexes of **3.2** shown in Figure 3.3. Unfortunately, similar problems as described earlier for the initial fully-rigidified complexes of **3.1** were faced. Hence, target **3.2** was altered to that based on the larger macrocycle **3.19**.

Using X-ray crystallography, characterization of the product **3.16** of the "crab-like" condensation reaction was possible. Crystals of **3.16** were obtained by dissolving the compound in $CHCl_3$ and layering with petroleum ether. After a series of similar steps earlier described, the semi-rigidified ligand **3.19** was obtained (Scheme 3.2).

The attempts to metalate the semi-rigidified ligand **3.19** with lanthanides also failed. In retrospect, it may be possible that the lanthanides partially coordinate to the fully-rigidified and semi-rigidified ligands at some point but falls out due to the distortion by the cyclohexyl groups appended to the backbone. Metalation with the same transition metals used for the fully-rigidified ligands was more successful and complexes **3.20** - **3.24** were obtained in good to excellent yields. Although the Ga^{3+} reaction was still unsuccessful, the metalation with Fe^{2+} worked. Based on this and previous observations, the fully-rigidified ligand is more selective than the semi-rigidified ligand. The reduced selectivity of the semi-rigidified ligand is likely due to the removal of a cyclohexyl group. Similar attempts to grow crystals for solid state analysis were not successful.

3.2.2 Crystal Structure

The crystal structure data of **3.16** is summarized in Table 3.1. The structure of **3.16** as shown in Figure 3.4a consists of three rings, the common points holding them together being two tertiary nitrogens, N1 and N4. This gives the molecule a "Y-like" appearance. One can image the cyclohexyl ring being the vertical stem and the other two nine-membered rings being the arms (Figure 3.4b). The cyclohexyl ring is not distorted and remains in its favourable chair conformation. The starting diamine salt **3.3** had an

absolute configuration of R, R-(+) (corresponding to C13 and C14). This configuration remained unchanged given that C13 and C14 are not sites of reactivity.
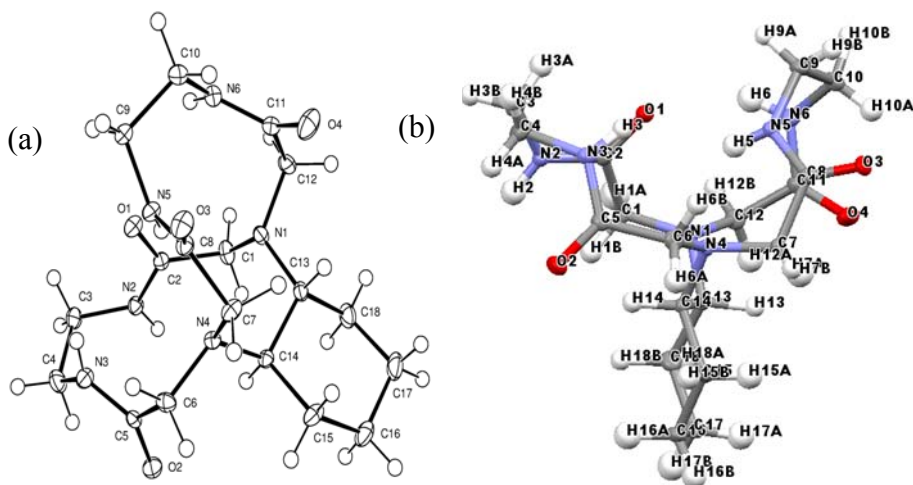
Figure 3.4: (a) ORTEP drawing of 3.16 showing naming and numbering scheme. Ellipsoids are at the 50% probability level and hydrogen atoms were drawn with arbitrary radii for clarity. Water of hydration omitted for clarity. (b) Ball and stick representation of 3.16, showing its Y-like shape.

The interesting feature of ligand **3.16** is the tertiary N1 and N4 that originated from the cyclohexyl diamine. The expected bond length for each N-C single bond in tertiary amines is 1.469 Å.[28] The three bonds to N1 consisted of two bonds (new bond N1-C12 and original bond N1-C13) that were close to the expected value of 1.469 Å (average length = 1.465 Å). The other new bond N1-C7 was much shorter by 0.021 Å (Table 3.2). On the other hand, two of the three bonds to N4 consisted of the shorter new N4-C7 bond (ΔÅ = 0.009) and the original N4-C14 bond (ΔÅ = 0.01) being the longest. Surprisingly, the bond length of N4-C14 is identical to the N-C bond of endo δ-lactams of the type C^1-N(-C^1)-C=O (1.479 Å).[28] The third bond N4-C6 (new) was identical to the expected value of 1.469 Å. The difference in bond length between the original bonds N1-C13 and N4-C14 may be due to the difference in the spatial orientation of these bonds. Each bond is pointing in opposite directions and the corresponding nitrogen atoms may require

different degrees of lengthening in order to each form two additional N-C bonds. Considering that the N4-C14 bond was the longest, this likely had to undergo the most change.

Table 3.1: Crystal data and structure refinements for 3.16.

Formula	$C_{18}H_{32}N_6O_5$
Formula Weight (*g/mol*)	412.49
Crystal Dimensions (*mm*)	0.325 × 0.320 × 0.122
Crystal Color and Habit	colourless prism
Crystal System	orthorhombic
Space Group	*P 2_1 2_1 2_1*
Temperature, K	110
Unit cell dimensions	
a, Å	9.504(2)
b, Å	14.103(3)
c, Å	14.726(4)
α,°	90
β,°	90
γ,°	90
V, Å^3	1973.9(8)
Z	4
F(000)	888
ρ (*g/cm*)	1.388
λ, Å, (MoKa)	0.71073
μ, (*cm^{-1}*)	0.103
Number of reflections to determine final unit cell	9608
Number of reflections measured	174049
Unique reflections measured	13523
R_1	0.0353
wR_2	0.0871
R_1 (all data)	0.0449
wR_2 (all data)	0.0916
GOF	1.066
Min & Max peak heights on final DF Map (e^-/Å)	-0.205, 0.473

Unpredictably, only one bond angle (C7-N4-C6) involving either of the tertiary N1 or N4 corresponded to a tetrahedral geometry for sp^3 nitrogens (Table 3.3). The other bond angles are greater than 109.5^o and range from 113° - 117°, thus falling between that of an sp^3 (109.5^o) and sp^2 (120°) nitrogen. It is possible that while in solution state, nitrogen inversion occurred, leading to the interconversion from tetrahedral to trigonal planar and

back to tetrahedral geometry. This interconversion may be possible since the ring systems involving N1 and N4 are large ring systems with less strain. However, upon forming crystals, a hybrid developed, thereby leading to bond angles between the two geometries.

Table 3.2: Selected bond lengths (Å) for 3.16.

N1-C1	1.4482(10)
N1-C13	1.4646(10)
N1-C12	1.4647(10)
C6-N4	1.4680(10)
N4-C7	1.4602(10)
N4-C14	1.4788(10)

Table 3.3: Selected bond angles (^{o}) for 3.16.

C1-N1-C13	117.07(7)	N4-C7-C8	113.11(6)
C1-N1-C12	116.77(7)	N4-C7-H7A	113.1(9)
C13-N1-C12	114.33(6)	N4-C7-H7B	108.3(10)
N1-C1-C2	112.67(7)	N1-C12-C11	108.55(6)
N1-C1-H1A	109.6(12)	N1-C12-H12A	113.6(11)
N1-C1-H1B	111.4(9)	N1-C12-H12B	111.2(10)
N4-C6-C5	112.68(6)	N1-C13-C18	114.15(7)
N4-C6-H6A	111.7(11)	N1-C13-C14	113.98(6)
N4-C6-H6B	107.1(9)	N1-C13-H13	103.9(9)
C7-N4-C6	108.85(6)	N4-C14-C15	113.18(6)
C7-N4-C14	113.84(6)	N4-C14-C13	112.30(6)
C6-N4-C14	113.82(6)	N4-C14-H14	104.6(9)

3.2.3 Magnetic Properties

Magnetic moments

The magnetic moments for the Co^{2+} (**3.11**) and Ni^{2+} (**3.12**) fully-rigidified complexes were determined and found to be 3.93 and 2.80 μ_B, respectively. These observations are in agreement with that of high spin Co^{2+} and Ni^{2+} complexes.[29] These values indicated that the coordination number (CN) for both complexes is six but due to distortion, the geometry is pseudo-octahedral rather than octahedral.[29]

The magnetic moments for the Co^{2+} (**3.21**) and Ni^{2+} (**3.22**) semi-rigidified complexes were 4.81 and 3.52 μ_B, respectively, which are in agreement with that of high spin Co^{2+}

and Ni^{2+}complexes.[29] The value reported for the Ni^{2+} complex (**3.22**) indicated that the coordination geometry is pseudo-tetrahedral rather than tetrahedral due to distortion (CN = 4).[29] Similarly, distortion of the Co^{2+} complex (**3.21**), led to a pseudo-octahedral geometry (CN = 6).[29]

A value of 2.49 μ_B for Fe^{2+} (**3.23**) indicated a low spin compound which could be either Fe^{2+} or Fe^{3+}, thus this value is considered to be anomalous.[29] However, there are a few things that should be considered in order to establish a reasonable oxidation state of iron in this complex. Firstly, if a fully-rigidified complex containing iron had been made, the oxidation state of iron and thus the ionic radii would be the same in both types of rigidified complexes. Secondly, octahedral Fe^{3+} has a smaller ionic radius (low spin = 0.55 Å and high spin = 0.645 Å) than Fe^{2+}, Ni^{2+} and Co^{2+} and metalation with iron did not occur with the fully-rigidified macrocycle **3.9**. Thirdly, the ionic radius of high spin Fe^{3+} is similar to that of Ga^{3+} (0.620 Å) which did not metalate either the semi-rigidified or fully-rigidified ligands, meaning that these metals are too small for the cavities of the ligands. Hence, it can be inferred that iron in the semi-rigidified complex must be the larger low spin Fe^{2+}, which was too large for the fully-rigidified ligand.

CEST studies

CEST data was collected at pH 6, 7 and 8 at T = 25°C and 37°C for the Co^{2+} and Ni^{2+} fully-rigidified complexes **3.11** and **3.12** as well as the Co^{2+}, Ni^{2+} and Fe^{2+} semi-rigidified complexes **3.21**, **3.22** and **3.23** (10 mM, 9:1 D_2O/H_2O). Unfortunately, no CEST signals were observed. Similarly, no signals were observed when CEST experiments of the complexes at 20 mM in pH 7 phosphate buffer (0.02 M) at 37°C were performed.

The most likely reason for the absence of an amide CEST signal is that the exchange rate of the amide protons may be outside the required regime for a CEST effect to be observed. This faster exchange rate could be due to the very rigid nature of the ligands, considering that Co^{2+}, Ni^{2+} and Fe^{2+} in simpler ligands such as DOTAM have shown amide CEST signals.[21, 22] While the coordination geometry of the transition metal in the complexes may also negatively impact the CEST signal generation, the exact geometries are unknown. The deviation from the lanthanide-containing DOTA-like complexes, as

represented in the original target complex structures (Figure 3.1), means that the definition of SAP and TSAP coordination geometries (nine-coordinate with respect to lanthanide ions) cannot be used in context with these highly rigidified macrocycles containing transition metals. Based on the results of the magnetic moments of the transition metals, their geometries may be tetrahedral (four-coordinate) and or octahedral (six-coordinate), with some distortions. The transition metals used to form these complexes are therefore coordinatively saturated and unlikely to form three additional coordinating bonds. Therefore, it cannot be reasonably concluded that the lack of a CEST signal is also due to the formation of the unwanted TSAP isomer, which in DOTA-based complexes, have faster exchange rates of exchangeable protons.

Relaxivity studies

The relaxivity properties of the Co^{2+} (**3.11**) and Ni^{2+} (**3.12**) fully-rigidified complexes as well as the Co^{2+} (**3.21**), Ni^{2+} (**3.22**) and Fe^{2+} (**3.23**) semi-rigidified complexes were determined and the results are shown in the Table 3.4. The low r_1 values of the complexes are comparable to those reported for macrocyclic complexes involving these metals. [21, 22, 24] Based on these values, it is likely that there is no water molecule bound to the metal center. The variation in r_1 values of the complexes were not based on the type of ligands, but rather on the type of metal, with the Ni^{2+} complexes having the highest values.

Table 3.4: r_1 and r_2 values of agents 3.11 - 3.12 and 3.21 - 3.23 at 37°C and pH 7.00 ± 0.03.

	M^{n+}	r_1 (mM^{-1}s^{-1})	r_2 (mM^{-1}s^{-1})	r_2/r_1
Fully-rigidified	Co^{2+} (**3.11**)	0.052	0.262	5.04
	Ni^{2+} (**3.12**)	0.268	0.345	0.507
Semi-rigidified	Co^{2+} (**3.21**)	0.081	0.463	5.72
	Ni^{2+} (**3.22**)	0.246	0.365	1.48
	Fe^{2+} (**3.23**)	0.097	3.17	32.7

On the other hand, while there was no significant variation in the r_2 values of Ni^{2+} complexes **3.12** and **3.22**, a difference was seen in the values for the Co^{2+} complexes **3.11**

and **3.21**, with the semi-rigidified complex having an r_2 value that is more than one and a half times that of the fully-rigidified complex. With the exception of the lone Fe^{2+} complex, these r_2 values were comparable to those previously reported. [21, 22]

The r_2 value of 3.17 $mM^{-1}s^{-1}$ for the Fe^{2+} complex **3.23** was the highest of all the complexes and higher than that reported previously for other Fe^{2+} macrocyclic complexes.[24] Nevertheless, in comparison to superparamagnetic iron oxide nanoparticles (SPIONs) that have r_2 values greater than 70 $mM^{-1}s^{-1}$ at 60 MHz,[30] the r_2 value of 3.17 $mM^{-1}s^{-1}$ for the Fe^{2+} complex **3.23** is obviously much lower at 400 MHz.

The r_2/r_1 ratio for both Co^{2+} complexes **3.11** and **3.21** are similar, while that of the semi-rigidified Ni^{2+} complex **3.22** is almost three -fold higher than the fully-rigidified Ni^{2+} complex **3.12**. The r_2/r_1 ratio of Fe^{2+}complex **3.23** is the highest of all the complexes described here as well as that of reported for various SPIONs such as TMAOH (tetramethylammonium hydroxide) SPION and Resovist®.[30] This recorded high value shows the preference of negative contrast enhancement (darkening effect), thus indicating that the interference from the T_1 effect (lightening effect) is small.[30]

3.2.4 UV Studies

Stability studies

Stability studies of the complexes (1 mM in H_2O) at pH 2-11 were carried out spectrophotometrically in order to further characterize the complexes made. At pH 7, the λ_{max} for the fully-rigidified Cu^{2+} complex **3.10** (Figure 3.5a) and Co^{2+} complex **3.11** (Figure 3.5c) was 584 nm and 525 nm, respectively. Although the Ni^{2+} complex **3.12** was a dark green solid, in solution it was almost colourless, making it difficult to obtain its λ_{max}. No stability studies were done with the Zn^{2+} complex **3.13** since it was naturally a cream -coloured compound.

The absorbances of complexes **3.10** and **3.11** at acidic pH were low, indicating possible demetalation. However, at basic pH a hyperchromic shift was observed, possibly

indicating increased stability. The solutions of **3.10** and **3.11** at pH 2 and 11 were left undisturbed for a week at room temperature and their UV absorbance re-measured. The Cu^{2+} complex **3.10** (Figure 3.5b) and Co^{2+} complex **3.11** (Figure 3.5d) showed no significant difference in absorbances at lower pH, but there was a slight increase in absorbance for the complexes at pH 11.
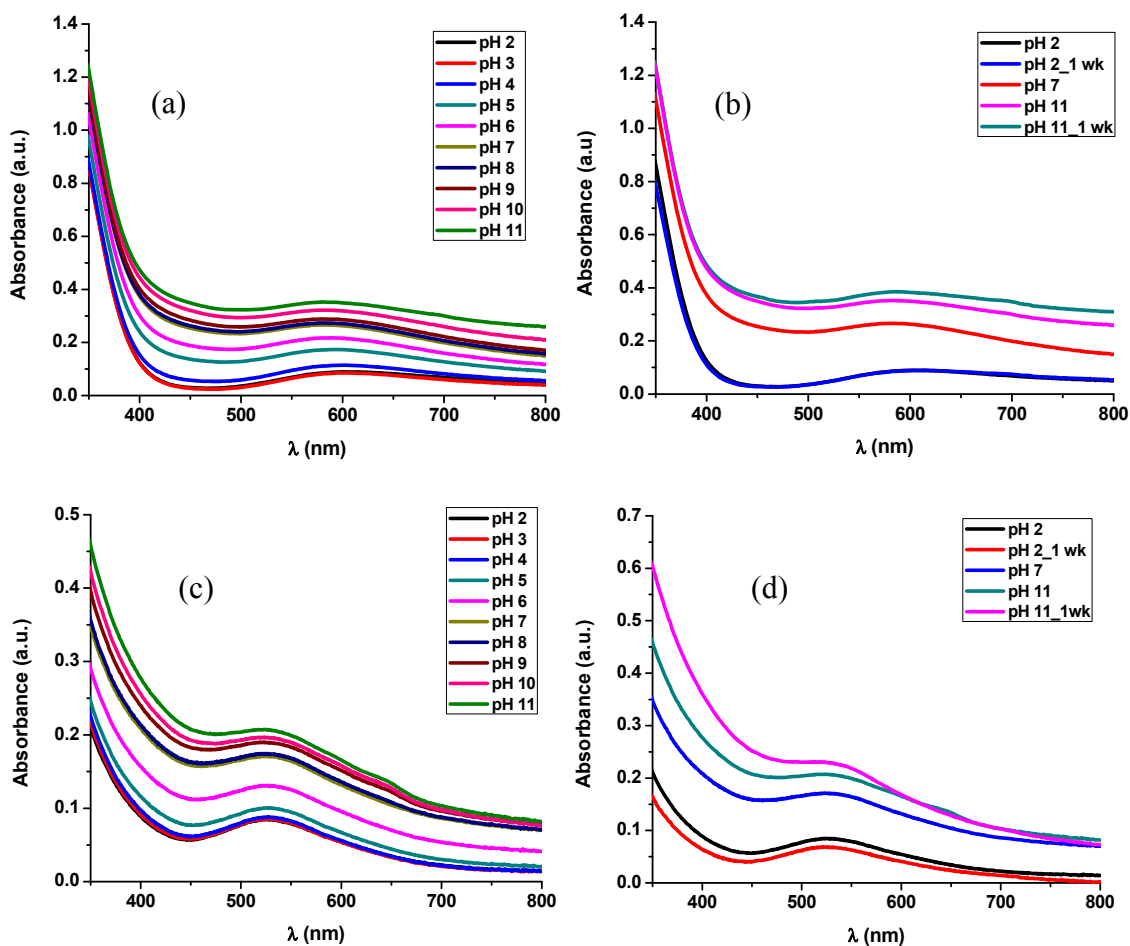
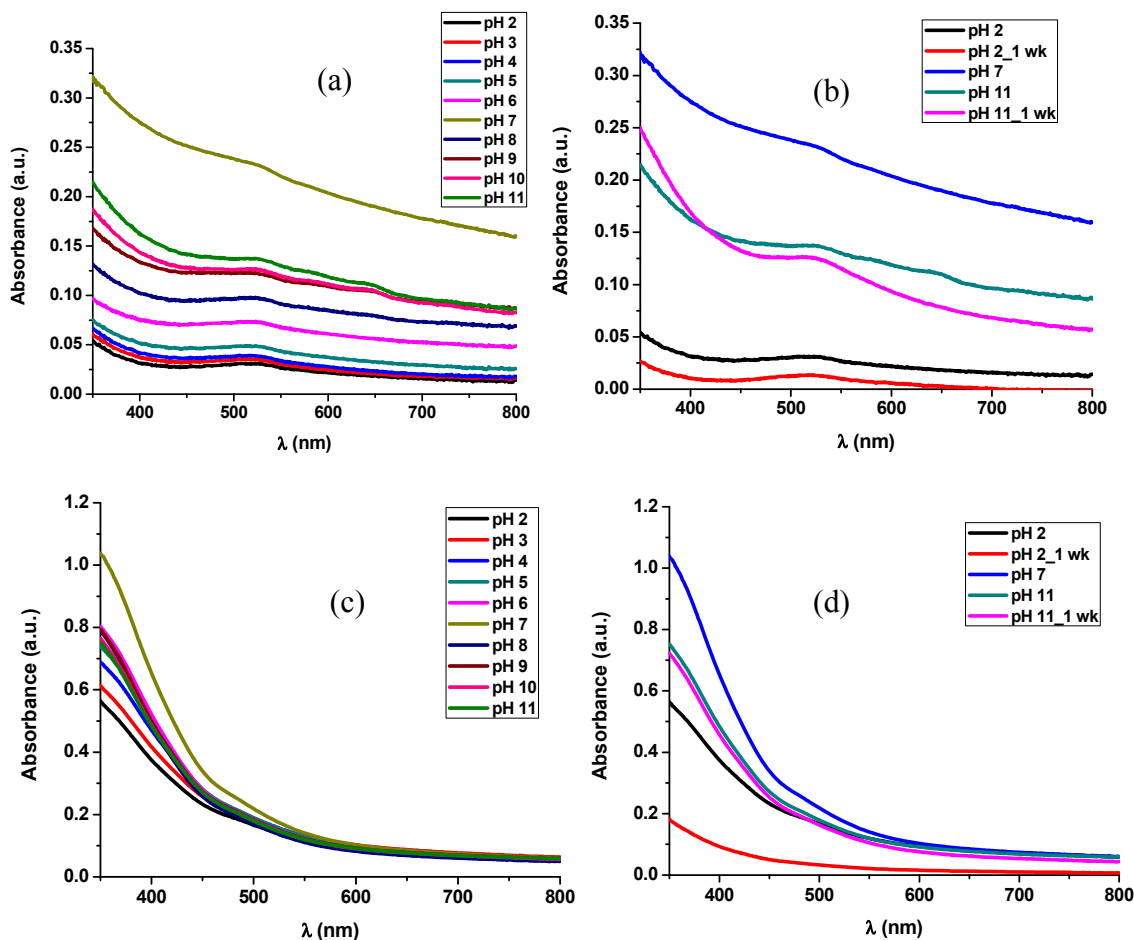

Figure 3.5: Absorption spectra of fully-rigidified complexes Cu^{2+} 3.10 (a) and (b) and Co^{2+} 3.11 (c) and (d). Figures (a) and (c) are at pH 2 - 11 and (b) and (d) are at pH 2 and 11 taken 1 week later. Each complex concentration was 1 mM in H_2O at $25^{o}C$.
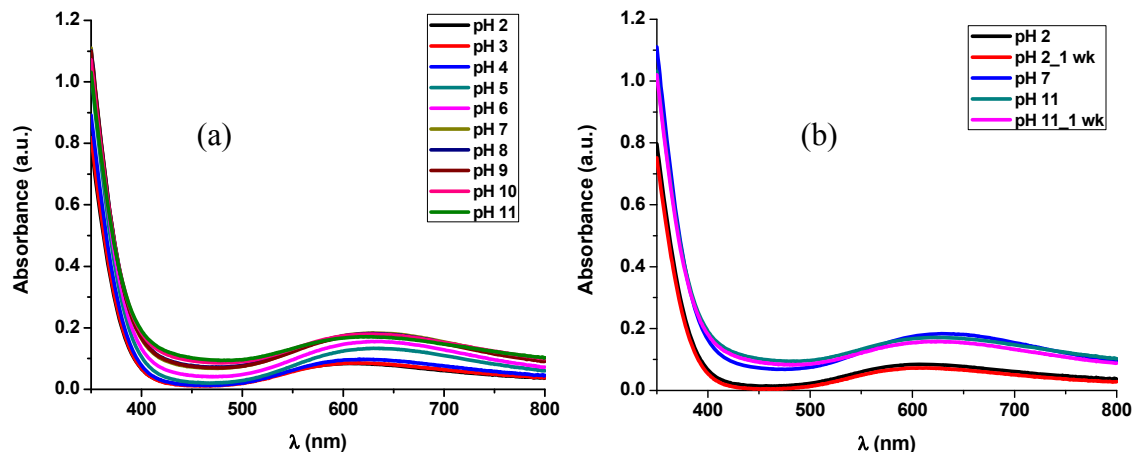
Figure 3.6: Absorption spectra of semi-rigidified complex Cu^{2+} 3.20 (a) at pH 2 - 11 and (b) pH 2 and 11 taken 1 week later Each complex concentration was 1 mM in H$_2$O at 25°C.

Similar stability studies at pH 2-11 were carried out for the semi-rigidified complexes **3.20**, **3.21** and **3.23**. Likewise, no stability studies were done with the Ni^{2+} **3.22** and Zn^{2+} **3.24** complexes for the reasons mentioned earlier. At pH 7, the λ_{max} in H$_2$O occurred at 637 nm for the Cu^{2+} complex **3.20** (Figure 3.6a), 525 nm for the Co^{2+} complex **3.21** (Figure 3.7a) and 473 nm for the Fe^{2+} complex **3.23** (Figure 3.7c). The Cu^{2+} complex **3.20** seemed to be more stable at pH 6 or greater since a slight hyperchromic shift was observed at those pH values. Both Co^{2+} **3.21** and the Fe^{2+} **3.23** complexes had their highest absorbance at pH 7, indicating higher stability.

The absorbances at pH 2 and pH 11 were re-measured one week later during which the solutions were left at room temperature. There was no difference in absorbance for the Cu^{2+} complex **3.20** (Figure 3.6b) and only a slight difference in the absorption spectra of the Co^{2+} complex **3.21** (Figure 3.7b) at those pH values. The Fe^{2+} complex **3.23** (Figure 3.7d) had a lower absorbance one week later at pH 2 but there was no difference in absorbance of the pH 11 values.

Figure 3.7: Absorption spectra of semi-rigidified complexes Co^{2+} 3.21 (a) and (b) and Fe^{2+} 3.23 (c) and (d). Figures (a) and (c) are at pH 2 - 11 and (b) and (d) are at pH 2 and 11 taken 1 week later. Each complex concentration was 1 mM in H$_2$O at 25°C.

The aqua complexes of Cu^{2+}, Fe^{2+}, Co^{2+} and Ni^{2+} have weak absorbances occurring in the near infrared region.[31] This may account for the small absorbances due to d-d transitions, seen in the aqueous solutions of the fully-rigidified and semi-rigidified complexes at 800 nm. That feature is comparable to that of Cu^{2+} complexes of tetraaza macrocycles such as DOTA[32] and DOTAM[33]. That feature is not restricted to DOTA or DOTAM. In Cu^{2+} polyaminocarboxylic acids such as ethylenediaminetetraacetic acid (EDTA), this has also been observed.[34] Although these complexes are more rigid in nature, it is not surprising

that they possess similar absorption characteristics as that of the unrigidified macrocycles, seeing that no additional chromophores were incorporated in the structures.

Ligand exchange studies
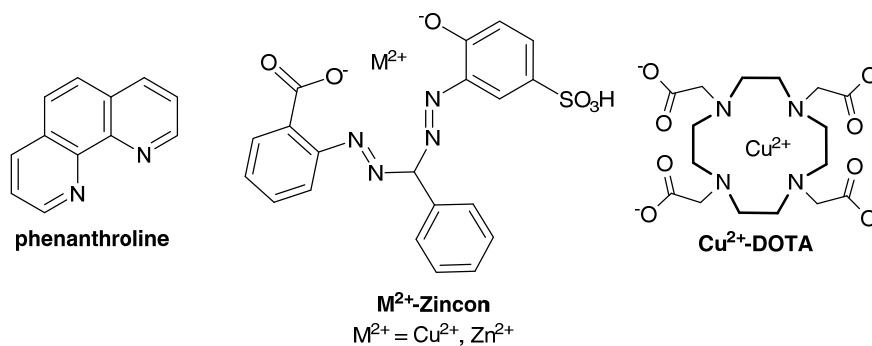
**Figure 3.8: Ligands and complexes used in the ligand exchange study.**

UV ligand exchange studies were attempted in order to determine the strength of binding of the ligands **3.9** and **3.19** to the metals. The first choice was phenanthroline (Figure 3.8) because it has a strong absorbance in both its free and complexed states. Figure 3.9a shows that the Cu^{2+}-phenanthroline complex had a λ_{max} of 273 nm while the free ligand had a λ_{max} of 262 nm in 1:1 H_2O/pH 7 phosphate buffer. The titration was carried out using the semi-rigidified Cu^{2+} complex **3.20**. Regrettably, there was an overlap of the peaks at 273 nm and 262 nm, which made it difficult to estimate how much Cu^{2+} was actually being released from the semi-rigidified ligand and being bound by phenanthroline. Additionally, with less than 0.5 µM of phenanthroline added, there was shift in λ_{max} from 273 nm to 262 nm.
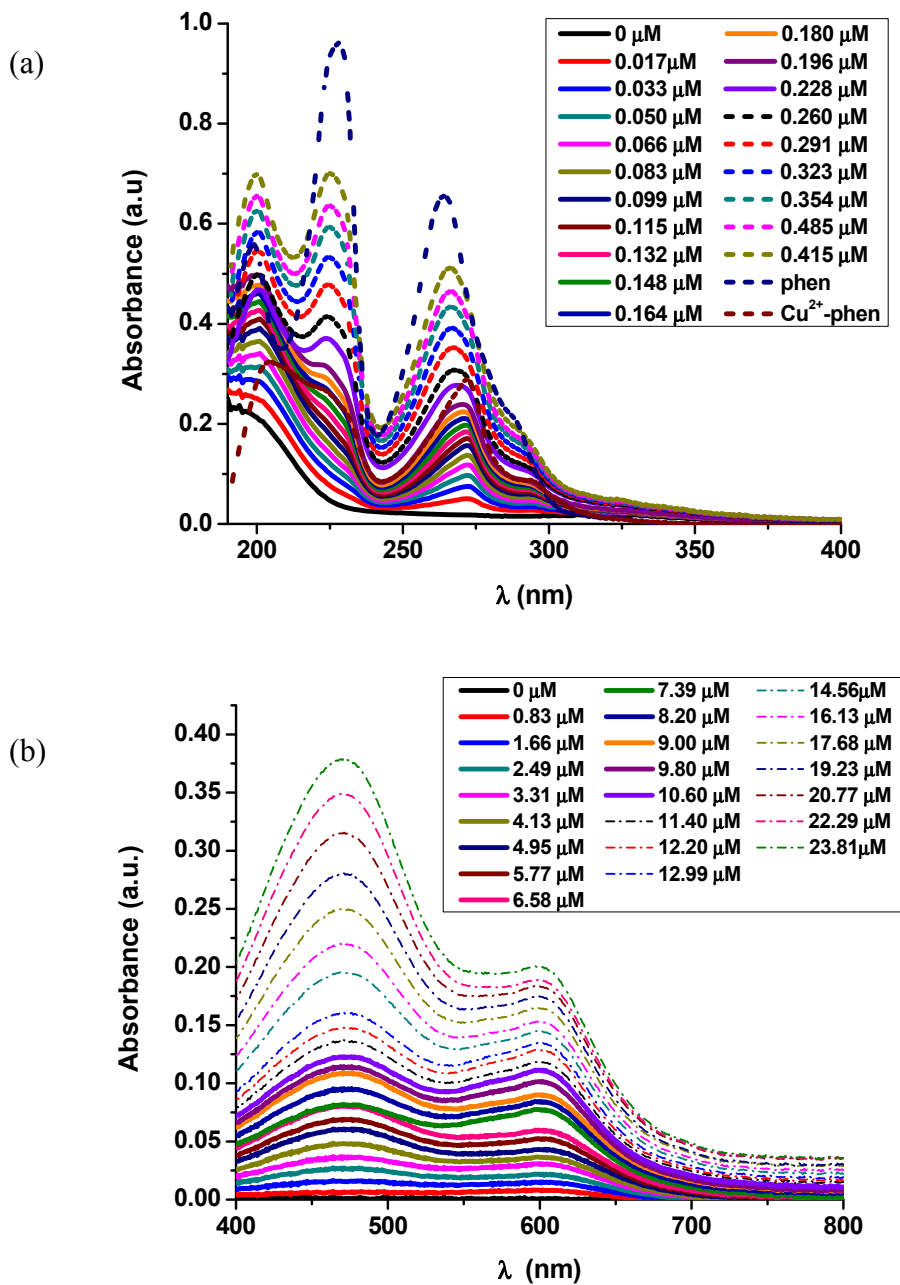
Figure 3.9: Titration absorption spectra at 25°C of semi-rigidified complexes (a) Cu²⁺ complex 3.20 (10 μM in 1 : 1 pH 7 (0.02 M) phosphate buffer/H₂O) with phenanthroline (500 μM in 10 μM Cu²⁺ complex 3.20 solution) and (b) Zn²⁺ complex 3.24 (10 μM in 1 : 1 pH 7 (0.02 M) phosphate buffer/H₂O) with Zincon (500 μM in 10 μM Zn²⁺ complex 3.24 solution).

The second choice of ligand for the afore-mentioned purpose was Zincon (Figure 3.8). Ligand exchange experiments were carried out with Zincon and the semi-rigidified Zn^{2+} complex **3.24**. Zincon binds strongly to Zn^{2+} (log β = 4.19, K_d = 64.44 μM).[35] The complex had a λ_{max} at 600 nm while the free Zincon had its λ_{max} at 470 nm in 1:1 pH 7 phosphate buffer/H_2O (Figure 3.9b). The λ_{max} of the Zn^{2+}-Zincon complex and the free Zincon has been observed at 620 and 488 nm, respectively, in borate buffer.[35] However, attempts to derive a K_d for complex **3.24** were unsuccessful, even although $\Delta\lambda_{max}$ was 130 nm. Addition of up to 25 μM addition of Zincon (2.5X), caused both peak absorbances at 470 and 600 nm to increase simultaneously, which is not an ideal response. The reason for the increase in absorbances for both peaks was not investigated.
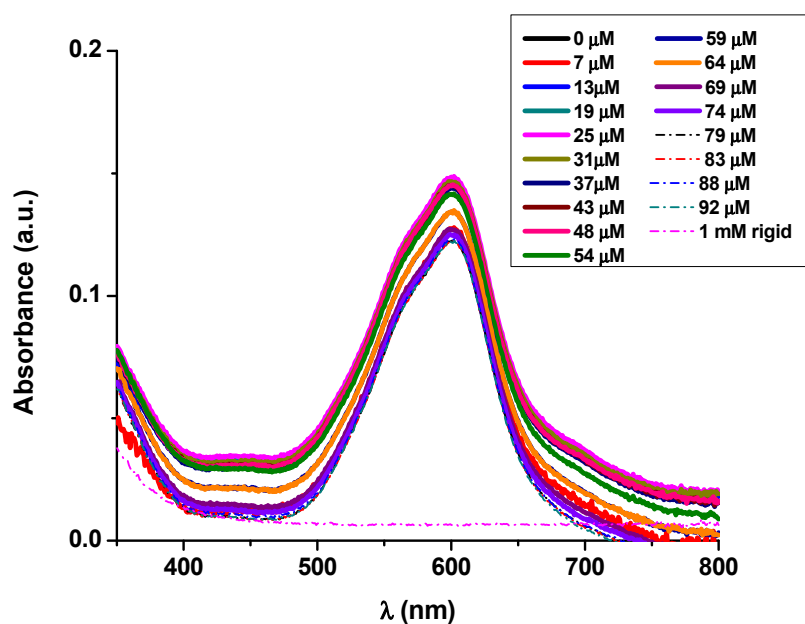
Figure 3.10: Titration absorption spectra of Cu^{2+}-Zincon complex (10 μM in 1 : 1 pH 8 (0.02 M) phosphate buffer/H_2O) with fully-rigidified ligand (500 μM in 10 μM Cu^{2+}-Zincon complex solution) at 25°C.

The Cu^{2+}-Zincon complex (Figure 3.8) was titrated with the fully-rigidified ligand **3.9**. The absorbance was measured for up to 95 μM of the ligand. As can be seen in Figure 3.10, there is no absorbance peak corresponding to the free Zincon. This reinforces that the Cu^{2+}-Zincon complex is a stable one (log β = 4.39, K_d = 40.01 μM).[35] Heating at 60°C

for overnight did not lead to formation of the Cu^{2+}-fully-rigidified complex **3.10**. The negative absorbances observed at longer wavelengths when the concentration of fully-rigidified ligand was increased, may be attributed to the formation of aggregates.
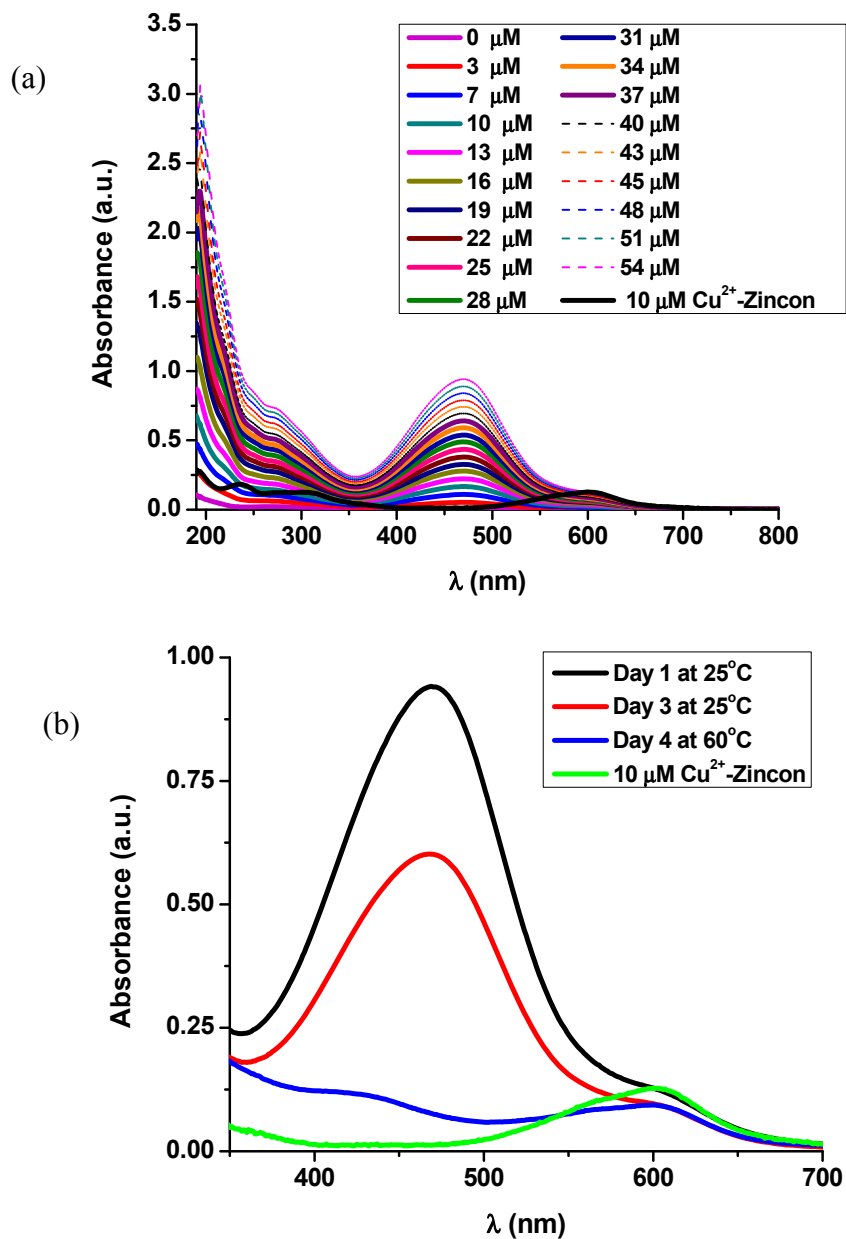
Figure 3.11: Absorption spectra of ligand exchange experiment with (a) Cu^{2+}-DOTA and Zincon at Cu^{2+}-DOTA complex (10 μM in 1 : 1 pH 8 (0.02 M) phosphate buffer/H_2O) with Zincon (500 μM in 10 μM Cu^{2+}-DOTA complex solution) at 25^oC and (b) Same solution at 60^oC, four days later.

The Cu^{2+}-DOTA complex (log β = 22.25)[36] was similarly titrated with Zincon. The UV spectrum showed that no exchange occurred between the two as evidenced by the absorption at ~488 nm which correlates to free Zincon (Figure 3.11a). The formation of the Cu^{2+}-Zincon complex was completed only upon overnight heating of the mixture at 60°C (Figure 3.11b).

Cu^{2+}-DOTA complex and fully-rigidified ligand **3.9** were reacted together at room temperature for overnight and the ligand exchange was monitored by UPLC. The chromatogram showed that no exchange occurred (data not shown). A similar experiment was done with the semi-rigidified ligand **3.19** giving the same results. Overnight heating at 60°C also did not lead to the formation of either the Cu^{2+}-fully-rigidified or semi-rigidified complexes.

Despite the fact that we were unable to quantitatively determine the stability of the fully-rigidified or semi-rigidified complexes, the afore-mentioned results of ligand exchange indicates that the stability of these complexes is in the order of semi-rigidified ligand ≈ fully-rigidified ligand < Zincon < DOTA.

3.3 Conclusion

The synthesis of the initial target lanthanide complexes containing one and two cyclohexyl rings appended to the backbone of DOTAM was met with several challenges. Based on the low yields obtained for these initially desired ligands during cyclization, the targets were modified to that of the very interesting and larger molecular weight by-products. These semi-rigidified and fully-rigidified ligands possessed a most unusual structure, as indicated by the X-ray crystal data of the intermediate semi-rigidified ligand. This intermediate ligand had an additional bisacetamide group attached, thereby forming a Y-shaped structure with two tertiary amines.

The new target ligands were observed to be selective towards the smaller transition metals, rather than the desired larger lanthanides. Within these two types of ligands, the fully-rigidified one was even more discriminating, since it did not form a complex with

Fe^{2+}. This observation of selectivity towards the transition metals indicated the smaller cavity sizes of these ligands and this may be useful for scavenging metals of similar sizes.

The research showed that a CEST signal cannot be generated for the Ni^{2+}, Co^{2+} and Fe^{2+} complexes under the different pH conditions and solvent mixtures used. At this time, it may be simply inferred that the lack of a CEST signal was due to the rigid ligand design that caused the exchange rate to fall outside of the desired regime for CEST. Considering that these modified complexes are fused structures that have severely deviated from DOTA-based ones, the definition of SAP and TSAP cannot be applied to these structures. While coordination geometry may play a role, it cannot be construed that the absence of a CEST signal is due to the exclusive formation the TSAP isomer, which is known to possess a fast exchange rate for the metal bound water protons. In regards to T_1 and T_2 relaxivities, all the complexes gave low values but these were comparable to published results. However, an exception was seen in the semi-rigidified Fe^{2+} complex, which had a much higher T_2 relaxivity.

The attempt to assess the selectivities of the ligands by performing exchange experiments was met with difficulty. Nonetheless, it was possible to conclude qualitatively that both types of rigidified ligands synthesized are weak chelators as compared to un-rigidified ones such as DOTA.

The information gained here has indicated that the degree of rigidity in DOTAM-like structures is important in binding of lanthanides as well as transition metals. More rigidified structures led to better selectivity but the rigidity negatively affected the generation of a CEST signal. It is still crucial to gain information regarding amide exchange and accordingly, the amide CEST effect in a SAP isomer. Hence, towards that goal, it may be necessary to reduce the level of rigidity in the target ligands. This may provide an easier way of driving the formation of the preferred SAP isomer, which is a promising advantage for good CEST signal generation.

# 3.4 Supplemental Information

3.4.1 General Experimental

General synthetic details can be found in Appendix 1.

CEST and Relaxivity Experiments

CEST spectra were acquired on a 600 MHz vertical bore NMR spectrometer, using a 15 μT, 2 s continuous wave presaturation pulse at offset frequencies ranging from -110 to 110 ppm in steps of 1 ppm at a concentration of 10 mM in D_2O/H_2O (9:1) at pH 6.00 ± 0.03, 7.00 ± 0.03 and 8.00 ± 0.03; 37 °C and at a concentration of 20 mM in pH 7 phosphate buffer; 37 °C. T_1 and T_2 relaxation time constant measurements were made on a 400 MHz vertical bore NMR spectrometer. T_1 relaxation time constant measurements were made for four different concentrations (1, 2, 4, 8 mM) of CA in H_2O, using an inversion recovery sequence (20 inversion times in the range of 0.1 s - 20 s) with a minimum $d_1 = 5T_1$ to ensure full recovery, pH 7.00 ± 0.03 and 37 °C. T_2 relaxation time constant measurements were made for four different concentrations (1, 2, 4, 8 mM) of CA in H_2O, using a CPMG pulse sequence (15 inversion times in the range of 0.001 s - 7 s) with a minimum $d_1 = 5T_1$ to ensure full recovery, pH 7.00 ± 0.03 and 37 °C. VNMRJ® software of the spectrometer automatically gave the T_1 and T_2 relaxation times from which the corresponding relaxation rates were calculated. The relaxivities were then determined from the slope of the linear regression fitting of the rates versus concentration in Microsoft Excel.

3.4.2 Synthetic Procedures

General procedure for cyclization. A solution of bisbromoacetamide, K_2CO_3 and LiBr were suspended in CH_3CN and refluxed for 1 h and (1R,2R)-cyclohexane-1,2-diamine tartrate in CH_3CN was added and stirring was continued for 36 h. The reaction mixture was filtered and the filtrate concentrated. The crude was purified by column chromatography (silica gel; $CH_2Cl_2/MeOH/NH_4OH$ (90:10:1); charring with $KMnO_4$).
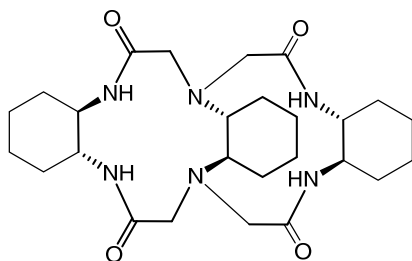
(4aR,8R,11aR,15aR,19R,22aR,23R,24R)-hexadecahydro-8,19-[1,2]benzenodibenzo[b,k][1,4,7,10,13,16]hexaazacyclooctadecine-6,10,17,21(7H,9H,18H,20H)-tetraone (3.5). Bisbromoacetamide (**3.4**) (0.889 g, 2.5 mmol), K$_2$CO$_3$ (2.07 g, 15 mmol) and LiBr (0.434 g, 5 mmol), (1R, 2R)-cyclohexane-1, 2-diamine tartrate **3.3** (0.661 g, 2.5 mmol) and CH$_3$CN (v$_{tot}$ = 80 mL). Title compound was obtained as a white solid (0.394 g, 31%). ^{1}H NMR (400 MHz ,CDCl$_3$): δ 8.67 (2H, d, *J* = 10Hz), 6.70 (2H, d), 3.86-3.64 (4H, m), 3.51-3.44 (3H, m), 3.16-3.09 (5H, m), 2.46-2.40 (2H, m), 2.01-1.93 (4H, m), 1.82-1.66 (8H, m), 1.56-1.29 (10H, m), 1.13-1.05 (2H, m). ^{13}C NMR (100 MHz, CDCl$_3$): δ 174.51, 174.13, 66.74, 62.85, 56.12, 55.00, 53.55, 31.98, 25.53, 24.89, 24.75. ESI-TOF *m/z* calcd for C$_{26}$H$_{43}$N$_6$O$_4$ (M + H)$^+$, calculated 503.3346, found 503.3350.
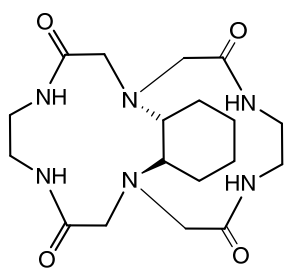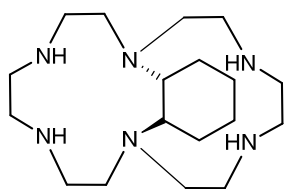

(1R,10R,10aR,14aR)-decahydro-1,10-(ethanoiminoethanoiminoethano)benzo[b][1,4,7,10]tetraazacyclododecine-3,8,16,21(2H,9H)-tetraone (3.16). Bisbromoacetamide **3.15** (1.755 g, 5.81 mmol), K$_2$CO$_3$ (3.9 g, 28.24 mmol) and LiBr (0.434 g, 5 mmol), (1R,2R)-cyclohexane-1,2-diamine tartrate **3.3** (1.536 g, 5.81 mmol) and CH$_3$CN (v$_{tot}$ = 170 mL). Recrystallization from petroleum ether-CHCl$_3$ gave the title compound as colourless crystals (0.529 g, 23%). ^{1}H NMR (400 MHz ,CDCl$_3$): δ 7.51 (2H, d) 7.17 (2H, d, *J* = 10Hz), 3.92 (2H, broad s), 3.48 (2H, broad s), 3.37 (2H, broad s), 3.30-3.17 (4H, m), 2.90-2.65 (8H, m), 1.95 (2H, broad s), 1.68 (2H, broad s), 1.10 (2H, broad s), 0.97 (2H, broad s). ^{13}C NMR

(100 MHz, CDCl$_3$): δ 174.07, 173.07, 61.12, 58.95, 53.59, 38.73, 37.74, 25.03, 23.97. m.p. 247.3 - 250.1°C. ESI-TOF *m/z* calcd for C$_{18}$H$_{31}$N$_6$O$_4$ (M + H)$^+$, calculated 395.2407, found 395.2392.

General procedure for amide reduction. Macrocycle was dissolved in 1M BH$_3$ in THF and then refluxed for 3 days. After quenching with H$_2$O, the mixture concentrated and acidified with 6M HCl at 0°C then refluxed for overnight. Mixture was co-evaporated with CH$_3$CH$_2$OH then dissolved in H$_2$O and lyophilized. The brown sticky solid was basified with NH$_4$OH and extracted with CHCl$_3$. The organic layers were collected, dried over Na$_2$SO$_4$, concentrated and the residue co-evaporated with acetone. Product was then carried forward to next step without further purification.
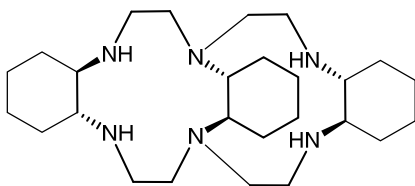
(4aR,8R,11aR,15aR,19R,22aR,23R,24R)-tetracosahydro-8,19-[1,2]benzenodibenzo[b,k][1,4,7,10,13,16]hexaazacyclooctadecine (**3.6**). Macrocycle **3.5** (0.335 g, 0.666 mmol), 1M BH$_3$ in THF (30 mL), and 6M HCl (5 mL). The title compound was obtained as a cream solid (0.242 g, 81%). ^{1}H NMR (400 MHz ,CDCl$_3$): δ 3.05 (2H, t, *J* = 14Hz), 2.72-2.65 (2H, m), 2.64-2.44 (10H, m), 2.40-2.28(4H, m), 2.28-2.15 (5H, m), 2.00 (2H, d, *J* = 13Hz), 1.95-1.85 (3H, m), 1.76-1.63 (8H, m), 1.33- 0.95 (14H, m). ^{13}C NMR (100 MHz, CDCl$_3$): δ 61.41, 59.97, 57.10, 48.63, 47.35, 43.71, 40.76, 32.50, 29.76, 26.16, 25.36, 24.85. ESI-TOF *m/z* calcd for C$_{26}$H$_{51}$N$_6$ (M + H)$^+$, calculated 447.4175, found 447.4156.

**(1R,10R,10aR,14aR)-tetradecahydro-1,10-(ethanoiminoethanoiminoethano)benzo[b][1,4,7,10]tetraazacyclododecine** **(3.17)**. Macrocycle **3.16** (0.467 g, 1.184 mmol), 1M BH$_3$ in THF (50 mL) and 6M HCl (9 mL). The title compound was obtained as a cream solid (0.353 g, 88%). ^{1}H NMR (400 MHz ,CDCl$_3$): δ 3.07 (2H, t, J = 13Hz), 3.03-2.96 (2H, m), 2.78-2.47 (20H, m), 2.25 (2H, d), 1.94 (2H, d, J = 13Hz), 1.78-1.72 (2H, m), 1.30-0.99 (8H, m). ^{13}C NMR (100 MHz, CDCl$_3$): δ 61.43, 48.54, 46.23, 45.84, 45.14, 30.07, 29.62, 25.67, 24.44. ESI-TOF m/z calcd for C$_{18}$H$_{39}$N$_6$ (M + H)$^+$, calculated 339.3236, found 339.3235.

General procedure for alkylation and deprotection. Starting material and K$_2$CO$_3$ were suspended in CH$_3$CN and ethyl (2-chloroacetyl)glycinate dissolved in CH$_3$CN () was added. The reaction mixture was heated to 60°C and left for 2 days. Reaction mixture was filtered and the filtrate concentrated. The crude was the carried forward to the next step as is.

Crude product was dissolved in MeOH/1M NaOH (1:1) and left stirring at rt for overnight. The reaction mixture was concentrated and neutralized with 1M HCl. The crude was purified by size exclusion column chromatography (100% H$_2$O) and the desired fractions were collected and lyophilized to give the desired compound.
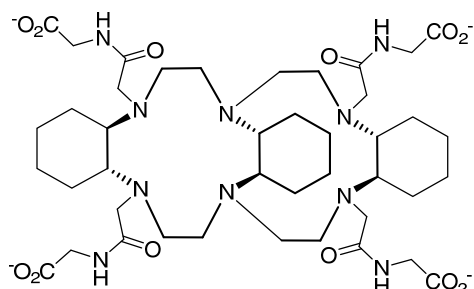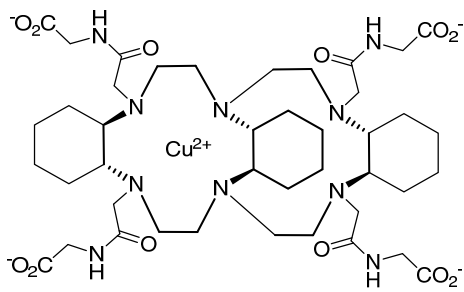

2,2',2'',2'''-((2,2',2'',2'''-((4aR,8R,11aR,15aR,19R,22aR,23R,24R)-icosahydro-8,19-

[1,2]benzenodibenzo[b,k][1,4,7,10,13,16]hexaazacyclooctadecine-5,11,16,22-tetrayl)tetrakis(acetyl))tetrakis(azanediyl))tetraacetic acid (3.9). Starting material **3.6** (0.200 g, 0.448 mmol), K_2CO_3 (0.310 g, 2.24 mmol), ethyl (2-chloroacetyl)glycinate **3.7** (0.402 g, 2.24 mmol), CH_3CN (v_{tot} = 7 mL) and MeOH/1M NaOH (v_{tot} =6 mL). The title compound was obtained as a cream solid (0.221 g, 54%). ESI-TOF *m/z* calcd for $C_{42}H_{71}N_{10}O_{12}$ $(M + H)^+$, calculated 907.5253, found 907.5295.
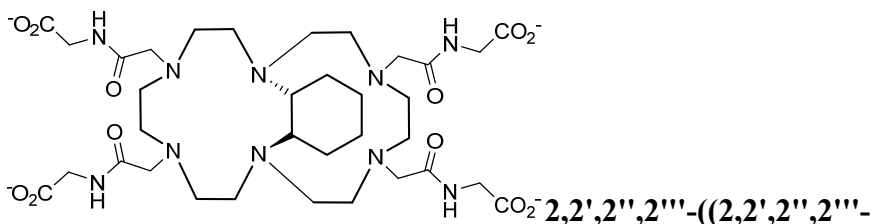
2,2',2'',2'''-((2,2',2'',2'''-((1R,10R,10aR,14aR)-dodecahydro-1,10-(ethanoiminoethanoiminoethano)benzo[b][1,4,7,10]tetraazacyclododecine-4,7,17,20-tetrayl)tetrakis(acetyl))tetrakis(azanediyl))tetraacetic acid (3.19). Starting material **3.17** (0.323 g, 0.954 mmol), K_2CO_3 (0.659 g, 4.77 mmol), ethyl (2-chloroacetyl)glycinate **3.7** (0.857 g, 4.77 mmol), CH_3CN (v_{tot} = 10 mL) and MeOH/1M NaOH (v_{tot} = 9 mL). The title compound was obtained as a cream solid (0.273 g, 36%). ESI-TOF *m/z* calcd for $C_{34}H_{59}N_{10}O_{12}$ $(M + H)^+$, calculated 799.4314, found 799.4346.

General procedure for metalation. Starting material was suspended in H_2O and the appropriate metal salts added. The pH was adjusted to 7 and the reaction mixture heated to 50^oC and left for overnight. The crude was dialyzed for 3 days and then lyophilized.
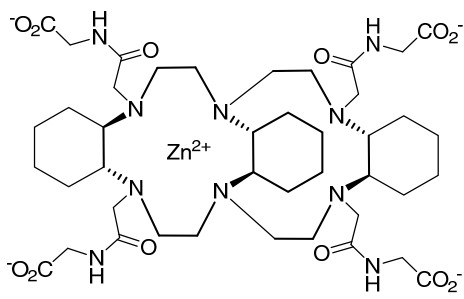
Copper(II) (2,2',2'',2'''-((2,2',2'',2'''-((4aR,8R,11aR,15aR,19R,22aR,23R,24R)-icosahydro-8,19-[1,2]benzenodibenzo[b,k][1,4,7,10,13,16]hexaazacyclooctadecine-5,11,16,22-tetrayl)tetrakis(acetyl))tetrakis(azanediyl))tetraacetate) (3.10). Starting material **3.9** (0.034 g, 0.0375 mmol), CuCl$_2$.2H$_2$O (0.0066 g, 0.0413 mmol) and H$_2$O (1 mL). The title compound was obtained as a blue solid (0.031 g, 86%). ESI-TOF *m/z* calcd for C$_{42}$H$_{68}$N$_{10}$O$_{12}$Cu (M - 2H)$^+$, calculated 967.4314, found 967.4296.
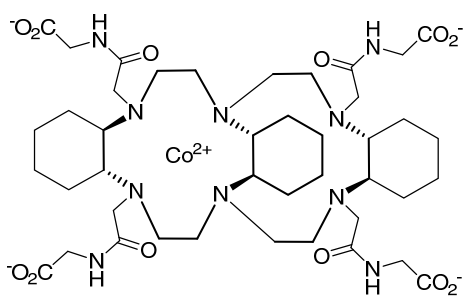

Cobalt(II) (2,2',2'',2'''-((2,2',2'',2'''-((4aR,8R,11aR,15aR,19R,22aR,23R,24R)-icosahydro-8,19-[1,2]benzenodibenzo[b,k][1,4,7,10,13,16]hexaazacyclooctadecine-5,11,16,22-tetrayl)tetrakis(acetyl))tetrakis(azanediyl))tetraacetate) (3.11). Starting material **3.9** (0.024 g, 0.0265 mmol), CoCl$_2$.6H$_2$O (0.0069g, 0.029 mmol) and H$_2$O (1 mL). The title compound was obtained as a purple solid (0.015 g, 58%). ESI-TOF *m/z* calcd for C$_{42}$H$_{68}$N$_{10}$O$_{12}$Co (M - 2H)$^+$, calculated 963.4350, found 963.4392.
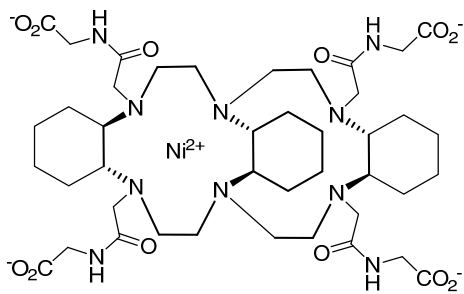
Nickel(II) **(2,2',2'',2'''-((2,2',2'',2'''-((4aR,8R,11aR,15aR,19R,22aR,23R,24R)-icosahydro-8,19-[1,2]benzenodibenzo[b,k][1,4,7,10,13,16]hexaazacyclooctadecine-5,11,16,22-tetrayl)tetrakis(acetyl))tetrakis(azanediyl))tetraacetate) (3.12)**. Starting material **3.9** (0.034 g, 0.0375 mmol), NiCl$_2$ (0.0054 g, 0.0413 mmol) and H$_2$O (1 mL). The title compound was obtained as a green solid (0.026 g, 72%). ESI-TOF *m/z* calcd for C$_{42}$H$_{68}$N$_{10}$O$_{12}$Ni (M - 2H)$^+$, calculated 962.4372, found 962.4348.

Zinc(II) **(2,2',2'',2'''-((2,2',2'',2'''-((4aR,8R,11aR,15aR,19R,22aR,23R,24R)-icosahydro-8,19-[1,2]benzenodibenzo[b,k][1,4,7,10,13,16]hexaazacyclooctadecine-5,11,16,22-tetrayl)tetrakis(acetyl))tetrakis(azanediyl))tetraacetate) (3.13)**. Starting material **3.9** (0.024 g, 0.026 mmol), ZnCl$_2$ (0.0035 g, 0.026 mmol) and H$_2$O (1 mL). The title compound was obtained as a white solid (0.017 g, 68%). ESI-TOF *m/z* calcd for C$_{42}$H$_{68}$N$_{10}$O$_{12}$Zn (M - 2H)$^+$, calculated 968.4310, found 968.4356.
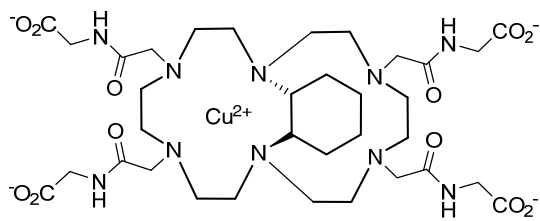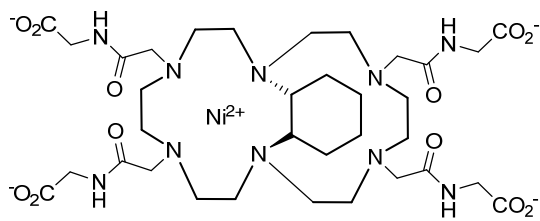
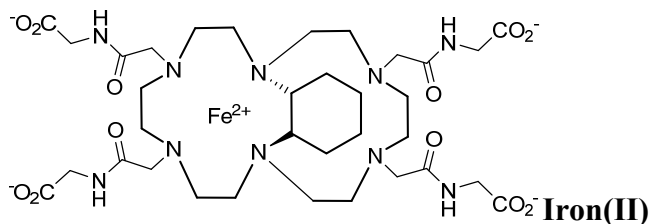 **Copper(II)** **(2,2',2'',2'''-((2,2',2'',2'''-((1R,10R,10aR,14aR)-dodecahydro-1,10-(ethanoiminoethanoiminoethano)benzo[b][1,4,7,10]tetraazacyclododecine-4,7,17,20-tetrayl)tetrakis(acetyl))tetrakis(azanediyl))tetraacetate)** (**3.20**). Starting material **3.19** (0.030 g, 0.0375 mmol), CuCl$_2$.2H$_2$O (0.0069 g, 0.0413 mmol) and H$_2$O (1 mL). The title compound was obtained as a blue solid (0.027 g, 84%). ESI-TOF *m/z* calcd for C$_{34}$H$_{56}$N$_{10}$O$_{12}$Cu (M - 2H)$^+$, calculated 859.3375, found 859.3398.
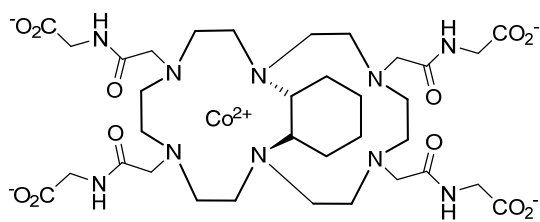
 Cobalt(II) **(2,2',2'',2'''-((2,2',2'',2'''-((1R,10R,10aR,14aR)-dodecahydro-1,10-(ethanoiminoethanoiminoethano)benzo[b][1,4,7,10]tetraazacyclododecine-4,7,17,20-tetrayl)tetrakis(acetyl))tetrakis(azanediyl))tetraacetate)** (**3.21**). Starting material **3.19** (0.041 g, 0.051 mmol), CoCl$_2$.6H$_2$O (0.013 g, 0.0547 mmol) and H$_2$O (1 mL). The title compound was obtained as a purple solid (0.032g, 73%). ESI-TOF *m/z* calcd for C$_{34}$H$_{56}$N$_{10}$O$_{12}$Co (M - 2H)$^+$, calculated 855.3411, found 855.3404.

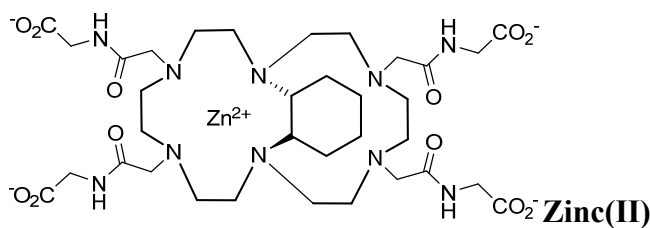 **Nickel(II)** **(2,2',2'',2'''-((2,2',2'',2'''-((1R,10R,10aR,14aR)-dodecahydro-1,10-(ethanoiminoethanoiminoethano)benzo[b][1,4,7,10]tetraazacyclododecine-4,7,17,20-**

tetrayl)tetrakis(acetyl))tetrakis(azanediyl))tetraacetate) (**3.22**). Starting material **3.19** (0.020 g, 0.025 mmol), NiCl$_2$ (0.0036 g, 0.0275 mmol) and H$_2$O (1 mL). The title compound was obtained as a green solid (0.014 g, 65%.). ESI-TOF *m/z* calcd for C$_{34}$H$_{56}$N$_{10}$O$_{12}$Ni (M - 2H)$^+$, calculated 854.3433, found 854.3400.

**Iron(II)** **(2,2',2'',2'''-((2,2',2'',2'''-((1R,10R,10aR,14aR)-dodecahydro-1,10-(ethanoiminoethanoiminoethano)benzo[b][1,4,7,10]tetraazacyclododecine-4,7,17,20-tetrayl)tetrakis(acetyl))tetrakis(azanediyl))tetraacetate)** (**3.23**). Starting material **3.19** (0.020 g, 0.025 mmol), Fe(CF$_3$SO$_3$)$_2$ (0.0088 g, 0.025 mmol) and H$_2$O (1 mL). The title compound was obtained as a red solid (0.021g, 95%). ESI-TOF *m/z* calcd for C$_{34}$H$_{56}$N$_{10}$O$_{12}$Fe (M - 2H)$^+$, calculated 852.3429, found 852.3394.

Zinc(II) **(2,2',2'',2'''-((2,2',2'',2'''-((1R,10R,10aR,14aR)-dodecahydro-1,10-(ethanoiminoethanoiminoethano)benzo[b][1,4,7,10]tetraazacyclododecine-4,7,17,20-tetrayl)tetrakis(acetyl))tetrakis(azanediyl))tetraacetate)** (**3.24**). Starting material **3.19** (0.025 g, 0.031 mmol), ZnCl$_2$ (0.0042 g, 0.031 mmol) and H$_2$O (1 mL). The title compound was obtained as a white solid (0.018 g, 65%). ESI-TOF *m/z* calcd for C$_{34}$H$_{56}$N$_{10}$O$_{12}$Zn (M - 2H)$^+$, calculated 860.3371, found 860.3356.

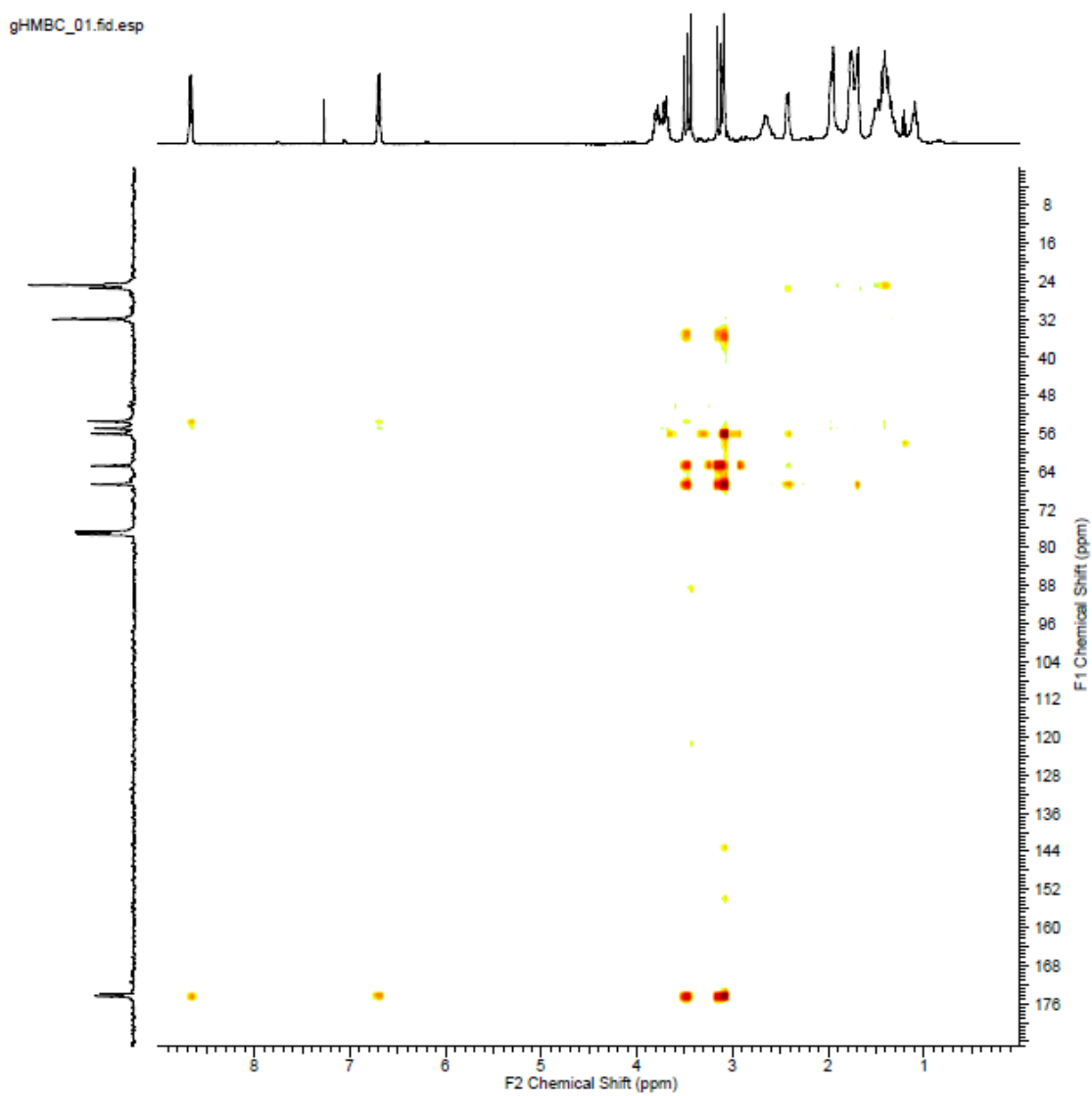## 3.4.3 Spectra

S 3.1: ^{1}H NMR Spectrum of **3.4**
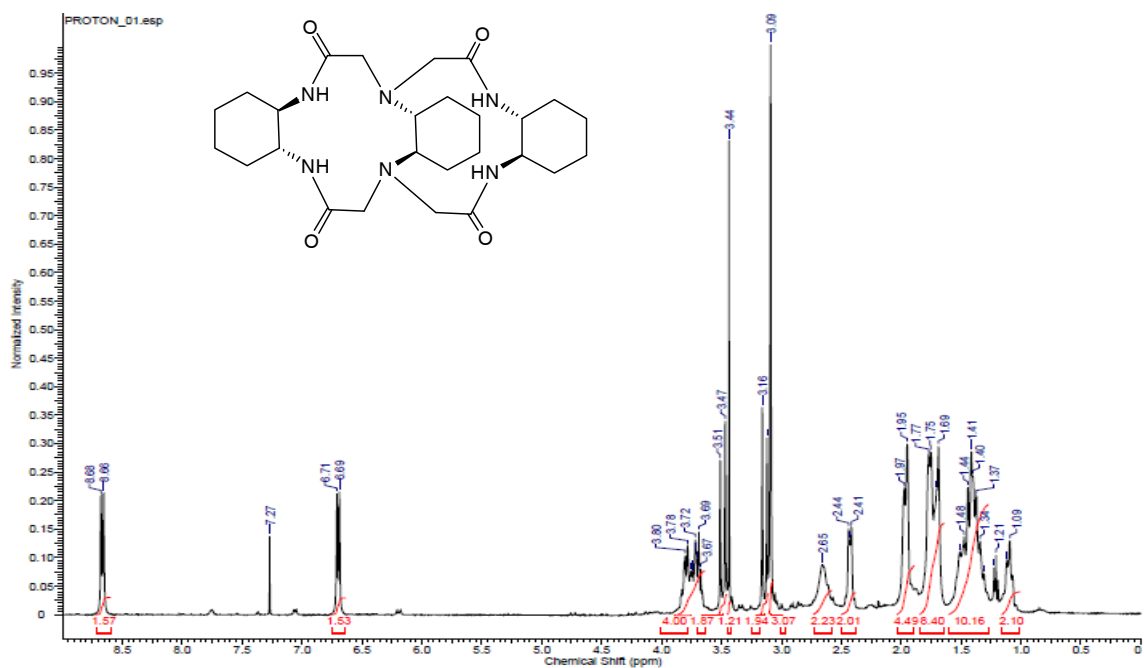
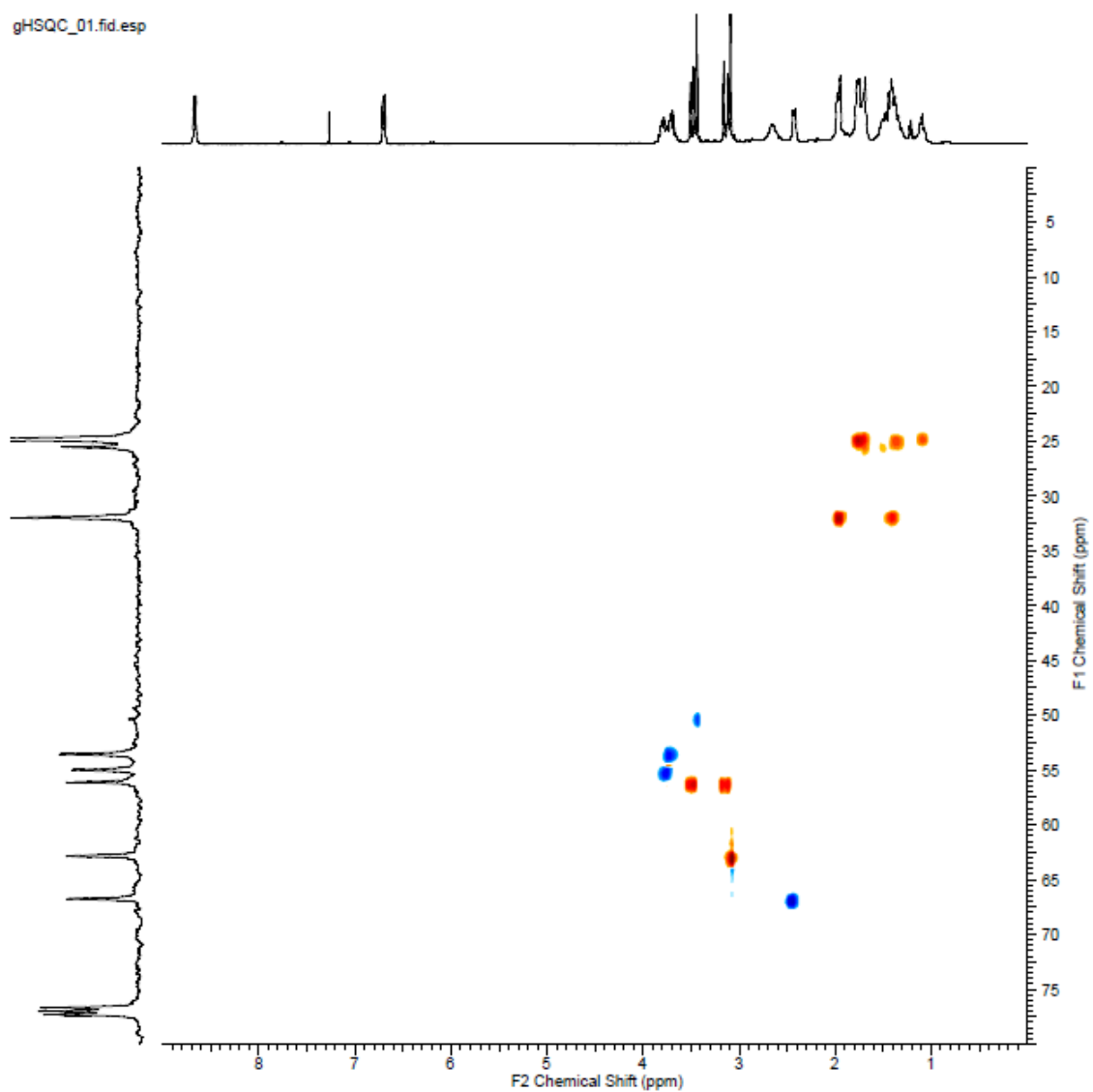**S 3.2:** ^{13}C NMR Spectrum of **3.4**
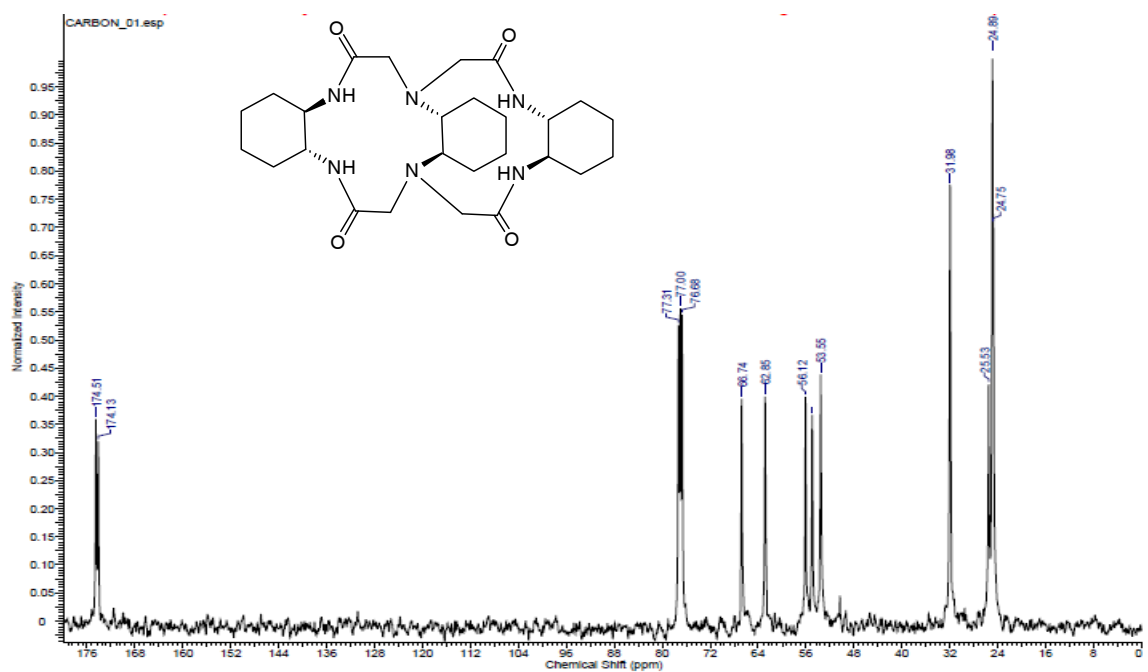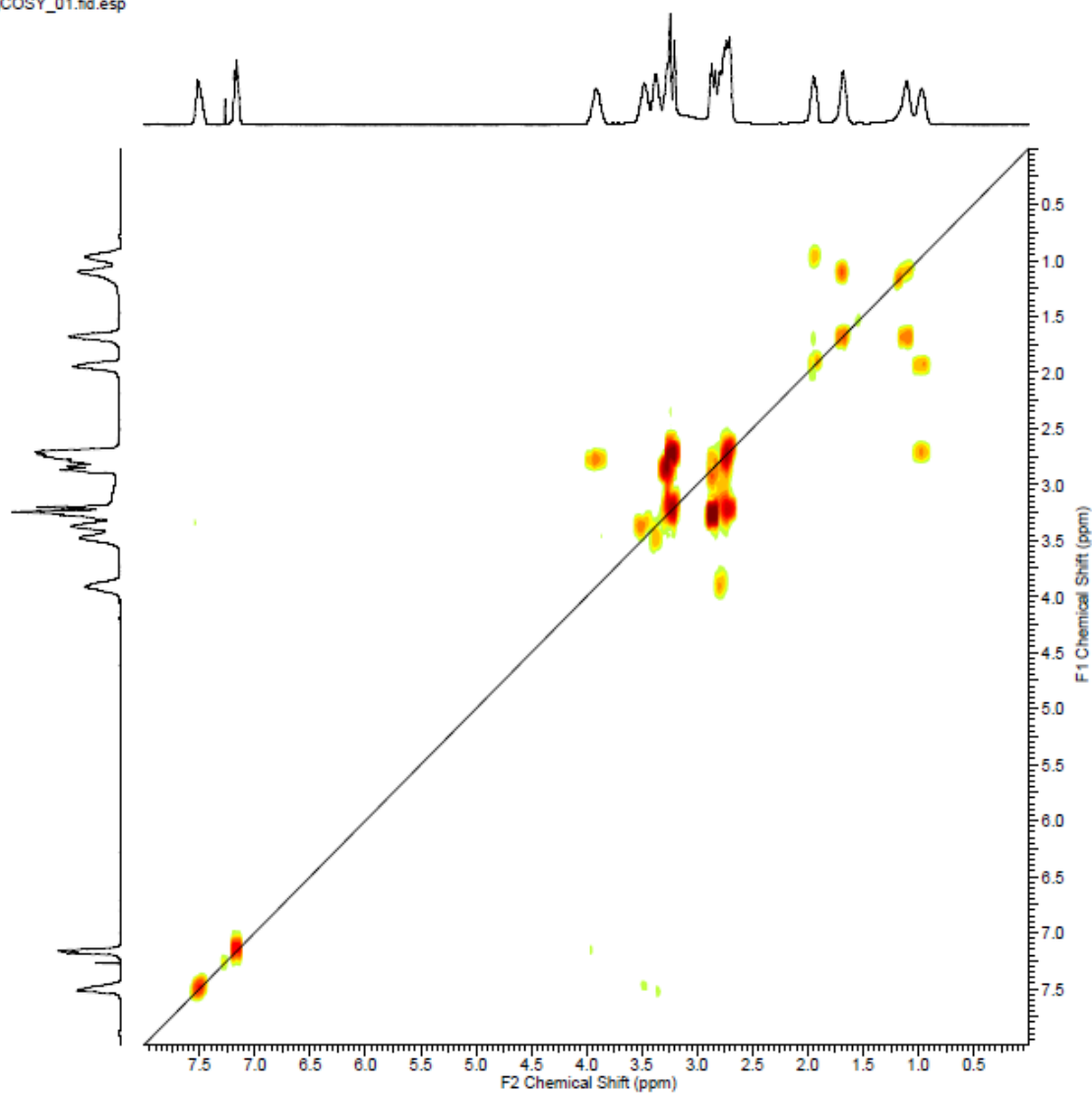
S 3.3: COSY Spectrum of **3.4**
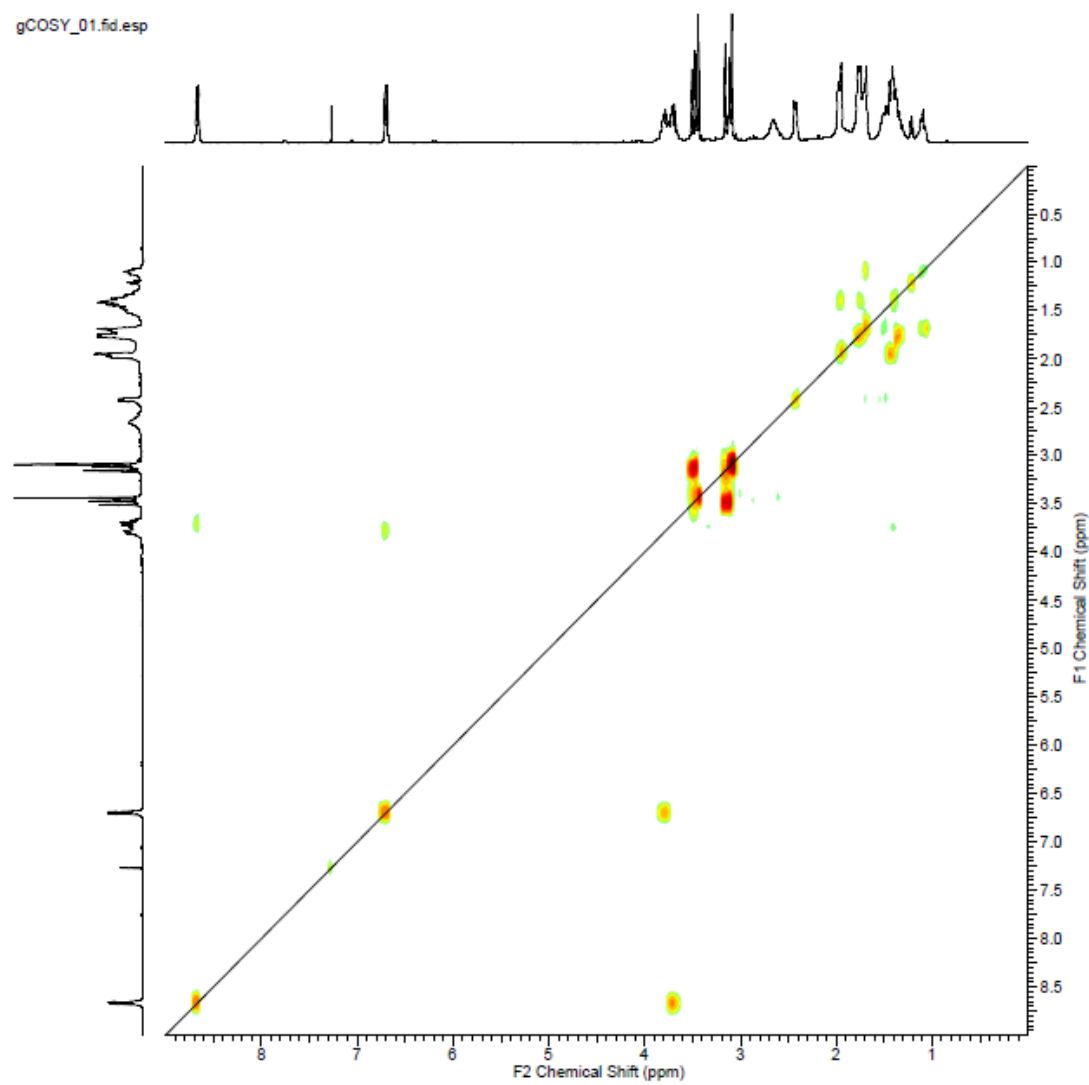
S 3.4: HMBC Spectrum of **3.4**

gHMBC_01.fid.esp

S 3.5: HSQC Spectrum of **3.4**

S 3.6: ^{1}H NMR Spectrum of **3.16**
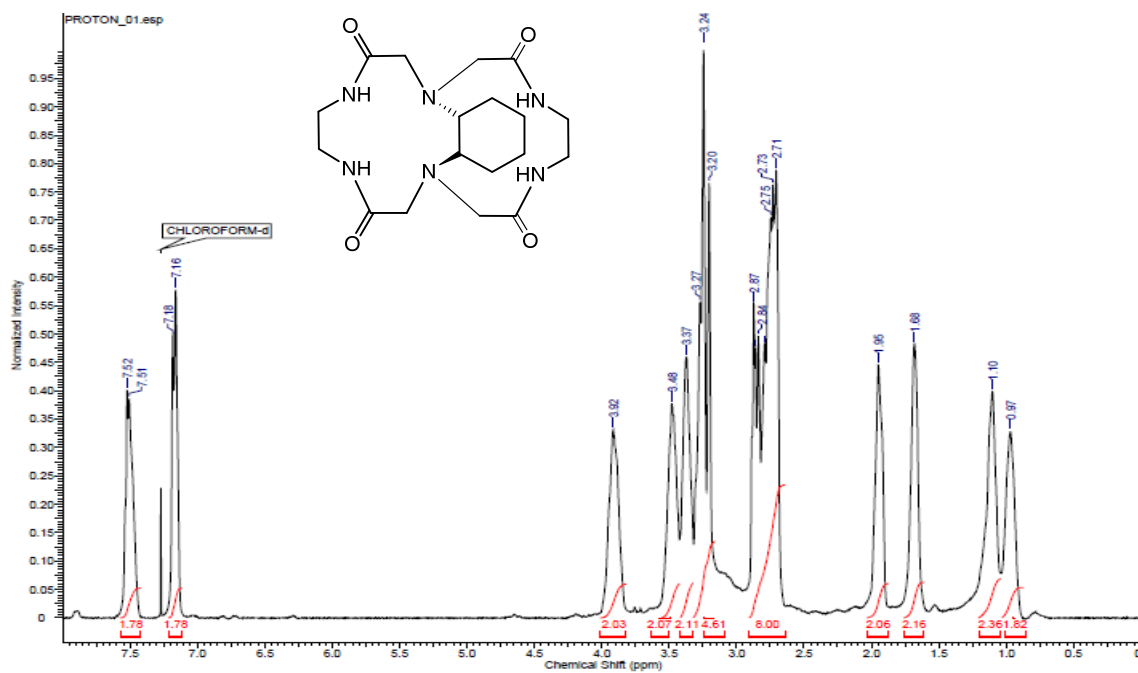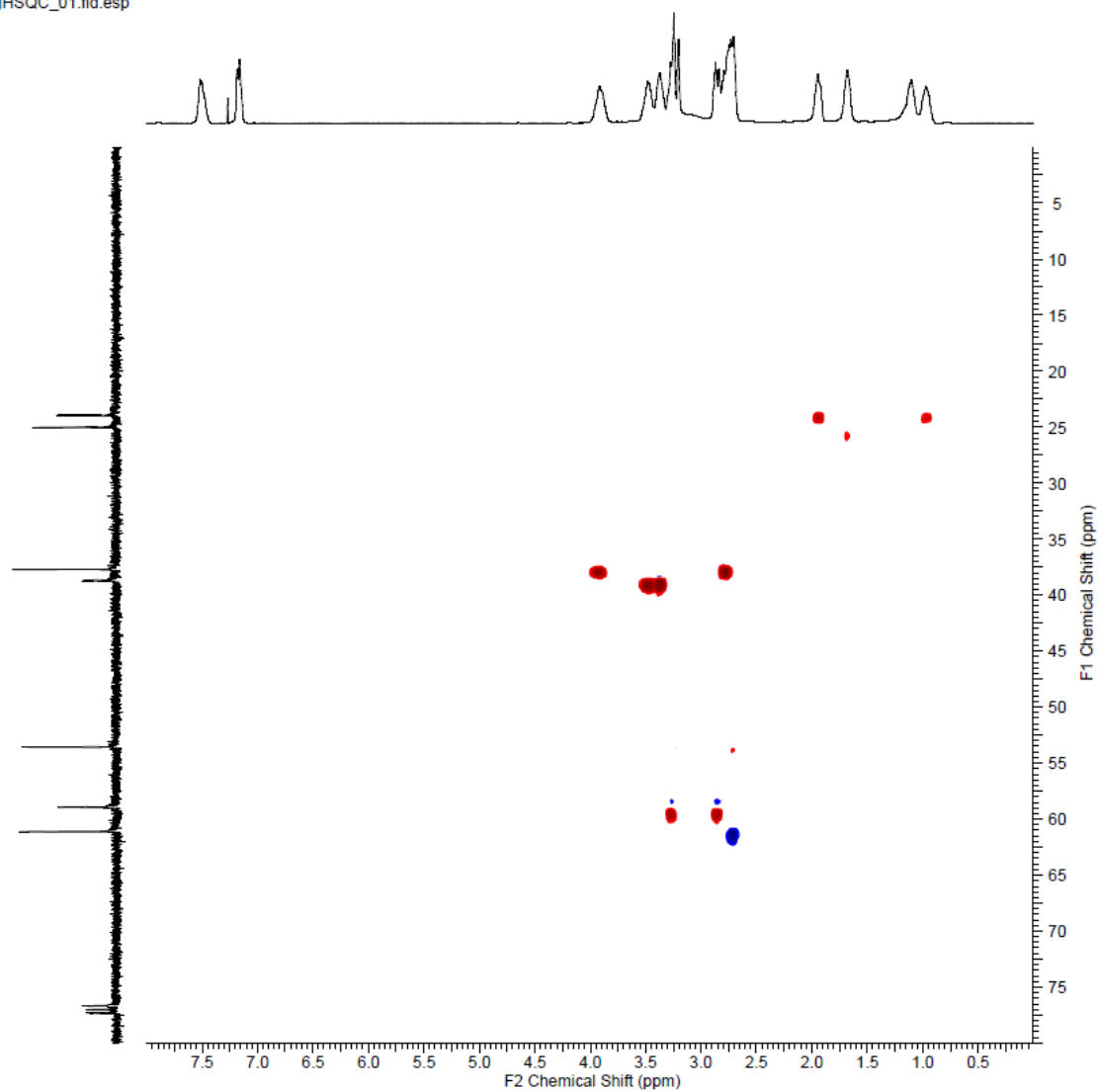

S 3.7: ^{13}C NMR Spectrum of **3.16**
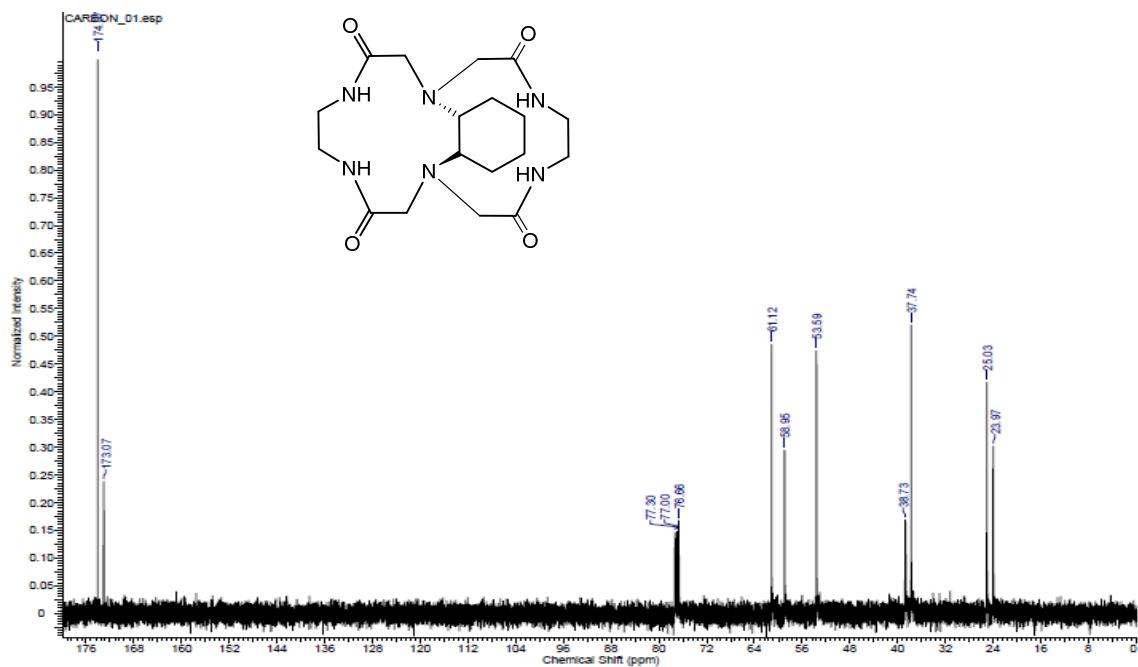
S 3.8: COSY Spectrum of **3.16**

gCOSY_01.fid.esp

S 3.9: HMBC Spectrum of **3.16**
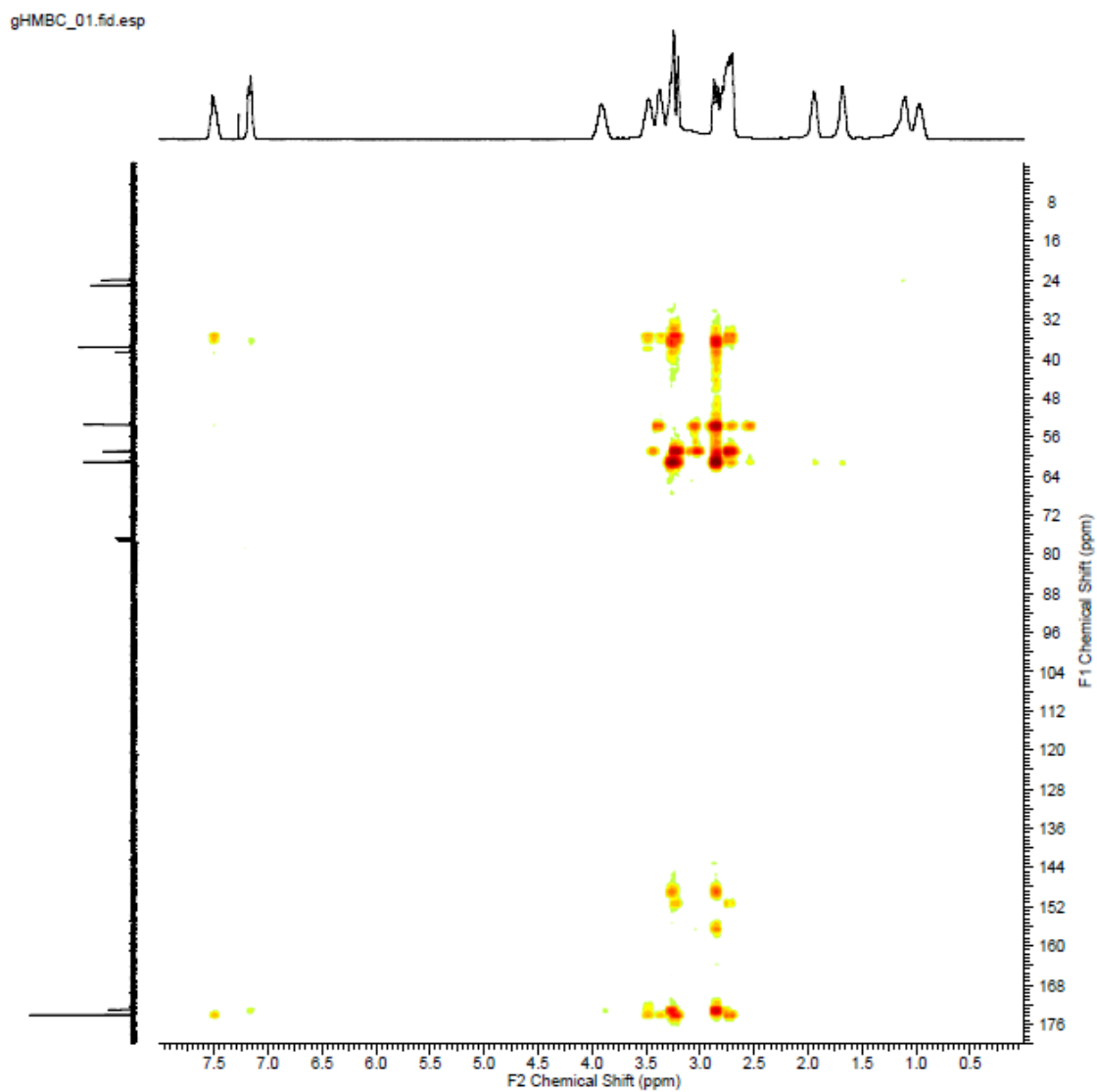
gHMBC_01.fid.esp

S 3.10: HSQC Spectrum of **3.16**

gHSQC_01.fid.esp

S 3.11: ^{1}H NMR Spectrum of **3.6**
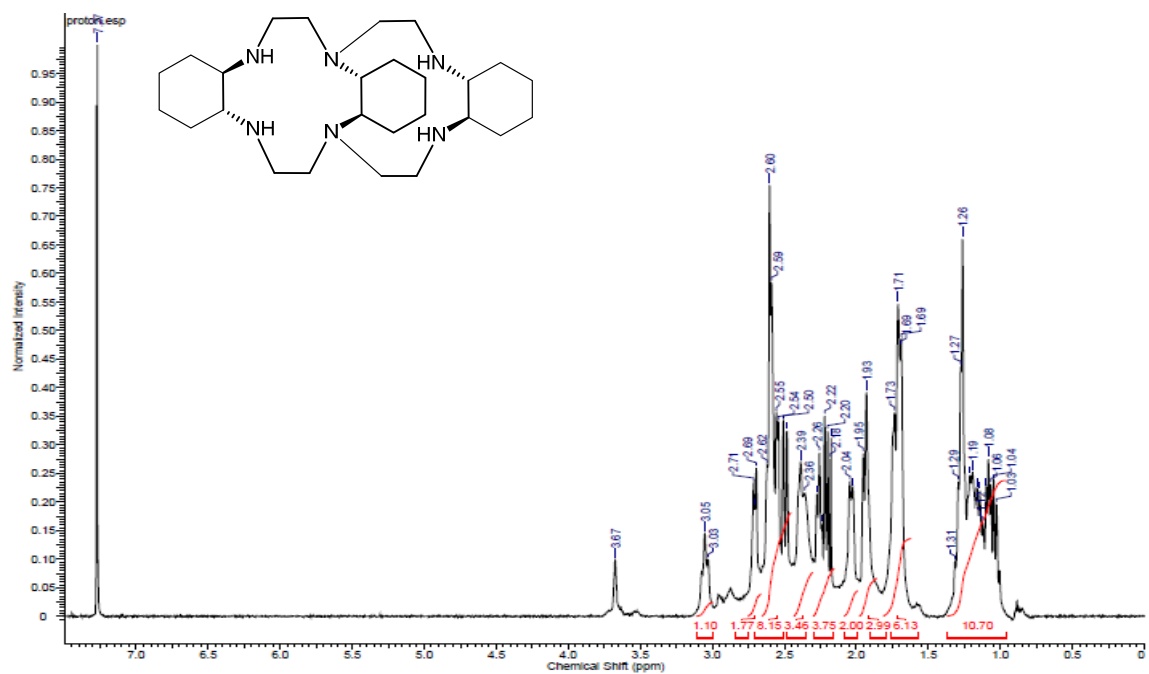
S 3.12: ^{13}C NMR Spectrum of **3.6**
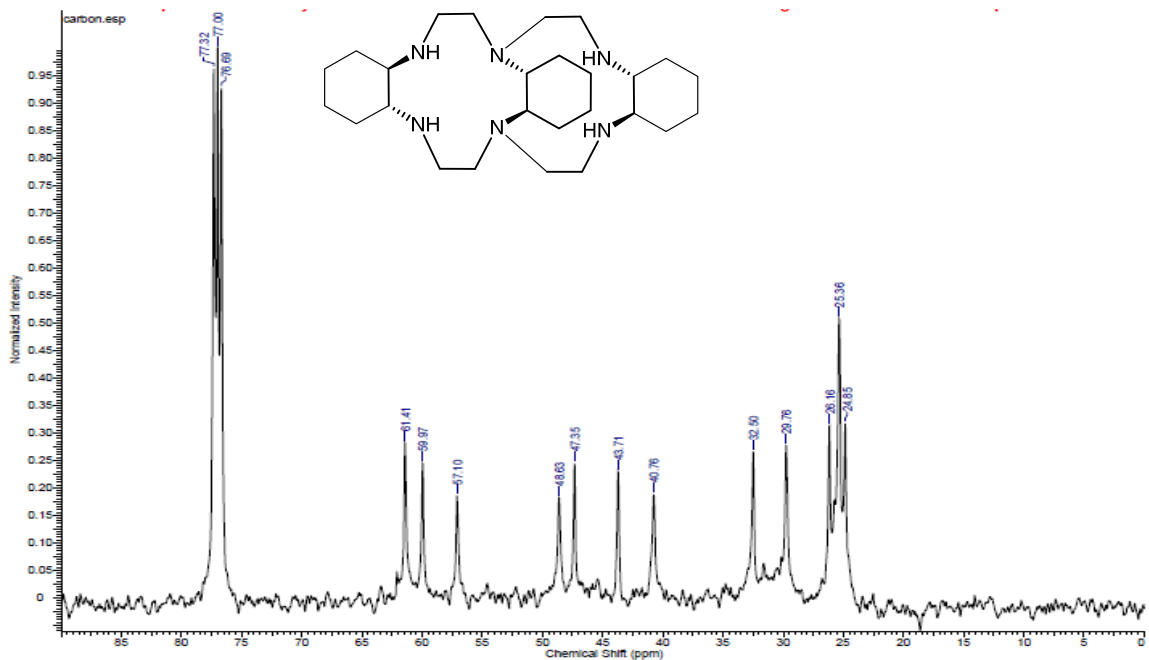
S 3.13: ¹H NMR Spectrum of **3.17**
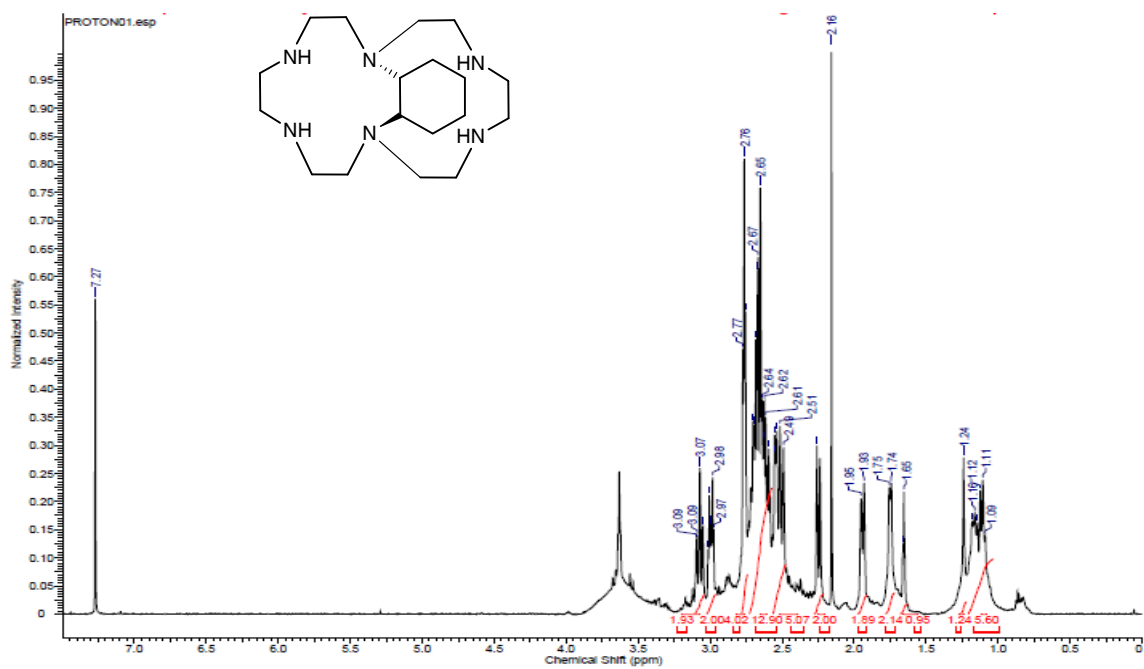
S 3.14: ¹³C NMR Spectrum of **3.17**

88
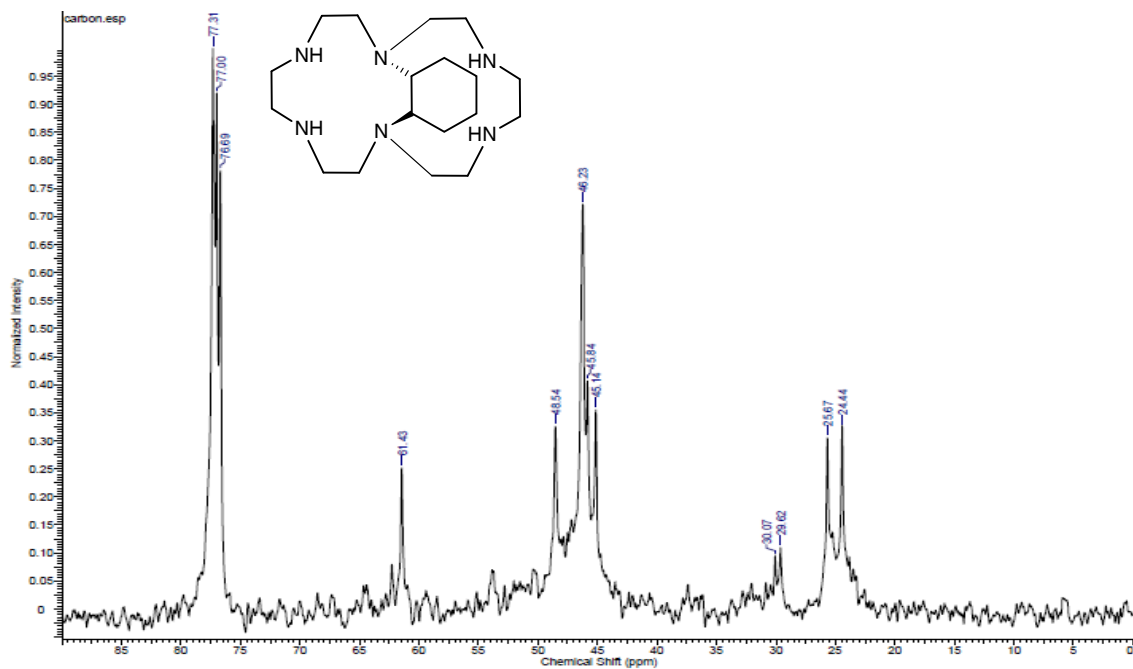
S 3.15: ^{1}H NMR Spectrum of 3.9
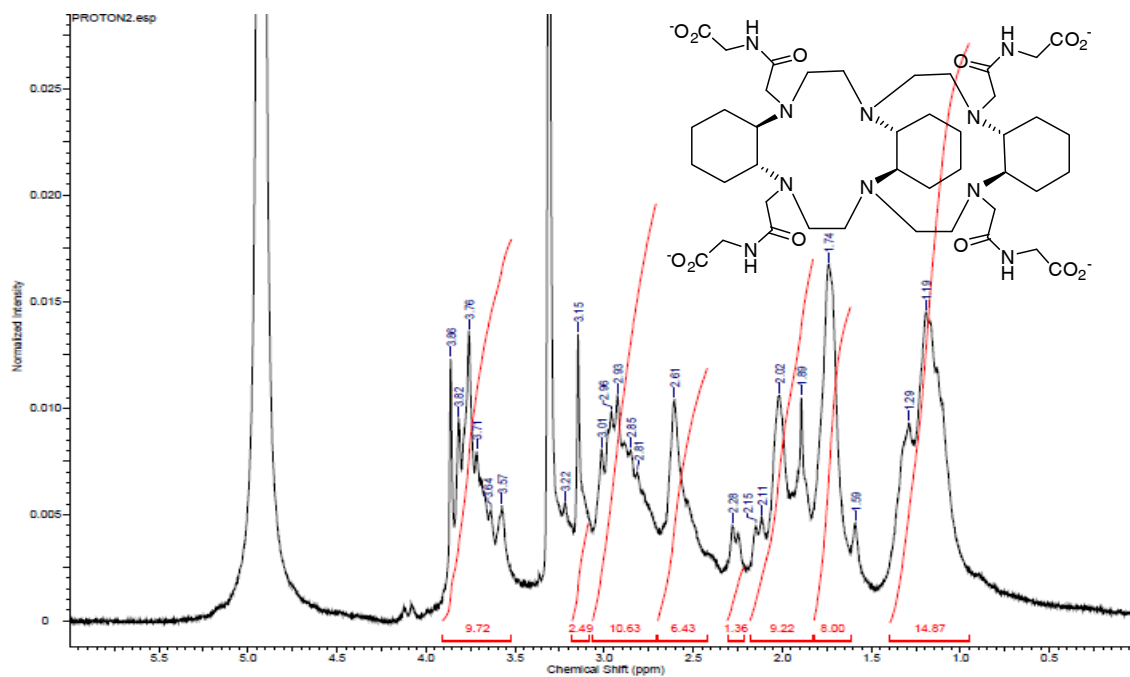
S 3.16: ^{1}H NMR Spectrum of 3.19
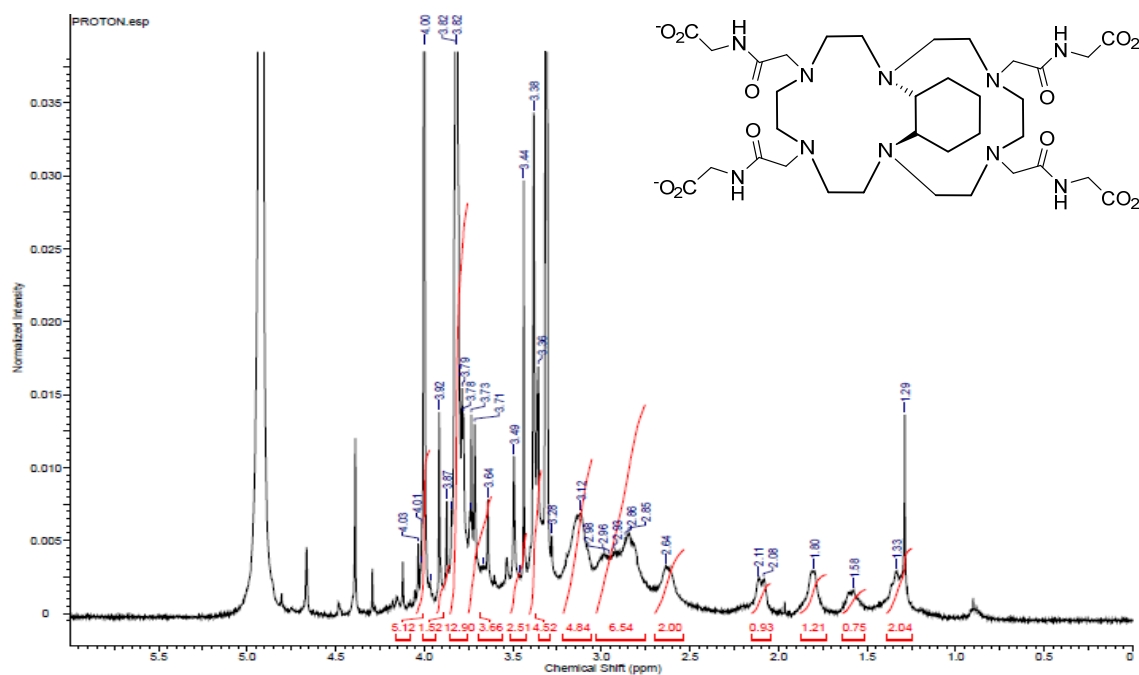
S 3.17: r_1 relaxivity profile of **3.11**
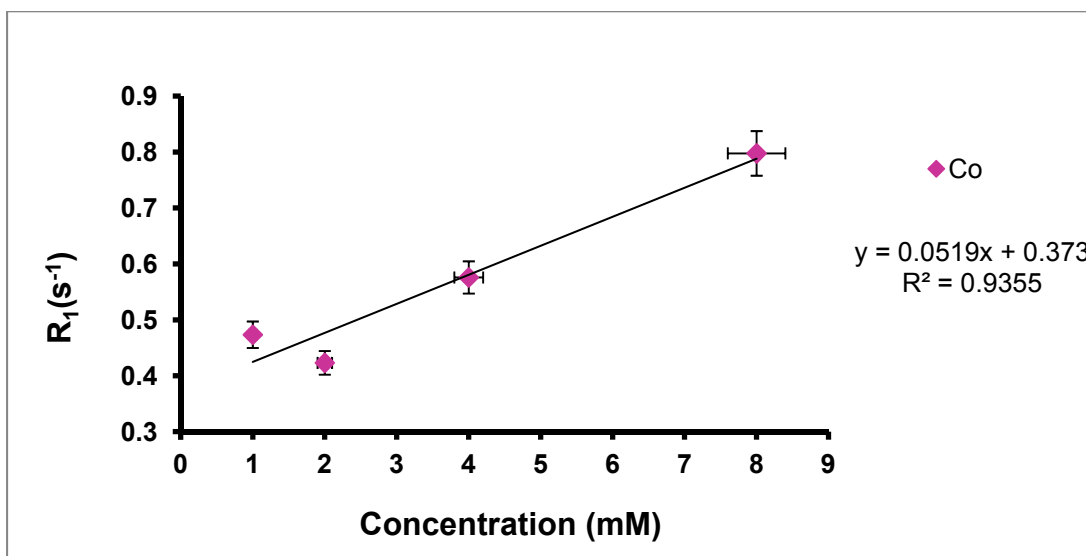
S 3.18: r_2 relaxivity profile of **3.11**
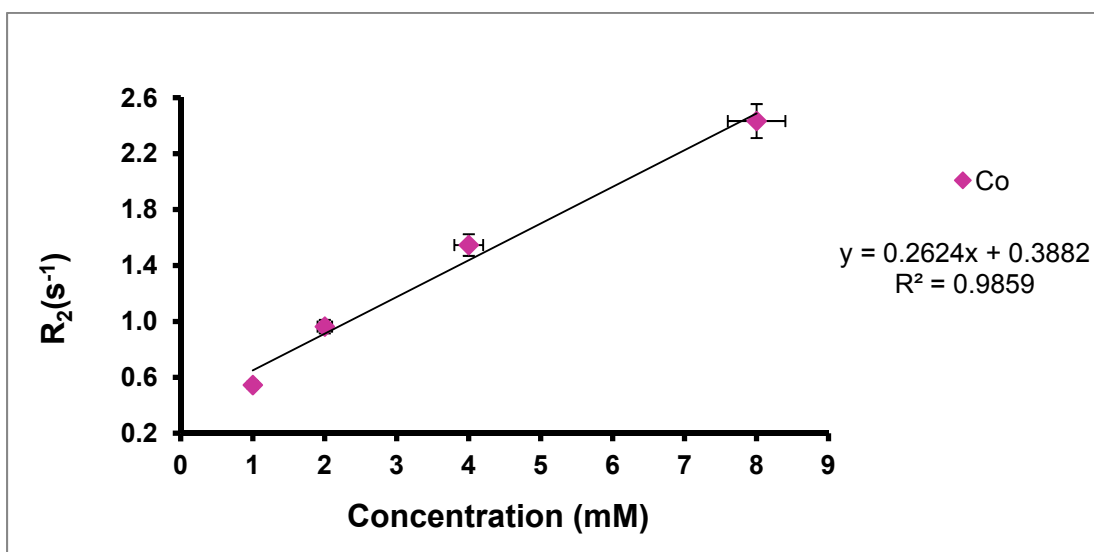
S 3.19: r_1 relaxivity profile of **3.12**
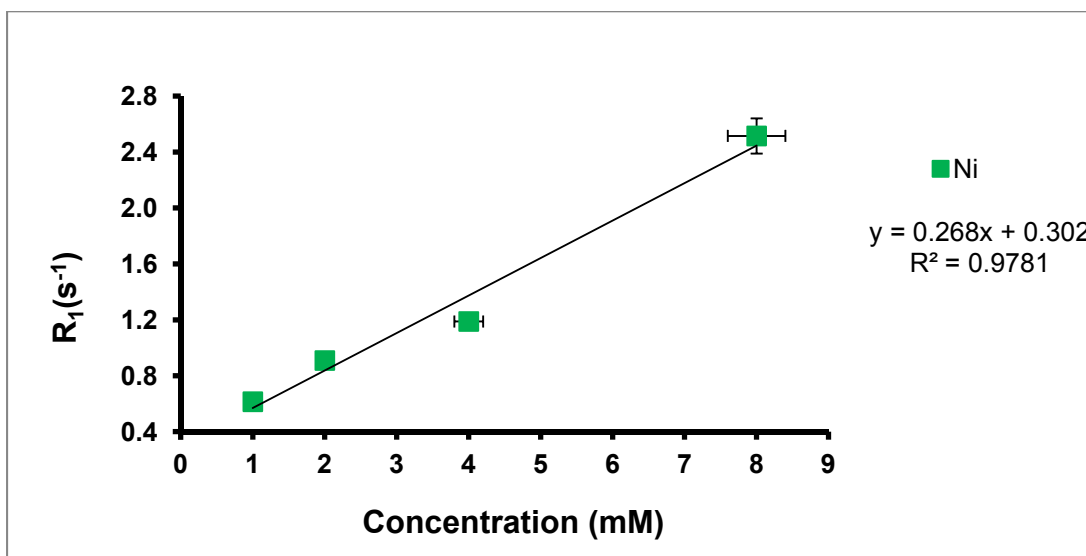
S 3.20: r_2 relaxivity profile of **3.12**
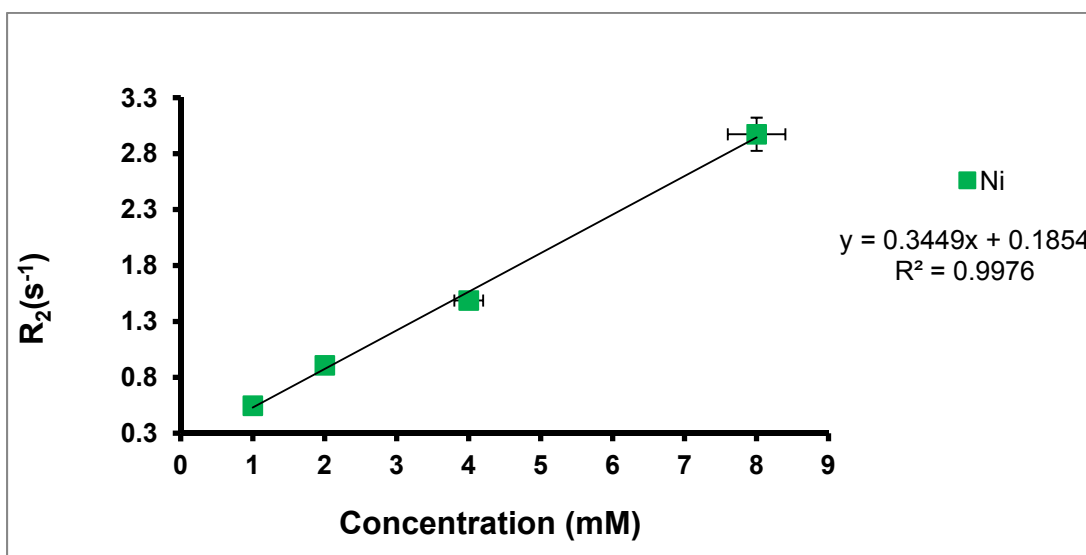
S 3.21: r_1 relaxivity profile of **3.21**
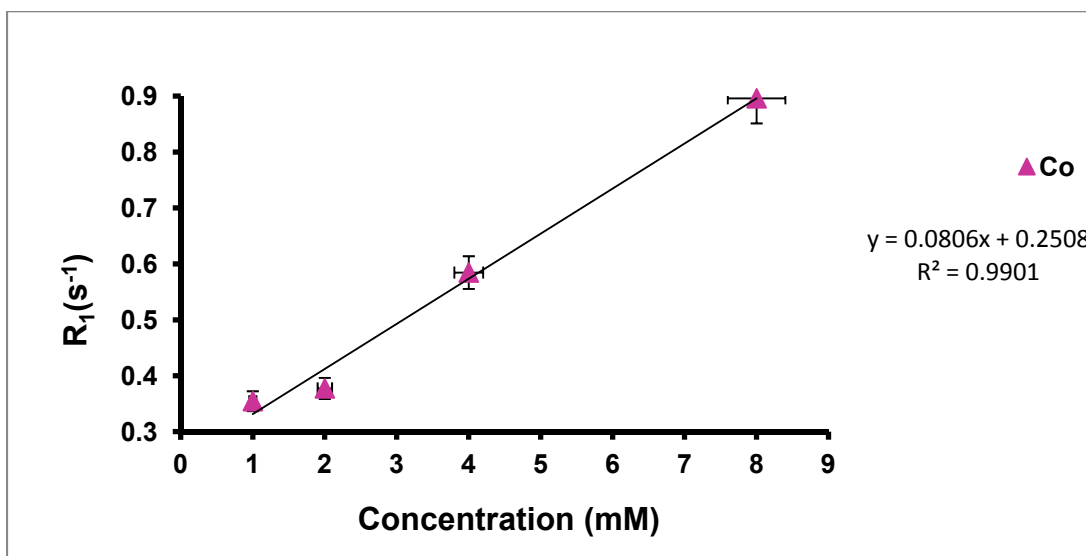
S 3.22: r_2 relaxivity profile of **3.21**
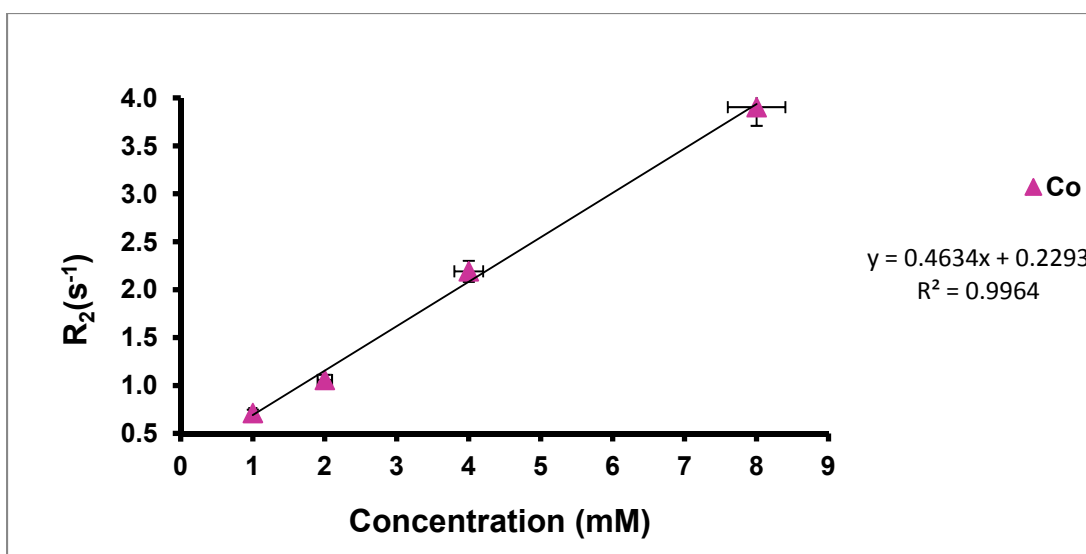
S 3.23: r_1 relaxivity profile of **3.22**

$$y = 0.2464x + 0.3051$$
$$R^2 = 0.9955$$
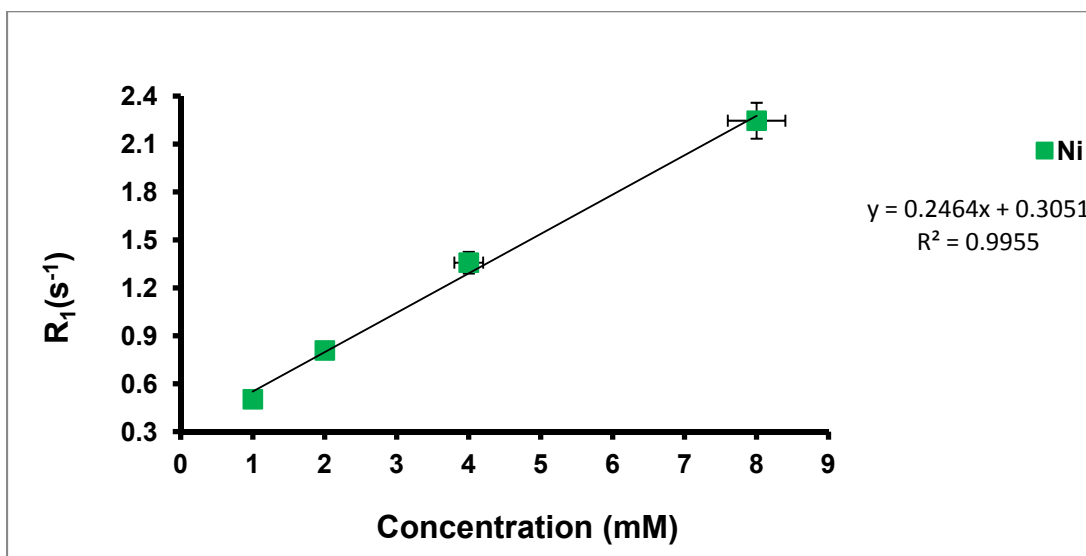
S 3.24: r_2 relaxivity profile of **3.22**

$$y = 0.365x + 0.493$$
$$R^2 = 0.9966$$
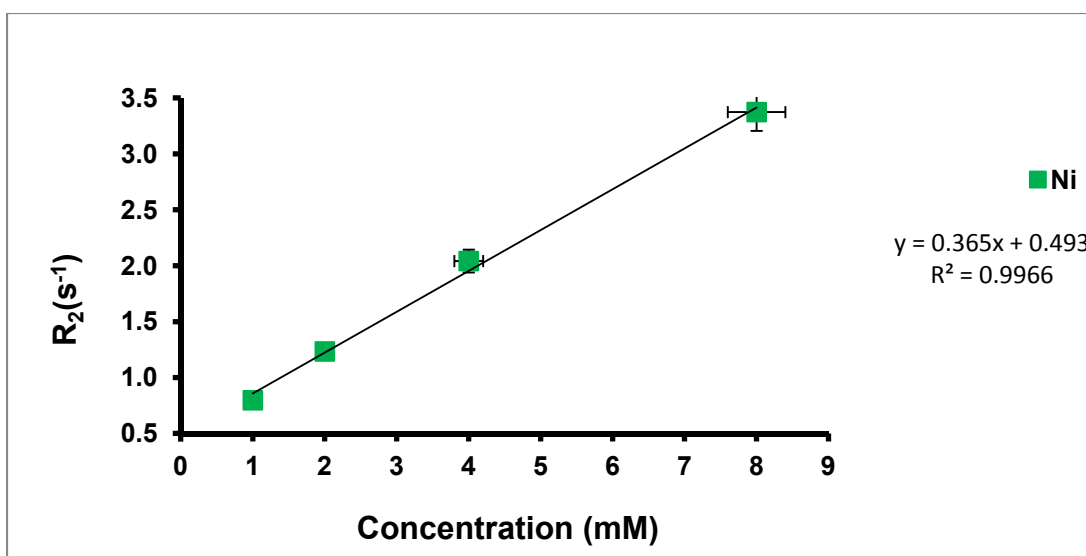
S 3.25: r_1 relaxivity profile of **3.23**
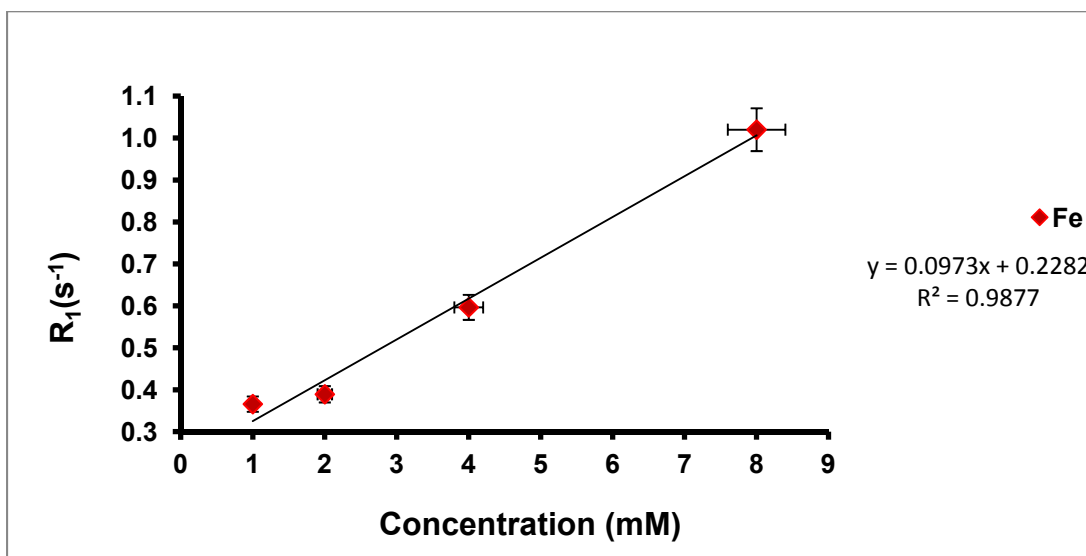
S 3.26: r_2 relaxivity profile of **3.23**
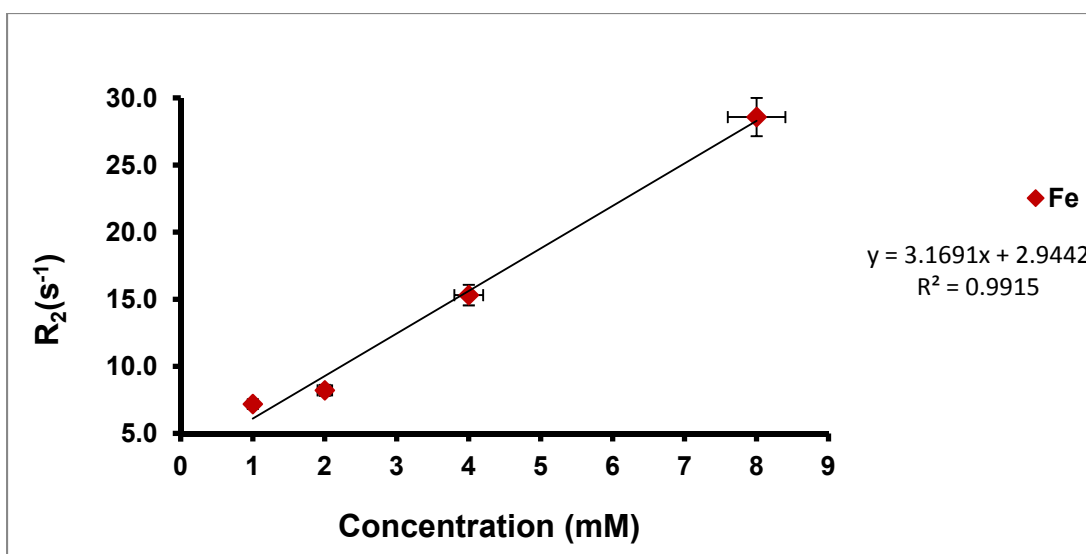
3.5 References

(1) Viswanathan, S.; Kovacs, Z.; Green, K. N.; Ratnakar, S. J.; Sherry, A. D. *Chem. Rev.* **2010,** *110,* 2960-3018.

(2) Woods, M.; Kovacs, Z.; Zhang, S.; Sherry, A. D. *Angew. Chem. Int. Ed.* **2003,** *42*, 5889-5892.

(3) Carney, C. E.; Tran, A. D.; Wang, J.; Schabel, M. C.; Sherry, A. D.; Woods, M. *Chem. Eur. J.* **2011,** *17*, 10372-10378.

(4) Aime, S.; Barge, A.; Bruce, J. I.; Botta, M.; Howard, J. A. K.; Moloney, J. M.; Parker, D.; de Sousa, A. S.; Woods, M. *J. Am. Chem. Soc.* **1999,** *121*, 5762-5771.

(5) Miller, K. J.; Saherwala, A. A.; Webber, B. C.; Wu, Y.; Sherry, A. D.; Woods, M. *Inorg. Chem.* **2010,** *49*, 8662-8664.

(6) Comblin, V.; Gilsoul, D.; Hermann, M.; Humblet, V.; Jacques, V.; Mesbahi, M.; Sauvage, C.; Desreux, J. F. *Coord. Chem. Rev.* **1999,** *185-186*, 451-470.

(7) Zhang, S.; Jiang, X.; Sherry, A. D. *Helv. Chim. Acta.* **2005,** *88*, 923-935.

(8) Tircso, G.; Webber, B. C.; Kucera, B. E.; Young, V. G.; Woods, M. *Inorg. Chem.* **2011,** *50*, 7966-7979.

(9) Desreux, J. F.; Marinelli, E. R.; Ratsep, P. C.; Tweedle, M. F.; Wagler, T. R. Canada Patent CA2150452A1, 1995.

(10) Alexakis, A.; Chauvin, A.; Stouvenel, R.; Vrancken, E.; Mutti, S.; Mangeney, P. *Tetrahedron: Asymmetry* **2001,** *12*, 1171-1178.

(11) Bolognesi, M. L.; Cavalli, A.; Andrisano, V.; Bartolini, M.; Banzi, R.; Antonello, A.; Rosini, M.; Melchiorre, C. *Il Farmaco* **2003,** *58*, 917-928.

(12) Saburi, M.; Yoshikawa, S. *Bull. Chem. Soc. Jpn.* **1974,** *47*, 1184-1189.

(13) Sharma, S. K.; Upreti, S.; Gupta, R. *Eur. J. Inorg. Chem.* **2007,** *2007*, 3247-3259.

(14) Neumann, W. L.; Franklin, G. W.; Sample, K. R.; Aston, K. W.; Weiss, R. H.; Riley, D. P.; Rath, N. *Tetrahedron Lett.* **1997,** *38*, 3143-3146.

(15) Ankner, T.; Hilmersson, G. *Org. Lett.* **2009,** *11*, 503-506.

(16) Haskell, B. E.; Bowlus, S. B. *J. Org. Chem.* **1976,** *41*, 159-160.

(17) Shohji, N.; Kawaji, T.; Okamoto, S. *Org. Lett.* **2011,** *13*, 2626-2629.

(18) Garrett, T.; Umbenhauer, J.; Romberger, G.; Smith, A.; Goulden, M.; Engle, J.; Harris, M. *J. Undergrad. Chem. Res.* **2008,** *7*, 19-26.

(19) Seshadri, R. *http://www.mrl.ucsb.edu/~seshadri/Periodic/* (accessed 03/22, 2014).

(20) Tsitovich, P. B.; Spernyak, J. A.; Morrow, J. R. *Angew. Chem. Int. Ed.* **2013,** *52*, 13997-14000.

(21) Dorazio, S. J.; Olatunde, A. O.; Spernyak, J. A.; Morrow, J. R. *Chem. Commun.* **2013,** *49*, 10025-10027.

(22) Olatunde, A. O.; Dorazio, S. J.; Spernyak, J. A.; Morrow, J. R. *J. Am. Chem. Soc.* **2012,** *134*, 18503-18505.

(23) Dorazio, S. J.; Morrow, J. R. *Inorg. Chem.* **2012,** *51*, 7448-7450.

(24) Dorazio, S. J.; Tsitovich, P. B.; Siters, K. E.; Spernyak, J. A.; Morrow, J. R. *J. Am. Chem. Soc.* **2011,** *133*, 14154-14156.

(25) Dorazio, S. J.; Morrow, J. R. *Eur. J. Inorg. Chem.* **2012,** *2012*, 2006-2014.

(26) Dorazio, S. J.; Tsitovich, P. B.; Gardina, S. A.; Morrow, J. R. *J. Inorg. Biochem.* **2012,** *117*, 212-219.

(27) Dorazio, S.; Olatunde, A.; Tsitovich, P.; Morrow, J. *J.Biol.Inorg.Chem.* **2013,** , 1-15.

(28) Allen, F. H.; Kennard, O.; Watson, D. G.; Brammer, L.; Orpen, A. G.; Taylor, R. *J. Chem. Soc. , Perkin Trans. 2* **1987,** , S1-S19.

(29) Barefield, E. K.; Busch, D. H.; Nelson, S. M. *Q. Rev. Chem. Soc.* **1968,** *22*, 457-498.

(30) Qin, J.; Laurent, S.; Jo, Y. â; Roch, A.; Mikhaylova, M.; Bhujwalla, Z. ; Muller, R.; Muhammed, M. *Adv. Mater.* **2007,** *19*, 1874-1878.

(31) Figgis, B. N. In *Introduction to Ligand Fields;* Interscience Publishers: New York, **1966**; pp 1- 351.

(32) Delgado, R.; da Silva, J. J. R. F.; Vaz, M. C. T. A. *Talanta* **1986,** *33*, 285-287.

(33) Pasha, A.; Tircsó, G.; Benyó, E. T.; Brücher, E.; Sherry, A. D. *Eur. J. Inorg. Chem.* **2007,** , 4340-4349.

(34) Da Silva, J. J. R. F.; Calado, J. C. G.; De Moura, M. L. *Talanta* **1965,** *12*, 467-473.

(35) Hilario, E.; Romero, I.; Celis, H. *J. Biochem. Biophys. Methods* **1990,** *21*, 197-207.

(36) Chaves, S.; Delgado, R.; Da Silva, J. J. R. F. *Talanta* **1992,** *39*, 249-254.

Chapter 4

4 MRI PARACEST Agents that Improve Amide-based pH Measurements by Limiting Inner Sphere Water T$_2$ Exchange

4.1 Introduction

The aim of this project was to modulate the pK_as of the amide protons and subsequently the amide CEST effect in DOTAM analogues. This was to be accomplished by synthesizing DOTAM tetraanilides that had electron-donating groups (EDGs) and electron-withdrawing groups (EWGs) in the *para* position of the aniline ring. One may expect the EWGs of the acetamide arms to make the amide protons more acidic, resulting in a faster exchange rate with the bulk water protons. On the other hand, EDGs should slow the rate of exchange of the amide protons with the bulk water protons. On account of this modulation, it was hoped these agents would be more sensitive to changes within the biologically relevant pH range, thus resulting in pH responsive PARACEST probes.

It has been previously demonstrated that the bound water exchange rate in PARACEST agents of Eu^{3+}-tetraamide complexes with one *para*-substituted aniline arm, can be modulated electronically using EDGs and EWGs.[1] A similar study involving amide protons has not yet been reported until now.[2] As a result of the interest in the CEST effect due to amide protons, the complexes synthesized here were based on Tm^{3+} and Dy^{3+}, which allowed for a larger chemical shift difference from the bulk water, in comparison to Eu^{3+}.

It was furthermore proposed that these PARACEST agents would not contain a bound water coordinated to the metal center. This is a highly feasible circumstance owing to the four aromatic rings of the acetamide pendant arms, which can provide steric bulk to the complex, thus blocking access of water to the metal center. The lack of a metal bound water would reduce signal losses due to T$_2$ relaxation. This relaxation is facilitated by T$_2$ exchange of the metal bound water with the surrounding water molecules. The impact of

this effect may be lessened by using pulse sequences such as the ultra-short echo-time (UTE) pulse.[3] It should be considered that the presence of any other exchangeable protons such as amide protons would still cause T_2 relaxation. However, the extent of relaxation will be lesser as compared to that of a metal bound water.

4.2 Results and Discussion

4.2.1 Synthesis
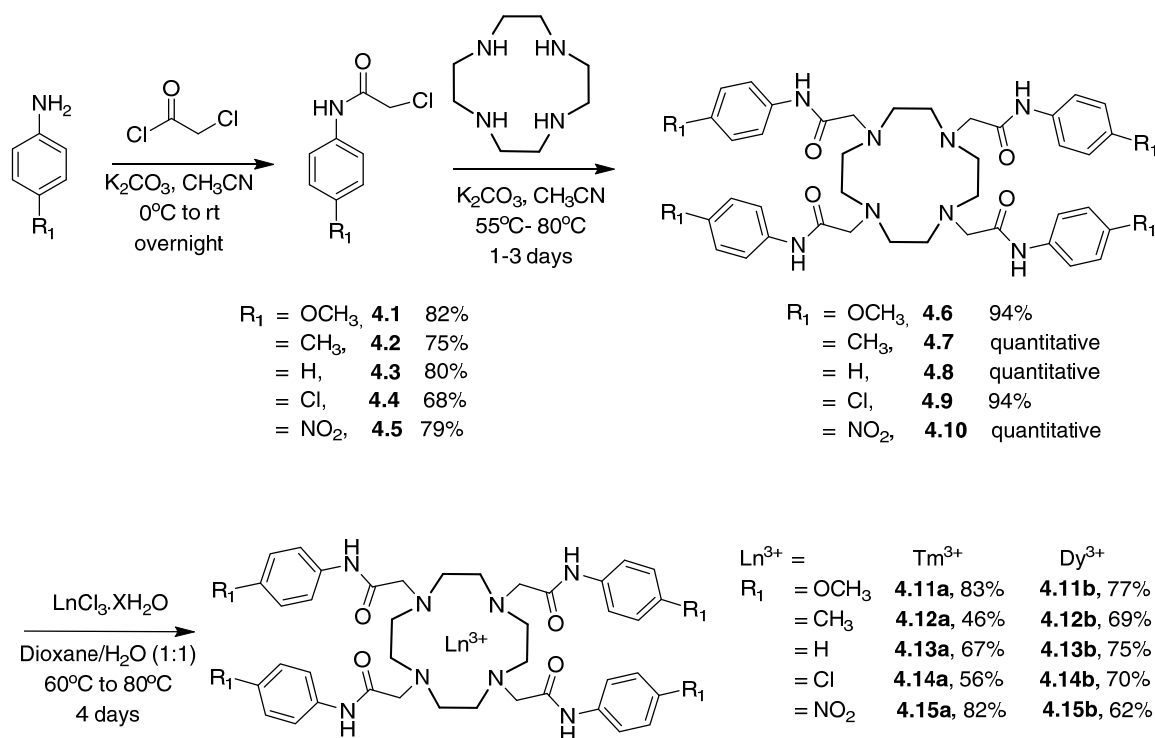
Scheme 4.1: Synthetic route to tetraanilide complexes 4.11a,b - 4.15a,b.

The electrophiles **4.1** - **4.5** were synthesized by adding chloroacetyl chloride to the appropriate aniline in CH_3CN while cooling in an ice bath in the presence of K_2CO_3 (Scheme 4.1). The reactions were stirred overnight at room temperature, then filtered and

the crude products were recrystallized from methanol. The average yield of these reactions was good (ca. 75%).

Syntheses of the tetra-substituted cyclens were performed by mixing cyclen with the appropriate electrophiles in CH_3CN in the presence of K_2CO_3. It was necessary to heat the reaction at 55 °C- 80 °C over 1-3 days to ensure complete tetraalkylation. The progress of these reactions was monitored by UPLC-MS. When the reaction was considered complete, the mixtures were cooled and the reaction mixture filtered. It was realized that the precipitates contained the desired products; therefore, they was washed with cold water to remove the K_2CO_3 and other salts. At this point, efforts to recrystallize these compounds from methanol were unsuccessful due to their highly insoluble nature. As such, the crude products were used in the next step without further purification. These tetraalkylated ligands **4.6 - 4.10** were mostly insoluble in a wide range of solvents such as MeOH, CH_3CN and H_2O.

The tetra-substituted ligands **4.6 - 4.10** were metalated using salts of Dy^{3+} and Tm^{3+} in a 1:1 H_2O/dioxane mixture at 80 °C over 4 days. The metalated complexes were subjected to dialysis against water across a membrane with a 500 Dalton molecular weight cutoff to remove salts carried through from the previous step as well as any unchelated lanthanide ion. The final products were isolated and lyophilized to give white powders, with exception of the p-NO_2 complexes **4.15a,b** being yellow powders. Identification of the metalated products was accomplished by high resolution mass spectrometry along with their UPLC trace which showed that all of the samples to be homogeneous tetra-substituted product. After metalation, solubility slightly improved for the Dy^{3+} and Tm^{3+} tetraaniline complexes of p-OMe (**4.11a,b**) and p-H (**4.13a,b**). Attempts were made to improve the solubilty of the p-NO_2 complexes **4.15a,b** for CEST analysis using Tween 20® but these were unsuccessful.

4.2.2 Crystal Structure

Figure 4.1 shows the X-ray crystal structure of Tm^{3+}-*p*-OMe complex **4.11a** with the corresponding crystallographic parameters listed in Table 4.1. The crystals were grown from slow evaporation of a concentrated solution of **4.11a** in water. In solution, DOTA-like complexes may adopt two possible coordination isomers. One isomer is the square antiprismatic (SAP) and the other is the twisted square antiprismatic (TSAP) isomer. The two isomers can be differentiated by their respective angles between the N-Ln-N and O-Ln-O planes (α). In the former geometry, that angle is ~ 40° and in the latter, is~ 30°.
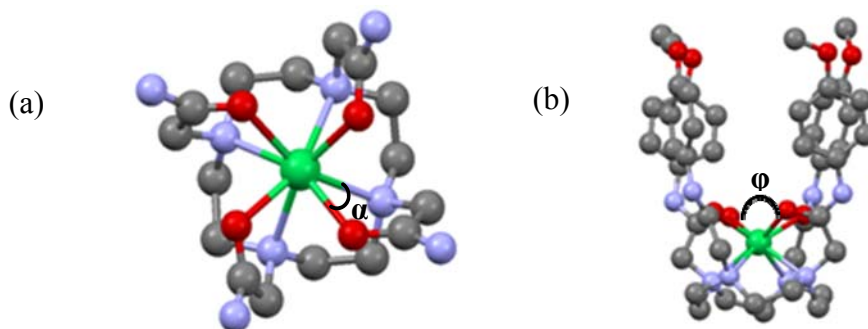
Figure 4.1: Molecular representation of the solid state structure of Tm^{3+}-*p*-OMe complex (4.11a) determined by single crystal X-ray studies. Hydrogens have been omitted for clarity. (a) Top down view of 4.11a. The aniline rings are omitted for clarity. α indicates the angle created between the planes of N–Ln–N and O–Ln–O and is listed in Table 4.2 along with selected angles and bond lengths and (b) side on view of 4.11a showing eightfold coordination of the Tm^{3+} by the nitrogens of cyclen and the oxygens of the amide pendant groups. φ denotes the trans O–Ln–O bond angle.

The solid state structure of the Tm^{3+}-*p*-OMe complex **4.11a** revealed that α was 27°, thus indicating a TSAP geometry (Figure 4.1). The structure also revealed that there was no bound water coordinated to Tm^{3+}, therefore that geometry is more correctly denoted as TSAP'. Lanthanide complexes based on the DOTA core structure, typically have eight coordination sites due to the four nitrogens of the macrocycle and the four oxygens from the pendant arms. These atoms coordinate to the metal center and the ninth coordination

site on the metal is typically occupied by a solvent molecule such as water. The distance between the centeroids of the O_4 and N_4 planes has a distance of 2.47 Å, which is comparable to other TSAP structures. This distance in SAP structures is ~2.35 Å.[4, 5] The distance between the centeroid of the four nitrogen atoms of the macrocycle and Tm^{3+} is 1.38 Å, which is shorter then a series of previously reported SAP DOTAM complexs (Dy^{3+} = 1.59 Å, Nd^{3+} = 1.66 Å, Tb^{3+} = 1.59 Å, Yb^{3+} =1.56 Å).[6]

Table 4.1: Crystal data and structure refinements for 4.11a.

Formula	$C_{44}H_{67}Cl_3N_8O_{13}Tm$
Formula Weight (*g/mol*)	1191.34
Crystal Dimensions (*mm*)	0.27 × 0.18 × 0.08
Crystal Colour and Habit	colourless prism
Crystal System	triclinic
Space Group	P -1
Temperature, K	110
a, Å	10.948(3)
b, Å	14.438(3)
c, Å	17.436(5)
α,°	77.345(10)
β,°	78.428(9)
γ,°	85.152(10)
V, Å^3	2632.1(12)
Number of reflections to determine final unit cell	9059
Min and Max 2q for cell determination,	4.88, 64.1
°Z	2
F(000)	1222
ρ (*g/cm*)	1.503
λ, Å, (MoKa)	0.71073
μ, (*cm^{-1}*)	1.904

Additionally, it was noted that the angles at the metal center (φ, O_1–Tm–O_3 and O_2–Tm–O_4) was about 123° (Table 4.2). This angle is expected to be at least 135°.[4, 7] The lower φ may be as a result of Tm^{3+} being positioned lower in the chelate cavity and the four oxygens of the carbonyl pendant arms being wrapped around the metal. This in turn blocked access to the metal by the water molecule. Taking into account that the chemical shift due of the amide CEST signal is distance dependent, the compact nature of the complex may have led to a highly shifted signal.[8]

Table 4.2: Summary of torsion angle α (°) and selected bond lengths (Å) for Tm^{3+}-*p*-OMe (4.11a).

Average α angle	26.95
N_1-C-C-O_1	12.4(3)
N_2-C-C-O_2	15.1(4)
N_3-C-C-O_3	14.7(4)
N_4-C-C-O_4	2.9(3)
N_1-Tm	2.508(2)
N_2-Tm	2.492(2)
N_3-Tm	2.469(3)
N_4-Tm	2.500(3)
O_1-Tm	2.295(2)
O_2-Tm	2.245(2)
O_3-Tm	2.313(2)
O_4-Tm	2.265(2)
φ angle O_1–Tm–O_3	123.64(7)
φ angle O_2–Tm–O_4	122.43(8)
Centeroid O_4–Tm	1.087
Centeroid N_4–Tm	1.382
Centeroid O_4–centeroid N_4	2.470

4.2.3 Magnetic Studies

CEST evaluation

As a consequence of insolubility, only the Tm^{3+} and Dy^{3+} tetraaniline complexes of *p*-OMe (**4.11a,b**) and *p*-H (**4.13a,b**) were further evaluated. CEST data for these complexes were acquired within the pH range of 6.5 to 9.0 for **4.13a,b** and the pH range of 5.1 to 8.0 for **4.11a,b** (Figure 4.2). These ranges were chosen because of the observation that the maximum CEST effect was close to pH 8.0 for the former and the latter had the maximum CEST effect between 7.0 and 7.5.

A 12% CEST signal was observed for the Tm^{3+}-*p*-H complex **4.13a**, while two signals of 17% and 12% were observed for Tm^{3+}-*p*-OMe complex **4.11a**. These signals may be attributed to the presence of the two conformational isomers in solution, that is, the SAP' and TSAP' isomers, respectively. This particular assignment was based on the previous observations for a series of DOTAM alkyl amides.[9, 10]
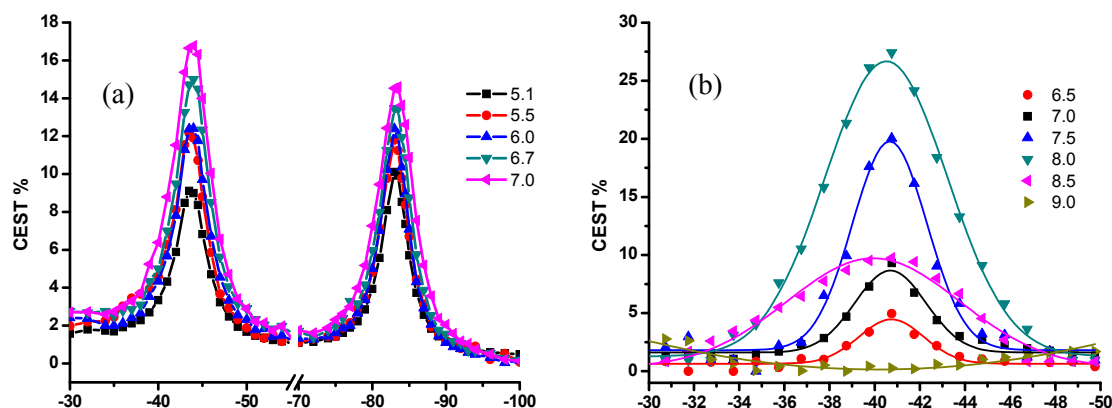
Figure 4.2: CEST spectra of (a) Tm^{3+}-*p*-OMe complex 4.11a over the pH range of 5.1–7.0 and (b) Tm^{3+}-*p*-H complex 4.13a over the pH range of 6.5–9.0. CEST spectra were acquired at 37 ^{o}C, with a 15 uT, 5 s presaturation pulse, 20 mM.

The CEST results for the Dy^{3+} tetraaniline complexes of *p*-OMe (**4.11b**) and *p*-H (**4.13b**) were more customary. While the Dy^{3+}-*p*-H complex **4.13b** still had one signal of 6%, the Tm^{3+}-*p*-OMe complex **4.11b** now had one signal of 3%. A summary of the CEST result for the Tm^{3+} and Dy^{3+} tetraaniline complexes of *p*-OMe (**4.11a,b**) and *p*-H (**4.13a,b**) are shown in Table 4.3.

Table 4.3: CEST % measured at pH 7, 37 °C, 20 mM with a 15 µT, 5 s continuous wave saturation pulse.

Agent	ppm (δ)	CEST %
4.11a	-43	17%
	-83	12%
4.13a	-41	12%
4.11b	74	3%
4.13b	70	6%
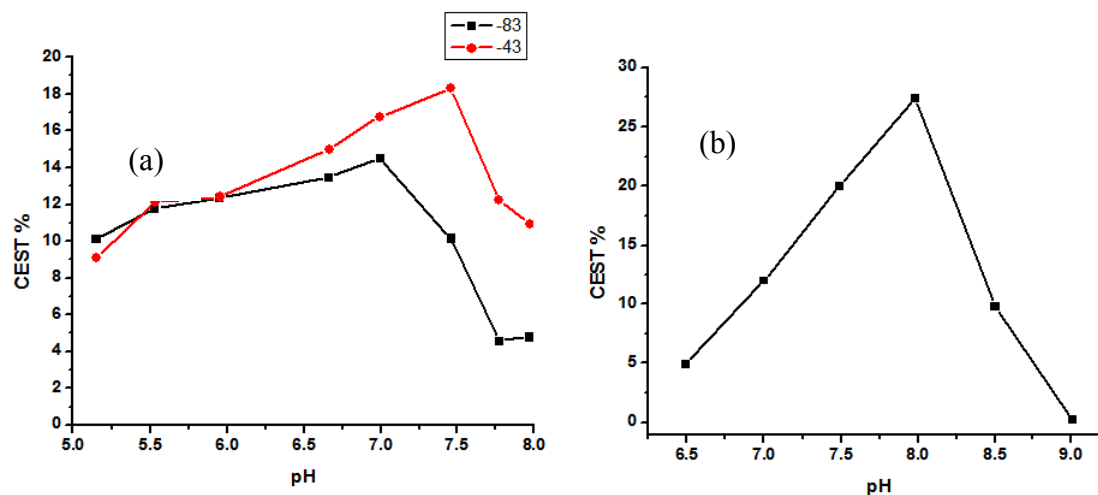
Figure 4.3: Maximum CEST effect as a function of pH (a) Tm^{3+}-*p*-OMe complex 4.11a shows a pH maximum at 7.5 for the signal at -43 ppm and at 7.0 for the signal at -83 ppm and (b) Tm^{3+}-*p*-H complex 4.13a shows a pH maximum at 8.0.

Figure 4.3 shows the changes in the CEST effect of agents Tm^{3+}-*p*-OMe complex **4.11a** and Tm^{3+}-*p*-H complex **4.13a** as a function of the pH ranges measured. The signal for the **4.11a** SAP' amide (-43 ppm) has a maximum signal at pH 7.5 compared to the TSAP' amide (-83 ppm) with its maximum signal at a slightly more acidic pH of 7.0. A similar effect has been previously reported for DOTAM agents, in which the signal having the greater chemical shift displayed a maximum CEST signal at lower pH, in comparison to the signal with a smaller chemical shift.[11]

The presence of the two signals seen for the Tm^{3+}-*p*-OMe complex **4.11a** was encouraging for ratiometric analysis. A ratiometric approach would eliminate the CEST effect dependency on concentration, thus allowing the agent to be used as a biological reporter.[12, 13] Unfortunately, preliminary results from the ratiometric studies indicated that this cannot be avoided. The CEST response for this complex between pH 6 and 7 seemed to be concentration dependent, which is highly likely due to the solubility issues. At high concentrations, **4.11a** is very insoluble but at lower concentrations, the solubility improves. These discrepancies preclude the use of this agent for ratiometric purposes.

Relaxometric studies

Table 4.4: r_1 and r_2 values of the Tm^{3+} based agents at 37 °C, pH 7.

Agent	r_1 (s^{-1} mM^{-1})	r_2 (s^{-1} mM^{-1})
Tm^{3+}-*p*-OMe (**4.11a**)	0.05	0.36
Tm^{3+}-*p*-H (**4.13a**)	0.06	0.67

The lack of a bound water in the Tm^{3+}-*p*-OMe complex **4.11a** should be advantageous in amide- based PARACEST imaging as water exchange contributing to the T$_2$ shortening mechanism has been eliminated. As mentioned earlier, the exchange of amide protons of the acetamide pendant arm still contributes to the T$_2$ relaxation of bulk water. However, the extent to which this happens is less compared to the highly shifted bound water (δ = 500 ppm).[14] The associated r_1 and r_2 values for Tm^{3+}-*p*-OMe (**4.11a**) and Tm^{3+}-*p*-H (**4.13a**) are provided in Table 4.4. The low values shown are representative of the lack of an inner sphere water molecule in these complexes. Moreover, Tm^{3+} is not known to act as a T$_1$ relaxation enhancer; therefore, it is not surprising that they did not produce a strong T$_1$ relaxation of the bulk water.[15]

4.3 Conclusions

A series of Dy^{3+} and Tm^{3+} *para*-substituted tetraaniline contrast agents were synthesized for the testing of their ability to respond to pH changes in the physiological pH range. Poor solubility of many of the compounds limited the possible measurements and prevented the complete analysis of structure and effects. As such, a proper analysis of the electronic effects on the pK_as of the amide protons could not be performed. Four of the compounds were soluble enough for further investigation. It was observed that the unsubstituted anilines (Dy^{3+} and Tm^{3+}-*p*-H) had a maximum CEST effect at a pH near 8, while the maximum CEST effect for both the Dy^{3+} and Tm^{3+}-*p*-OMe agents was between pH 7 - 7.5. A crystal structure indicated that the geometry of Tm^{3+}-*p*-OMe complex is TSAP', which potentially leads to the highly shifted signal at -83 ppm. A signal for a Tm^{3+} agent above 100 ppm has been previously observed,[10] but due to the inability to

grow a crystal suitable for analysis by X-ray crystallography, the presence of an inner sphere water cannot be determined. A concentration and pH study was attempted to determine if the Tm^{3+}-*p*-OMe complex could be used as a ratiometric agent to measure pH *in vivo*, independent of concentration, but due to solubility limitations, no suitable measurements could be performed. With the lack of inner sphere water, the Tm^{3+} aniline agents may produce appreciable amide CEST contrast without decreasing image signal intensity due to lowering of the bulk water T_2 relaxation time constant.

4.4   Supplemental Information

4.4.1 General Experimental

General synthetic details can be found in Appendix 1.

CEST and Relaxivity Experiments

All samples were studied at 20 mM concentration, 37 °C. CEST spectra (Tm^{3+} and Dy^{3+}) were acquired using a 15µT, 5s continuous wave presaturation pulse at offset frequencies ranging from -100 to 100 ppm in steps of 1 ppm. T_1 relaxation time constant measurements were made for 4 different concentrations (1, 2, 4, 8 mM) of CA using an inversion recovery sequence (10 inversion times in the range of 10 ms – 10 s) with a 20 second repetition time to ensure full recovery, pH 7 and 37 °C. T_2 relaxation time constant measurements were made for 4 different concentrations (1, 2, 4, 8 mM) of CA using a CPMG pulse sequence (10 train echo times in the range of 10 ms – 10 s) with a 20 second repetition time to ensure full recovery, pH 7 and 37 °C.

4.4.2 Synthetic Procedures

General procedure for synthesis of *N*-aryl-chloroacetamides. Anilines **4.1** - **4.5** (7.84 mmol) and K_2CO_3 (15.68 mmol) were suspended in CH_3CN (50 mL) and cooled to 0°C in an ice bath while stirring. Chloroacetyl chloride (15.68 mmol) was added dropwise and

reaction mixture warmed to room temperature and left stirring overnight. Reaction mixture was filtered and the filtrate collected and concentrated. The residue was recrytallized from hot CH_3OH.
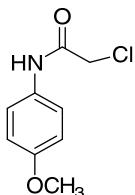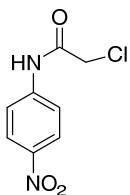
2-Chloro-N-(4-methoxyphenyl)acetamide (4.1). The title compound was obtained as silver crystals (1.29 g, 82%) ^{1}H NMR (400 MHz, DMSO-d$_6$): δ 10.17 (1H, s); 7.51 (2H, d, J = 8.6 Hz); 6.90 (2H, d, J = 8.6 Hz); 4.22 (2H, s); 3.72 (3H, s). ^{13}C NMR (100 MHz, DMSO-d$_6$): δ 164.5, 156.0, 132.0, 121.4, 114.3, 55.6. 43.9. ESI-TOF m/z calcd for $C_9H_{11}ClNO_2$ (M+H)$^+$, calculated 200.0478, found 200.0477.
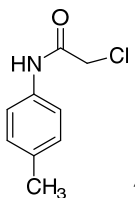
2-Chloro-N-(p-tolyl)acetamide (4.2). The title compound was obtained as white crystals (1.08 g, 75%) ^{1}H NMR (400 MHz, DMSO-d$_6$): δ 10.21 (1H, s); 7.50 (2H, d, J = 7.4 Hz); 7.13 (2H, d, J = 7.4 Hz); 4.24 (2H, s); 2.26 (3H, s). ^{13}C NMR (100 MHz, DMSO-d$_6$): δ 164.8, 136.4, 133.2, 129.6, 119.8, 44.0, 20.8. ESI-TOF m/z calcd for $C_9H_{11}ClNO$ (M+H)$^+$, calculated 184.0529, found 184.0524.
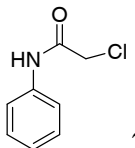
2-Chloro-N-phenylacetamide (4.3). The title compound was obtained as white crystals (1.06 g, 80%) ^{1}H NMR (400 MHz, DMSO-d$_6$): δ 10.36 (1H, s); 7.60 (2H, d, J = 7.4 Hz); 7.33 (2H, t, J =7.4 Hz); 7.08 (1H, t, J = 7.4 Hz); 4.26 (2H, s,). ^{13}C NMR (100

MHz, DMSO-d$_6$): δ 165.0, 138.9, 129.2, 124.2, 119.8, 44.0. ESI-TOF *m/z* calcd for C$_8$H$_9$ClNO (M+H)$^+$, calculated 170.0373, found 170.0366.
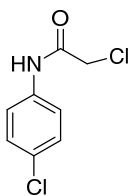

2-Chloro-N-(4-chlorophenyl)acetamide (4.4). The title compound was obtained as white crystals (1.08 g, 68%) ^{1}H NMR (400 MHz, DMSO-d$_6$): δ 10.43 (1H, s); 7.62 (2H, d, *J* = 8.6 Hz); 7.38 (2H, d, *J* = 8.6 Hz); 4.26 (2H, s). ^{13}C NMR (100 MHz, DMSO-d$_6$): δ 165.2, 137.8, 129.2, 127.9, 121.3, 43.9. ESI-TOF *m/z* calcd for C$_8$H$_8$Cl$_2$NO (M+H)$^+$, calculated 203.9983, found 203.9983.

2-Chloro-N-(4-nitrophenyl)acetamide (4.5). The title compound was obtained as yellow crystals (1.80 g, 79%) ^{1}H NMR (400 MHz, DMSO-d$_6$): δ 10.97 (1H, s); 8.22 (2H, d, *J* = 9.0 Hz); 7.84 (2H, d, *J* = 9.0 Hz); 4.35 (2H, s). ^{13}C NMR (100 MHz, DMSO-d$_6$): δ 166.0, 145.0, 143.0, 125.4, 119.5, 44.0. ESI-TOF *m/z* calcd for C$_8$H$_8$ClN$_2$O$_3$ (M+H)$^+$, calculated 215.0223, found 215.0220.

General procedure for synthesis of tetrakis-*N*-aryl-acetamides. 1,4,7,10-tetraazacyclododecane (cyclen), (0.5 mmol) and K$_2$CO$_3$ (2.25 mmol) were suspended in CH$_3$CN (12 mL) and acetamides **4.1 - 4.5** (2.25 mmol) dissolved in CH$_3$CN (3 mL) were added. The reaction mixture was heated to 55°C-80°C and left for 1-3 days. Reaction mixture was filtered and the precipitate washed with H$_2$O then collected and dried.
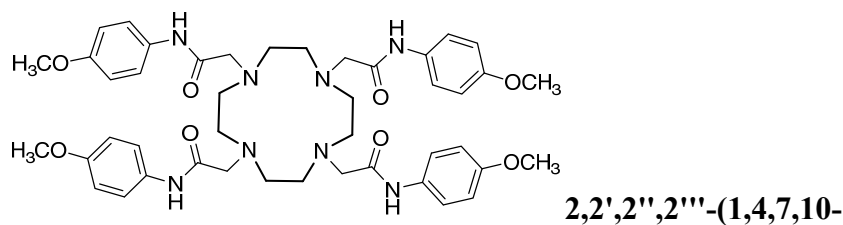
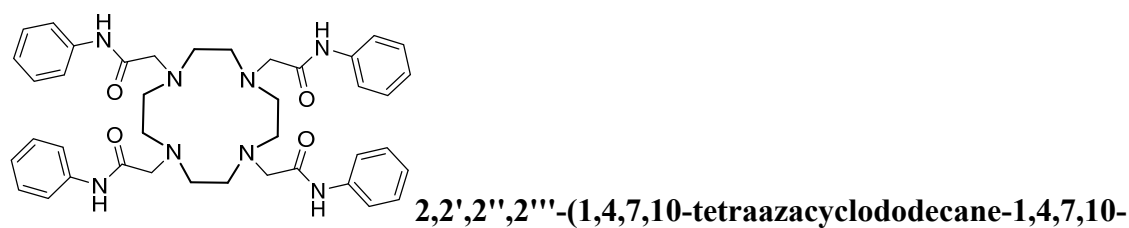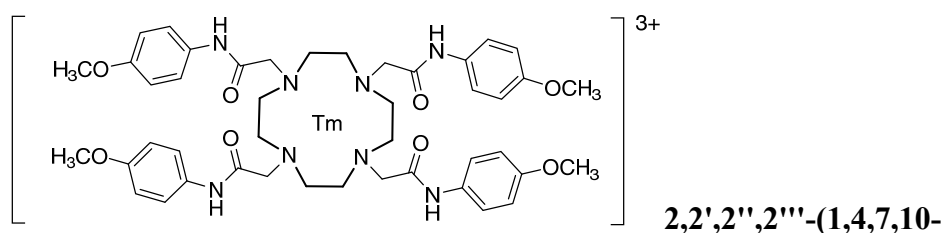**2,2',2'',2'''-(1,4,7,10-tetraazacyclododecane-1,4,7,10-tetrayl)tetrakis(N-(4-methoxyphenyl)acetamide) (4.6)**. The title compound was obtained as a white powder (0.389 g, 94%) ^{1}H NMR (400 MHz, DMSO-d$_6$): 10.04 (4H, broad s); 7.51 (8H, s); 6.80 (8H, s); 3.68 (16H, s,); 3.25 (12H, s); 2.84 (8H, broad s). ^{13}C NMR (100 MHz, DMSO-d$_6$): δ 168.8, 155.1, 131.7, 120.8, 113.6, 58.1, 55.0, 52.0. ESI-TOF *m/z* calcd for C$_{44}$H$_{57}$N$_8$O$_8$ (M+H)$^+$, calculated 825.4299, found 825.4284.
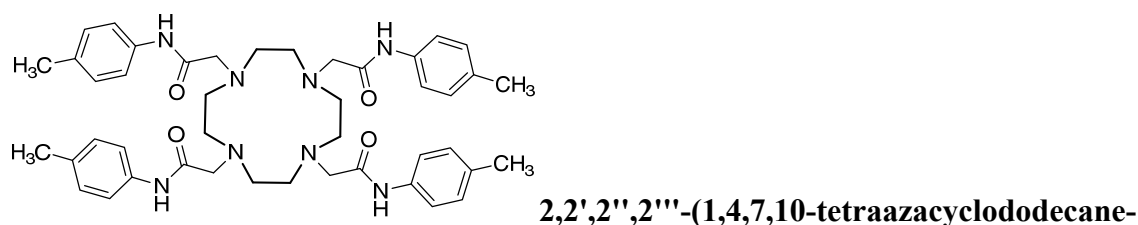
2,2',2'',2'''-(1,4,7,10-tetraazacyclododecane-1,4,7,10-tetrayl)tetrakis(N-(p-tolyl)acetamide) (4.7). The title compound was obtained as a white powder (0.375 g, quantitative) ^{1}H NMR (400 MHz, DMSO-d$_6$): δ 10.05 (4H, broad s); 7.47 (8H, d, *J* = 6.6 Hz); 7.03 (8H, d, *J* = 6.6 Hz); 3.26 (16H, s); 2.82 (8H, broad s); 2.22 (12H, s). ^{13}C NMR (100 MHz, DMSO-d$_6$): δ 169.0, 135.9, 131.9, 128.7, 119.3, 58.1, 52.3, 20.1. ESI-TOF *m/z* calcd for C$_{44}$H$_{57}$N$_8$O$_4$ (M+H)$^+$, calculated 761.4503, found 761.4529.
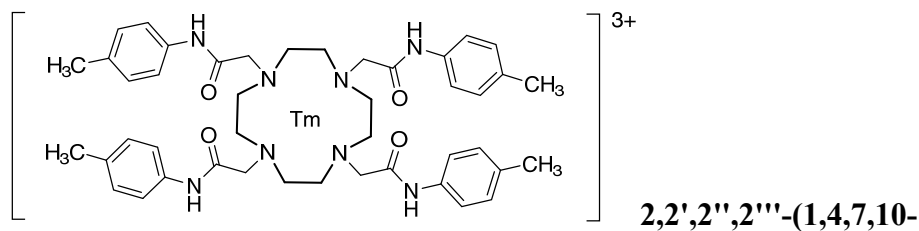

2,2',2'',2'''-(1,4,7,10-tetraazacyclododecane-1,4,7,10-tetrayl)tetrakis(N-phenylacetamide) (4.8). The title compound was obtained as a white powder (0.348 g, quantitative) ^{1}H NMR (400 MHz, DMSO-d$_6$): δ 10.32 (4H, broad s);

7.61 (8H, d, J = 7.8 Hz); 7.22 (8H, t, J =7.8 Hz); 7.01 (4H, t, J = 7.8 Hz); 3.38 (16H, s); 2.81 (8H, broad s). ^{13}C NMR (100 MHz, DMSO-d$_6$): δ 169.3, 138.5, 128.3, 123.0, 119.3, 58.1, 51.9. ESI-TOF m/z calcd for C$_{40}$H$_{49}$N$_8$O$_4$ (M+H)$^+$, calculated 705.3877, found 705.399.
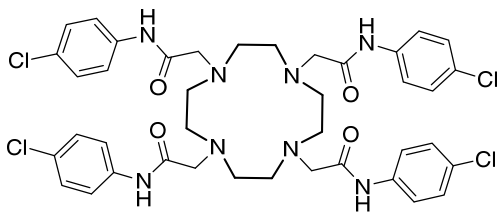
2,2',2'',2'''-(1,4,7,10-tetraazacyclododecane-1,4,7,10-tetrayl)tetrakis(N-(4-chlorophenyl)acetamide) (4.9). The title compound was obtained as a white powder (0.394 g, 94%)^{1}H NMR (400 MHz, DMSO-d$_6$): δ δ 10.6 (4H, broad s); 7.64 (8H, d, J = 8.8 Hz); 7.26 (8H, d, J = 8.8 Hz); 3.37 (16H, s); 2.78 (8H, broad s). ^{13}C NMR (100 MHz, DMSO-d$_6$): δ 169.5, 137.4, 128.1, 126.6, 120.8, 57.8, 51.7. ESI-TOF m/z calcd for C$_{40}$H$_{45}$Cl$_4$N$_8$O$_4$ (M+H)$^+$, calculated 841.2318, found 841.2325.
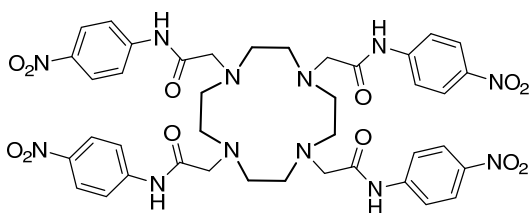
2,2',2'',2'''-(1,4,7,10-tetraazacyclododecane-1,4,7,10-tetrayl)tetrakis(N-(4-nitrophenyl)acetamide) (4.10). The title compound was obtained as a yellow powder (0.437 g, quantitative) ^{1}H NMR (400 MHz, DMSO-d$_6$): δ 10.69 (4H, broad s); 8.10 (8H, s); 7.81 (8H, s); 3.39 (16H, s); 2.87 (8H, broad s). ^{13}C NMR (100 MHz, DMSO-d$_6$): δ 170.2, 144.5, 142.0 124.3, 118.7, 57.7, 52.0. ESI-TOF m/z calcd for C$_{40}$H$_{45}$N$_{12}$O$_{12}$ (M+H)$^+$, calculated 885.3280, found 885.3254.

General procedure for synthesis of metalated compounds. Compounds **4.6 - 4.10** (0.07 mmol) were dissolved (or suspended) in dioxane/H_2O (1:1) (4 mL total) then the appropriate lanthanide chloride salts (0.07 mmol) added. The pH was adjusted to 6 and the reaction mixture heated to 60-80°C and left for 1 - 4 days. The crude was dialysed for 3 days then lyophilized to obtain desired products.
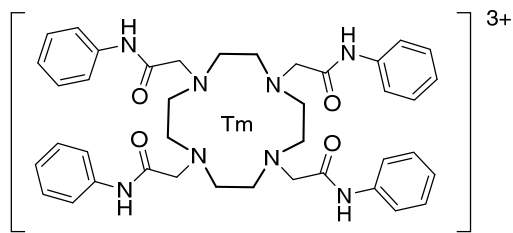

2,2',2'',2'''-(1,4,7,10-tetraazacyclododecane-1,4,7,10-tetrayl)tetrakis(N-(4-methoxyphenyl)acetamide), thulium(III) salt (4.11a). The title compound was obtained as a white powder (58 mg, 83%). ESI-TOF *m/z* calcd for $C_{44}H_{54}N_8O_8Tm$ (M-2H)$^+$, calculated 991.3407, found 991.3387.
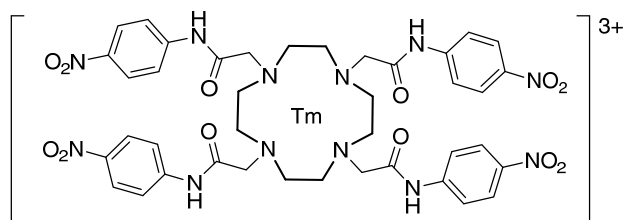

2,2',2'',2'''-(1,4,7,10-tetraazacyclododecane-1,4,7,10-tetrayl)tetrakis(N-(p-tolyl)acetamide), thulium(III) salt (4.12a). The title compound was obtained as a white powder (30 mg, 46%). ESI-TOF *m/z* calcd for $C_{44}H_{54}N_8O_4Tm$ (M-2H)$^+$, calculated 927.3610, found 927.3647.

2,2',2'',2'''-(1,4,7,10-tetraazacyclododecane-1,4,7,10-tetrayl)tetrakis(N-phenylacetamide), thulium(III) salt (4.13a). The title compound was obtained as a white powder (41 mg, 67%). ESI-TOF *m/z* calcd for $C_{40}H_{46}N_8O_4Tm$ (M-2H)$^+$, calculated 871.2984, found 871.2974.
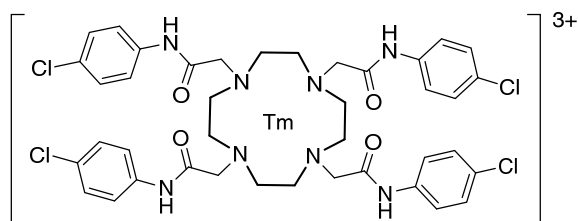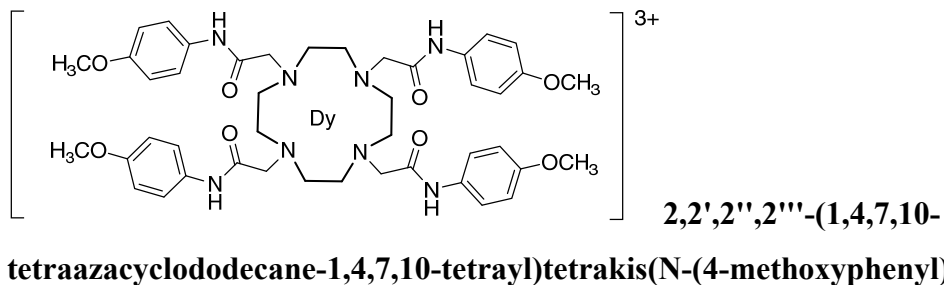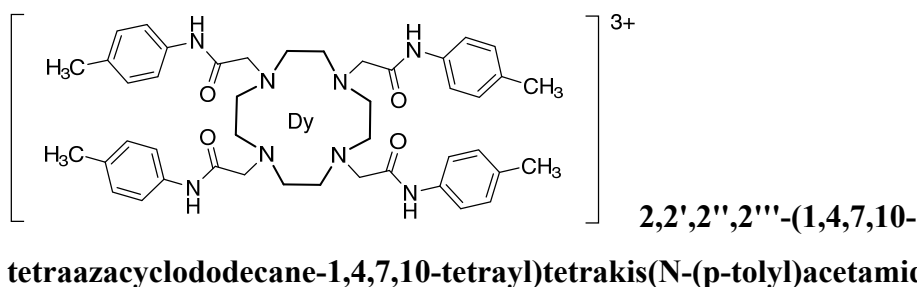

2,2',2'',2'''-(1,4,7,10-tetraazacyclododecane-1,4,7,10-tetrayl)tetrakis(N-(4-chlorophenyl)acetamide), thulium(III) salt (4.14a). The title compound was obtained as a white powder (40 mg, 56%). ESI-TOF *m/z* calcd for $C_{40}H_{42}Cl_4N_8O_4Tm$ (M-2H)$^+$, calculated 1007.1425, found 1007.1412.
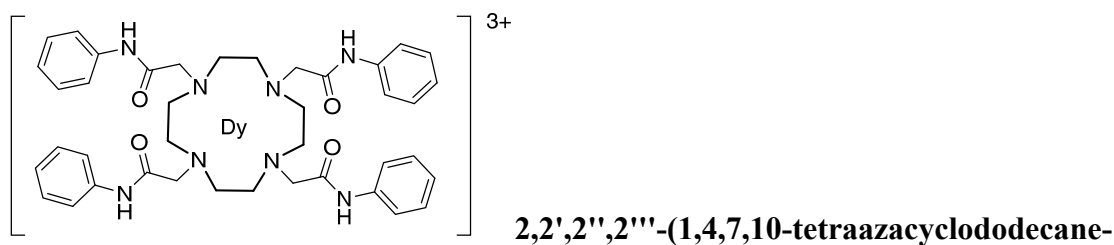

2,2',2'',2'''-(1,4,7,10-tetraazacyclododecane-1,4,7,10-tetrayl)tetrakis(N-(4-nitrophenyl)acetamide), thulium(III) salt (4.15a). The title compound was obtained as a yellow powder (61mg, 82%). ESI-TOF *m/z* calcd for $C_{40}H_{42}N_{12}O_{12}Tm$ (M-2H)$^+$, calculated 1051.2387, found 1051.2408.
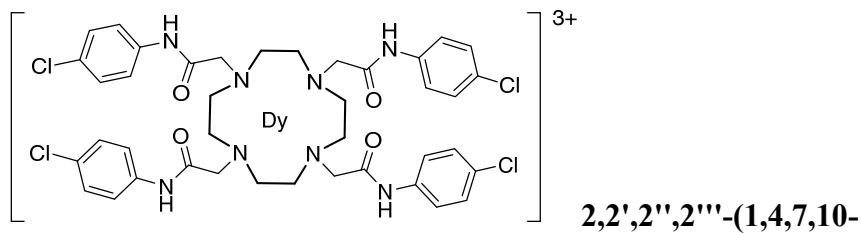
2,2',2'',2'''-(1,4,7,10-tetraazacyclododecane-1,4,7,10-tetrayl)tetrakis(N-(4-methoxyphenyl)acetamide), dysprosium(III) salt (4.11b). The title compound was obtained as a white powder (53 mg, 77%). ESI-TOF *m/z* calcd for $C_{44}H_{54}N_8O_8Dy$ (M-2H)$^+$, calculated 986.3356, found 986.3383.

2,2',2'',2'''-(1,4,7,10-tetraazacyclododecane-1,4,7,10-tetrayl)tetrakis(N-(p-tolyl)acetamide), dysprosium(III) salt (4.12b). The title compound was obtained as a white powder (43 mg, 69%). ESI-TOF *m/z* calcd for $C_{44}H_{54}N_8O_4Dy$ (M-2H)$^+$, calculated 922.3560, found 922.3586.
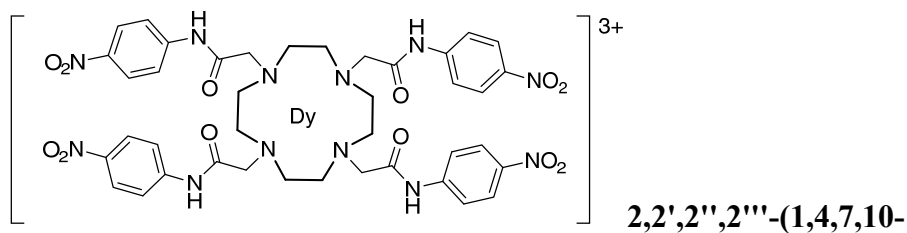

2,2',2'',2'''-(1,4,7,10-tetraazacyclododecane-1,4,7,10-tetrayl)tetrakis(N-phenylacetamide), dysprosium(III) salt (4.13b). The title compound was obtained as a white powder (45 mg, 75%). ESI-TOF *m/z* calcd for $C_{40}H_{46}N_8O_4Dy$ (M-2H)$^+$, calculated 866.934, found 866.2903.

**2,2',2'',2'''-(1,4,7,10-tetraazacyclododecane-1,4,7,10-tetrayl)tetrakis(N-(4-chlorophenyl)acetamide), dysprosium(III) salt (4.14b).** The title compound was obtained as a white powder (49 mg, 70%). ESI-TOF *m/z* calcd for $C_{40}H_{42}Cl_4N_8O_4Dy$ (M-2H)$^+$, calculated 1002.1375, found 1002.1343.
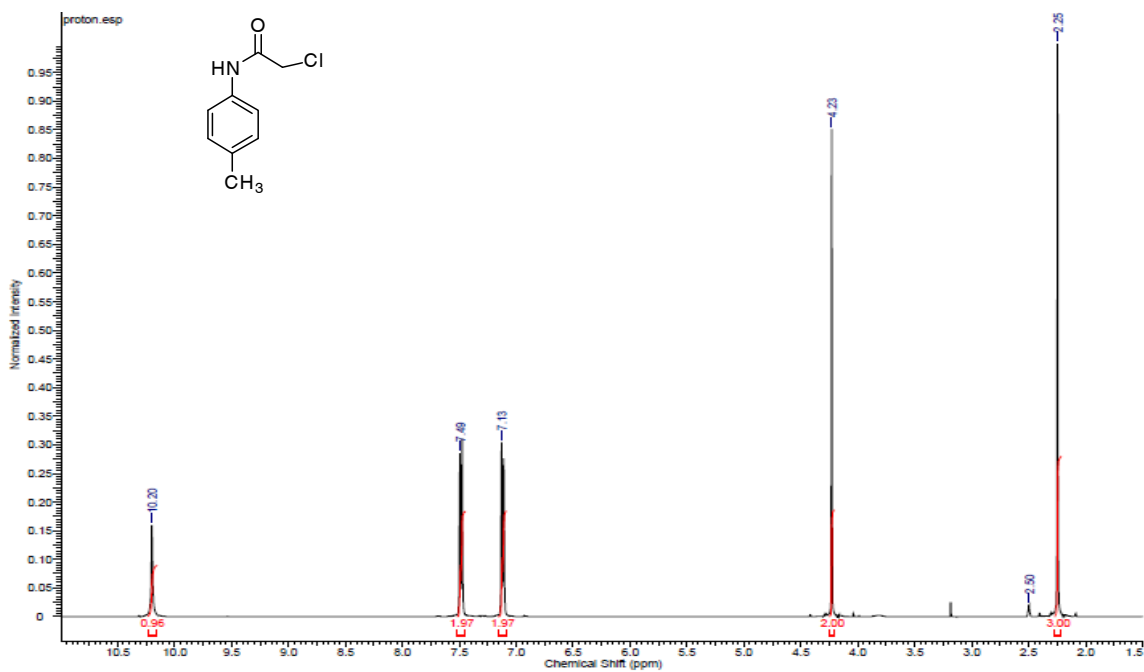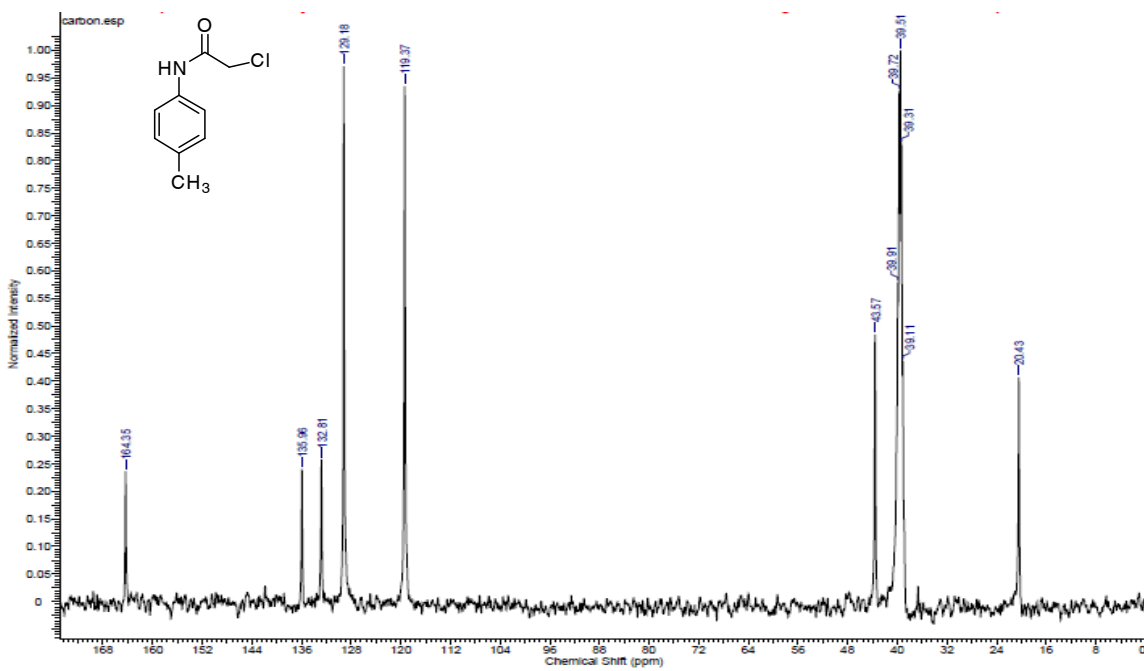

**2,2',2'',2'''-(1,4,7,10-tetraazacyclododecane-1,4,7,10-tetrayl)tetrakis(N-(4-nitrophenyl)acetamide), dysprosium(III) salt (4.15b)**. The title compound was obtained as a yellow powder (45 mg, 62%). ESI-TOF *m/z* calcd for $C_{40}H_{42}N_{12}O_{12}Dy$ (M-2H)$^+$, calculated 1046.2337, found 1046.2336.

4.4.3 Spectra

S 4.1: ^{1}H-NMR Spectrum of **4.1**
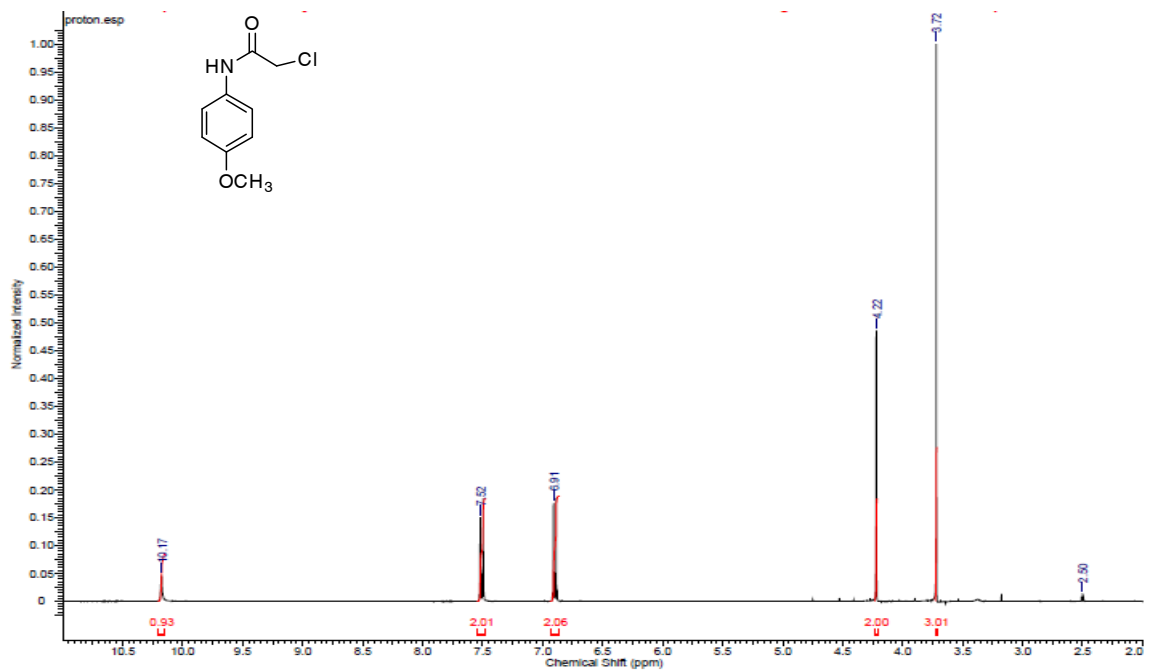
S 4.2: ^{13}C-NMR Spectrum of **4.1**
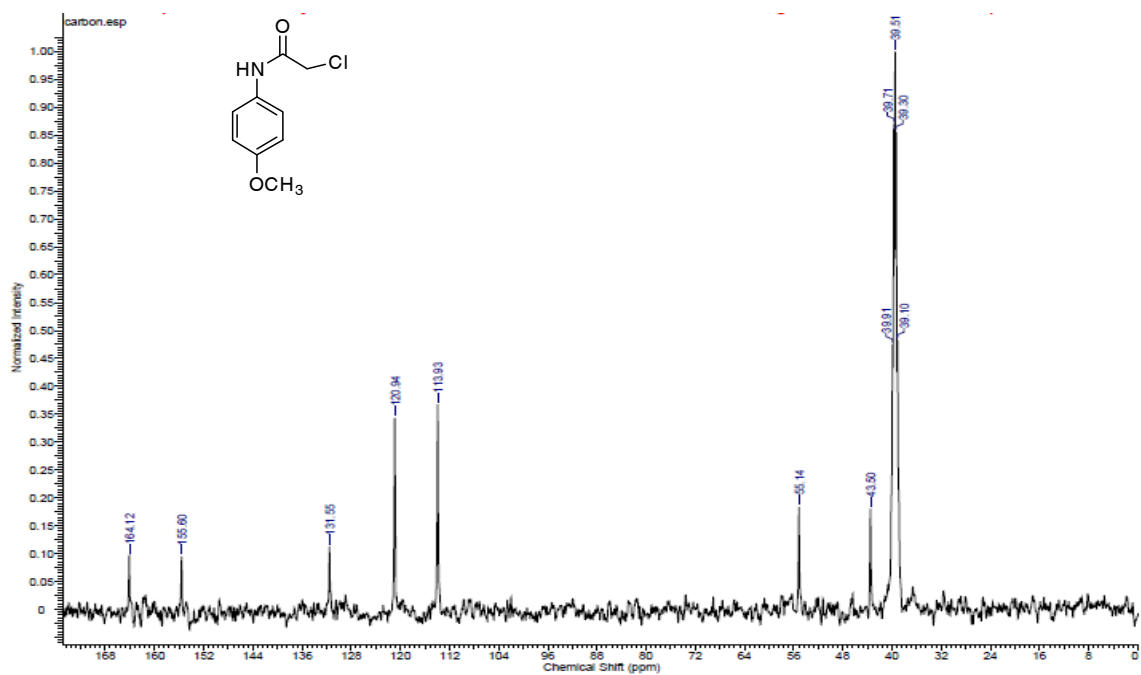
S 4.3: ^{1}H-NMR Spectrum of **4.2**

S 4.4: ^{13}C-NMR Spectrum of **4.2**

S 4.5: ^{1}H-NMR Spectrum of **4.3**
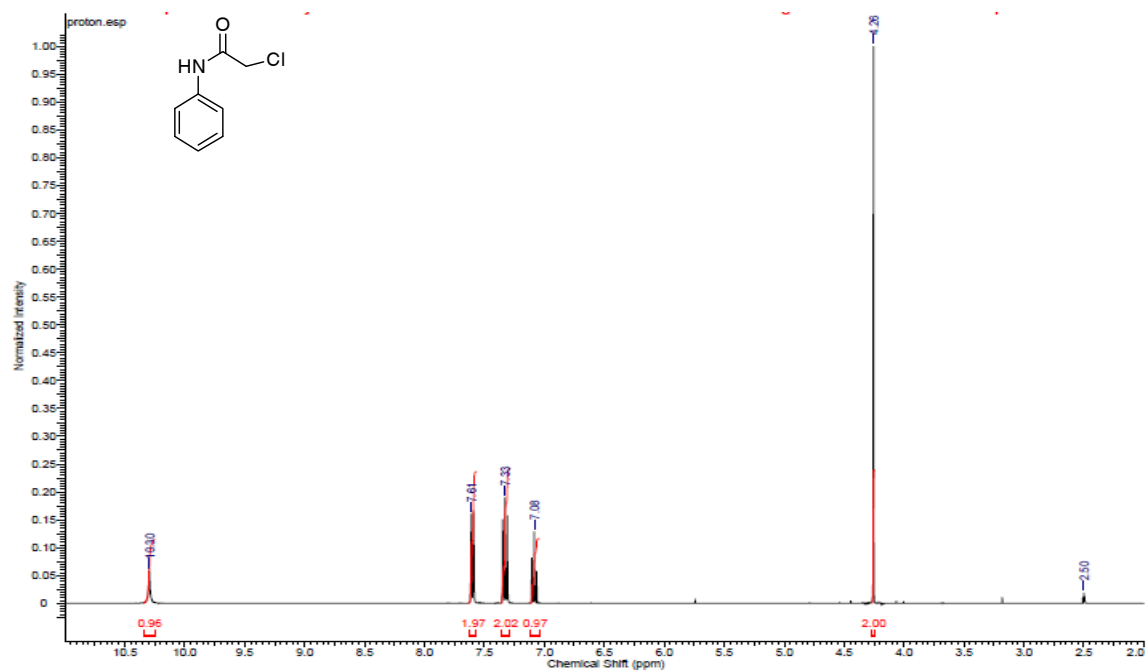
S 4.6: ^{13}C-NMR Spectrum of **4.3**
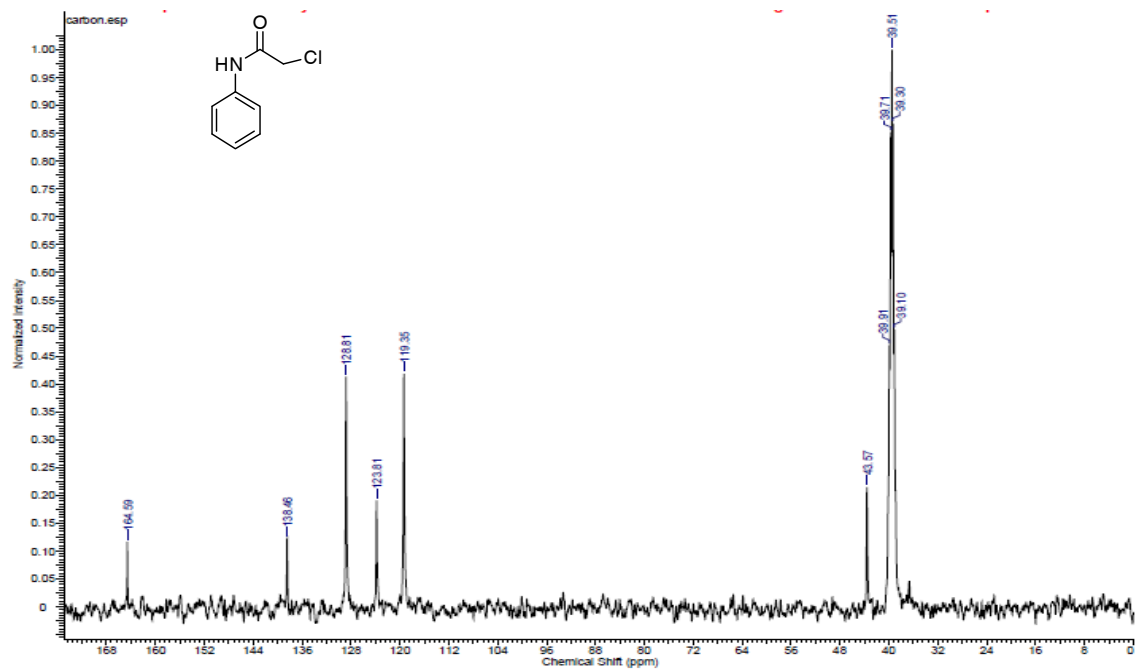
S 4.7: ¹H-NMR Spectrum of **4.4**
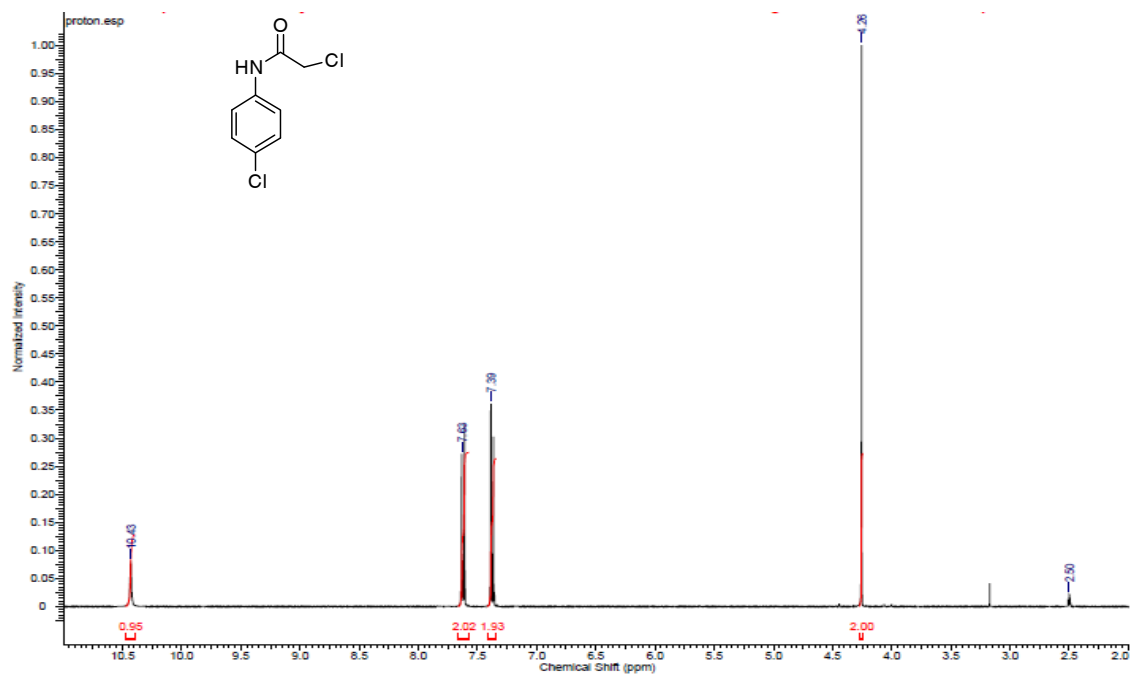
S 4.8: ¹³C-NMR Spectrum of **4.4**
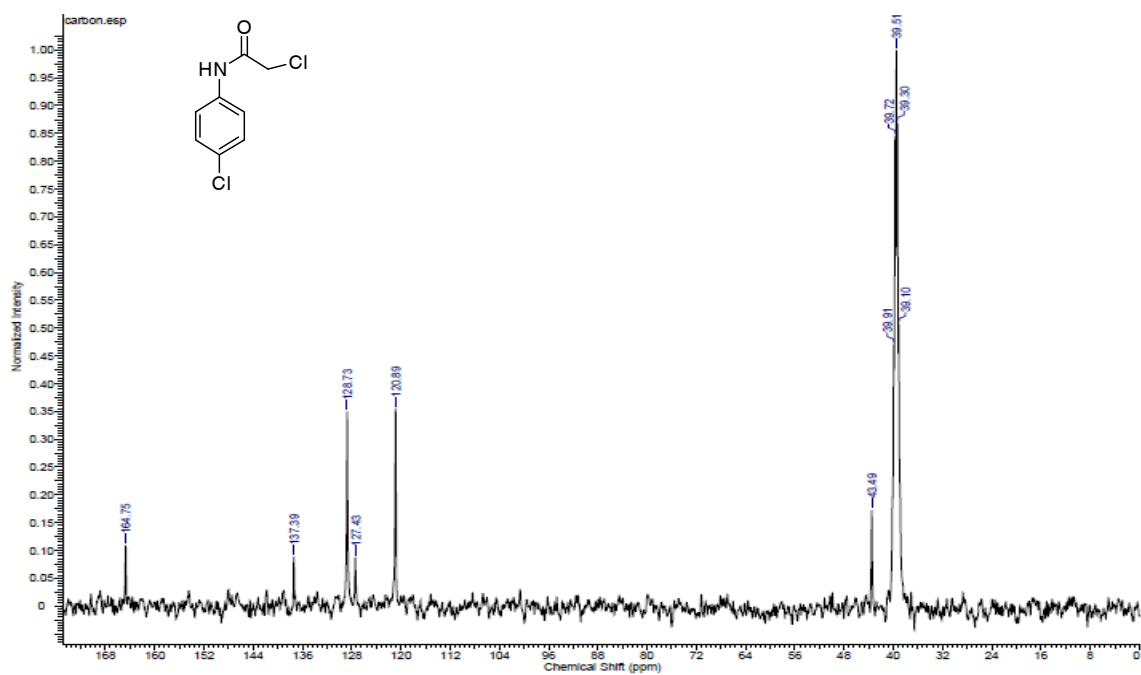
S 4.9: ^{1}H-NMR Spectrum of **4.5**
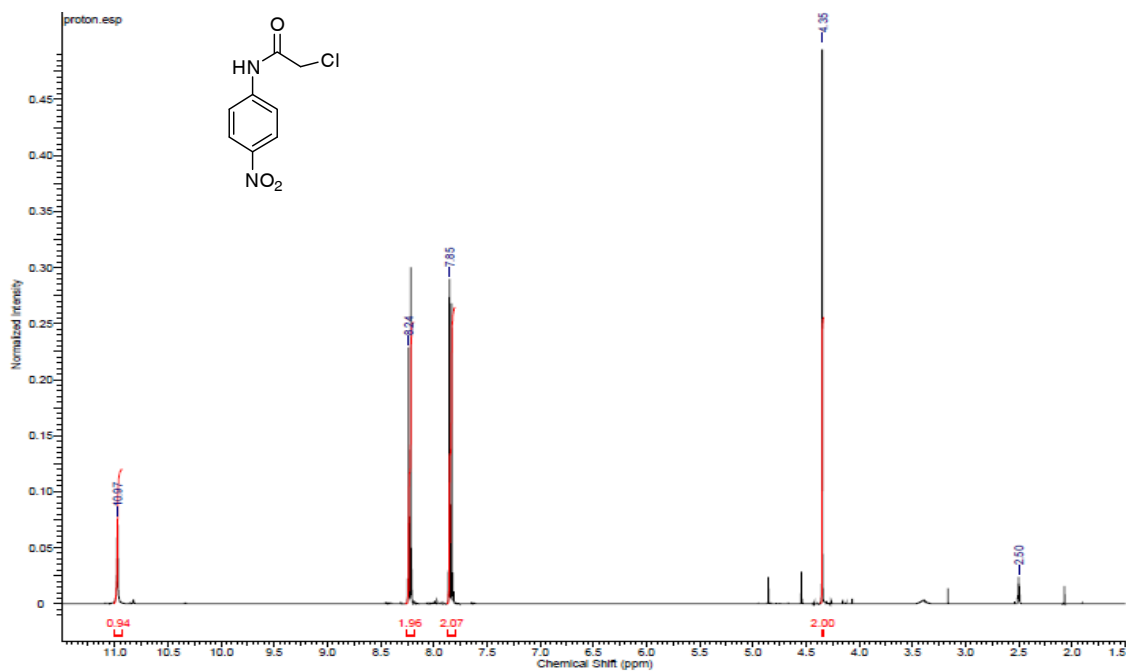
S 4.10: ^{13}C-NMR Spectrum of **4.5**
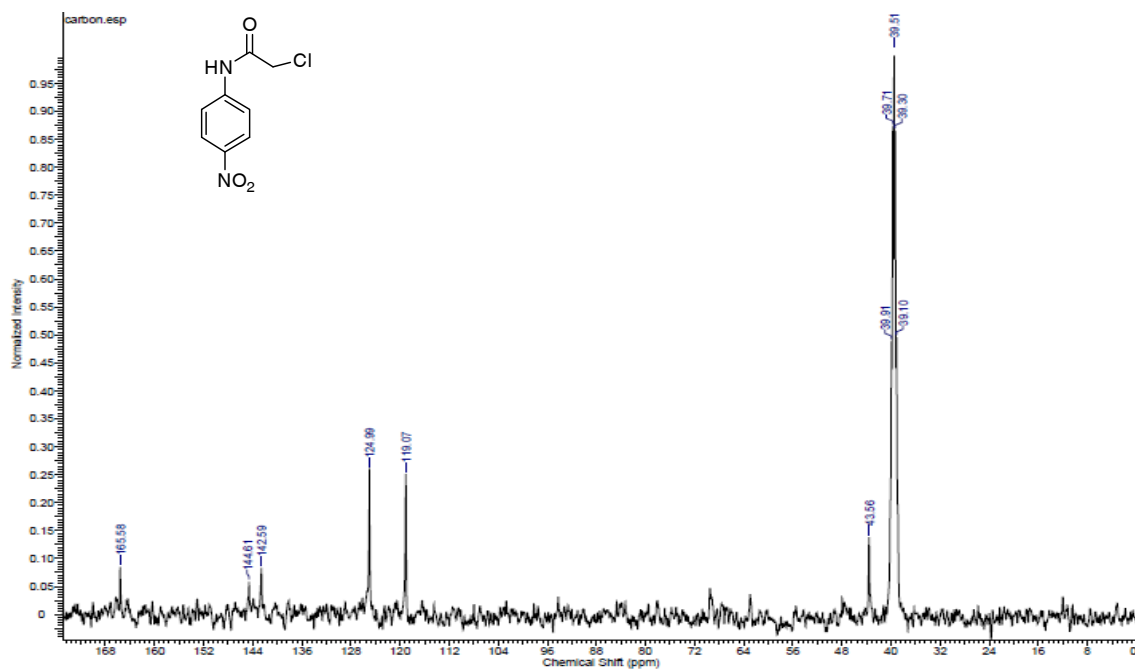
S 4.11: ^{1}H-NMR Spectrum of **4.6**
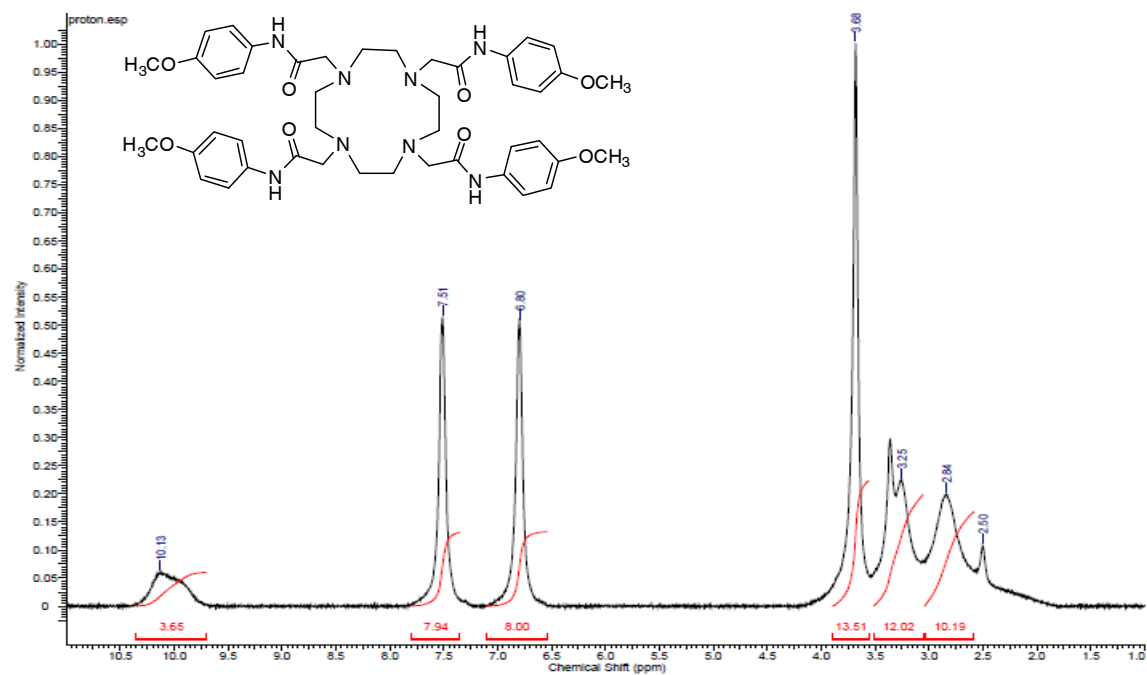
S 4.12: ^{13}C-NMR Spectrum of **4.6**
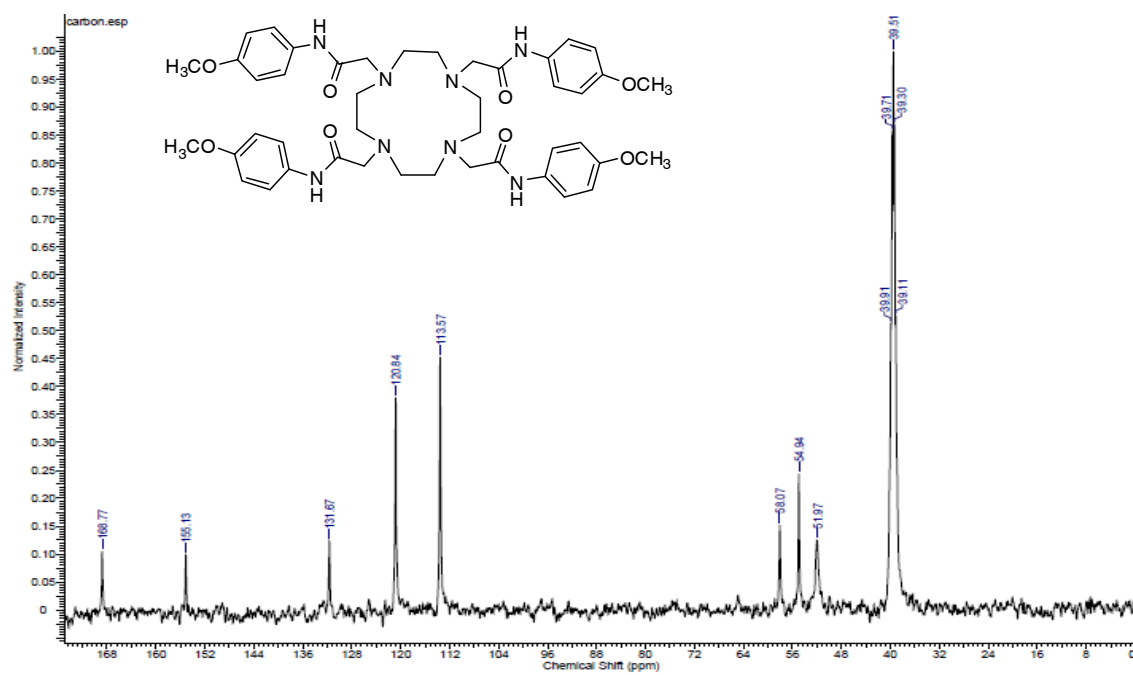
S 4.13: ¹H-NMR Spectrum of **4.7**
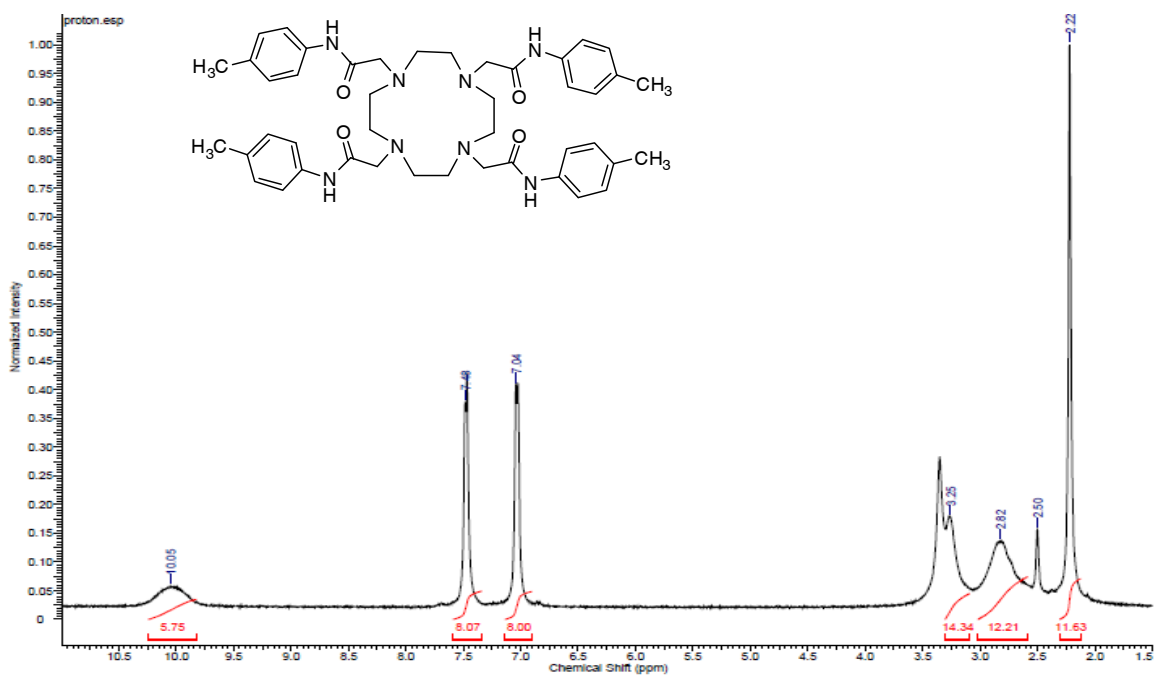
S 4.14: ¹³C-NMR Spectrum of **4.7**
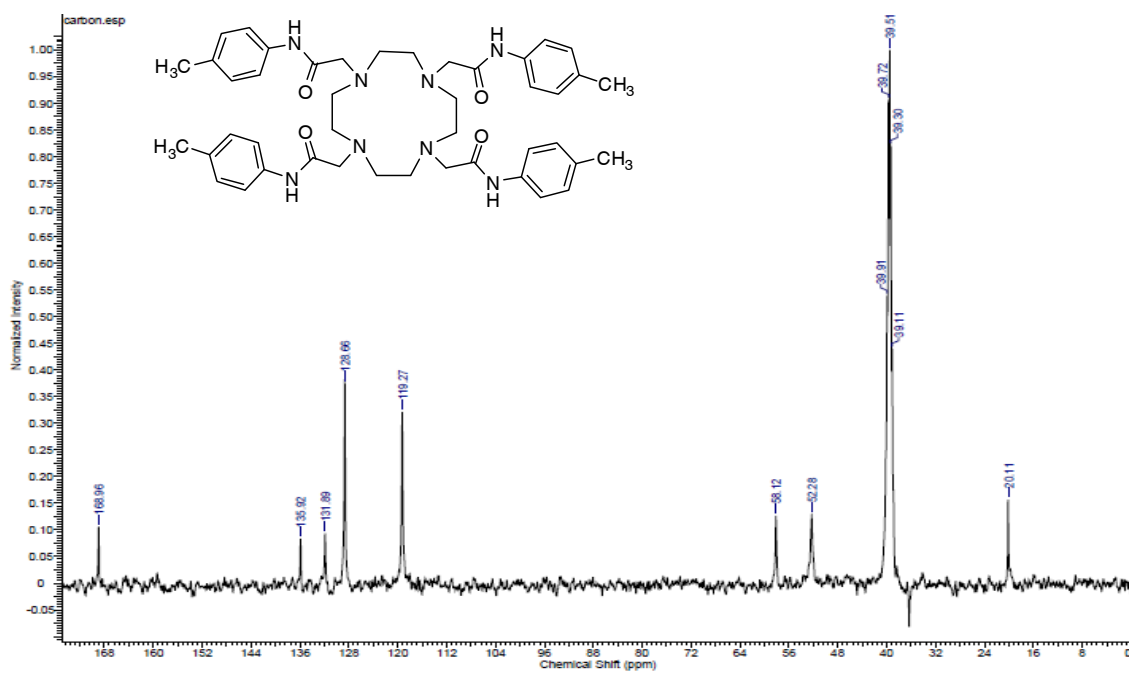
S 4.15: ^{1}H-NMR Spectrum of **4.8**
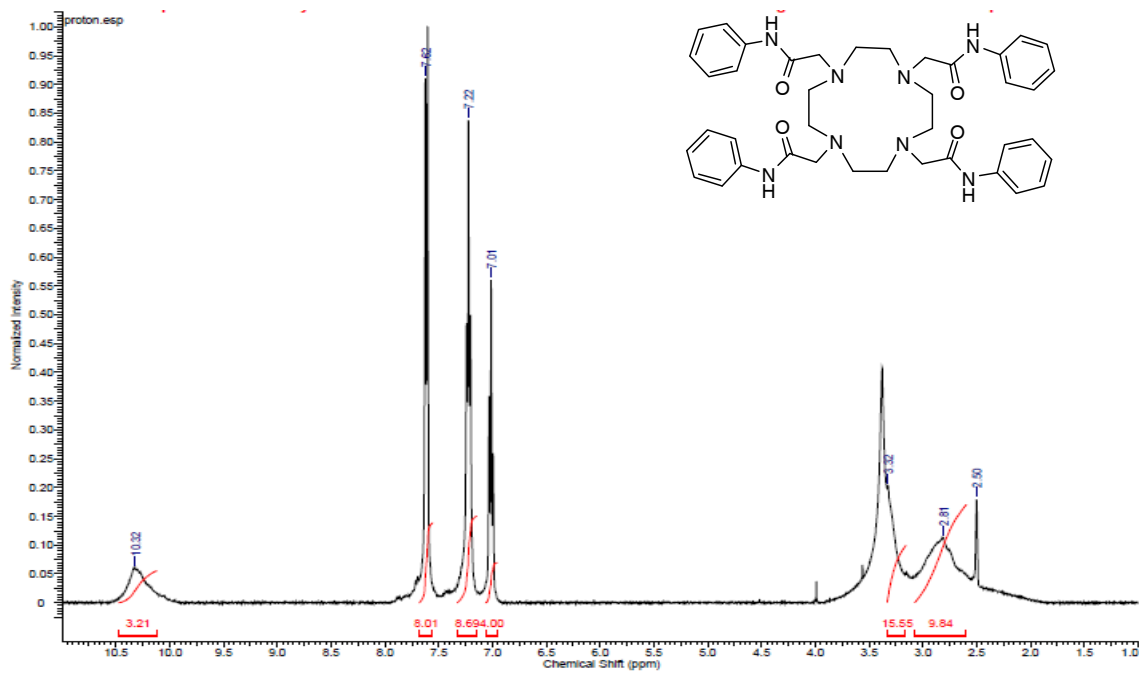
S 4.16: ^{13}C-NMR Spectrum of **4.8**
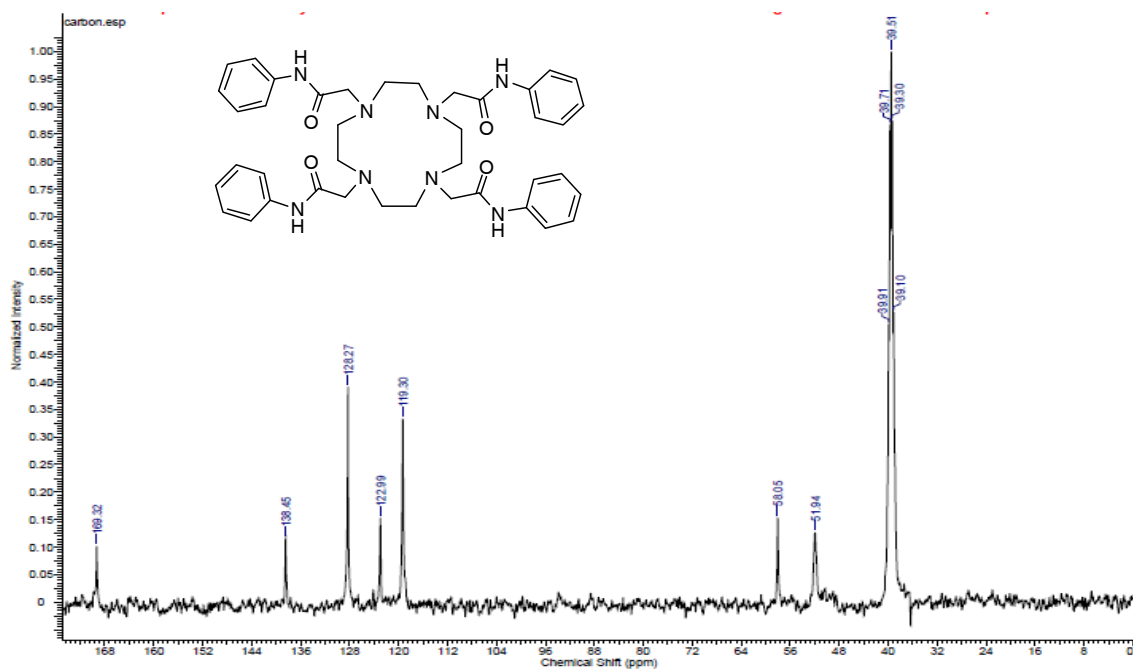
S 4.17: ^{1}H-NMR Spectrum of **4.9**
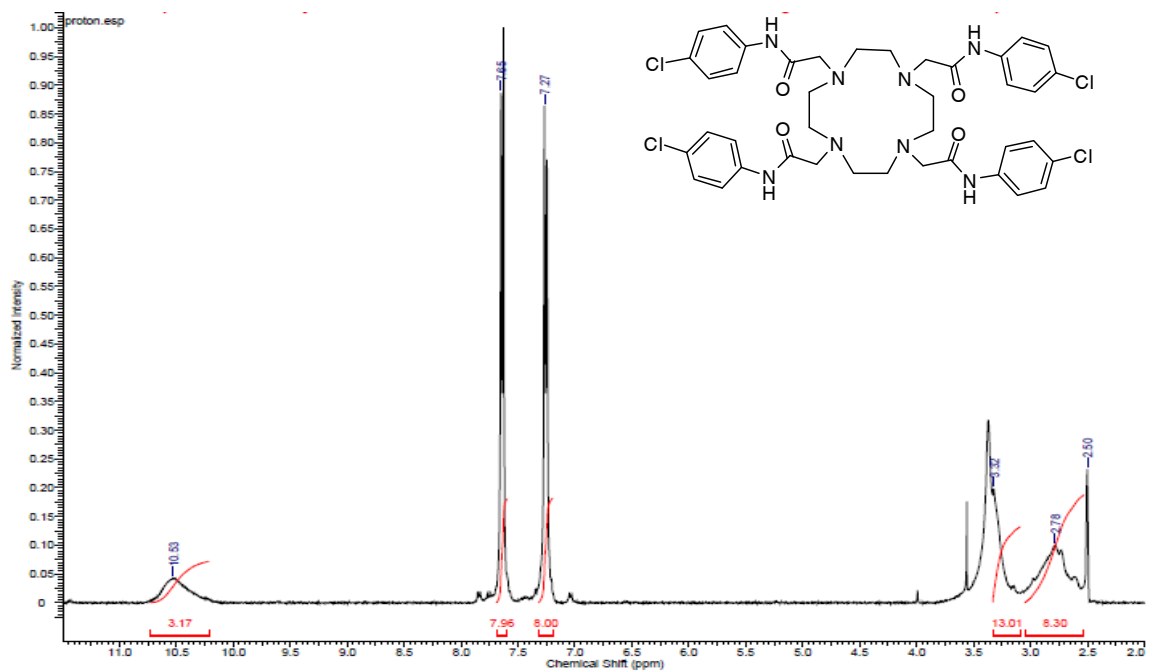
S 4.18: ^{13}C-NMR Spectrum of **4.9**
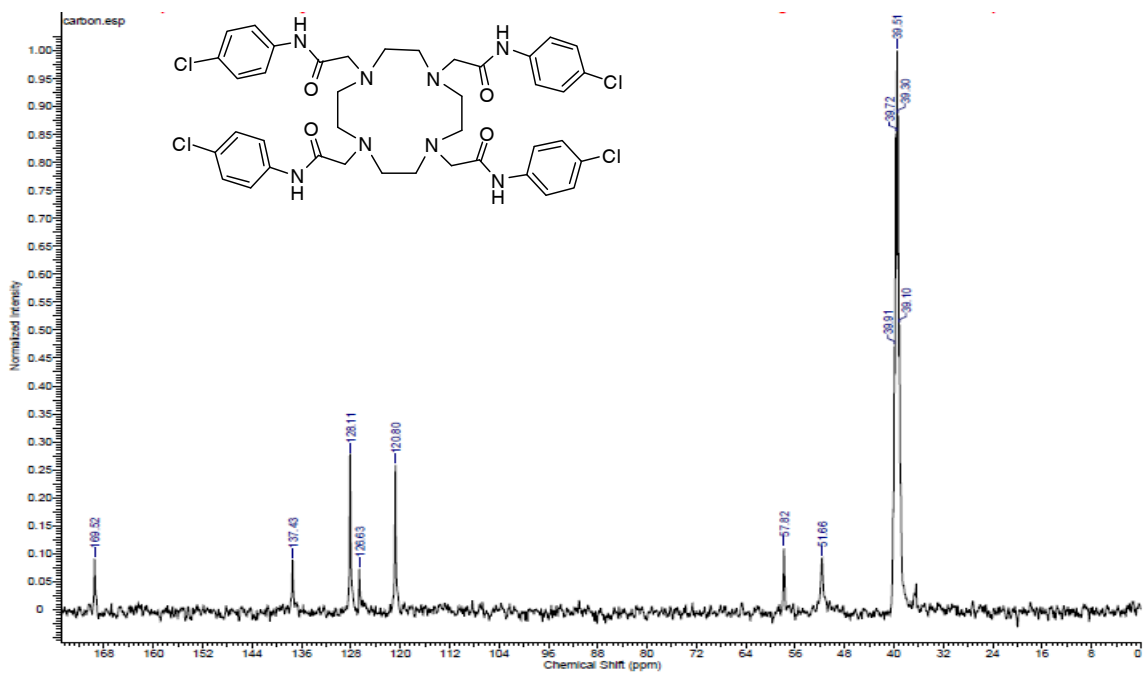
S 4.19: ^{1}H-NMR Spectrum of **4.10**
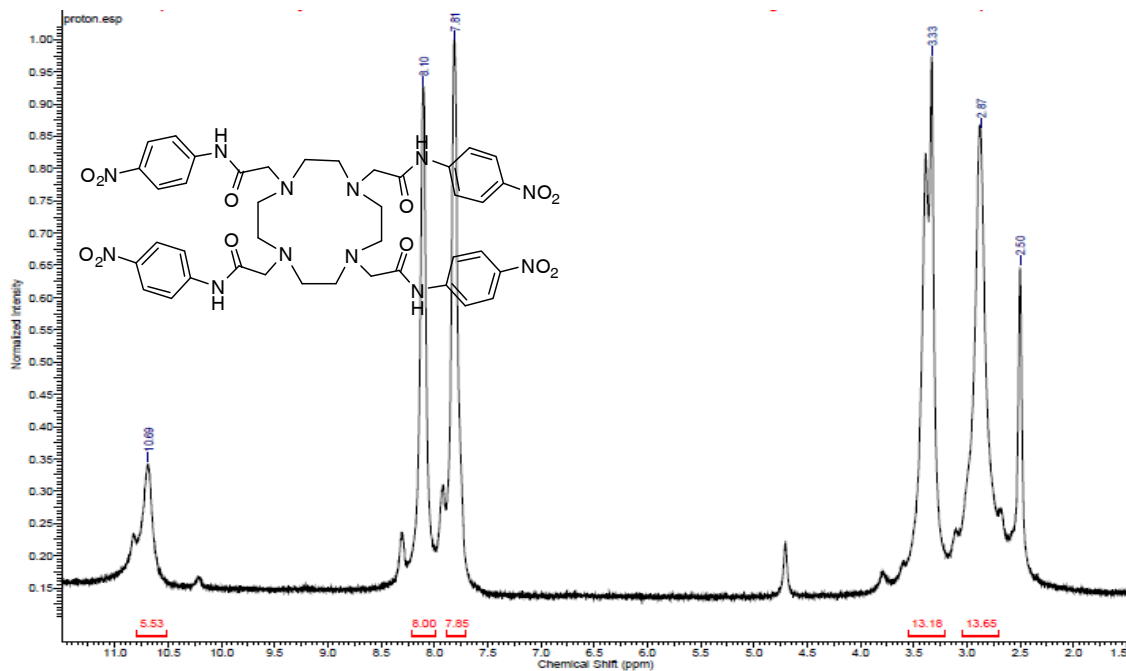
S 4.20: ^{13}C-NMR Spectrum of **4.10**
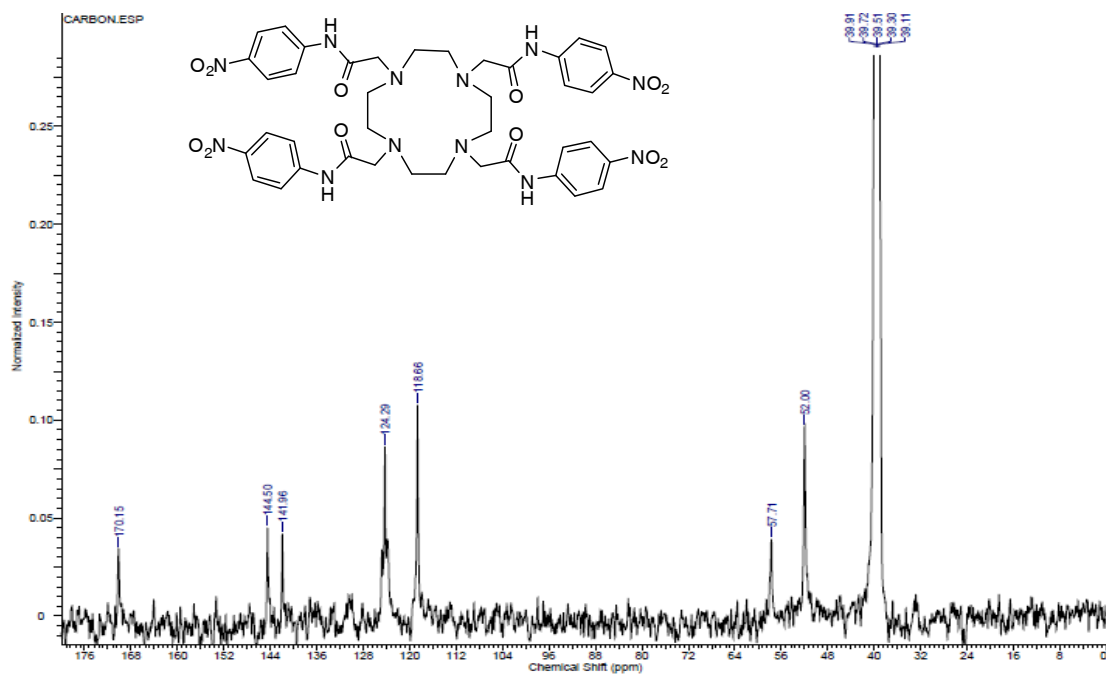
4.5   References

(1) Ratnakar, S. J.; Woods, M.; Lubag, A. J. M.; Kovács, Z.; Sherry, A. D. *J. Am. Chem. Soc.* **2008,** *130*, 6-7.

(2) Milne, M.; Lewis, M.; McVicar, N.; Suchý, M.; Bartha, R.; Hudson, R. H. E. *RSC Adv.* **2014,** *4*, 1666-1674.

(3) Soesbe, T. C.; Togao, O.; Takahashi, M.; Sherry, A. D. *Magn.Reson.Med.* **2012,** *68*, 816-821.

(4) Kotek, J.; Rudovský, J.; Hermann, P.; Lukeš, I. *Inorg. Chem.* **2006,** *45*, 3097-3102.

(5) Vipond, J.; Woods, M.; Zhao, P.; Tircsó, G.; Ren, J.; Bott, S. G.; Ogrin, D.; Kiefer, G. E.; Kovacs, Z.; Sherry, A. D. *Inorg. Chem.* **2007,** *46*, 2584-2595.

(6) Milne, M.; Chicas, K.; Li, A.; Bartha, R.; Hudson, R. H. E. *Org. Biomol. Chem.* **2012,** *10*, 287-292.

(7) Lukeš, I.; Kotek, J.; Vojtíšek, P.; Hermann, P. *Coord. Chem. Rev.* **2001,** *216-217*, 287-312.

(8) Singh, M.; Reynolds, J. J.; Sherry, A. D. *J. Am. Chem. Soc.* **1983,** *105*, 4172-4177.

(9) Stevens, T. K.; Milne, M.; Elmehriki, A. A. H.; Suchý, M.; Bartha, R.; Hudson, R. H. E. *Contrast Media Mol. Imaging* **2013,** *8*, 289-292.

(10) Elmehriki, A. A. H.; Milne, M.; Suchý, M.; Bartha, R.; Hudson, R. H. E. *Can. J. Chem.* **2013,** *91*, 211-219.

(11) Sherry, A. D.; Wu, K.; Zhang, S. WO2002043775 A2, 2002.

(12) Castelli, D. D.; Terreno, E.; Aime, S. *Angew. Chem. Int. Ed.* **2011,** *50*, 1798-1800.

(13) Pacheco-Torres, J.; Calle, D.; Lizarbe, B.; Negri, V.; Ubide, C.; Fayos, R.; Lopez Larrubia, P.; Ballesteros, P.; Cerdan, S. *Curr. Top. Med. Chem.* **2011,** *11*, 115-130.

(14) Soesbe, T. C.; Merritt, M. E.; Green, K. N.; Rojas-Quijano, F.; Sherry, A. D. *Magn. Reson. Med.* **2011,** *66*, 1697-1703.

(15) Jones, C. K.; Li, A. X.; Suchý, M.; Hudson, R. H. E.; Menon, R. S.; Bartha, R. *Magn. Reson. Med.* **2010,** *63*, 1184-1192.

Chapter 5

5 Dysprosium(III) and Thulium(III) Complexes of DO3A-monoanilides: An Investigation of Electronic Effects on their Relaxometric and Amide-based PARACEST Properties

5.1 Introduction

As described in Chapter 4, a study of DOTAM-tetraanilide PARACEST agents which were varied about their *para* (*p*-)-substituents was completed.[1] The aim of that work was to modulate the amide proton exchange rate to increase the CEST contrast produced by these protons. Unfortunately, with the exception of the Dy^{3+}- and Tm^{3+}-*p*-H and -*p*-OMe complexes (Figure 5.1), the other complexes were insoluble and could not be further studied.[1]
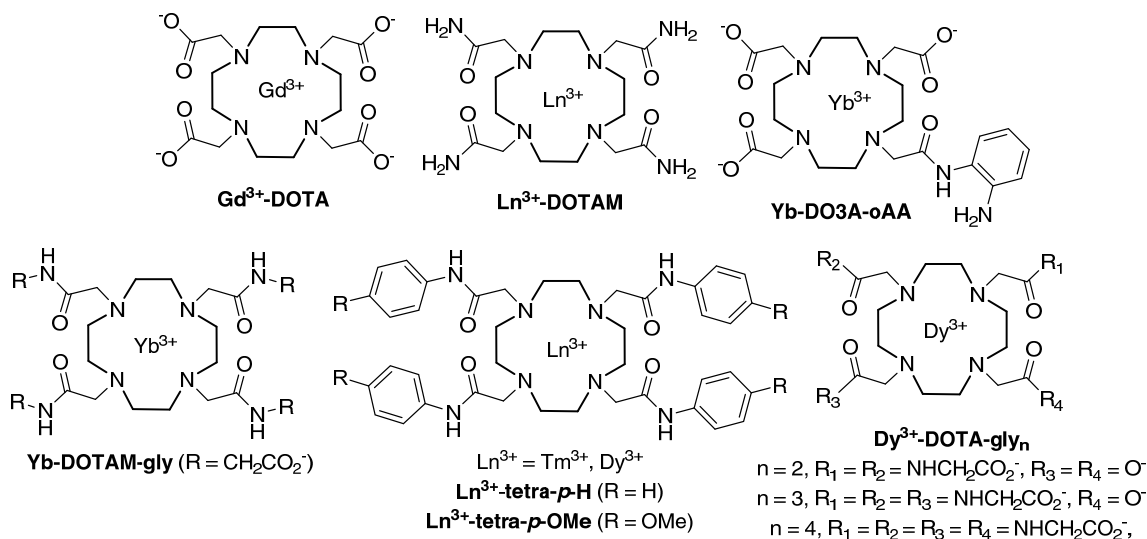
Figure 5.1: Chemical structures of some complexes discussed in this work.

In order to produce water soluble complexes, a series of analogues, the DO3A-monoanilide ligands, was prepared. The intent was to utilize this series to investigate the

influence of the nature of the *para*-substituent on the amide proton CEST signal. These complexes represent a simplified system compared to the tetraanilide complexes possessing not only aqueous solubility but also only a single carboxamide proton. The presence of three acetate arms and the use of Tm^{3+} and Dy^{3+} would produce large LIS and engender fast water exchange at the metal center. However, the effect on exchange of the amide proton should be smaller and hence a CEST signal is expected. Congruent with this expectation, is the observation of an amide proton based CEST signal for the Yb^{3+}-DO3A-oAA complex (Chart 1).[2, 3]

The lone acetamide arm was designed with the *para*-substituted anilines spanning a large range of electronic effects ranging from strong electron-donating groups (EDG, e.g. -NMe_2) to powerful electron-withdrawing groups (EWGs, e.g. -NO_2). Anilines that are substituted in the *para* position on the aromatic ring can provide information about electronic effects, charge state (pK_a) and polarity. Since the CEST effect is due to the single carboxamide proton, these studies should provide insight regarding the amide pK_a and provide some insight on the ability to tune the pK_a and CEST effect to biologically relevant pHs potentially laying the foundation for development of a pH responsive PARACEST contrast agent.

In lanthanide complexes, where CEST due to amide protons is to be observed, one may expect EWGs of the acetamide arm to make the amide proton more acidic. This should result in a faster exchange with bulk water. On the other hand, the opposite effect should be observed for EDGs: the amide proton becomes more basic resulting in slower exchange with the surrounding water. According to Terreno *et al.*, an increase in pH up to 9 increases the amide exchange rate and subsequently, the amide CEST.[4] It is expected that EWGs would allow for a decrease in the pH at which the maximum CEST effect occurs. This feature would make agents possessing these functional moieties more applicable as pH sensors for detecting biological anomalies, such as cancerous tissues, which have an acidic extracellular pH.[5]

Our second focus was to examine the influence of the nature of the *para*-substituent on the complex relaxivity. These complexes were expected to have fast water exchange at

the metal center that may be affected by the electronics of the single amide arm. For example, EDGs are envisioned to promote faster exchange of bound water due to an increase in electron density at the metal center, while the converse would ensue with the presence of EWGs. These effects should be apparent in the relaxivity measurements. In support of this notion, Ratnakar *et al.* have reported that Eu^{3+}-tetraamide complexes with one *para*-substituted aniline arm, can electronically affect the CEST effect due to a bound water molecule.[6]

5.2   Results and Discussion

5.2.1 Synthesis

Treatment of Et_3DO3A with the chlorine-containing electrophiles **5.1 - 5.5**,[1] in the presence of K_2CO_3, gave the desired bifunctional compounds **5.6 - 5.10** in low to moderate yields after purification by column chromatography (Scheme 5.1). All the ester-protected compounds **5.6 - 5.9** were subjected to saponification at 60^oC without any problems, with the exception of **5.10**. The saponified compounds **5.11 - 5.14** were obtained with excellent yields (Scheme 5.1). In contrast, the amide bond of **5.10** hydrolysed, leading to the formation of DOTA (Figure 5.1), as seen by UPLC. Consequently, the ethyl groups of compound **5.10** were removed under milder conditions at 5^oC[7] and compound **5.19** was obtained with excellent yield (Scheme 5.2).
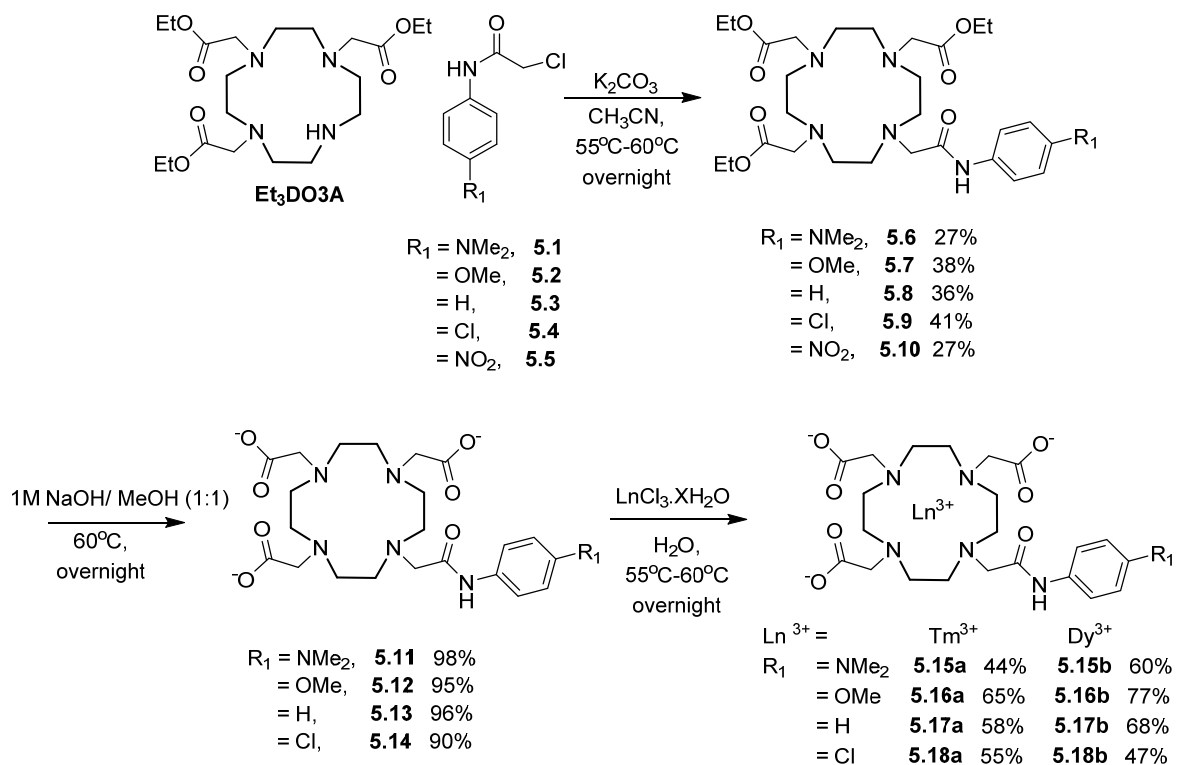
Scheme 5.1: Conditions for synthesis of contrast agents 5.15a,b - 5.18a,b.
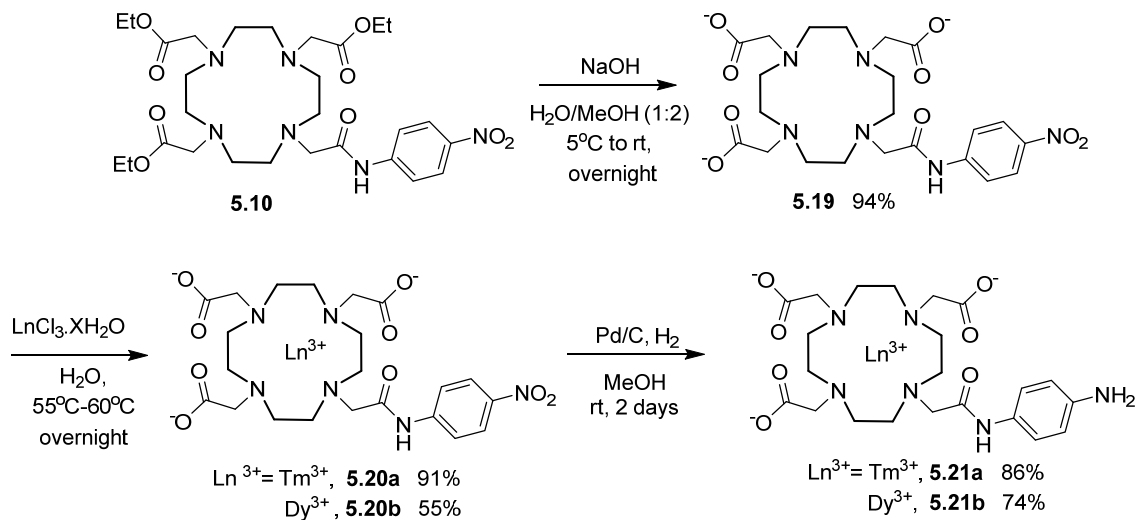
Scheme 5.2: Conditions for synthesis of contrast agents 5.20a,b and 5.21a,b.

Metalation of the ligands **5.11 - 5.14** with lanthanide salts of Tm^{3+} and Dy^{3+}, afforded the Tm^{3+} complexes **5.15a - 5.18a** and Dy^{3+} **5.15b - 5.18b** in moderate to good yields (Scheme 5.1). In order to prevent the hydrolysis of the amide bond, as seen previously during the saponification of **5.10**, the metalation of ligand **5.19** with Tm^{3+} and Dy^{3+} was performed at room temperature and **5.20a,b** were obtained in good yield (Scheme 5.2). The metalated complexes **5.20a,b** were subjected to catalytic hydrogenation to produce **5.21a,b** in excellent yields (Scheme 5.2).

5.2.2 CEST Measurements of Tm^{3+} Complexes
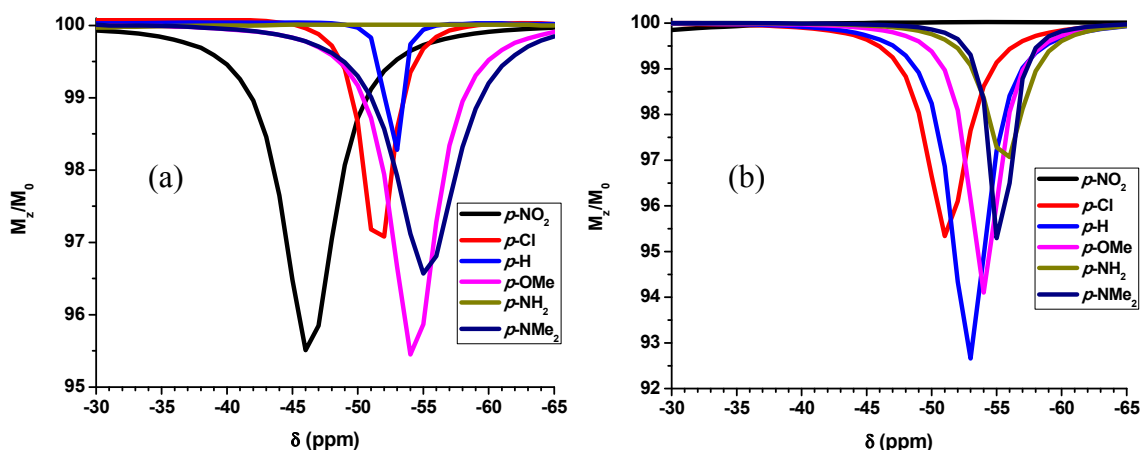
Figure 5.2: (a) CEST spectra of 5.15a - 5.18a and 5.20a - 5.21a at pH 7.00 ± 0.03 and (b) CEST spectra of 5.15a - 5.18a and 5.20a - 5.21a at pH 8.00 ± 0.03. CEST spectra were acquired at 37°C, with a 15 µT, 2 s saturation pulse, 10 mM in D_2O/H_2O (9:1). Data was processed with Origin® software by performing a Lorentzian fitting of the raw data.

The CEST data for the Tm^{3+} compounds were obtained at pH 6, 7, 8 and 9. CEST signals were not observed at pH 6 and 9 (data not shown), however, there were signals at pH 7 and 8 (Figure 5.2). The magnitude of the CEST effect ranged from 1 - 8% at these pH values, with the *p*-H complex **5.17a** having the highest signal of almost 8% at pH 8.

While these values may be considered low, only a 3-5% change in the water signal intensity is needed to see contrast in an MR image. [5]

CEST signal intensity as a function of EDG/EWG

Figure 5.3 shows the trend in CEST signal intensity with respect to the Hammett substituent constants associated with groups in the *para* position (δ_{para}). Hammett substituent constants give a measure of the total electronic (polar) effect exerted by a substituent on the aromatic ring, in comparison to the absence of the substituent. [8, 9] These values are derived from the rate of equilibrium of the ionization of unsubitituted benzoic acid and that of a substituted benzoic acid.[8, 9] A δ_{para} value of zero (*p*-H) indicates no electronic effect, while increasing negative δ_{para} values indicate EDGs (increasing order of strength: *p*-OMe, *p*-NH$_2$ and *p*-NMe$_2$). On the other hand, increasing positive δ_{para} values indicate EWGs (increasing order of strength: *p*-Cl and *p*-NO$_2$).
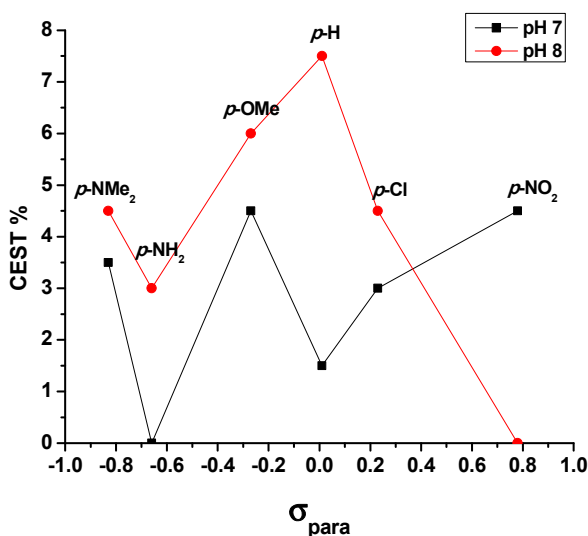
Figure 5.3: CEST intensity with respect to σ_{para} at 37°C and pH 7.00 ± 0.03 and 8.00 ± 0.03 for 5.15a - 5.18a and 5.20a - 5.21a. CEST spectra were acquired at 37°C, with a 15 µT, 2 s saturation pulse, 10 mM in D$_2$O/H$_2$O (9:1).

At pH 7, with the exception of the *p*-NH$_2$ complex **5.21a**, which displayed no CEST signal, the presence of EDGs led to an increase in the amide CEST effect, in comparison

to the p-H complex **5.17a**. At pH 8, the CEST effect was greatest for the complexes **5.15a**, **5.16a** and **5.21a**. However, their CEST effect was lower than that of the p-H complex **5.17a**. These results seem to support the hypothesis made earlier. The increased electron-density, due to EDGs, resulted in the amide proton being less acidic, therefore requiring a higher pH for deprotonation and subsequent exchange.

At pH 7, CEST signals were seen for both **5.18a** and **5.20a**, which bore EWGs. Both complexes gave higher signals in contrast to the p-H complex **5.17a**. At pH 8, there was a reduction in the signal of the p-Cl complex **5.18a** and a complete disappearance of the signal for the p-NO$_2$ complex **5.20a**, (as compared to the p-H complex **5.17a**). These observations also appear to be in agreement with the afore-mentioned expectations that EWGs should lead to more acidic amide protons due to lower pK_as. At pH 8, the acidic proton seems to be exchanging rather quickly with the bulk water, thereby negatively affecting the CEST signal and causing obliteration of the signal. The reduction rather than eradication of the CEST signal of the p-Cl complex **5.18a** implies that the amide proton exchange rate is still within the limits of the rate requirement for a CEST signal to be generated. Thus, these EWGs allowed a maximum CEST effect to be seen at pH 7 instead of at pH 8 or 9.

The pK_as (unknown) for all these complexes are prone to be dissimilar, even although there are some similarities in pH where the maximum CEST signal occurs. From these results, one may infer that there are also similarities in the amide proton exchange rates.

The interesting phenomena of the p-NO$_2$ complex **5.20a** having a CEST signal at pH 7 and no signal at pH 8 (*vice versa* for the p-NH$_2$ complex **5.21a**), may serve as a starting point for the design of a potential dual pH and redox probe using more than one p-NO$_2$ substituents. The reduced CEST effect in the p-NH$_2$ complex **5.21a** as compared to p-NO$_2$ **5.20a**, has been similarly demonstrated for the Eu^{3+}-DOTAM-p-NO$_2$ and -p-NH$_2$ monoaniline complexes (Figure 5.1) reported by Ratnakar *et al.*[6]

Observed chemical shift as a function of EDG/EWG

The chemical shift at which the amide CEST signal arises in Tm^{3+}-DOTAM complexes is -51 ppm.[4] The chemical shifts observed for the CEST signals of the Tm^{3+}- DO3A-monoaniline complexes **5.15a** - **5.18a** and **5.20a** - **5.21a** fall close to this expected value. Furthermore, it was observed that the chemical shifts of these complexes were independent of pH (Table 5.1). In comparison to the *p*-H complex **5.17a** at -53 ppm (at pH 7 and 8), the EDGs had upfield chemical shifts and the EWGs had downfield chemical shifts. Surprisingly at pH 7, the *p*-NO_2 complex **5.20a** had the most downfield chemical shift at -46 ppm. The slight downfield shift produced by the EWGs and upfield shift produced by the EDGs are likely a result of shielding effects propagated through the aromatic ring system to the amide proton rather than changes in the chelate conformation which would result in larger chemical shift changes, *vide infra*.

Table 5.1: Chemical shifts (δ) of Tm^{3+} based agents 5.15a - 5.18a and 5.20a - 5.21a at 37°C and pH 7.00 ± 0.03 and 8.00 ± 0.03.

	δ (ppm)	
	7.00 ± 0.03	8.00 ± 0.03
p-NMe_2	-55	-55
p-NH_2	n.o.	-56
p-OMe	-54	-54
p-H	-53	-53
p-Cl	-52	-51
p-NO_2	-46	n.o
n.o. indicates not observed		

The Yb^{3+}-DO3A-oAA complex (Figure 5.1) reported had two signals, each due to the amide proton and the *o*-NH_2 substituent (δ (ppm) = -11 and +8 ppm, respectively; pH 7, 37°C).[2] A single signal for the *p*-NH_2 complex **5.21a** was only observed at pH 8 (37°C). The difference in the number of signals seen in both complexes may be attributed to the position of the NH_2 group, rather than pH. In order for a signal to be generated by the NH_2 group, intramolecular hydrogen-bonding with the carboxylate arm may be necessary.[10] In complex **5.21a**, the NH_2 group in the *para* position is not conducive to intramolecular hydrogen-bonding with a carboxylate arm, therefore, no CEST signal was

seen for these exchangeable protons. In contrast, the Yb^{3+}-DO3A-oAA complex has the NH_2 group in the *ortho* position, an ideal location for this interaction and thus, an additional CEST signal for these protons was observed. The small chemical shift difference in Yb^{3+}-DO3A-oAA complex is a shortcoming of using Yb^{3+}, since the signals were close to that of the bulk water signal.

As previously reported, Tm^{3+}-tetraaniline-*p*-H complex had a CEST signal at -41 ppm. The Tm^{3+}-tetraaniline-*p*-OMe complex had two CEST signals at -43 and -83 ppm due to the square antiprismatic (SAP) and twisted square antiprismatic (TSAP) isomers, respectively.[1] The solid state structure of the Tm^{3+}-tetraaniline *p*-OMe complex indicated no bound water, therefore those geometries are more correctly denoted as SAP' and TSAP'.[1] Only one signal was seen in the Tm^{3+}- DO3A complexes **5.15a** - **5.18a** and **5.20a** - **5.21a**. Hence, this suggests that there is only one isomer (most likely SAP) present in solution.

CEST signal were not produced by the Dy^{3+} complexes as the T_2 relaxation was too great, thus no comparisons to the Tm^{3+} complexes can be made.

5.2.3 Relaxometric Evaluation of Dy^{3+} and Tm^{3+} Complexes

Tm^{3+} Complexes

The relaxivity data for the Tm^{3+} complexes **5.15a** - **5.18a** and **5.20a** - **5.21a** was acquired and these results are seen in Table 2. These low relaxivity values are comparable to those reported for the complexes of Tm^{3+}- tetraaniline-*p*-H (r_1 = 0.06 $mM^{-1}s^{-1}$ and r_2 = 0.66 $mM^{-1}s^{-1}$) and -*p*-OMe (r_1 = 0.05 $mM^{-1}s^{-1}$ and r_2 = 0.40 $mM^{-1}s^{-1}$).[1] In comparison to the *p*-H complex **5.17a**, the r_1 values indicated an overall slight increase for EDGs and a slight decrease for EWGs (Figure 5.4). On the other hand, with respect to **5.17a**, both EWGs and EDGs showed a decrease in r_2, with the exception being the *p*-NMe$_2$ complex **5.15a** (Figure 5.4).

Table 5.2: r_1 and r_2 values of Tm^{3+} based agents 5.15a - 5.18a and 5.20a - 5.21a at 25°C and pH 7.00 ± 0.03

	r_1 (mM^{-1} s^{-1})	r_2 (mM^{-1} s^{-1})
p-NMe$_2$	0.06	0.19
p-NH$_2$	0.06	0.09
p-OMe	0.10	0.12
p-H	0.05	0.15
p-Cl	0.03	0.15
p-NO$_2$	0.03	0.12
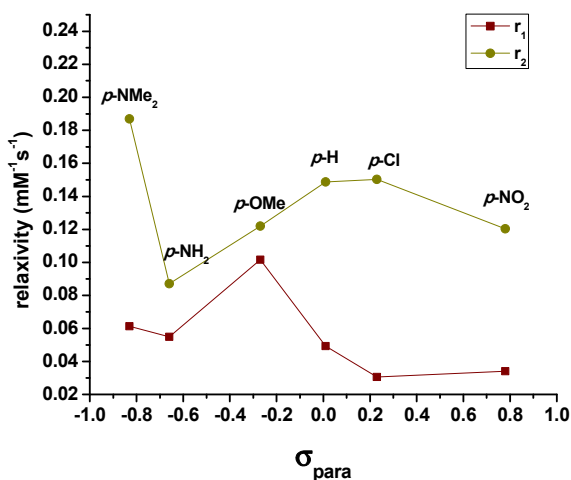
Figure 5.4: r_1 and r_2 with respect to σ_{para} at 25°C and pH 7.00 ± 0.03 for 5.15a - 5.18a and 5.20a - 5.21a.

The relationship between r_2 and the strengths of the EDGs or EWGs, is not straightforward. A maximal value for *p*-H complex **5.17a** (or *p*-Cl complex **5.18a**) is observed with falling off as $|\sigma_{para}| > 0$ with the exception for *p*-NH$_2$ complex **5.20a**
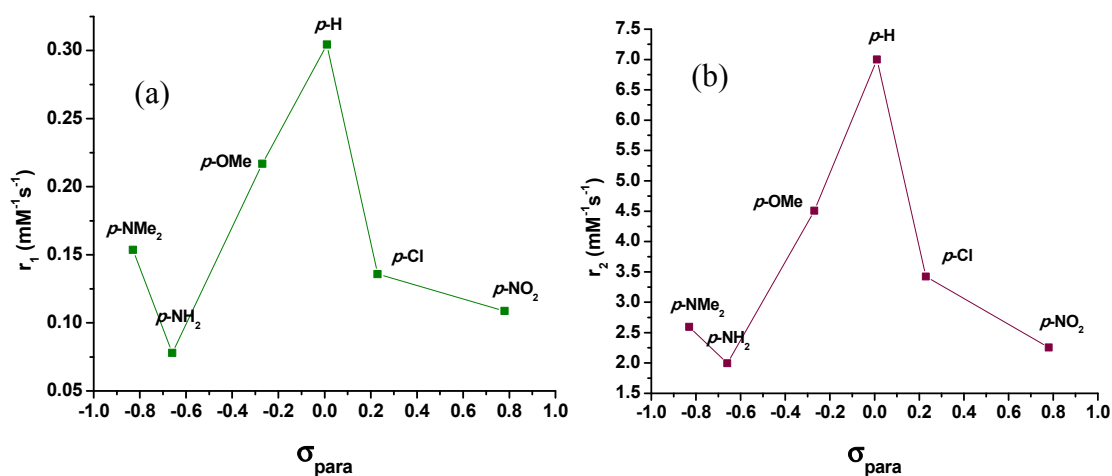
Dy^{3+} complexes

Dy^{3+} complexes have been shown to act as T$_2$ shortening agents.[11] This is evident as these agents **5.15b - 5.18b and 5.20b - 5.21b** had much higher r_2 than r_1 values (Table 5.3). In particular, the *p*-OMe **5.16b** and *p*-H **5.17b** complexes had r_2 values of

approximately twice that of the other complexes. These r_2 values were also higher in comparison to Dy^{3+}-DOTA (r_2 = 1.5 mM^{-1} s^{-1} at 22°C; Figure 5.1),[11] indicating that having at least one amide arm is advantageous. This assumption was made based on previous results by Soesbe *et al*., where derivatives of Dy^{3+}-DOTA-gly$_n$ (Figure 5.1), with n = 2, 3 and 4 had r_2 values of 18.8 mM^{-1} s^{-1}, 4.2 mM^{-1} s^{-1} and 1.4 mM^{-1} s^{-1}, respectively, at 22°C.[11]

Table 5.3: r_1 and r_2 values of Dy^{3+} based agents 5.15b - 5.18b and 5.20b - 5.21b at 25 °C and pH 7.00 ± 0.03.

	r_1 (mM^{-1} s^{-1})	r_2 (mM^{-1} s^{-1})
p-NMe$_2$	0.2	2.6
p-NH$_2$	0.1	2.0
p-OMe	0.2	4.5
p-H	0.3	7.0
p-Cl	0.1	3.4
p-NO$_2$	0.1	2.3

Figure 5.5: (a) r_1 with respect to σ_{para} at pH 7.00 ± 0.03 for 5.15b - 5.18b and 5.20b - 5.21b and (b) r_2 with respect to σ_{para} at pH 7.00 ± 0.03 for 5.15b - 5.18b and 5.20b - 5.21b.

The r_1 values with respect to δ_{para} of both the EDGs and EWGs substituents showed a decrease in comparison to the unsubstituted *p*-H complex **5.17b**. This trend was similarly observed for the r_2 values. Nevertheless, there was an inverse relationship between the strengths of the groups and the r_1 and r_2 values. This trend was similarly seen in the r_2 values of the Tm^{3+} complexes.

Table 5.4: Relaxivity parameters r_1 and r_2 (mM^{-1} s^{-1}) of Dy^{3+} based agents 5.17b and 5.21b at pH 7.00 ± 0.03 and $10^{o}C$, 25 °C and $37^{o}C$.

T	*p*-NH$_2$		*p*-H	
	r_1	r_2	r_1	r_2
10°C	0.07	3.4	0.16	8.7
25°C	0.08	2.0	0.30	7.0
37°C	0.05	0.71	0.12	3.2

The study involving complexes of Dy^{3+}-DOTA-gly$_n$ also demonstrated that Swift-Connick theory can be used to envisage the trend in r_2 with respect to the lifetime of bound water (τ_m), at several temperatures.[12] This is given by the equation 5.1:

$$r_{2ex} = (1.8 \text{ X } 10^{-5}) \frac{\tau_m \Delta\omega^2}{1 + \tau_m^2 \Delta\omega^2} \qquad \text{equation [5.1]}$$

where r_{2ex} is the transverse relaxivity due to molecular water exchange, $\Delta\omega$ is the chemical shift difference of bound water in rad s^{-1} and τ_m is the lifetime of the bound water.[13, 14] It was shown that when n = 0 and 2, the exchange rates were faster than optimal for generating T_2 contrast.[11] On the other hand, when n = 3 and 4 the exchange rate was slower, with n = 2 being optimal.[11] However, no data about monoacetamides was reported. In order to compare the Dy^{3+}-DO3A-monoanilines, temperature studies were carried out on the *p*-H complex **5.17b** (one with higher r_2 values) and *p*-NH$_2$ **5.21b** (one with lower r_2 values). Results for both complexes indicated that as the temperature is increased, the r_2 decreased (Table 5.4). This highlights that the exchange rate should fall on the fast side of the Swift-Connick plot (τ_m < 545 ns; between n = 0 and n = 2), as is expected for fast inner-sphere water exchange systems.[11, 15] Due to the fact that these

complexes represent each extreme (high and low r_2), it is therefore expected that all of these Dy^{3+} complexes would also have fast inner-sphere exchange of water. Because the p-H complex **5.17b** gave the greatest r_1 and r_2 values, the substituent effect appears to be steric in nature rather than dictated by subtle changes in the electronics of the amide arm, given that hydrogen is the smallest substituent. The steric nature of substituent may influence the conformation of the complex, but perhaps more likely influence the second sphere of solvation and lead to the observed trend.
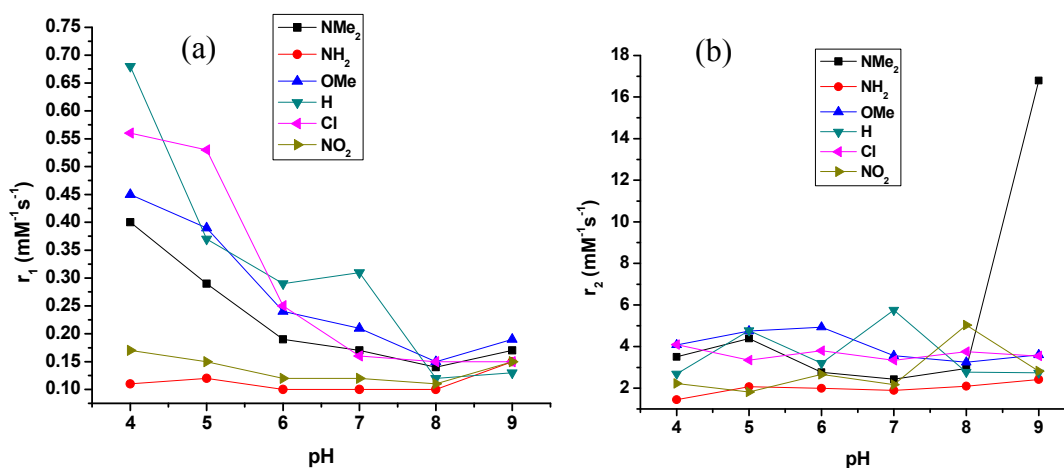
Figure 5.6: (a) r_1 with respect to pH at 25^oC for 4mM each of 5.15b - 5.18b and 5.20b - 5.21b and (b) r_2 with respect to pH at 25^oC for 4mM each of 5.15b - 5.18b and 5.20b - 5.21b.

In order to determine the potential of these complexes as the basis for development of pH probes for the physiologically interesting range (pH < 7),[5] a study was carried out with 4 mM of each complex over a pH range of 4 - 9 (Figure 5.6). Within this range, the r_1 values of the complexes were mainly low at the more basic pH then increased as the pH became more acidic.

This trend may be caused by an increase in the number of coordinated water molecules at low pH (inner-sphere interaction).[16, 17] The increase at low pH was less noticeable for the p-NH$_2$ **5.21b** and p-NO$_2$ **5.20b** complexes. On the other hand, the r_2 values of the

complexes had no trend with respect to pH over the range tested. Unexpectedly, the *p*-NMe$_2$ complex **5.15b** demonstrated a dramatic increase in relaxivity at pH 9, which may be due to OH- catalyzed prototropic exchange.[16, 17]

In order to be applicable as a responsive probe, a change in relaxivity approximately 2.0 mM^{-1} s^{-1} or more is needed.[18] None of the complexes met this requirement within the biologically relevant pHs.

5.3   Conclusions

It has been shown that several Tm^{3+}- and Dy^{3+}-DO3A-monoanilide complexes can be synthesized and obtained in moderate to excellent yields starting from monoalkylation of Et$_3$DO3A with various *para*-substituted anilines.

It was also demonstrated that a CEST signal could be generated from an amide proton in the Tm^{3+} complexes. The amide CEST signal is slightly modulated under varying pH conditions, by using EDGs or EWGs. Complexes containing EDGs gave higher CEST intensities at pH 8, while those with EWGs had higher CEST intensities at pH 7. The observed chemical shifts of the CEST signals were independent of pH but were influenced by the nature of the *para*-substitutent.

It has been furthermore established that the relaxivities for the Tm^{3+} complexes were very weak, while those of the Dy^{3+} complexes were stronger. However, the presence of either strongly electron-donating or withdrawing groups in the Dy^{3+}complexes, resulted in weaker relaxivities.

The observed trends in CEST intensity and relaxivity are not simply dependent on the electronic nature of the *para*-substitutent and are a result of complex interplay of metal-bound water exchange rate, amide-proton exchange rate, outer sphere solvation and conformation of the complex – contributing factors that cannot be deconvoluted in these studies.[19]

Although the complexes reported herein are not very promising as responsive contrast agents for *in vitro* or *in vivo* use, the information gleaned is still valuable for the development of agents that can provide a CEST signal due to amide proton(s). This information can assist in the design of ligands to achieve agents with CEST responses that would fall within the physiological pH range of interest (pH 6.5-7.5). One step towards this objective would be to investigate variation of the position of substitution with other EDGs or EWGs on the aniline ring as well as bis(amide)-bis(carboxylate) ligands.

5.4   Supplemental Information

5.4.1 General Experimental

General synthetic details can be found in Appendix 1.

CEST and Relaxivity Experiments

CEST spectra of complexes were acquired on a 600 MHz vertical bore NMR spectrometer, using a 15 µT, 2 s continuous wave presaturation pulse at offset frequencies ranging from -110 to 110 ppm in steps of 1 ppm at a concentration of 10 mM in D_2O/H_2O (9:1) at pH 6.00 ± 0.03, 7.00 ± 0.03 and 8.00 ± 0.03; 37 °C. T_1 and T_2 relaxation time constant measurements were made on a 400 MHz vertical bore NMR spectrometer. T_1 and T_2 relaxation time constant measurements were made for four different concentrations (1, 2, 4, 8 mM) of Dy^{3+} complexes and three different concentrations (2, 4, 8 mM) of Tm^{3+} complexes in H_2O. T_1 relaxation time constant was measured using an inversion recovery sequence (15-20 inversion times in the range of 200 ms – 25 s) with a minimum $d_1 = 5T_1$ to ensure full recovery (pH 7.00 ± 0.03 and 25°C). T_2 relaxation time constant measurements were made using a CPMG pulse sequence (15-20 train echo times) with a minimum $d_1 = 5T_1$ to ensure full recovery (pH 7.00 ± 0.03 and 25°C). Additional T_1 and T_2 temperature studies were done at 25°C and 37°C (pH 7.00 ± 0.03). VNMRJ® software of the spectrometer automatically gave the T_1

and T_2 relaxation rate constants. The relaxivities were then determined by linear regression fitting of the rate constants versus concentration in Microsoft Excel.

5.4.2 Synthetic Procedures

General procedure for monoalkylation. Et₃DO3A and K_2CO_3 were suspended in CH_3CN (3-5 mL) and acetamides **5.1 - 5.5** dissolved in CH_3CN (1.5-2.5 mL) were added. The reaction mixture was heated to $55^{o}C$-$60^{o}C$ and left for overnight. Reaction mixture was filtered and the filtrate concentrated. The crude material was purified by silica gel column chromatography with 5% MeOH in CH_2Cl_2. The desired fractions were collected and concentrated to give the desired compounds.
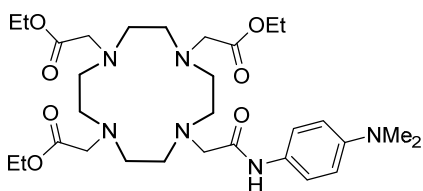
Triethyl 2,2',2''-(10-(2-((4-(dimethylamino)phenyl)amino)-2-oxoethyl)-1,4,7,10-tetraazacyclododecane-1,4,7-triyl)triacetate (5.6). Et₃DO3A (1.027 mmol), compound **5.1** and K_2CO_3 (1.550 mmol each). The title compound was obtained as a brown oil (168 mg, 27%). ¹H NMR (400 MHz, CDCl₃): δ 10.75 (1H, s); 7.67 (2H, d, J = 9.3 Hz); 6.55 (2H, d); 4.17 - 4.07 (8H, m); 3.49 (2H, s); 3.33 - 1.96 (16H, m); 1.23 - 1.19 (12H, m). ¹³C NMR (100 MHz, CDCl₃): δ 173.0, 169.9, 147.0, 130.0, 121.1, 112.9, 61.1, 56.8, 55.0, 51.1, 49.1, 41.1, 14.0. ESI-TOF m/z calcd for $C_{30}H_{51}N_6O_7$ (M+H)⁺, calculated 607.3819, found 607.3813.
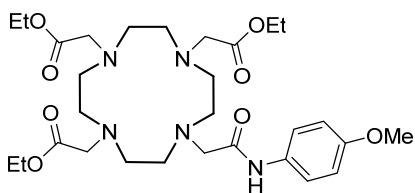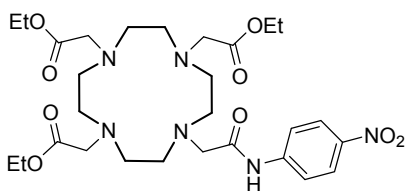
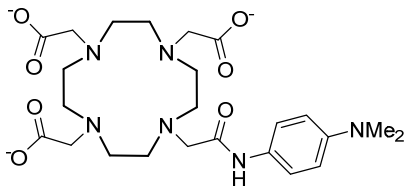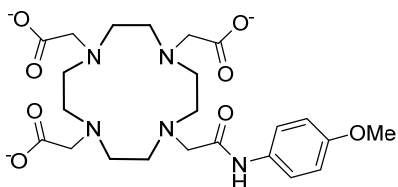**Triethyl 2,2',2''-(10-(2-((4-methoxyphenyl)amino)-2-oxoethyl)-1,4,7,10-tetraazacyclododecane-1,4,7-triyl)triacetate (5.7)**. Et$_3$DO3A (1.039 mmol), compound **5.2** and K$_2$CO$_3$ (1.632 mmol each).The title compound was obtained as a colourless oil (234 mg, 38%). ^{1}H NMR (400 MHz, CDCl$_3$): δ 10.93 (1H, s); 7.72 (2H, d, J = 8.7 Hz); 6.65 (2H, d); 4.17 - 4.07 (8H, m); 3.67 (3H, s); 3.50 (2H, s); 3.37 - 1.97 (16H, m); 1.22 - 1.17 (12H, m). ^{13}C NMR (100 MHz, CDCl$_3$): δ 173.0, 170.8 132.5, 121.3, 113.7, 61.1, 56.8, 55. 2, 55.0, 52.1, 48.9, 41.1, 14.0. ESI-TOF m/z calcd for C$_{29}$H$_{48}$N$_5$O$_8$ (M+H)$^+$, calculated 594.3503, found 594.3522.
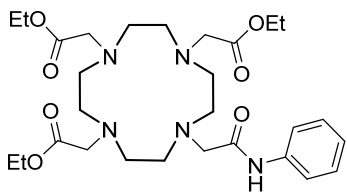
Triethyl 2,2',2''-(10-(2-oxo-2-(phenylamino)ethyl)-1,4,7,10-tetraazacyclododecane-1,4,7-triyl)triacetate (5.8). Et$_3$DO3A (1.039 mmol), compound **5.3** and K$_2$CO$_3$ (1.632 mmol each). The title compound was obtained as a colourless oily residue (211 mg, 36%). ^{1}H NMR (400 MHz, CDCl$_3$): δ 11.1 (1H, s); 7.84 (2H, d, J = 7.8 Hz); 7.13 (2H, t); 6.94 (1H, t, J = 7.4 Hz); 4.16 - 4.09 (6H, m); 3.55 (2H, s); 3.41 - 1.93 (16H, m); 1.24 - 1.19 (9H, m). ^{13}C NMR (100 MHz, CDCl$_3$): δ 173.0, 170.9, 139.1, 128.1, 123.2, 120.0, 61.2, 56.9, 55.0, 51.4, 49.2, 14.0. ESI-TOF m/z calcd for C$_{28}$H$_{46}$N$_5$O$_7$ (M+H)$^+$, calculated 564.3397, found 564.3399.
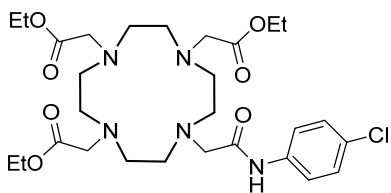
Triethyl 2,2',2''-(10-(2-((4-chlorophenyl)amino)-2-oxoethyl)-1,4,7,10-tetraazacyclododecane-1,4,7-triyl)triacetate (5.9). Et$_3$DO3A (1.039

mmol), compound **5.4** and K_2CO_3 (1.632 mmol each). The title compound was obtained as a colourless oily residue (254 mg, 41%). ^{1}H NMR (400 MHz, CDCl$_3$): δ 11.46 (1H, s); 7.89 (2H, d, J = 9.0 Hz); 7.13 (2H, d); 4.20 - 4.14 (6H, m); 3.65 (2H, s); 3.57-1.97 (16H, m); 1.29 -1.24 (9H, m). ^{13}C NMR (100 MHz, CDCl$_3$): δ 173.0, 171.2, 137.9, 128.1, 121.5, 110.1, 61.3, 57.0, 55.1, 52.1, 48.7, 14.1. ESI-TOF *m/z* calcd for $C_{28}H_{45}ClN_5O_7$ (M+H)$^+$, calculated 598.3008, found 598.2999.

Triethyl 2,2',2''-(10-(2-((4-nitrophenyl)amino)-2-oxoethyl)-1,4,7,10-tetraazacyclododecane-1,4,7-triyl)triacetate (5.10). Et$_3$DO3A (1.039 mmol), compound **5.5** and K_2CO_3 (1.632 mmol each). The title compound was obtained as a yellow oily residue (171 mg, 27%). ^{1}H NMR (400 MHz, CDCl$_3$): δ 12.02 (1H, s); 8.13 (2H, d, J = 8.9 Hz); 8.06 (2H, d); 4.22 - 4.10 (8H, m); 3.73 (2H, s); 3.54 - 2.18 (16H, m); 1.30 -1.24 (9H, m). ^{13}C NMR (100 MHz, CDCl$_3$): δ 173.1, 172.3, 145.3, 142.8, 124.3, 119.8, 61.4, 57.2, 55.1, 52.1, 48.7, 14.1. ESI-TOF *m/z* calcd for $C_{28}H_{45}N_6O_9$ (M+H)$^+$, calculated 609.3248, found 609.3222.

General procedure for saponification. Et$_3$DO3A-monoanilines **5.6 - 5.9** were dissolved in MeOH (1.5-2.5 mL) and 1M NaOH (1.5-2.5 mL) added, then heated to 60°C and left for overnight. The reaction mixture was concentrated and neutralized with 1M HCl. The crude was purified by size exclusion column chromatography (100% H$_2$O) and the desired fractions were collected and lyophilized to give the desired compounds.
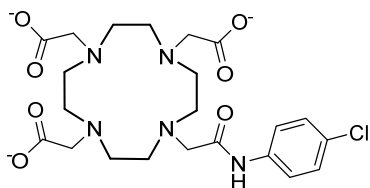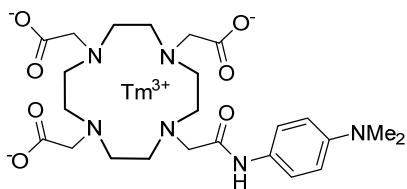
2,2',2''-(10-(2-((4-(dimethylamino)phenyl)amino)-2-oxoethyl)-1,4,7,10-tetraazacyclododecane-1,4,7-triyl)triacetic acid (5.11). Compound **5.6** (115 mg, 0.190 mmol). Title compound was obtained as a brown solid (110 mg, 98%). ^{1}H NMR (400 MHz, D$_2$O): δ 7.32 (2H, d, *J* =8.0 Hz); 6.68 (2H, d); 3.91 (2H, s); 3.80-2.12 (16H, m). ESI-TOF *m/z* calcd for C$_{24}$H$_{39}$N$_6$O$_7$ (M+H)$^+$, calculated 523.2880, found 523.2889.

2,2',2''-(10-(2-((4-methoxyphenyl)amino)-2-oxoethyl)-1,4,7,10-tetraazacyclododecane-1,4,7-triyl)triacetic acid (5.12). Compound **5.7** (170 mg, 0.286 mmol). Title compound was obtained as a brown solid (157 mg, 95%).^{1}H NMR (400 MHz, D$_2$O): δ 7.38 (2H, d); 6.98 (2H, d *J* = 8.0 Hz)); 3.93 (2H, s); 3.89-2.78 (16H, m). ESI-TOF *m/z* calcd for C$_{23}$H$_{36}$N$_5$O$_8$ (M+H)$^+$, calculated 510.2564, found 510.2569.
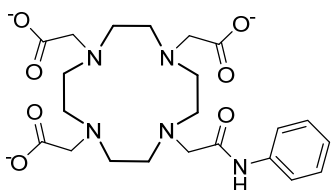
2,2',2''-(10-(2-oxo-2-(phenylamino)ethyl)-1,4,7,10-tetraazacyclododecane-1,4,7-triyl)triacetic acid (5.13). Compound **5.8** (160 mg, 0.284 mmol). Title compound was obtained as a cream solid (149 mg, 96%). ^{1}H NMR (400 MHz, D$_2$O): δ 7.59-7.36 (4H, m); 7.25 (1H, t, J = 6 Hz); 6.83 (~0.5H, t, *J* = 7 Hz); 3.95 (2H, s); 3.88-2.24 (16H, m). ESI-TOF *m/z* calcd for C$_{22}$H$_{34}$N$_5$O$_7$ (M+H)$^+$, calculated 480.2458, found 480.2441.
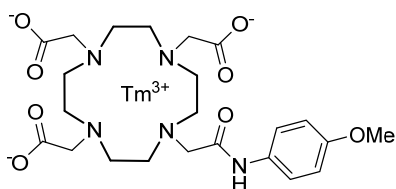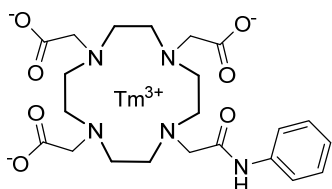
2,2',2''-(10-(2-((4-chlorophenyl)amino)-2-oxoethyl)-1,4,7,10-tetraazacyclododecane-1,4,7-triyl)triacetic acid (5.14).

Compound **5.9** (240 mg, 0.401 mmol). Title compound was obtained as a cream solid (210 mg, 90%). ^{1}H NMR (400 MHz, D$_2$O): δ 7.54-7.33 (4H, m); 3.95 (2H, s); 3.90-2.21 (16H, m). ESI-TOF *m/z* calcd for C$_{22}$H$_{33}$ClN$_5$O$_7$ (M+H)$^+$, calculated 514.2069, found 514.2073.
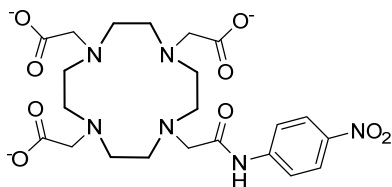
2,2',2''-(10-(2-((4-nitrophenyl)amino)-2-oxoethyl)-1,4,7,10-tetraazacyclododecane-1,4,7-triyl)triacetic acid (5.19). Compound **5.10** (115 mg, 0.189 mmol) was dissolved in MeOH (3 mL) and cooled to 5°C. NaOH (38 mg, 0.945 mmol) was added and the mixture left sirring at 5°C for 3 hrs then brought to rt and left for overnight. The reaction mixture was concentrated and neutralized with 1M HCl. The crude was purified by size exclusion column chromatography (100% H$_2$O) and the desired fractions were collected and lyophilized to give the desired compound. Title compound was obtained as a yellow solid (105 mg, 94%). ^{1}H NMR (400 MHz, D$_2$O): δ8.18 (2H, d); 7.67 (2H, d *J* = 9.0 Hz)); 3.94 (2H, s); 3.89-2.99 (16H, m). ESI-TOF *m/z* calcd for C$_{22}$H$_{33}$N$_6$O$_9$ (M+H)$^+$, calculated 525.2309, found 525.2316.

General procedure for metalation. Compounds **5.11 - 5.14** and **5.19** were dissolved in H$_2$O (2 mL) then the appropriate lanthanide chloride salts added. The pH was adjusted to 6 and the reaction mixture heated to 55°C and left for overnight.

Thulium(III) 2,2',2''-(10-(2-((4-(dimethylamino)phenyl)amino)-2-oxoethyl)-1,4,7,10-tetraazacyclododecane-1,4,7-triyl)triacetate (5.15a). Compound **5.11** (43 mg, 0.073 mmol) and TmCl$_3$.6H$_2$O (30 mg, 0.073 mmol). Title compound was obtained as a brown solid (24 mg, 44%). ESI-TOF *m/z* calcd for C$_{24}$H$_{36}$N$_6$O$_7$Tm (M+H)$^+$, calculated 689.1988, found 689.2010.

Thulium(III) 2,2',2''-(10-(2-((4-methoxyphenyl)amino)-2-oxoethyl)-1,4,7,10-tetraazacyclododecane-1,4,7-triyl)triacetate (5.16a). Compound **5.12** (42 mg, 0.073 mmol) and TmCl$_3$.6H$_2$O (30 mg, 0.073 mmol). Title compound was obtained as a cream solid (35 mg, 65%). ESI-TOF *m/z* calcd for C$_{23}$H$_{33}$N$_5$O$_8$Tm (M+H)$^+$, calculated 676.1671, found 676.1659.

Thulium(III) 2,2',2''-(10-(2-oxo-2-(phenylamino)ethyl)-1,4,7,10-tetraazacyclododecane-1,4,7-triyl)triacetate (5.17a). Compound **5.13** (40 mg, 0.073mmol) and TmCl$_3$.6H$_2$O (30 mg, 0.073 mmol). Title compound was obtained as a cream solid (30 mg, 58%). ESI-TOF *m/z* calcd for C$_{22}$H$_{31}$N$_5$O$_7$Tm (M+H)$^+$, calculated 646.1566, found 646.1588.
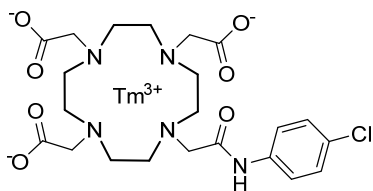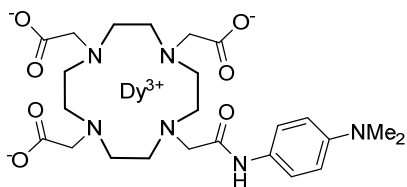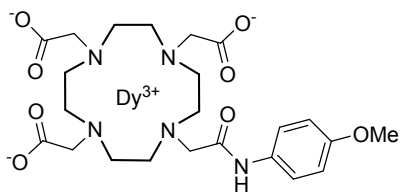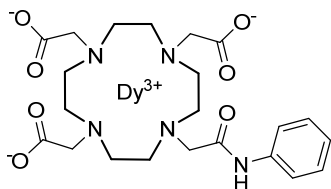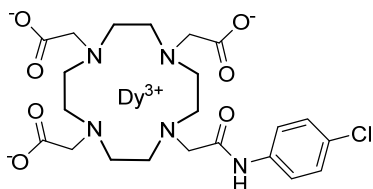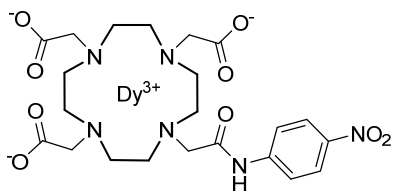
Thulium(III) 2,2',2''-(10-(2-((4-chlorophenyl)amino)-2-oxoethyl)-1,4,7,10-tetraazacyclododecane-1,4,7-triyl)triacetate (5.18a). Compound **5.14** (42 mg, 0.073mmol) and TmCl$_3$.6H$_2$O (30 mg, 0.073 mmol). Title compound was obtained as a cream solid (30 mg, 55%). ESI-TOF *m/z* calcd for C$_{22}$H$_{30}$ClN$_5$O$_7$Tm (M+H)$^+$, calculated 680.1176, found 680.1178.
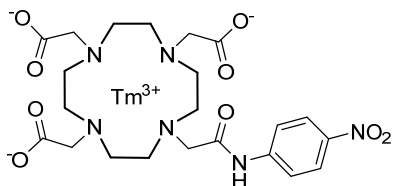
Thulium(III) 2,2',2''-(10-(2-((4-nitrophenyl)amino)-2-oxoethyl)-1,4,7,10-tetraazacyclododecane-1,4,7-triyl)triacetate (5.20a). Compound **5.19** (43 mg, 0.073 mmol) and TmCl$_3$.6H$_2$O (30 mg, 0.073 mmol). Title compound was obtained as a yellow solid (50 mg, 91%). ESI-TOF *m/z* calcd for C$_{22}$H$_{30}$N$_6$O$_9$Tm (M+H)$^+$, calculated 691.1417, found 691.1404.
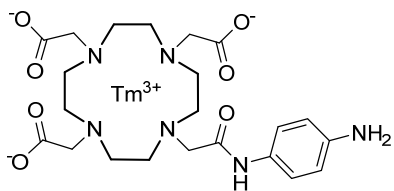

Dysprosium(III) 2,2',2''-(10-(2-((4-(dimethylamino)phenyl)amino)-2-oxoethyl)-1,4,7,10-tetraazacyclododecane-1,4,7-triyl)triacetate (5.15b). Compound **5.11** (60 mg, 0.102 mmol) and DyCl$_3$.6H$_2$O (38 mg, 0.102 mmol). Title compound was obtained as a brown solid (46 mg, 60%). ESI-TOF *m/z* calcd for C$_{24}$H$_{36}$N$_6$O$_7$Dy (M+H)$^+$, calculated 683.1859, found 683.1874

Dysprosium(III) 2,2',2''-(10-(2-((4-methoxyphenyl)amino)-2-oxoethyl)-1,4,7,10-tetraazacyclododecane-1,4,7-triyl)triacetate (5.16b). Compound **5.12** (59 mg, 0.102 mmol) and DyCl$_3$.6H$_2$O (38 mg, 0.102 mmol). Title compound was obtained as a cream solid 58 mg, 77%). ESI-TOF *m/z* calcd for C$_{23}$H$_{33}$N$_5$O$_8$Dy (M+H)$^+$, calculated 670.1543, found 670.1569.

Dysprosium(III) 2,2',2''-(10-(2-oxo-2-(phenylamino)ethyl)-1,4,7,10-tetraazacyclododecane-1,4,7-triyl)triacetate (5.17b). Compound **5.13** (56 mg, 0.102 mmol) and DyCl$_3$.6H$_2$O (38 mg, 0.102 mmol). Title compound was obtained as a cream solid (48 mg, 68%). ESI-TOF *m/z* calcd for C$_{22}$H$_{31}$N$_5$O$_7$Dy (M+H)$^+$, calculated 640.1437, found 640.1457.
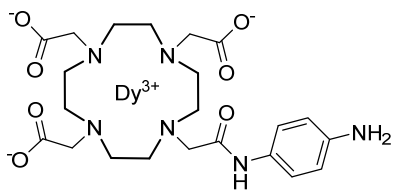

Dysprosium(III) 2,2',2''-(10-(2-((4-chlorophenyl)amino)-2-oxoethyl)-1,4,7,10-tetraazacyclododecane-1,4,7-triyl)triacetate (5.18b). Compound **5.14** (59 mg, 0.102 mmol) and DyCl$_3$.6H$_2$O (38 mg, 0.102 mmol). Title compound was obtained as a cream solid (36 mg, 47%). ESI-TOF *m/z* calcd for C$_{22}$H$_{30}$ClN$_5$O$_7$Dy (M+H)$^+$, calculated 674.1047, found 674.1048.

Dysprosium(III) 2,2',2''-(10-(2-((4-nitrophenyl)amino)-2-oxoethyl)-1,4,7,10-tetraazacyclododecane-1,4,7-triyl)triacetat (5.20b). Compound **5.19** (60 mg, 0.102 mmol) and DyCl$_3$.6H$_2$O (38 mg, 0.102 mmol). Title compound was obtained as a yellow solid (42 mg, 55%). ESI-TOF *m/z* calcd for C$_{22}$H$_{30}$N$_6$O$_9$Dy (M+H)$^+$, calculated 685.1288, found 685.1319.

Reduction of 5.20a,b. Compounds **5.20a,b** were each dissolved in MeOH (2 mL) and Pd/C (10 mol %) added. The suspension was purged with H$_2$ under vacuum and left stirring for 2 days at rt under H$_2$. The reaction mixture was filtered and the filtrate concentrated then redissolved in H$_2$O and lyophilized.

Thulium(III) 2,2',2''-(10-(2-((4-aminophenyl)amino)-2-oxoethyl)-1,4,7,10-tetraazacyclododecane-1,4,7-triyl)triacetate (5.21a). Compound **5.20a** (30 mg, 0.040 mmol) and TmCl$_3$.6H$_2$O (15 mg, 0.040 mmol). Title compound was obtained as a white solid (29 mg, 86%). ESI-TOF *m/z* calcd for C$_{22}$H$_{32}$N$_6$O$_7$Tm (M+H)$^+$, calculated 661.1675, found 661.1656.
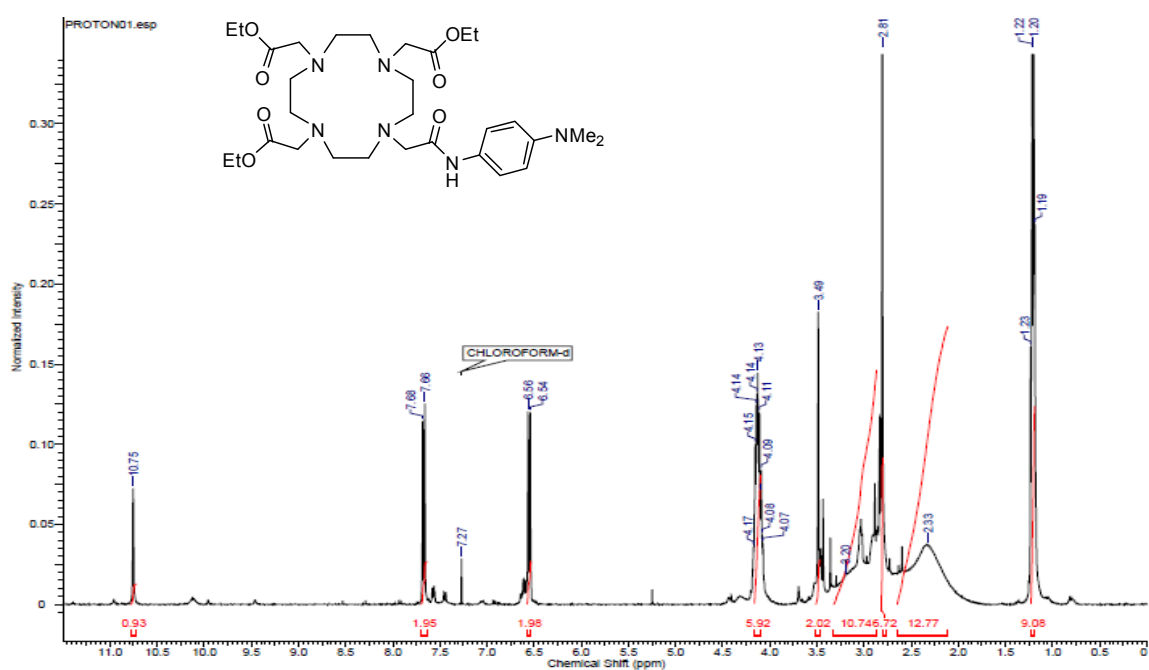

Dysprosium(III) 2,2',2''-(10-(2-((4-aminophenyl)amino)-2-oxoethyl)-1,4,7,10-tetraazacyclododecane-1,4,7-
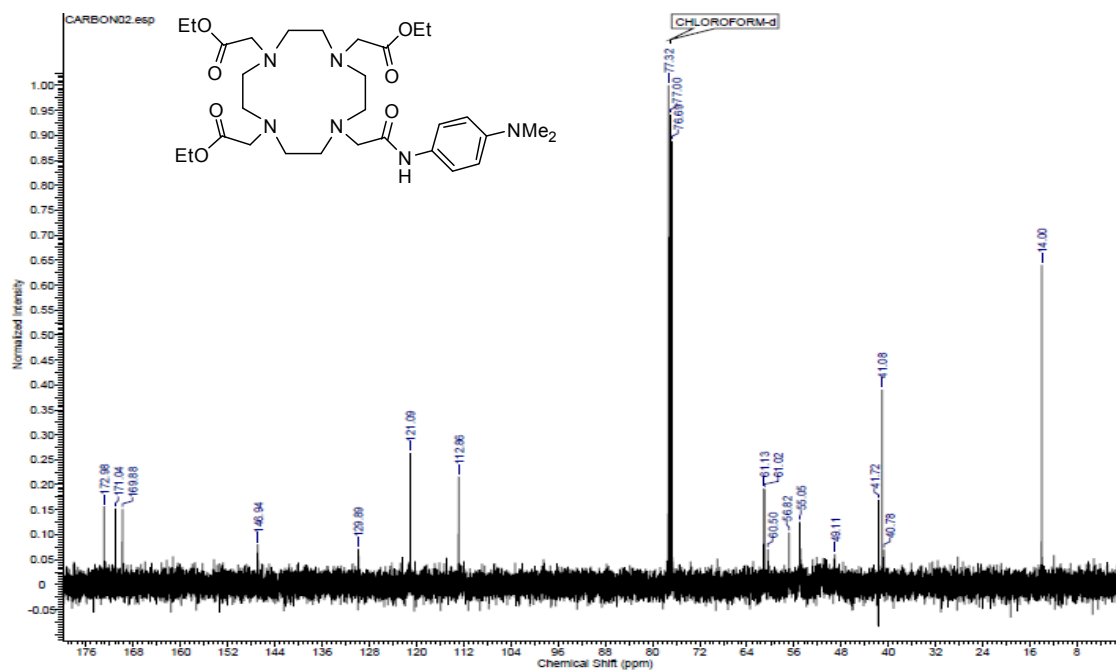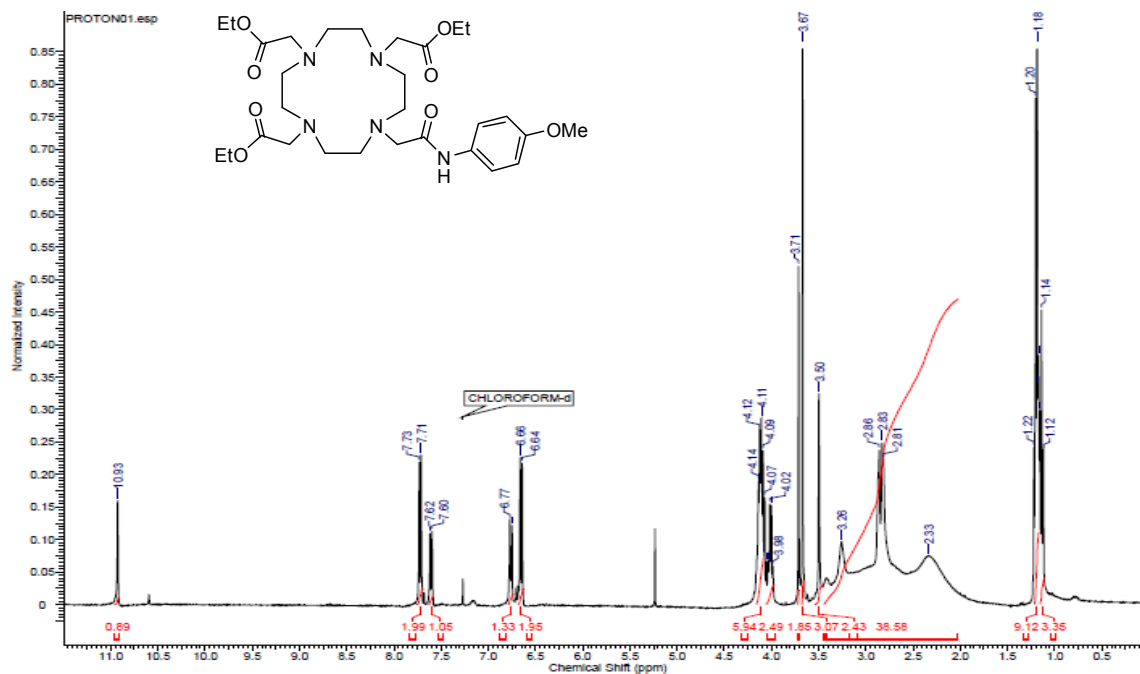
triyl)triacetate (5.21b). Compound **5.20b** (20 mg, 0.027 mmol) and $DyCl_3.6H_2O$ (10 mg, 0.027 mmol). Title compound was obtained as a white solid (14 mg, 74%). ESI-TOF *m/z* calcd for $C_{22}H_{32}N_6O_7Dy$ $(M+H)^+$, calculated 655.1546, found 655.1518.

5.4.3 Spectra

S 5.1: ^{1}H-NMR Spectrum of **5.6**

S 5.2: ^{13}C-NMR Spectrum of 5.6
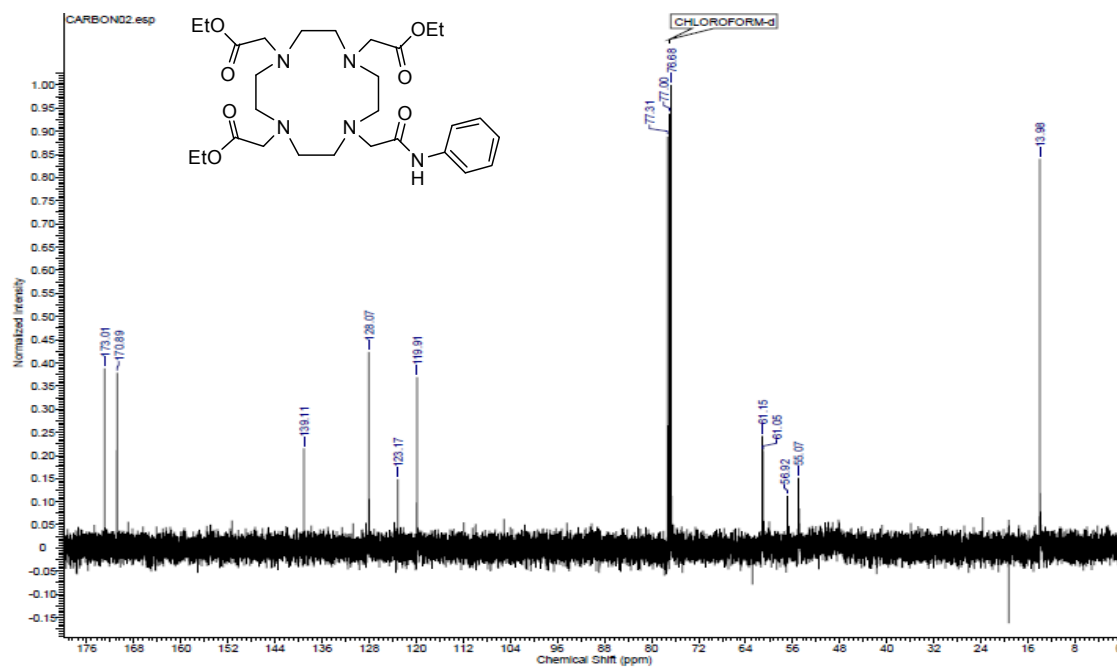

S 5.3: ^{1}H-NMR Spectrum of 5.7

S 5.4: ^{13}C-NMR Spectrum of **5.7**
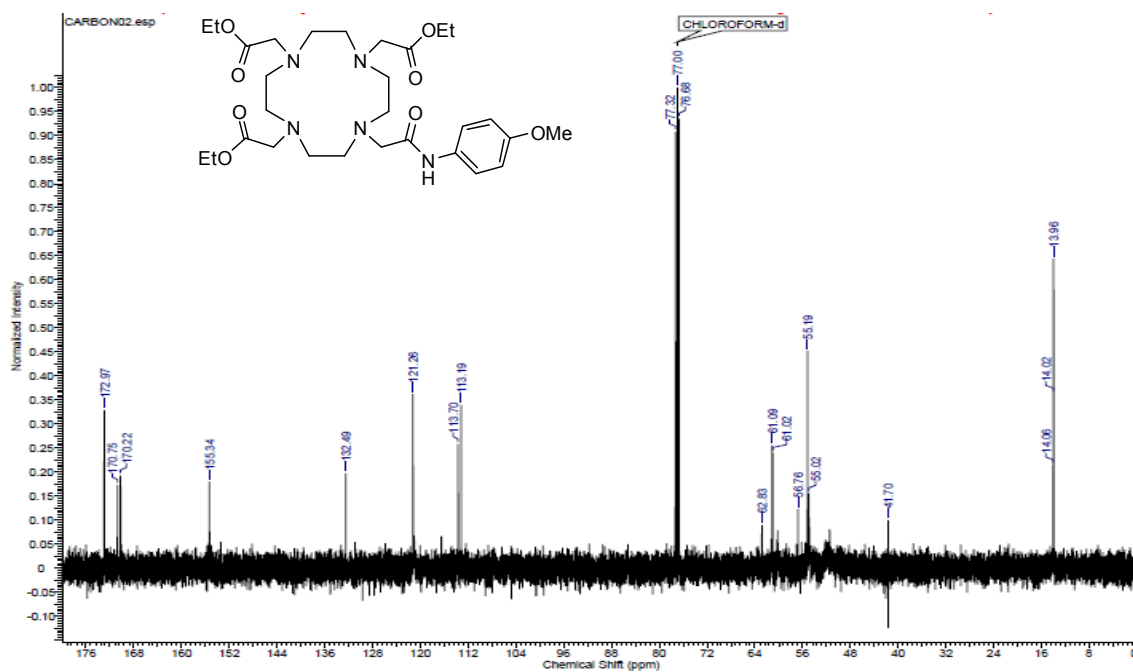
S 5.5: ^{1}H-NMR Spectrum of **5.8**
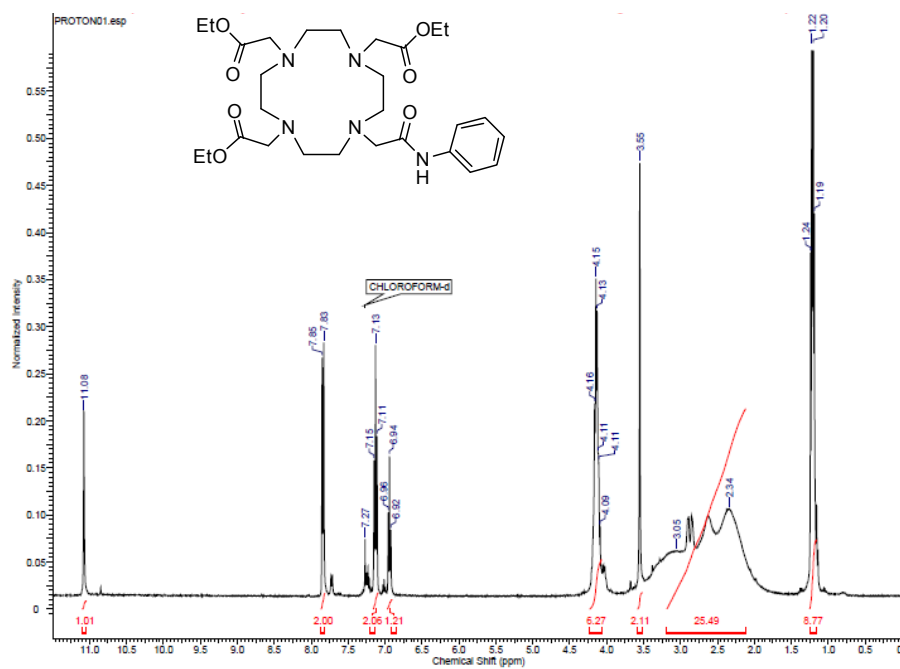
S 5.6: ^{13}C-NMR Spectrum of **5.8**

S 5.7: ^{1}H-NMR Spectrum of **5.9**
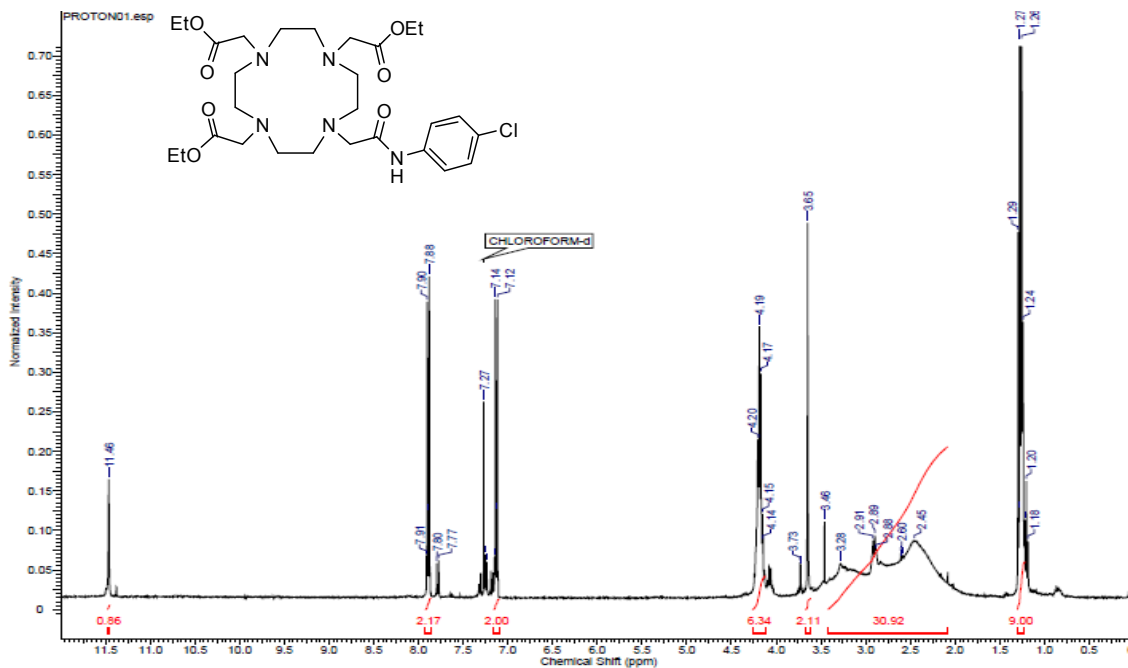
S 5.8: ^{13}C-NMR Spectrum of **5.9**
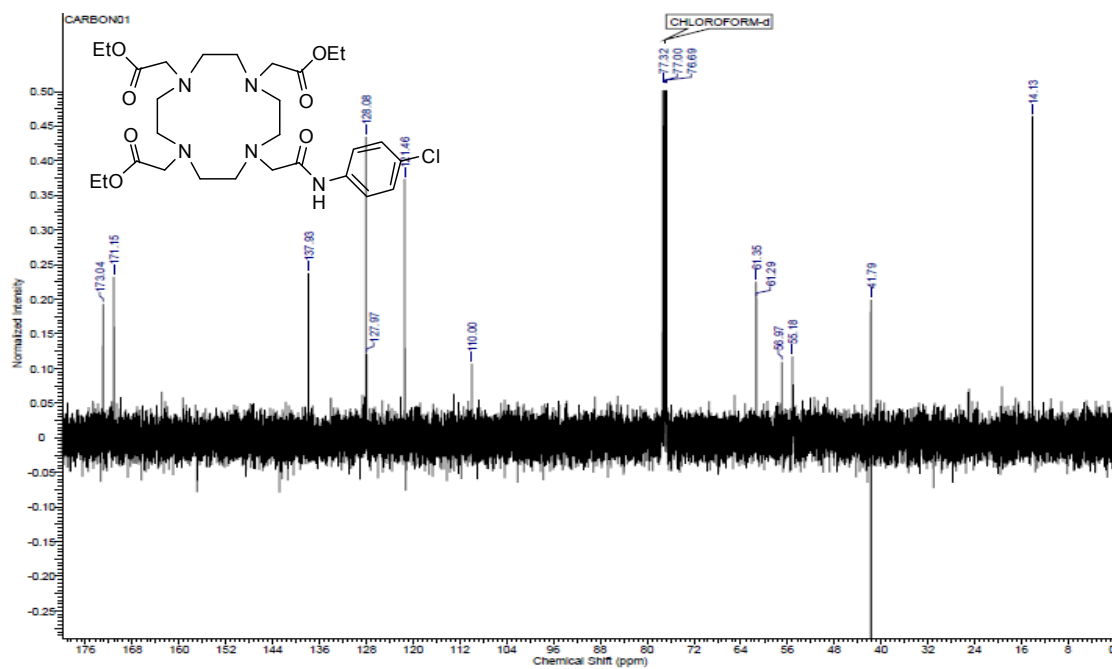
S 5.9: ^{1}H-NMR Spectrum of **5.10**
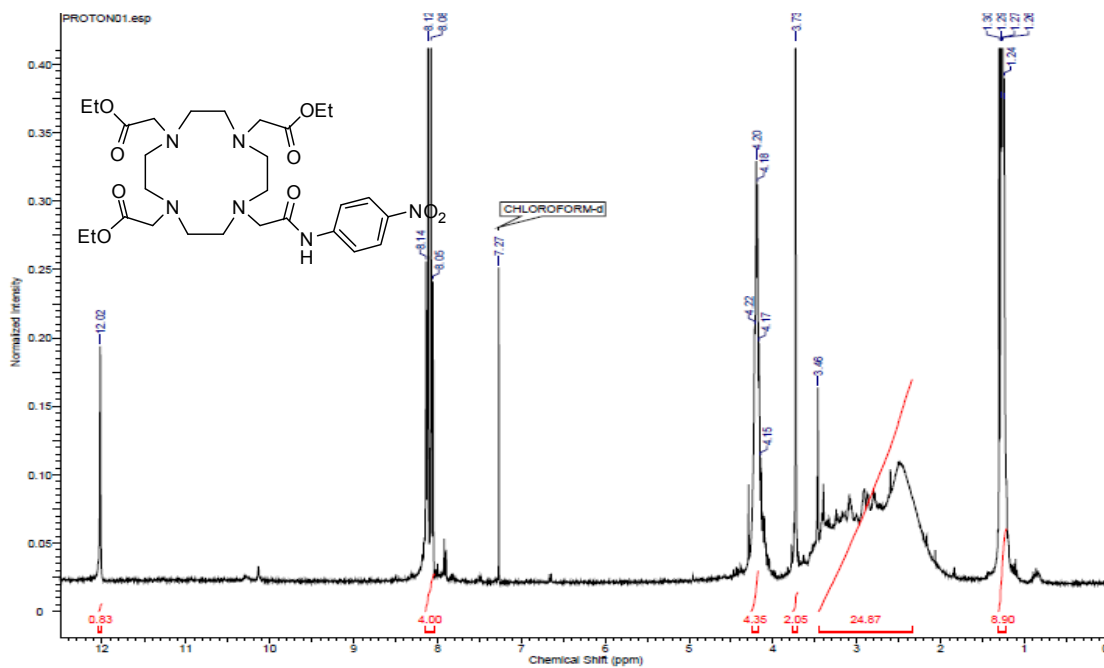
S 5.10: ^{13}C-NMR Spectrum of **5.10**
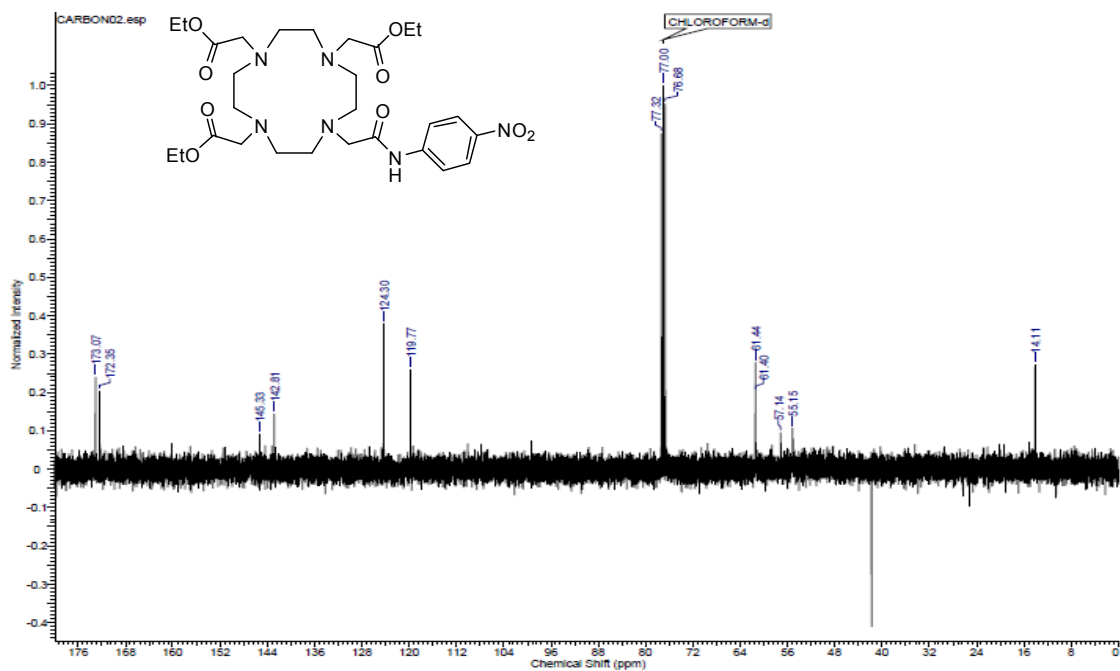
S 5.11: ^{1}H-NMR Spectrum of **5.11**
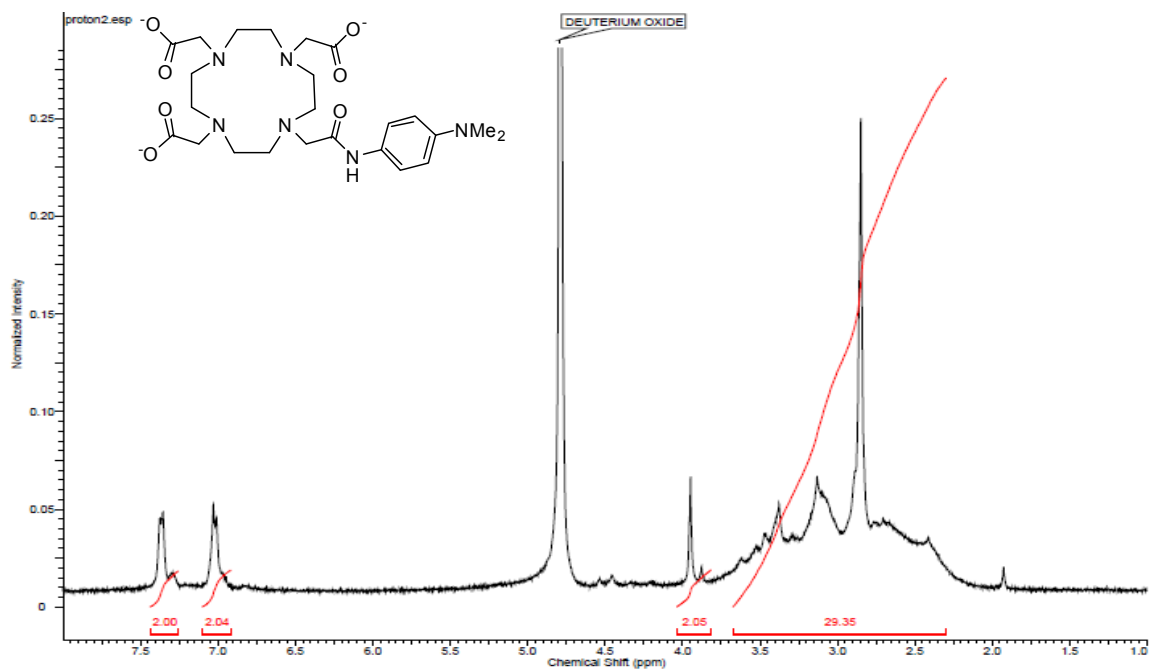
S 5.12: ^{1}H-NMR Spectrum of **5.12**
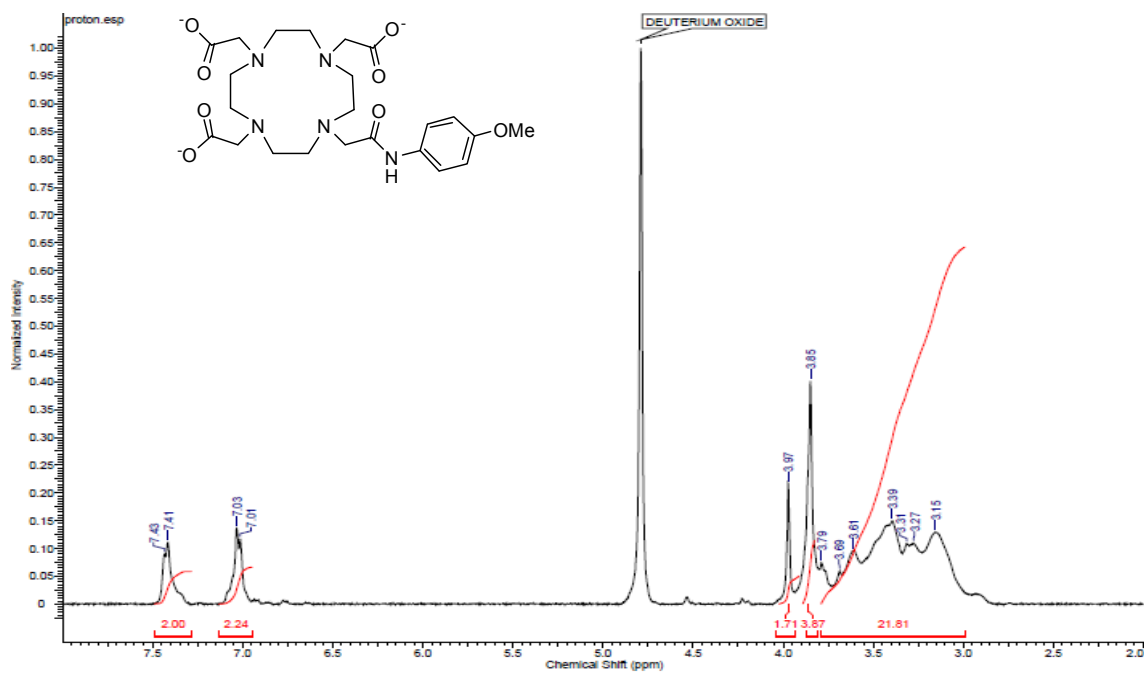
S 5.13: ^{1}H-NMR Spectrum of **5.13**
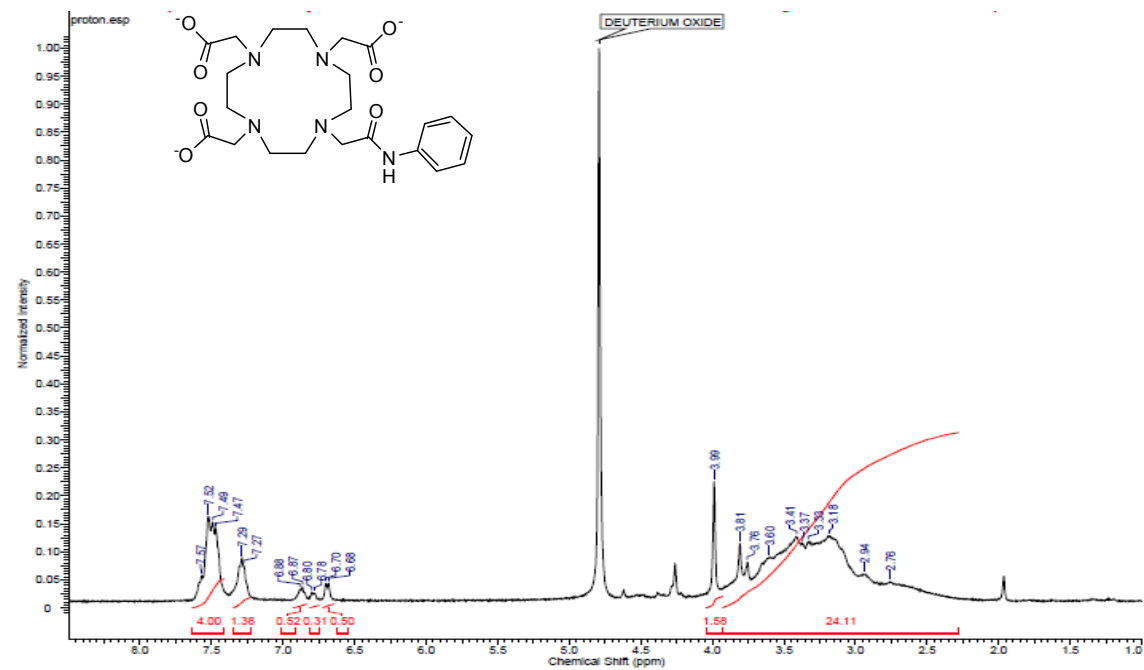
S 5.14: ^{1}H-NMR Spectrum of **5.14**
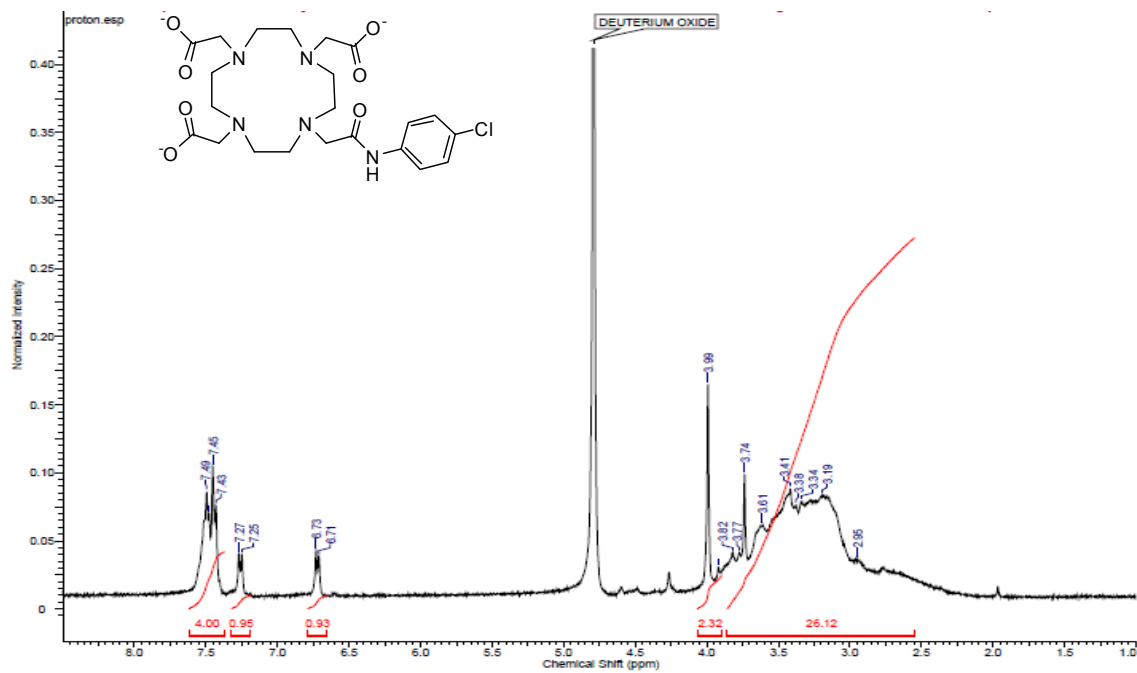
S 5.15: ^{1}H-NMR Spectrum of **5.19**
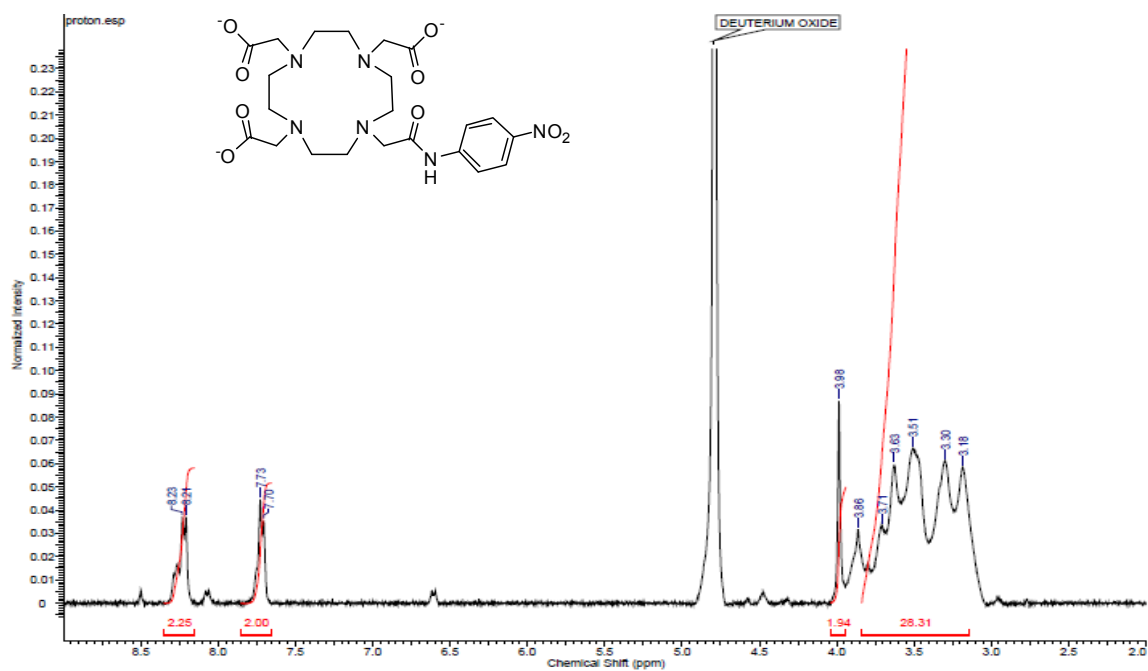
S 5.16: r_1 relaxivity profile of **5.15a**
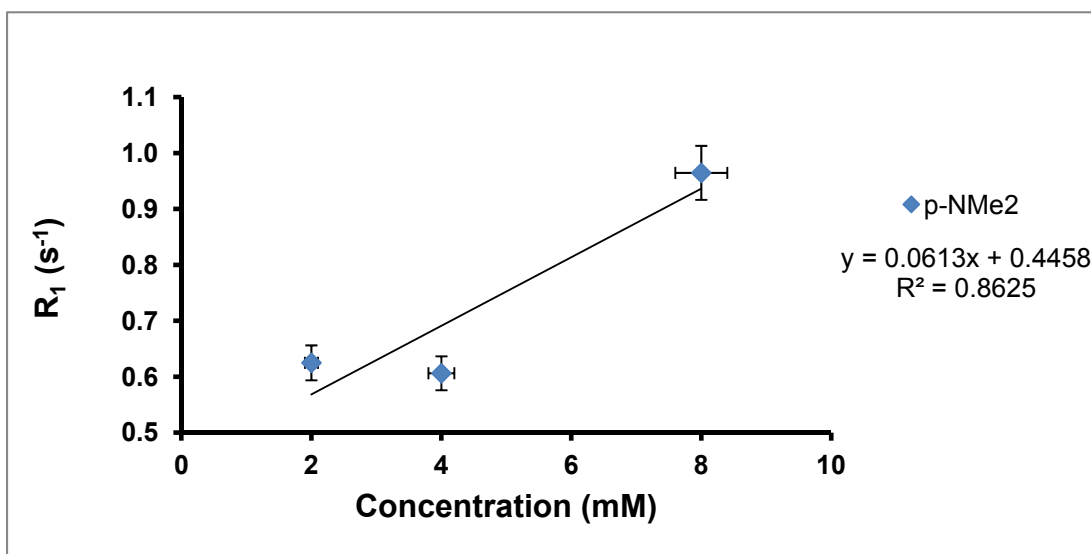
S 5.17: r_2 relaxivity profile of **5.15a**
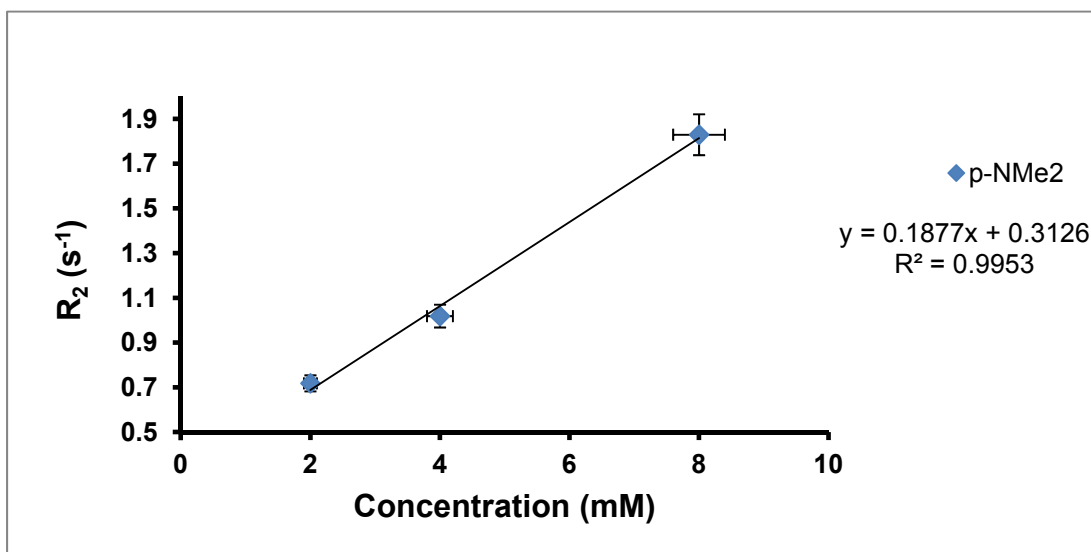
S 5.18: r_1 relaxivity profile of **5.16a**
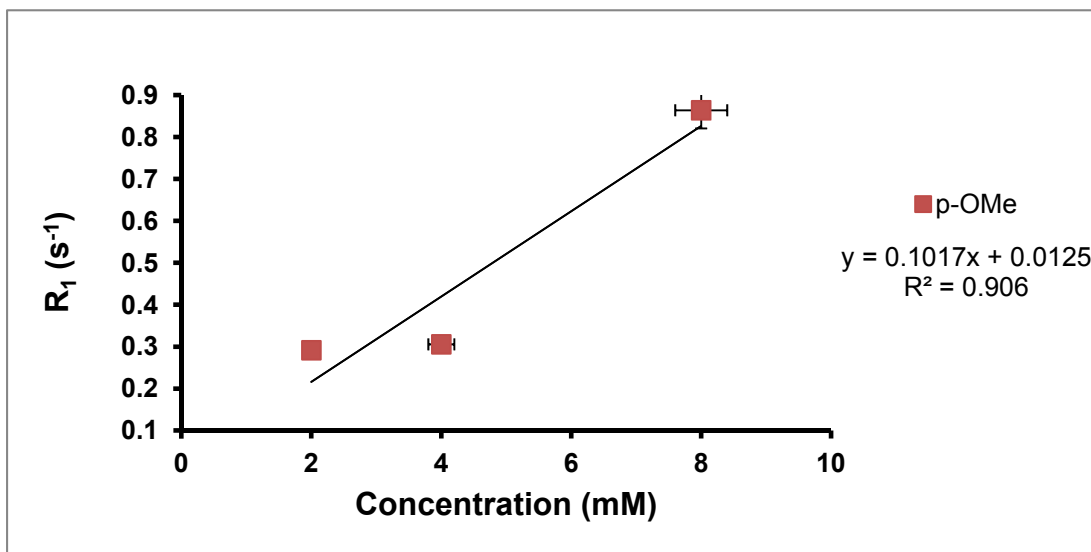
S 5.19: r_2 relaxivity profile of **5.16a**
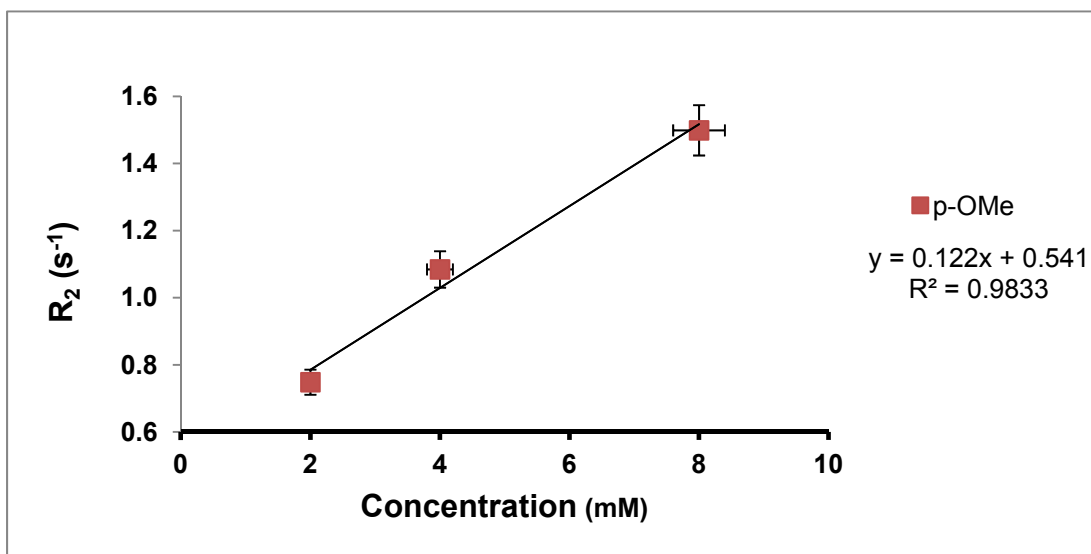
S 5.20: r_1 relaxivity profile of **5.17a**
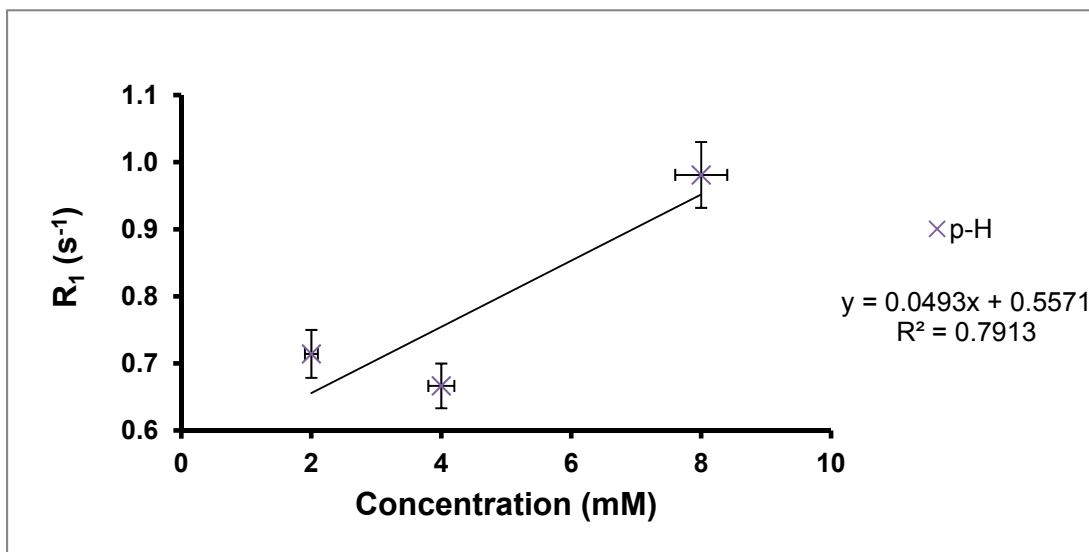
S 5.21: r_2 relaxivity profile of **5.17a**
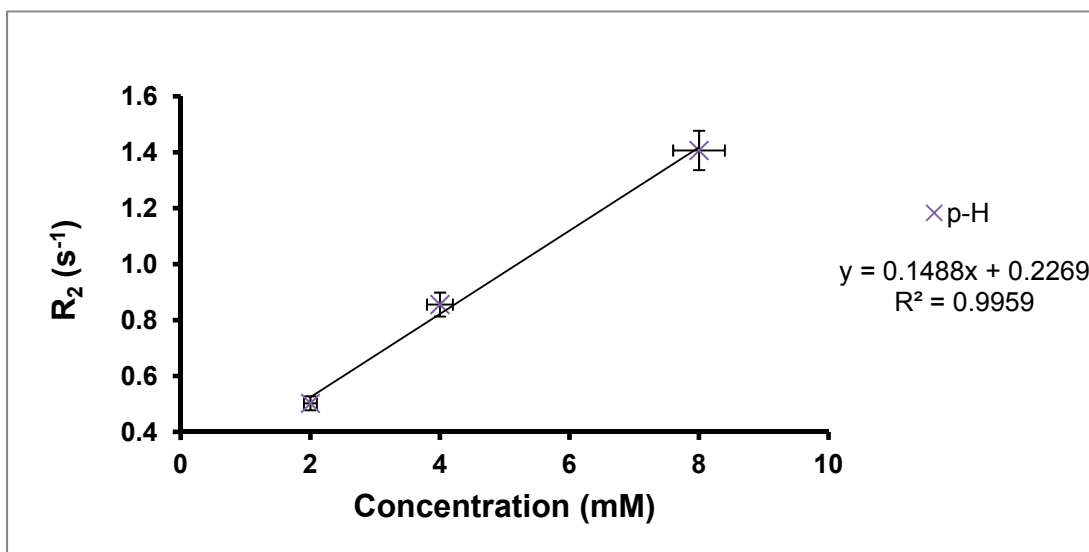
S 5.22: r_1 relaxivity profile of **5.18a**
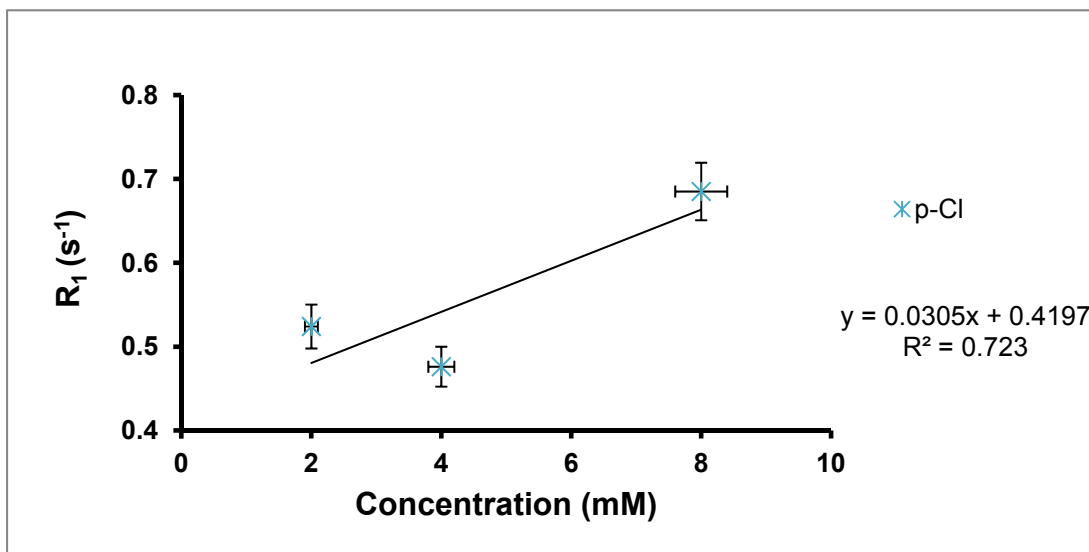
S 5.23: r_2 relaxivity profile of **5.18a**
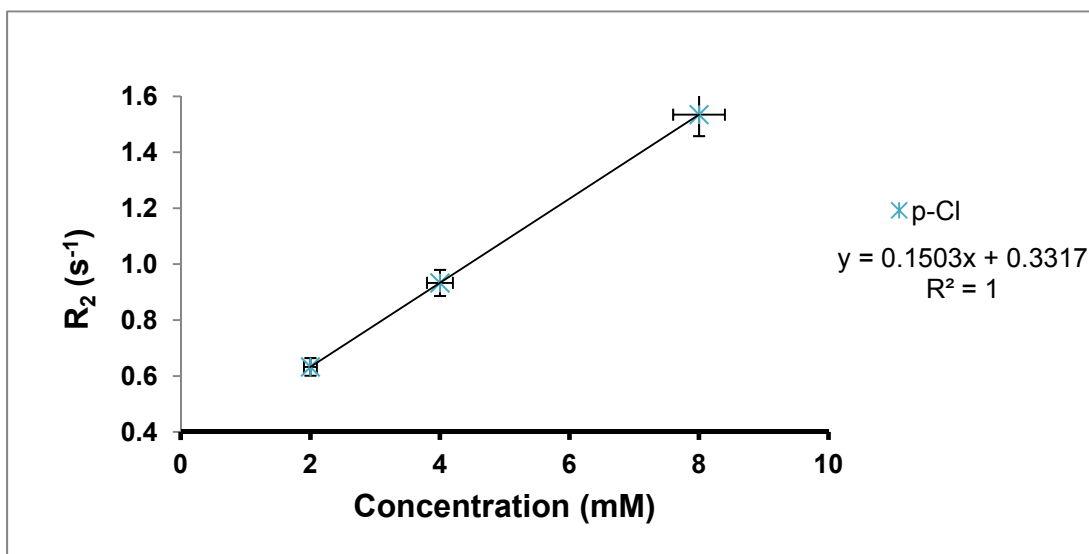
S 5.24: r_1 relaxivity profile of **5.20a**
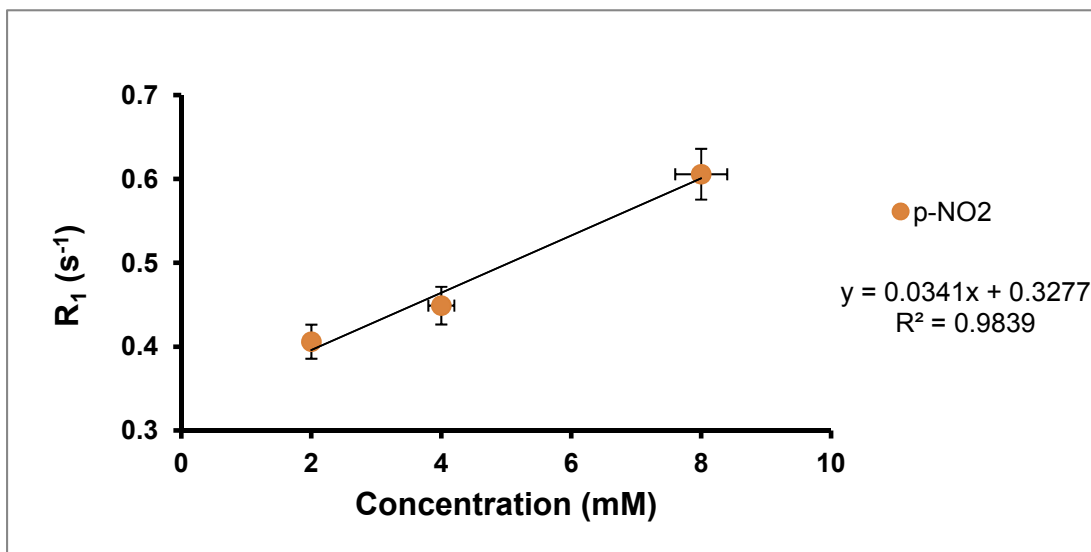
S 5.25: r_2 relaxivity profile of **5.20a**
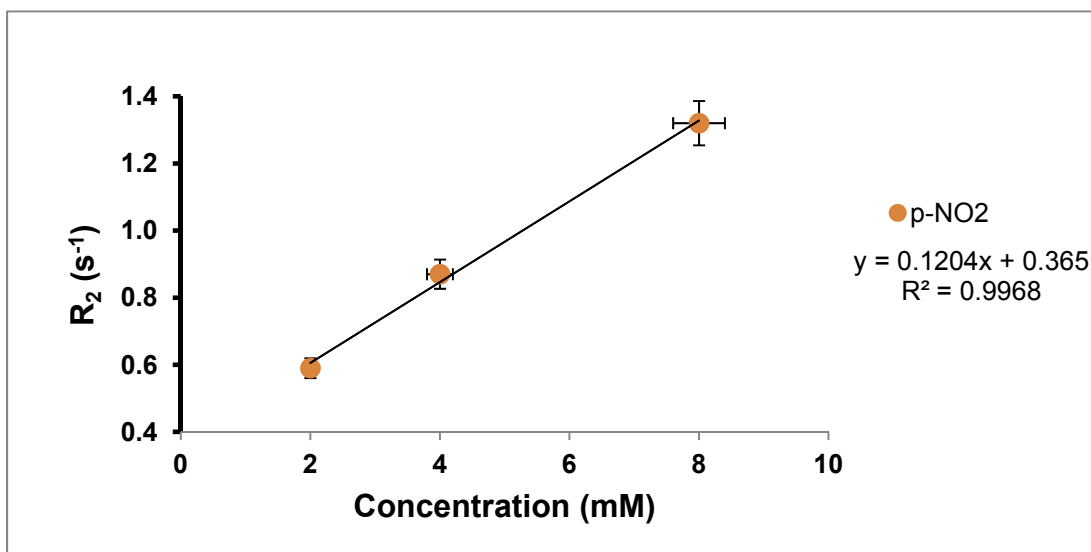
S 5.26: r$_1$ relaxivity profile of **5.21a**
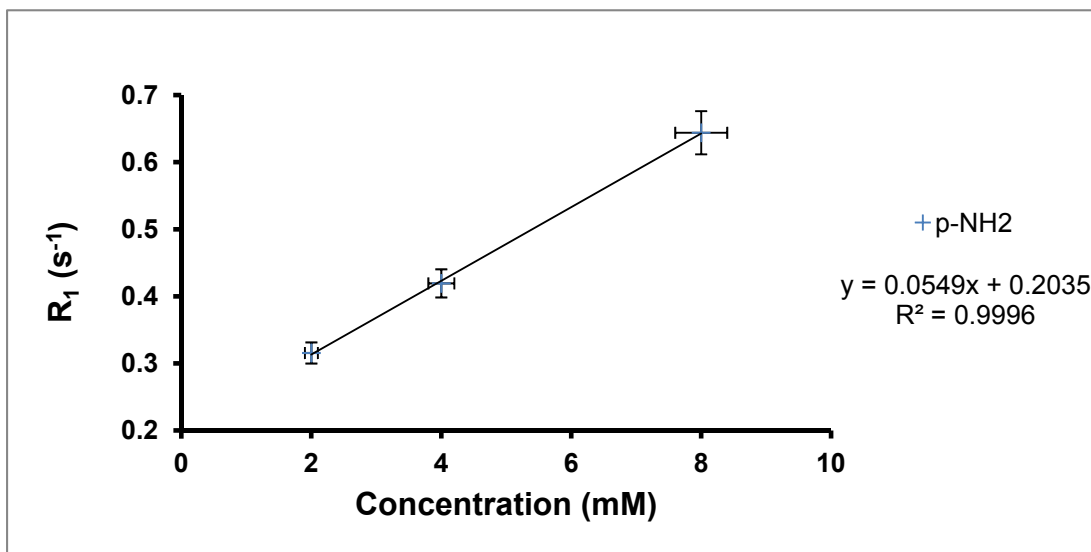
S 5.27: r$_2$ relaxivity profile of **5.21a**
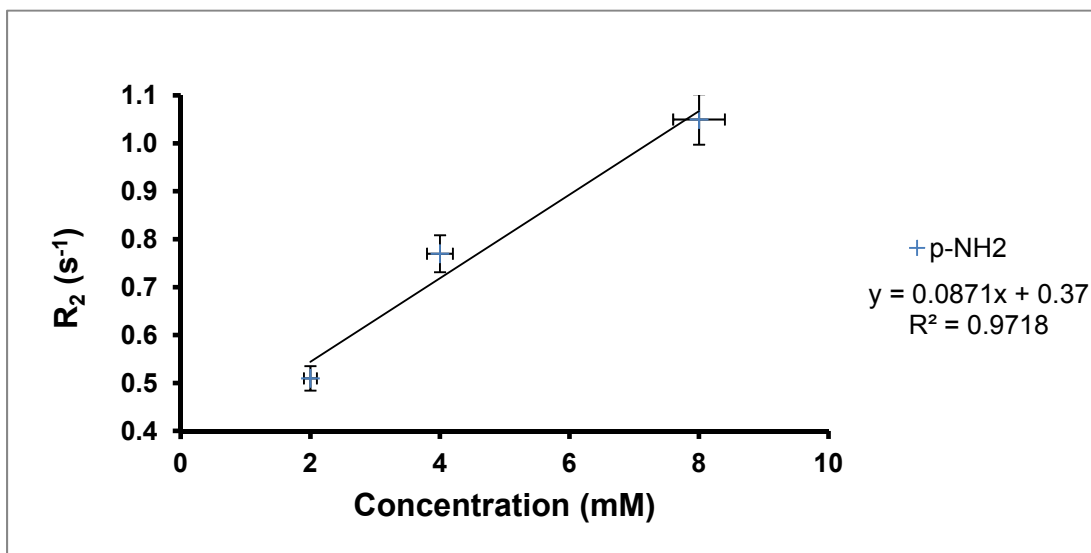
S 5.28: r_1 relaxivity profile of **5.15b**
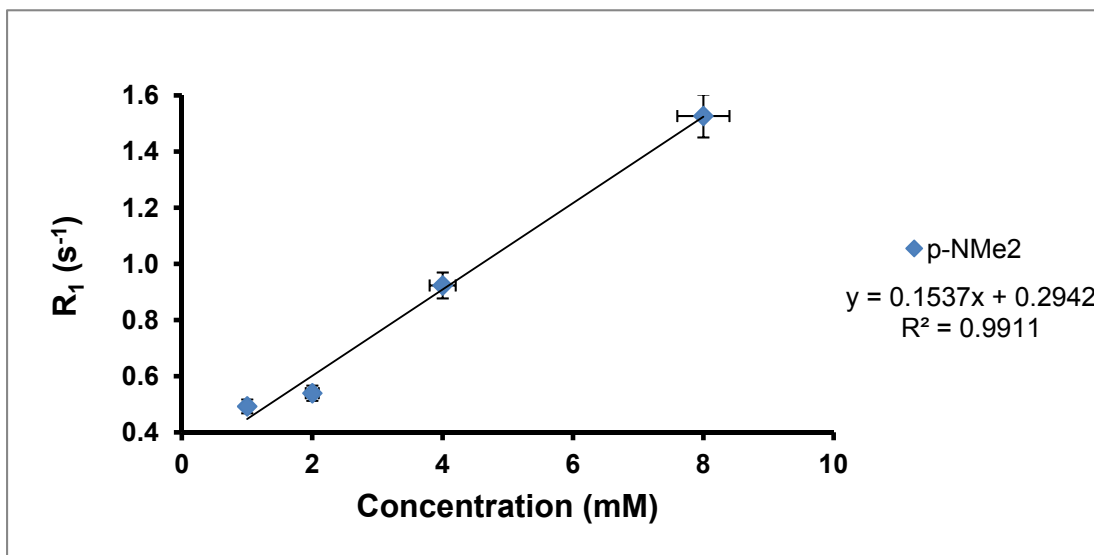
S 5.29: r_2 relaxivity profile of **5.15b**
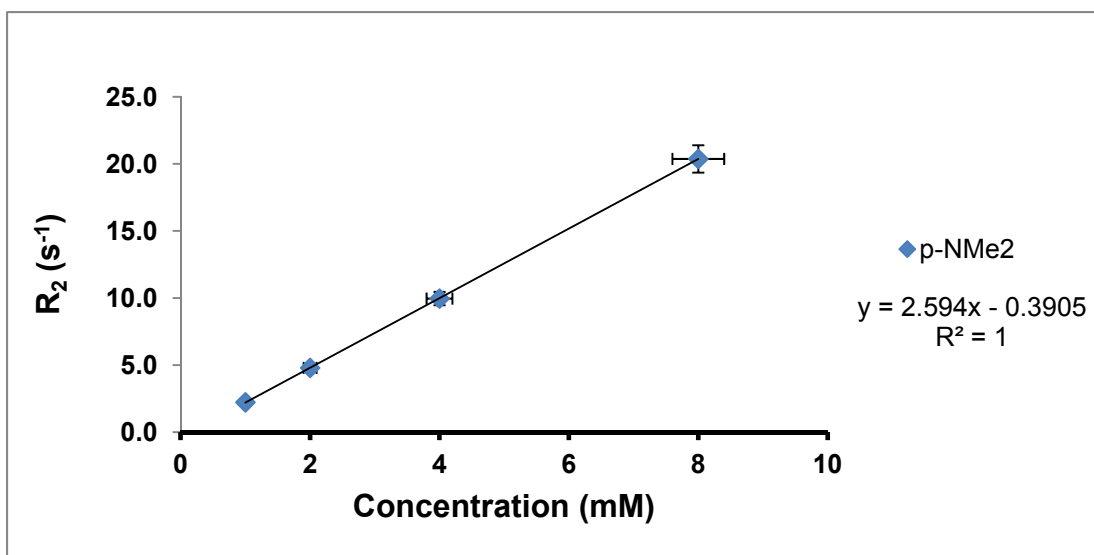
S 5.30: r_1 relaxivity profile of **5.16b**
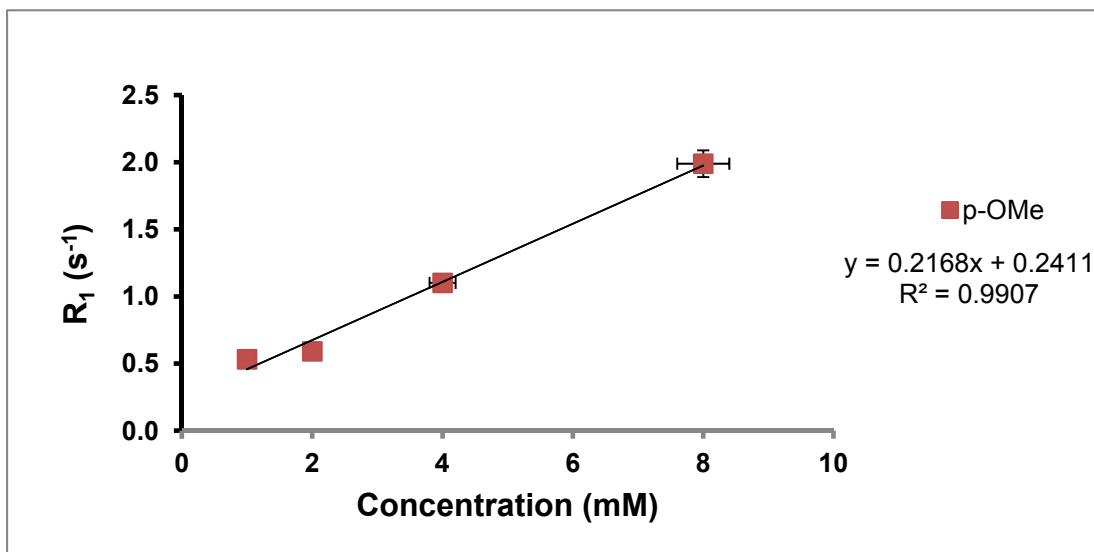
S 5.31: r_2 relaxivity profile of **5.16b**
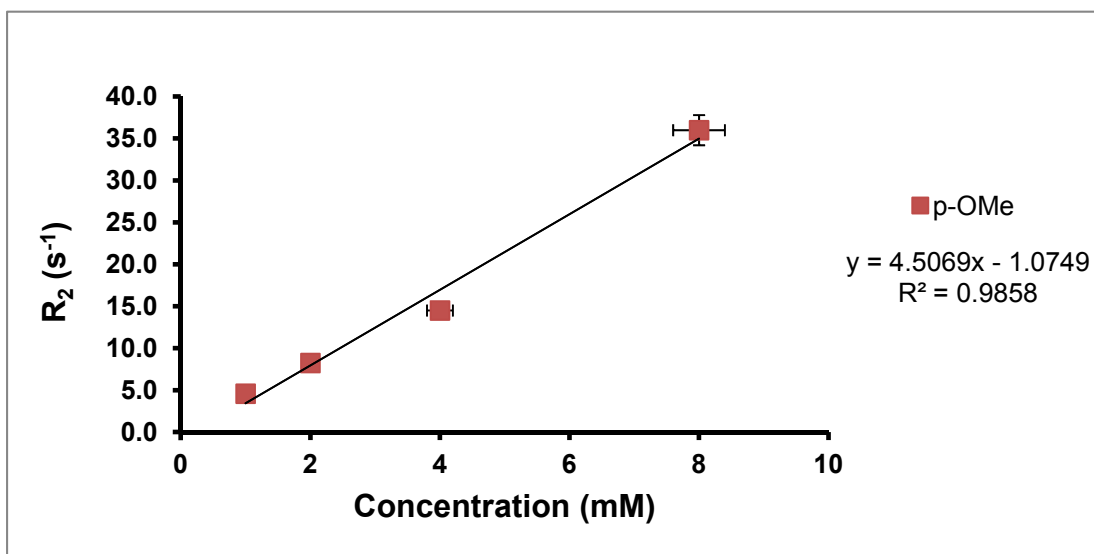
S 5.32: r_1 relaxivity profile of **5.17b**
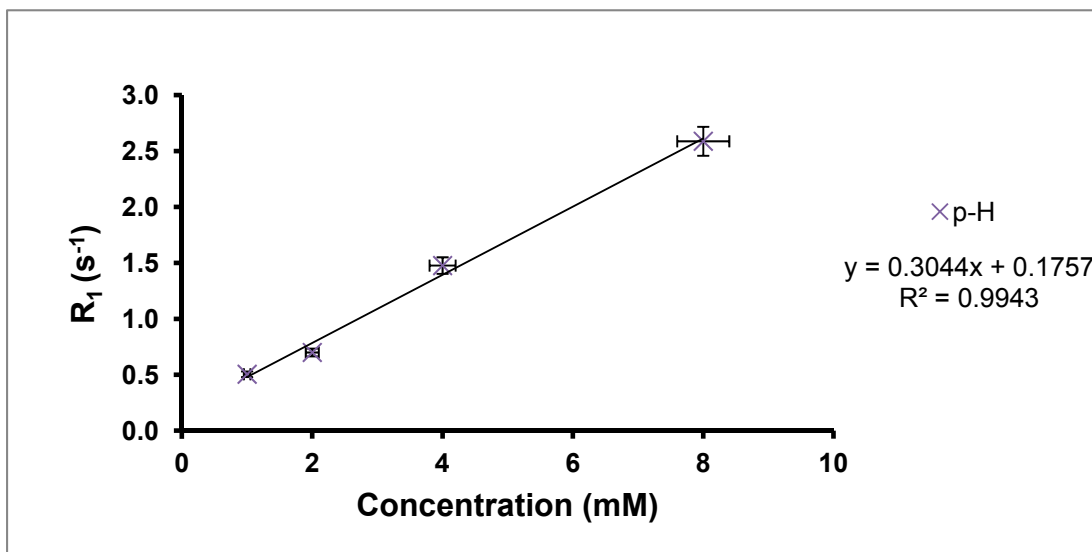
S 5.33: r_2 relaxivity profile of **5.17b**
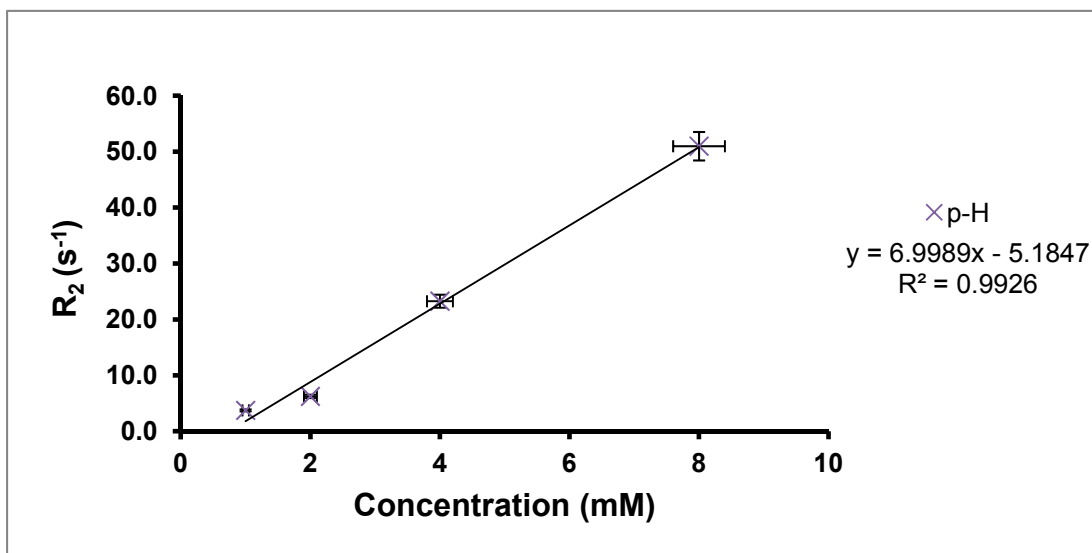
S 5.34: r_1 relaxivity profile of **5.18b**
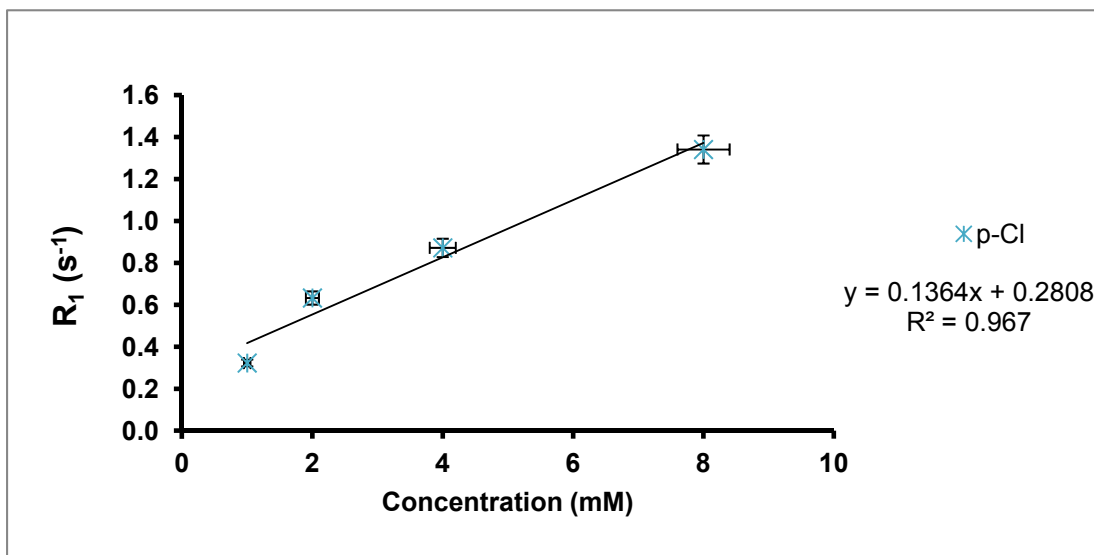
S 5.35: r_2 relaxivity profile of **5.18b**
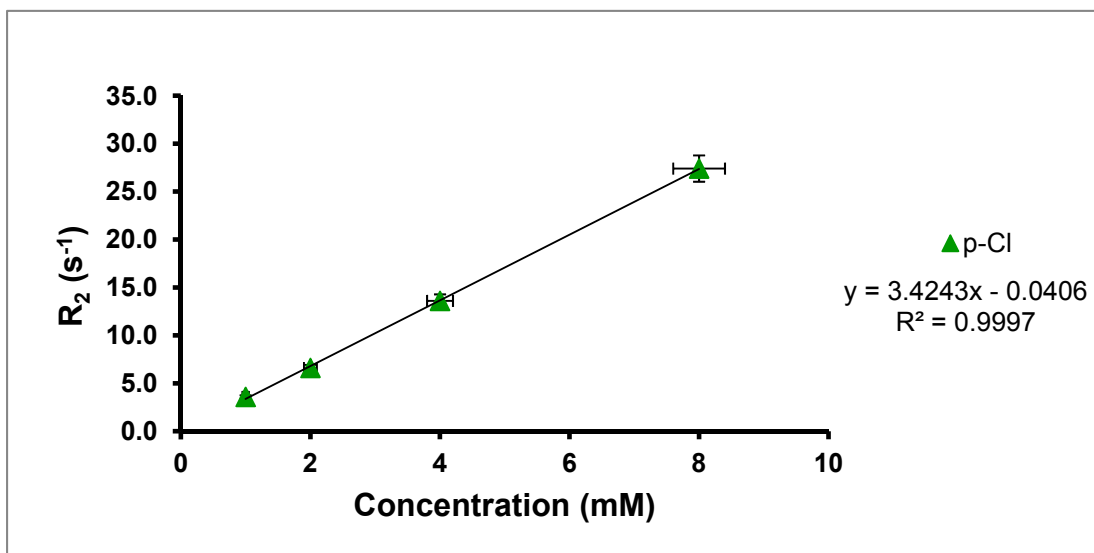
S 5.36: r_1 relaxivity profile of **5.20b**
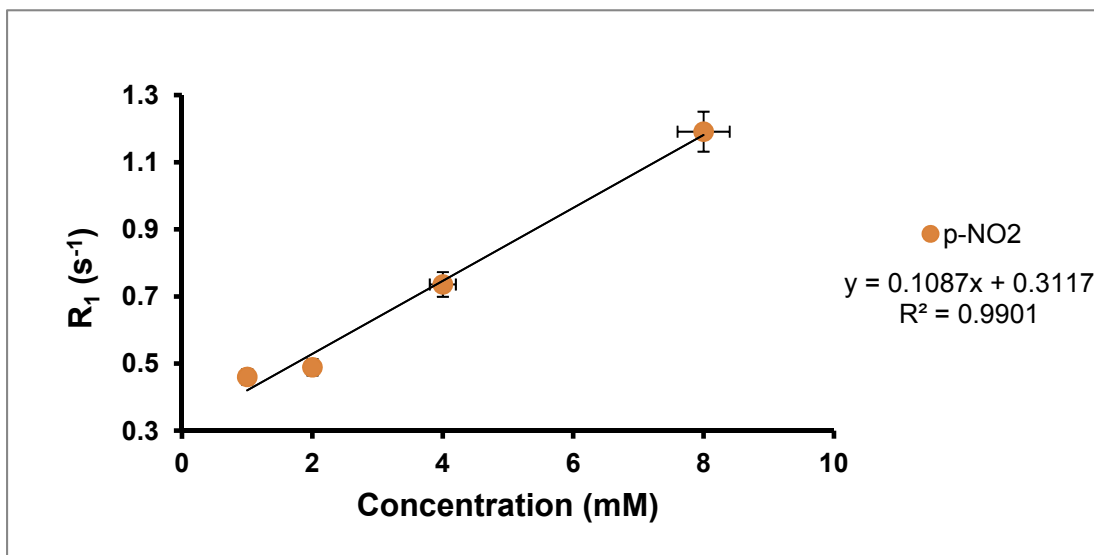
S 5.37: r_2 relaxivity profile of **5.20b**
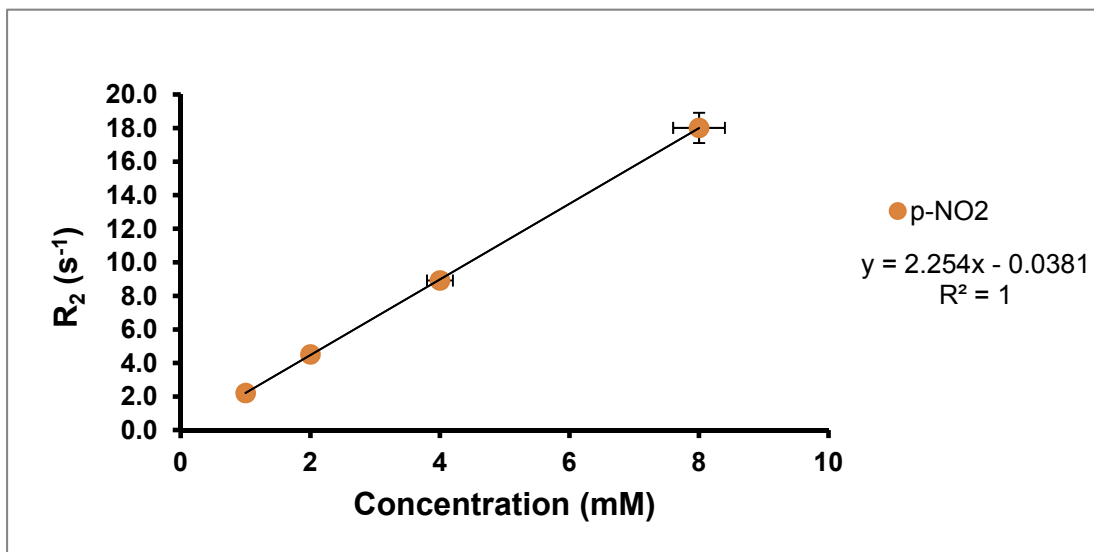
S 5.38: r_1 relaxivity profile of **5.21b**
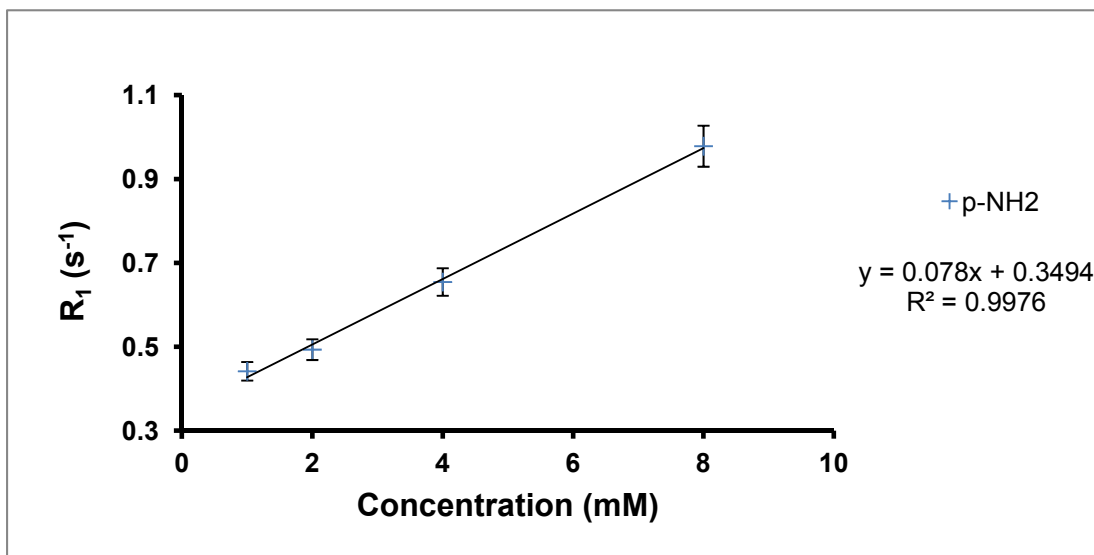
S 5.39: r_2 relaxivity profile of **5.21b**
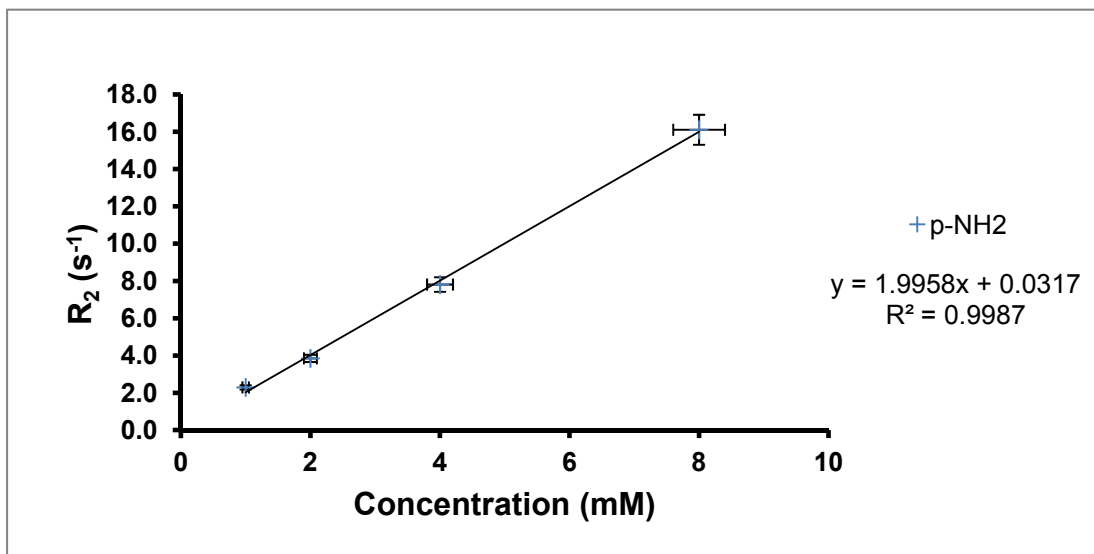
S 5.40: Temperature profile of r_1 relaxivity of **5.17b**
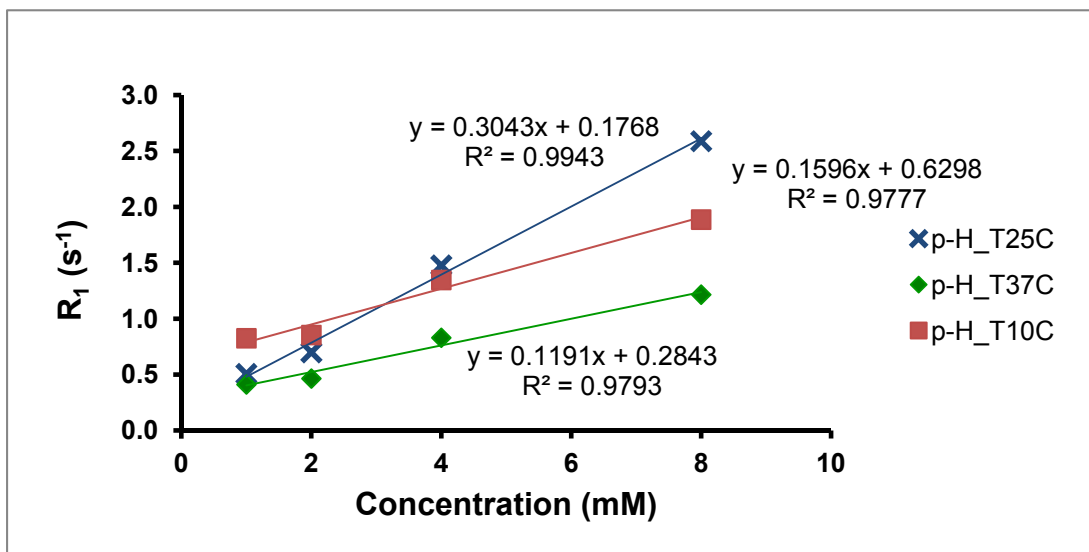
S 5.41: Temperature profile of r_2 relaxivity of **5.17b**
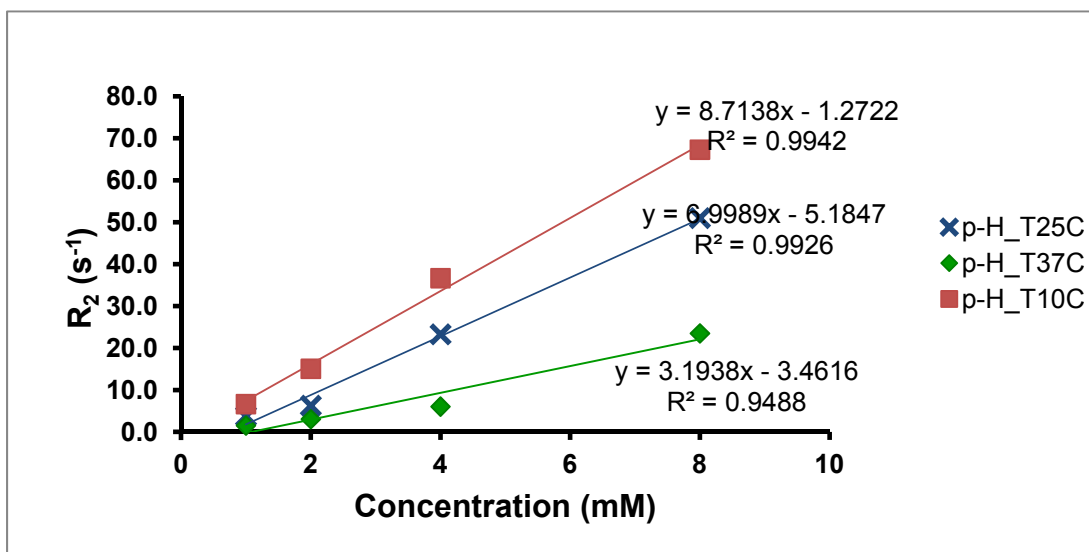
S 5.42: Temperature profile of r_1 relaxivity of **5.21b**
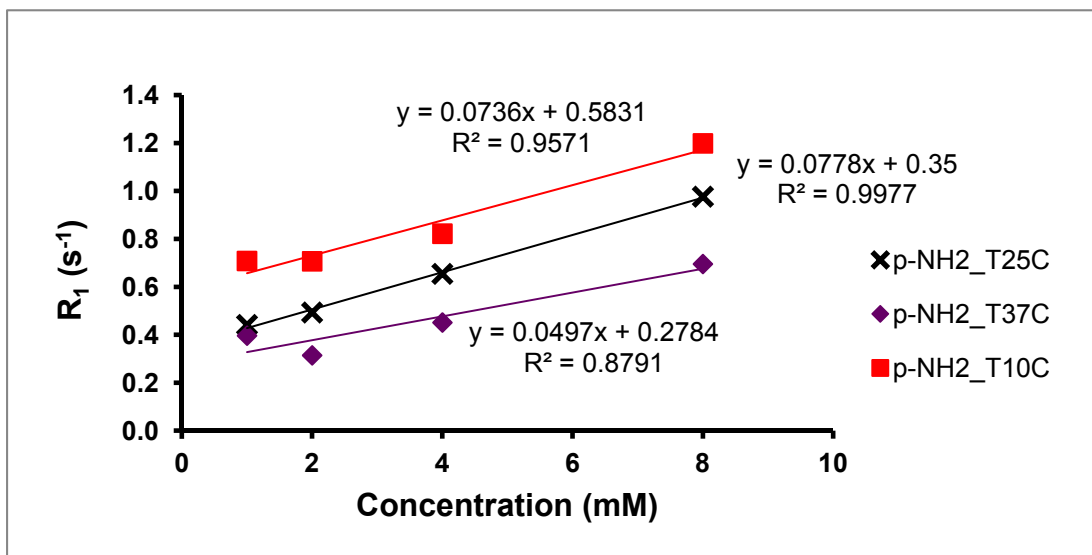
S 5.43: Temperature profile of r_2 relaxivity of **5.21b**

5.5   References

y
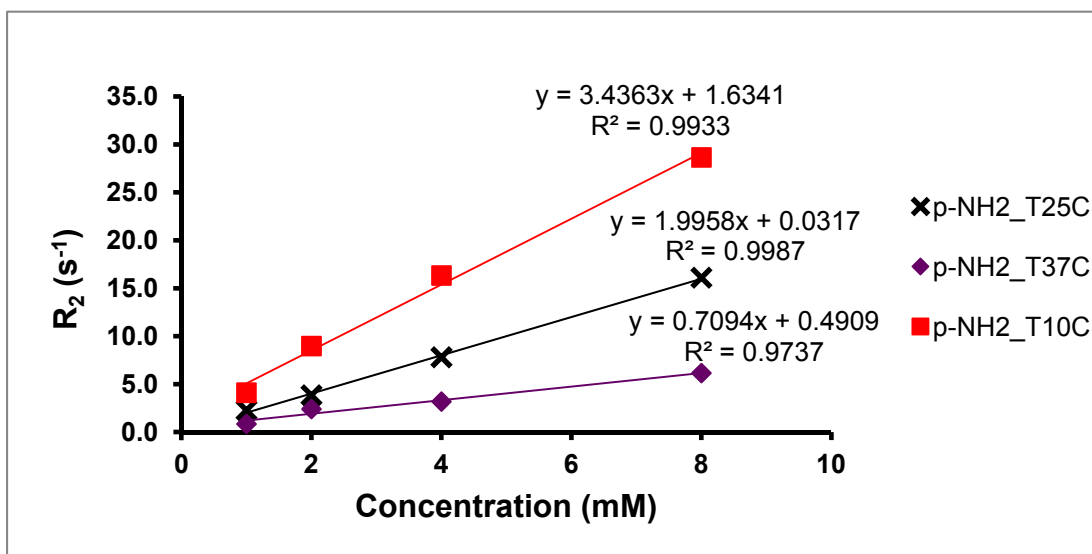
(1) Milne, M.; Lewis, M.; McVicar, N.; Suchý, M.; Bartha, R.; Hudson, R. H. E. *RSC Adv.* **2014,** *4*, 1666-1674.

(2) Liu, G.; Li, Y.; Pagel, M. D. *Magn. Reson. Med.* **2007,** *58*, 1249-1256.

(3) Li, Y.; Sheth, V. R.; Liu, G.; Pagel, M. D. *Contrast Media Mol. Imaging* **2011,** *6*, 219-228.

(4) Terreno, E.; Castelli, D. D.; Cravotto, G.; Milone, L.; Aime, S. *Invest. Radiol.* **2004,** *39*, 235-243.

(5) Viswanathan, S.; Kovacs, Z.; Green, K. N.; Ratnakar, S. J.; Sherry, A. D. *Chem. Rev.* **2010,** *110*, 2960-3018.

(6) Ratnakar, S. J.; Woods, M.; Lubag, A. J. M.; Kovács, Z.; Sherry, A. D. *J. Am. Chem. Soc.* **2008,** *130*, 6-7.

(7) Corey, E. J.; Székely, I.; Shiner, C. S. *Tetrahedron Lett.* **1977,** *18*, 3529-3532.

(8) Hammett, L. P. *Chem. Rev.* **1935,** *17*, 125-136.

(9) Hammett, L. P. *J. Am. Chem. Soc.* **1937,** *59*, 96-103.

(10) Liu, G.; Li, Y.; Sheth, V.; Pagel, M. *Mol. Imaging* **2011,** *11*, 47-57.

(11) Soesbe, T. C.; Ratnakar, S. J.; Milne, M.; Zhang, S.; Do, Q. N.; Kovacs, Z.; Sherry, A. D. *Magn. Reson. Med.* **2014,** *71*, 1179-1185.

(12) Swift, T. J.; Connick, R. E. *J. Chem. Phys.* **1962,** *37*, 307-320.

(13) Granot, J.; Fiat, D. *J.Magn.Reson.* **1974,** *15*, 540.

(14) Soesbe, T. C.; Merritt, M. E.; Green, K. N.; Rojas-Quijano, F.; Sherry, A. D. *Magn. Reson. Med.* **2011,** *66*, 1697-1703.

(15) Rojas-Quijano, F. A.; Tircso, G.; Benyo, E. T.; Baranyai, Z.; Hoang, H. T.; Kalman, F. K.; Gulaka, P. K.; Kodibagkar, V. D.; Aime, S.; Kovacs, Z.; Sherry, A. D. *Chem. Eur. J.* **2012,** *18*, 9669-9676.

(16) Zhang, S.; Wu, K.; Sherry, A. D. *Angew. Chem. Int. Ed.* **1999,** *38*, 3192-3194.

(17) Aime, S.; Barge, A.; Botta, M.; Parker, D.; De Sousa, A. S. *J. Am. Chem. Soc.* **1997,** *119*, 4767-4768.

(18) Giovenzana, G. B.; Negri, R.; Rolla, G. A.; Tei, L. *Eur. J. Inorg. Chem.* **2012,** *2012*, 2035-2039.

(19) Miller III, W. A.; Moore, P. B. *J.Org. Biomol. Simul.* **2014,** *1*, 1-13.

Chapter 6

6 Synthesis Towards Modified Dy^{3+} and Tm^{3+} DOTAM-tetraanilide Complexes Bearing a *para*-phosphonate Monoanilide for *In vivo* Studies

6.1 Introduction

A previous report was made regarding the study of DOTAM-tetraanilide PARACEST agents which were varied with regards to their *para*-substituents.[1] This was done with the aim of exploring the adjustment of the amide exchange rate by the presence of electron-withdrawing groups (EWGs) and electron-donating groups (EDGs). The adjustment of the amide exchange rate in turn would affect the CEST due to amide protons. Unfortunately, with the exception of the Dy^{3+} and Tm^{3+}-*p*-H and -*p*-OMe complexes (Figure 6.1), the other complexes were insoluble and could not be further analyzed after synthesis.[1] The solid state structure of the Tm^{3+}-*p*-OMe complex revealed that the angle between the N-Ln-N and O-Ln-O planes (α) was 27°, thus indicating a twisted square antiprismatic (TSAP) geometry. It was also noted that the complex lacked a metal bound water molecule and was more accurately termed as the TSAP' isomer. Additionally, the Tm^{3+}-*p*-OMe complex had an interesting feature of two CEST signals of moderate intensities at -43 and -83 ppm, corresponding to the square antiprismatic (SAP') and TSAP' isomers, respectively.[1] These features reported for the Tm^{3+}-*p*-OMe complex are unique and so warrants further studies.

Ln^{3+} = Dy^{3+}, Tm^{3+}

Ln^{3+}-tetra-*p*-H (R = H)

Ln^{3+}-tetra-*p*-OMe (R = OMe)
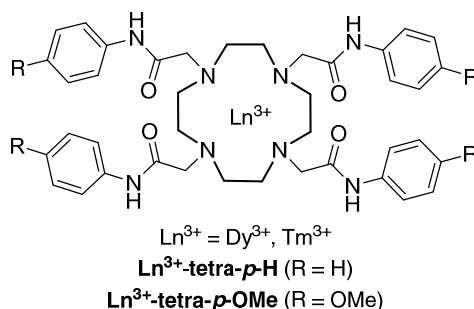
Figure 6.1: Chemical structures of some complexes discussed in this work.

It has been reported that non-ionic complexes are more tolerable than ionic ones due to better blood compatible viscosity and osmolality.[2] Therefore, for the tetraanilide Tm^{3+}-*p*-OMe complex to be used *in vivo* (in mice or other animal models), the overall charge of the complex needs to be reduced to neutral or close to neutral. To meet the charge requirements, it was decided that a phosphonate group should be installed in the *para*-position of the unsubstituted aniline ring. This derivative would be a lone arm on the macrocycle, with the remaining arms being the unmodified *para*-substituted aniline of *p*-OMe. The corresponding *p*-H complex would also be synthesized for comparison purposes. As a result, our lanthanide metalated complexes would have an overall charge of +1, which should be more tolerable for *in vivo* studies, should the opportunity present itself. Additionally, we hoped for an increase in solubility in aqueous solvents. It is anticipated that the presence of the two CEST signals seen in the unmodified tetraanilide Tm^{3+}-*p*-OMe complex would still be present in this modified analogue. If so, it would allow for ratiometric analysis that would eliminate the CEST effect dependency on concentration, thus allowing the agent to be used as a biological reporter.[3, 4] The ratiometric analysis of the unmodified tetraanilide Tm^{3+} -*p*-OMe complex was attempted but due to solubility restrictions, no appropriate measurements could be performed.[1]

6.2   Results and Discussion

6.2.1 Synthesis

The synthetic route as shown in Schemes 6.1 and 6.2 represent the attempts to the modified DOTAM tetraanilide possessing a phosphonate group. The initial reactions attempted in order to achieve **6.4** without using a protecting group for the amino moiety was met with difficulty. Starting with the *p*-I-aniline **6.1**, several conditions were tried. These included using various solvents (toluene, CH_3CN), reaction times (up to 3 days), and temperatures (90^oC - 155^oC). Under these conditions, multiple products were formed including the desired compound but purification of the mixture was challenging.
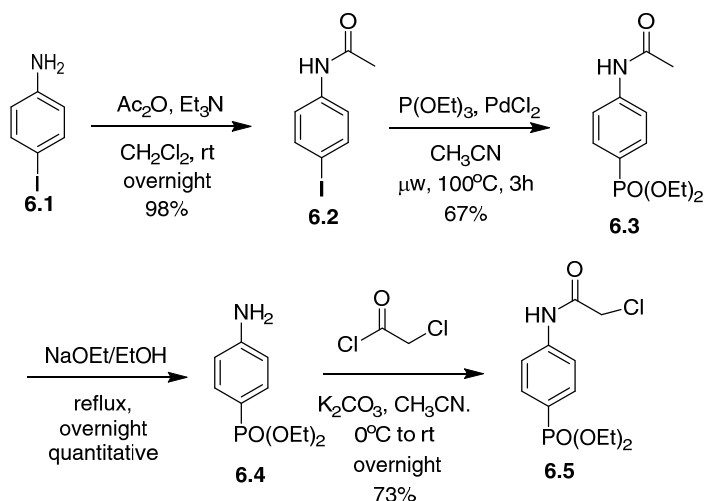
Scheme 6.1: Synthetic route to phosphonate ester electrophile.

To further optimize the desired reaction conditions whereby the phosphonate diester was produced, several metal-catalyzed cross couplings of **6.1** and triethyl phosphite were attempted based on literature precedence.[5] NiCl$_2$, Pd(OAc)$_2$ and PdCl$_2$ were used as catalysts. However, all gave the same results as previously observed, that is, multiple products being formed. This occurred whether or not the reaction was carried out at room temperature or heated to high temperatures.

A model reaction with iodobenzene was performed using the PdCl$_2$ catalyst so as to determine whether or not the amine of **6.1** was inhibiting the progress of the desired reaction. This reaction was successful and thus highlighted the need of a protecting group for the amine moiety.

Following literature procedure,[6] the amino group of the *p*-I-aniline **6.1** was protected with an aceyl group to give **6.2**. The palladium-mediated cross coupling reaction was then re-attempted with **6.2** and the alkylphosphite. While this reaction was met with more success as compared to that with the free amine, the reaction times were long and the yields were unsatisfactory. To reduce the reaction times while possibly increasing the yields of **6.3**, microwave-assisted synthesis of the palladium-catalyzed cross coupling

reaction was performed.[7] Moderate yields of the desired phosphonate diester compound **6.3** were accomplished following purification by column chromatography.
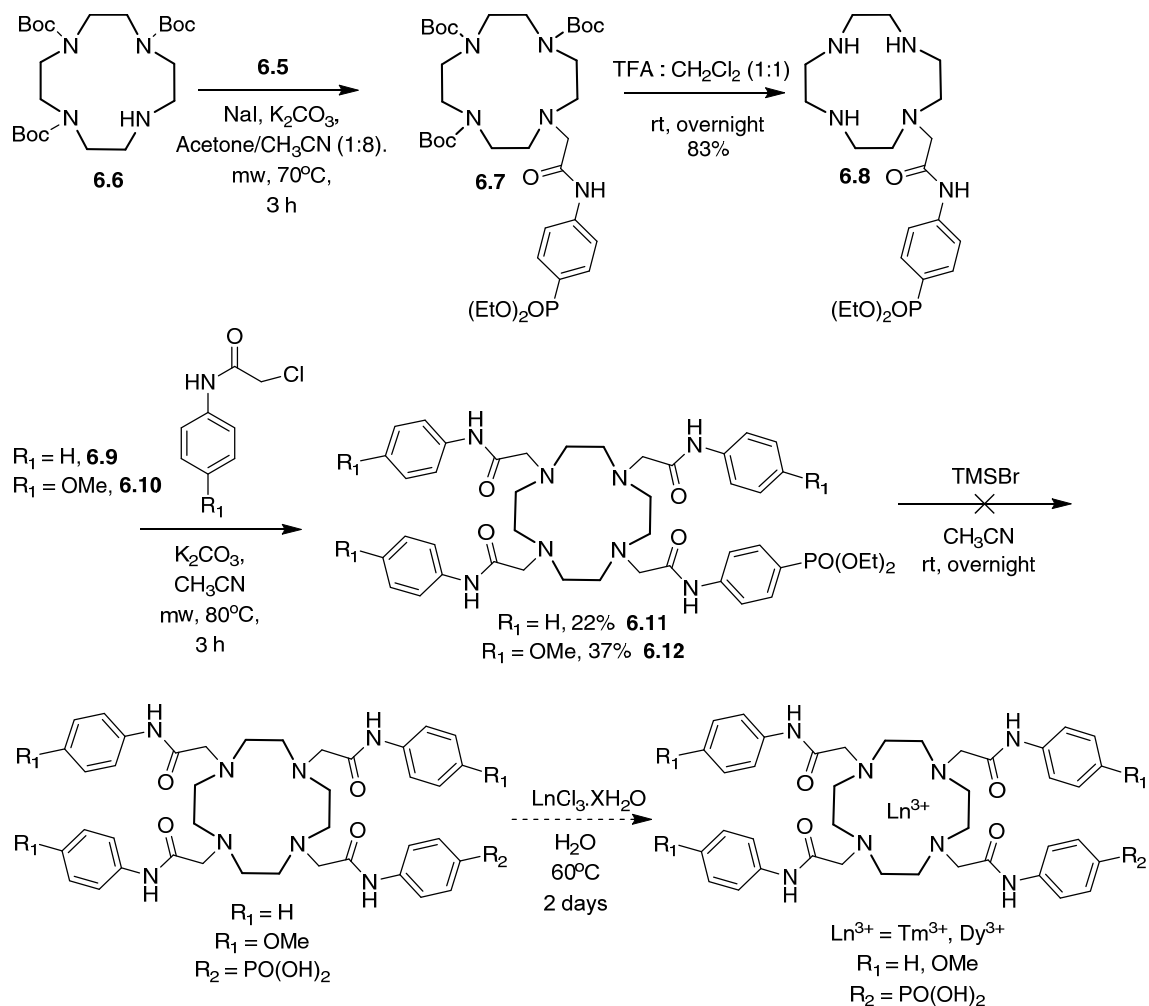
Scheme 6.2: Synthetic attempt to obtain metalated phosphonate complexes.
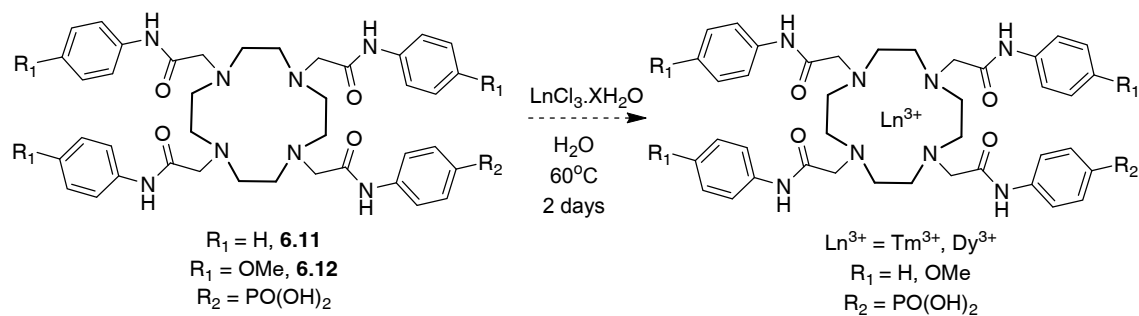
Scheme 6.3: Synthetic approach to metalated phosphonate diester complexes.

The cross-coupling reaction between palladium and the protected *p*-I-aniline **6.2** relies on the Pd (II) of the catalyst being reduced to Pd (0) by the triethyl phosphite. In order for this reduction to occur, it has been demonstrated that at least five equivalents of the triethy phosphite is needed, in addition to heating the reaction mixture to at least 80°C.[7, 8]
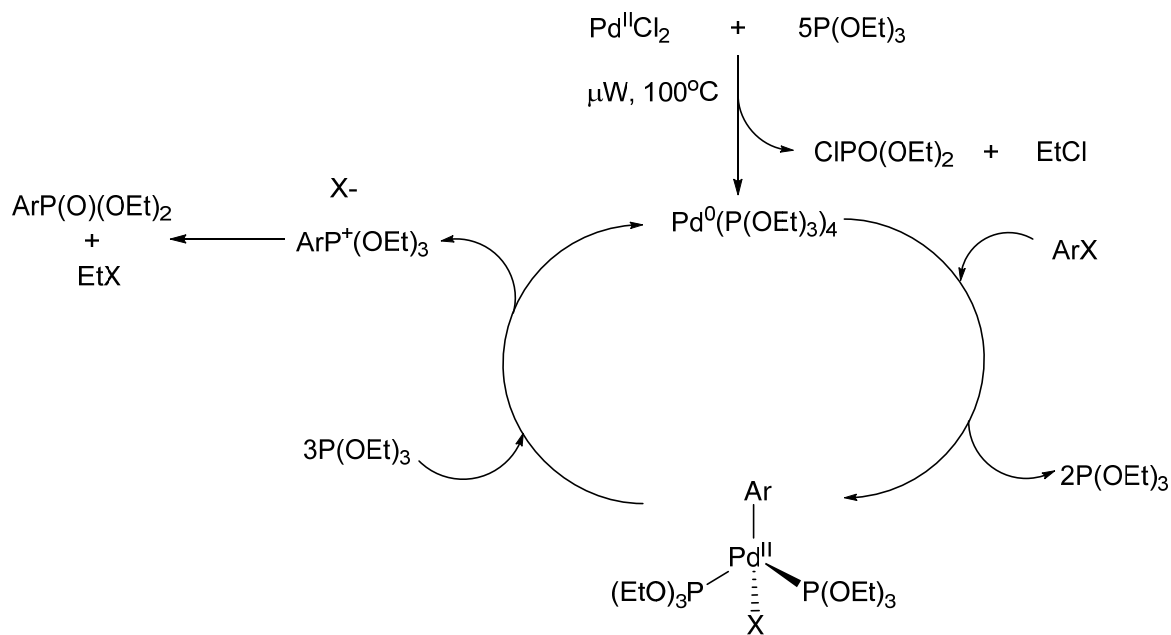
Scheme 6.4: Proposed mechanism of palladium-catalyzed microwave-assisted synthesis of a phosphonate diester.

The mechanism of the catalysis by Pd(0) is more complicated than the corresponding reaction with Ni(0). This complication arises as a result of factors such as the source of Pd(0), the types of ligands of the catalyst and the electronic and steric factors of the aryl (or alkyl halide).[9] The proposed mechanism for this cross coupling is shown in Scheme 6.4 and is derived from that of the nickel-mediated reaction.[9]

The amino-protecting group of **6.3** was removed and a reaction involving **6.4** and chloroacetyl chloride was carried out to afford compound **6.5** (Scheme 6.1). Monoalkylation of the triBoc-protected cyclen **6.6** with the electrophile **6.5** using traditional conditions were problematic. Initial conditions were done at room temperature

followed by heating at 50°C for up to 3 days but the reaction was quite sluggish. The reaction was also carried out with the assistance of the microwave, initially at 60°C and then at 80°C for up to 3 hrs. At these higher temperatures, even although the reaction proceeded with some improvement, UPLC-MS also showed deprotected products. As such, the subsequent monoalkylation reaction was carried out at 70°C. Additionally, rather than separate the products at this stage, the crude reaction mixture of **6.7** was carried forward to the deprotection step to facilitate a less complicated purification step. Over two steps, the monoalkylated product **6.8** was obtained in low yield (Scheme 6.2).

Trialkylation of **6.8** with the unmodified aniline electrophiles of *p*-H (**6.9**) and *p*-OMe (**6.10**) proceeded sluggishly as that of the monoalkylation and the reaction did not go to completion. The outcome was the same whether the reaction was done for 3 days heating at 60°C or in the microwave for 3 hrs at 80°C. Creation of an *in situ* iodide-containing electrophile of **6.9** and **6.10** via a Finklestein reaction did not improve the formation of the desired peralkylated products **6.11** and **6.12**. The reaction mixture consisted mostly of trialkylated and tetraalkylated products that were difficult to separate by silica gel column chromatography as both products were very polar and eluted together. Purification was also attempted by semi-preparative thin layer chromatography with a solvent system of H$_2$O/*sec*-butanol/acetic acid in 2.5:2.0.5 ratio. Those conditions also proved unsuccessful. As a last attempt and based on the polarity of the products, HPLC purification using a C$_{18}$ column was attempted. This was met with some success but the desired products **6.11** and **6.12** were obtained in low yields.

The dealkylation step of the phosphonate diesters of the peralkylated compounds **6.11** and **6.12** was the most difficult step (Scheme 6.2). Several reaction conditions were attempted in order to cleave the ester bonds. These ester bonds were very stable under refluxing conditions or heating in the microwave at high temperatures in concentrated HCl.[10] A reaction mixture of incomplete dealkylation products ensued when TMSBr was used at room temperature in varying solvents for prolonged reaction times.[6, 11] This phenomenon was also observed when neat TMSBr was used. Although the reaction conditions with TMSBr produced some of desired phosphonate compound, UPLC-MS also indicated various bromide adducts of these products, which were still present even

after neutralization with NaOH and 2 days of dialysis. This was the norm when more than 90% TMSBr was used. Quenching the reaction with CH_3OH as typically done after concentration of the reaction mixture,[6] led to decomposition products.

As a result of the challenges faced during removal of the phosphonate diesters of **6.11** and **6.12**, it was decided that metalation of the diesters **6.11** and **6.12** as seen in Scheme 6.3 should be pursued so as to be able to preliminarily characterize the complexes based on their magnetic properties. This approach does not represent an ideal situation, considering that these complexes would still have a +3 charge and the charge requirements for future *in vivo* studies would not be met.

6.3   Conclusions and Future Work

The synthesis of DOTAM-*para*-substituted tetraanilide Dy^{3+} and Tm^{3+} complexes with one aniline arm bearing a phosphonate group in the *para*-position of the aniline ring and the remaining arms containing *p*-OMe or *p*-H was attempted. This modification was based on published results regarding the intriguing observation of two amide CEST signals in the unmodified tetraanilide Tm^{3+}-*p*-OMe complex.[1] The purpose of the phosphonate group was to reduce the overall charge of the complex for prospective *in vivo* studies. Unfortunately, the synthesis was fraught with difficulties such as low yields and unsuccessful reactions. Consequently, at this time, the desired target complexes cannot be attained.

The inability to acquire the desired target phosphonate metal complexes, necessitated temporary alteration of the target metalated complexes to that containing the phosphonate diesters. Once these precursor compounds are obtained in yields sufficient for metalation, the lanthanides Dy^{3+} and Tm^{3+} will be incorporated into the these ligands containing *p*-OMe or *p*-H. At this juncture, comparative evaluation of the magnetic properties of these complexes similar to that carried out for the unmodified tetraanilide complexes for which no inner sphere water was present will be performed.[1]

More importantly, the condition for efficient removal of the phosphonate diester needs to be determined. This may involve changing the type of alkyl groups of the phosphonate diester. Once this has been accomplished, metalation with the desired lanthanides can be carried out. The magnetic properties of the complexes can then be evaluated and compared to both the unmodified DOTAM tetraanilide complexes and those having the phosphonate diester present. Depending on the results obtained, *in vivo* assessments of the modified tetraanilides containing the phosphonate group may be completed.

6.4 Supplemental Information

6.4.1 General Experimental

General synthetic details can be found in Appendix 1.

6.4.2 Synthetic Procedures
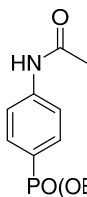
Diethyl (4-acetamidophenyl)phosphonate (6.3). Triethylphosphite (1.25 mL, 7.173 mmol) and $PdCl_2$ (0.159 g, 0.897 mmol) were added to a solution of **6.2** (1.17 g, 4.483 mmol) in CH_3CN (18 mL) in a 20 mL microwave vial which was then sealed. The mixture was irradiated at 100°C and maintained for 3 h with stirring in a Biotage Initiator® microwave reactor. The temperature was monitored by external IR temperature sensor. After 3 h, the reaction was checked by TLC and UPLC-MS and the solution was transferred to a round bottom flask for concentration under reduced pressure. The crude product was purified by column chromatography (silica, 1:1 EtOAc/hexanes then 5% MeOH in CH_2Cl_2). The title compound was obtained as a yellow sticky solid (1.03 g, 85%). [12] ^{1}H NMR (400 MHz, CDCl$_3$): δ 8.21 (1H, s); 7.78 -7.63 (4H, m); 4.18-3.99 (4H, m (2 x dq), $^{3}J_{PH}$ = 10.0 Hz); 2.21 (3H, s); 1.32 (6H, t, J = 7.0 Hz). ^{13}C NMR (100 MHz, CDCl$_3$): δ 169. 5, 142.7, 132.7, 119.2, 62.2, 24.4, 16.2. ^{31}P NMR (161.97 MHz, CDCl$_3$):

δ 18.8. ESI-TOF *m/z* calcd for $C_{12}H_{19}NO_4P$ (M+H)$^+$, calculated 272.1052, found 272.1043.
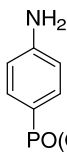
Diethyl 4-aminophenylphosphonate (6.4). Sodium (0.245 g, 10.64 mmol) dissolved in dry EtOH (21 mL) under N_2 was added to a solution of 6.3 (1.03 g, 3.80 mmol) in dry EtOH (10 mL) and the reaction mixture was refluxed under nitrogen atmosphere for overnight. After the reaction was complete (monitored by TLC and UPLC-MS), the solvent was removed under reduced pressure and the crude black mixture then suspended in $CHCl_3$ and was washed with H_2O. The organic layer was collected and dried over Na_2SO_4, filtered and concentrated under reduced pressure. The crude product was purified by column chromatography (silica, 20-100% EtOH in $CHCl_3$). The product **6.4** was obtained as a yellow sticky solid (0.740 g, 85%).[11] ^{1}H NMR (400 MHz, $CDCl_3$): δ 7.61 - 7.53 (2H, dd, *J* = 8 Hz, $^3J_{PH}$ = 12.0 Hz); 6.72 - 6.66 (2H, dd, $^4J_{PH}$ = 3.0 Hz); 41.5 -. 3.96 (4H, m (2 x dq), $^3J_{PH}$ = 10.0 Hz); 1.30 (6H, t, *J* = 7.0 Hz). ^{13}C NMR (100 MHz, $CDCl_3$): δ 133.7, 133.6, 114.2, 114.1, 61.7, 61.7, 61.7, 16.3, 16.3. ^{31}P NMR (161.97 MHz, $CDCl_3$): δ 21.4. ESI-TOF *m/z* calcd for $C_{10}H_{17}NO_3P$ (M+H)$^+$, calculated 230.0946, found 230.0941.
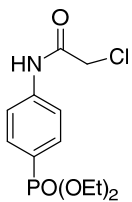
Diethyl 4-(chloroacetamido)phenylphosphonate (6.5). A suspension of K_2CO_3 (0.536 g, 3.876 mmol) in a solution of **6.4** (0.740 g, 3.23 mmol) in CH_3CN (12mmL) was cooled to 0°C. A solution of chloroacetyl chloride (0.31 mL, 3.876 mmol) in CH_3CN (2 mL) was then added dropwise. The reaction mixture was slowly warmed to room temperature and then stirred overnight (monitored by TLC and HR-ESI-MS). The reaction mixture was filtered, the filtrate collected and concentrated under reduced

pressure. The crude product was used without further purification in the next step.[11] The resulting oil was evaporated with toluene three times to give the crude product as a yellow solid (0.756 g, 77%) which was used without further purification in the next step. ^{1}H NMR (400 MHz, CDCl$_3$): δ 8.68 (1H, s); 7.84 - 7.75 (2H, dd, J = 9 Hz, $^3J_{PH}$ = 13.0 Hz); 7.74 - 7.68 (2H, dd, $^4J_{PH}$ = 3.0 Hz); 4.22 (2H, s); 4.19-4.03 (4H, m (2 x dq), $^3J_{PH}$ = 10.0 Hz); 1.32 (6H, t, J = 7.0 Hz). ^{13}C NMR (100 MHz, CDCl$_3$): δ 164.5, 140.8, 140.8, 133.0, 132.9, 119.6, 119.4, 62.5, 62.4, 42.9, 16.3, 16.2. ^{31}P NMR (161.97 MHz, CDCl$_3$): δ 18.3. ESI-TOF m/z calcd for C$_{12}$H$_{18}$ClNO$_4$P (M+H)$^+$, calculated 306.0662, found 306.0652.
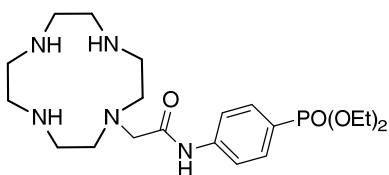
Diethyl (4-(2-(1,4,7,10-tetraazacyclododecan-1-yl)acetamido)phenyl)phosphonate (6.8). K$_2$CO$_3$ (0.423 g, 3.06 mmol), NaI (0.238 g, 1.591 mmol), **6.5** (0.486 g, 1.591 mmol) and **6.6** (0.723 g, 1.530 mmol) were suspended in acetone/CH$_3$CN (2:16 mL) in a 20 mL microwave vial which was then sealed. The mixture was irradiated at 70°C and maintained for 3h with stirring in a Biotage Initiator® microwave reactor. The temperature was monitored by an external IR temperature sensor. After 3 h, the reaction was checked by HR-ESI-MS and TLC and the mixture was filtered. The filtrate was collected and concentrated under reduced pressure. The crude product **6.7** was used without further purification in the next step.

Crude **6.7** was dissolved in CH$_2$Cl$_2$ (4 mL) and an equal volume of TFA added. The reaction mixture was left stirring for 3.5 hrs at room temperature (monitored by UPLC-MS). The crude product was purified by column chromatography (silica, 1.5:5:93.5 NH$_4$OH/MeOH in CHCl$_3$). The product **6.8** was obtained as an orange sticky solid (0.561 g, 83%). ^{1}H NMR (400 MHz, CD$_3$OD): 7.83 - 7.77 (2H, dd, J = 9 Hz, $^4J_{PH}$ = 3.0 Hz); 7.75 - 7.67 (2H, dd, $^3J_{PH}$ = 13.0 Hz,); 4.16 - 4.01 (4H, m (2 x dq), $^3J_{PH}$ = 10.0 Hz); 3.67 (2H, s); 3.30-3.14 (16H, m); 1.31 (6H, t, J = 7.0 Hz). ^{13}C NMR (100 MHz, CD$_3$OD): δ 163.3, 133. 8, 121.0, 116.8, 63.9, 57.5, 51.6, 45.9, 44.7, 44.2, 43.9, 39.5, 16.7. ^{31}P NMR

(161.97 MHz, CD$_3$OD): δ 19.1. ESI-TOF *m/z* calcd for C$_{20}$H$_{36}$N$_5$O$_4$P (M+H)$^+$, calculated 442.2583, found 442.2590.

General procedures for synthesis of tetra-substituted cyclen. Starting material **6.8**, electrophiles **6.9** or **6.10** and K$_2$CO$_3$ were suspended in CH$_3$CN in a 20 mL microwave vial which was then sealed. The mixture was irradiated at 80°C and maintained for 3 h with stirring in a Biotage Initiator® microwave reactor. The temperature was monitored by an external IR temperature sensor. After 3 h, the reaction was checked by HR-ESI-MS and the mixture was filtered and the filtrate collected and concentrated under reduced pressure. The crude product was first purified by column chromatography (silica gel, 5-10% MeOH in CH$_2$Cl$_2$, then 100% EtOH) then by HPLC (C18, gradient over 19 mins 99:1 to 45:55 H$_2$O/CH$_3$CN). The fractions were concentrated to reduce the volume then lyophilized.
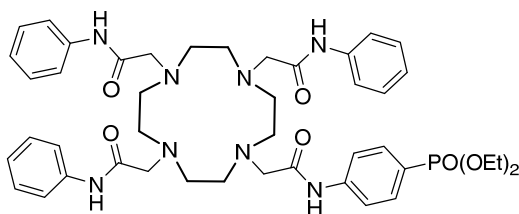
Diethyl (4-(2-(4,7,10-tris(2-oxo-2-(phenylamino)ethyl)-1,4,7,10-tetraazacyclododecan-1-yl)acetamido)phenyl)phosphonate (6.11). Starting material **6.8** (0.250 g, 0.566 mmol), electrophile **6.9** (0.384 g, 2.264 mmol) and K$_2$CO$_3$ (0.313 g, 2.264 mmol) were suspended in CH$_3$CN (6 mL). The product **6.11** was obtained as a yellow oil (0.105 g, 22%). ^{1}H NMR (400 MHz, CD$_3$OD): δ 7.81 - 6.76 (17H, m); 6.71 - 6.30 (2H, m); 4.42 - 3.43 (20H, m); 3.21-2.91 (8H, m); 1.28 (6H, m). ^{31}P NMR (161.97 MHz, CD$_3$OD): δ 19.49. ESI-TOF *m/z* calcd for C$_{44}$H$_{58}$N$_8$O$_7$P (M+H)$^+$, calculated 841.4166, found 841.4157.
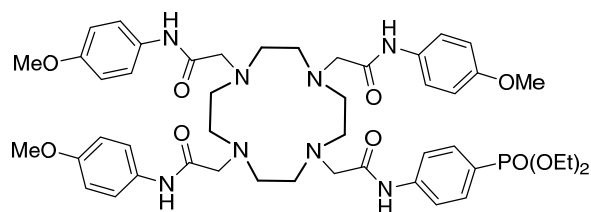
Diethyl (4-(2-(4,7,10-tris(2-((4-methoxyphenyl)amino)-2-oxoethyl)-1,4,7,10-tetraazacyclododecan-1-yl)acetamido)phenyl)phosphonate (6.12). Starting material **6.8** (0.250 g, 0.566 mmol), electrophile **6.10** (0.452 g, 2.264 mmol) and K$_2$CO$_3$ (0.313 g, 2.264 mmol) were suspended in CH$_3$CN (8 mL). The product **6.12** was obtained as a cream solid (0.195 g, 37%). ^{1}H NMR (400 MHz, CD$_3$OD): δ 7.66 - 6.93 (12H, m); 6.66 (4H, s); 4.33 - 3.86 (10H, m); 3.82 - 3.56 (19H, m); 3.28-3.05 (8H, m); 1.29 (6H, m). ^{31}P NMR (161.97 MHz, CD$_3$OD): δ 19.34. ESI-TOF *m/z* calcd for C$_{47}$H$_{64}$N$_8$O$_{10}$P (M+H)$^+$, calculated 931.4483, found 931.4448.

6.4.3 Spectra

S 6.1: ^{1}H-NMR Spectrum of **6.3**
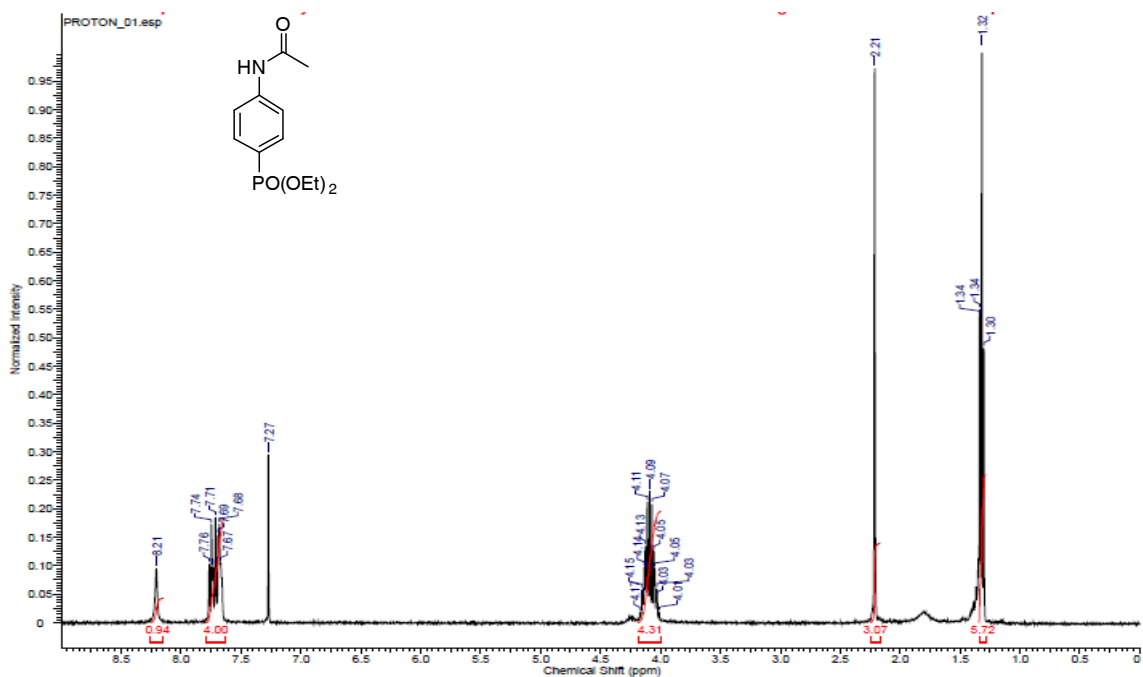
S 6.2: ^{13}C-NMR Spectrum of **6.3**
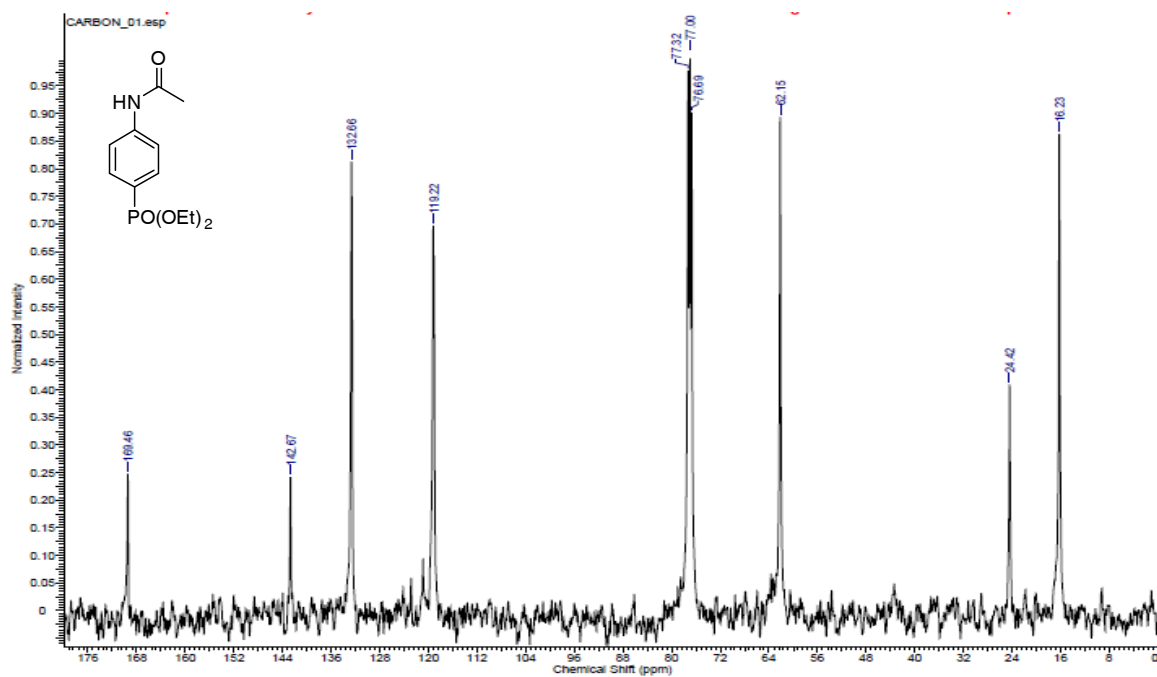
S 6.3: ^{31}P-NMR Spectrum of **6.3**
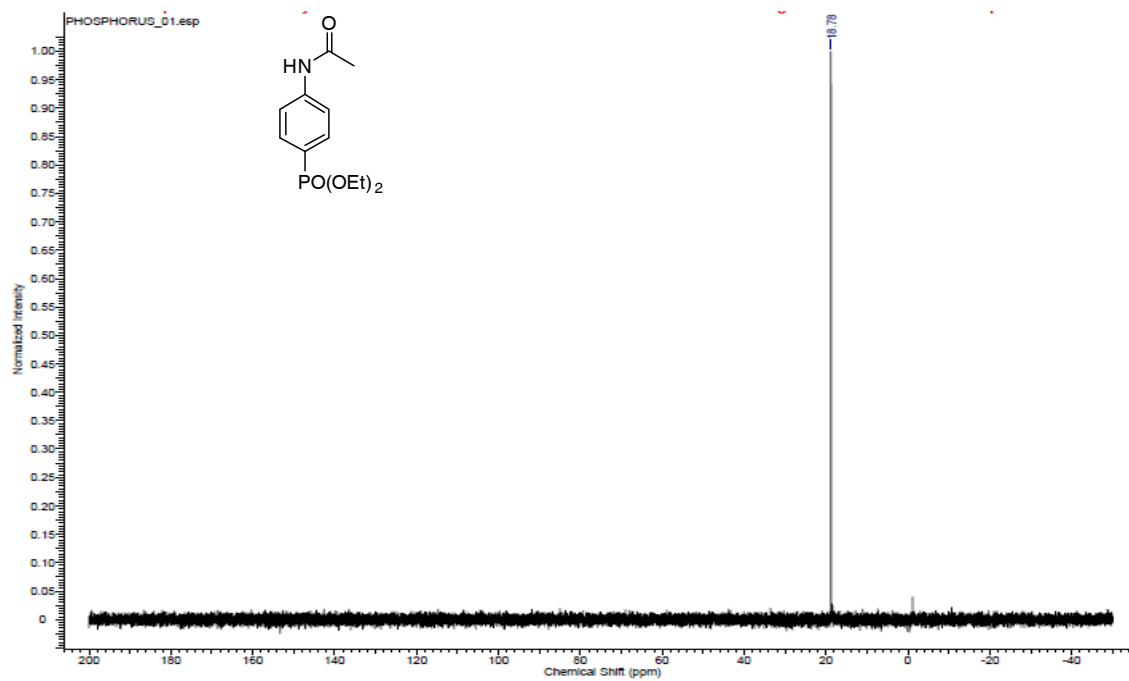
S 6.4: ^{1}H-NMR Spectrum of **6.4**
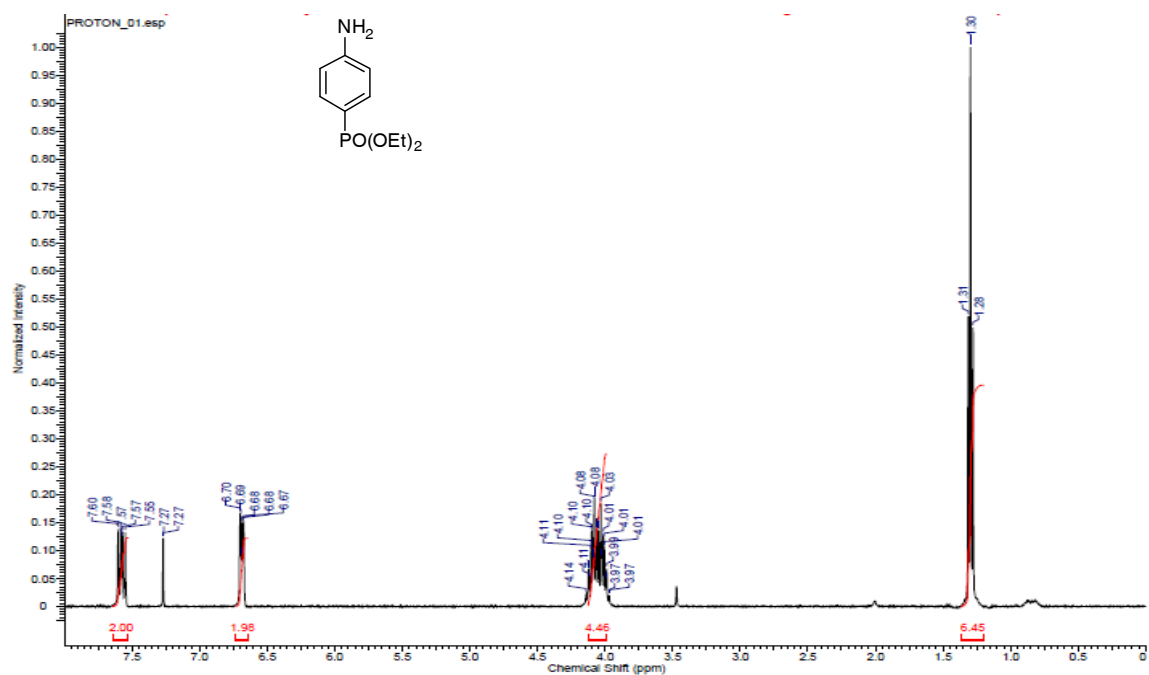
S 6.5: ^{13}C-NMR Spectrum of **6.4**
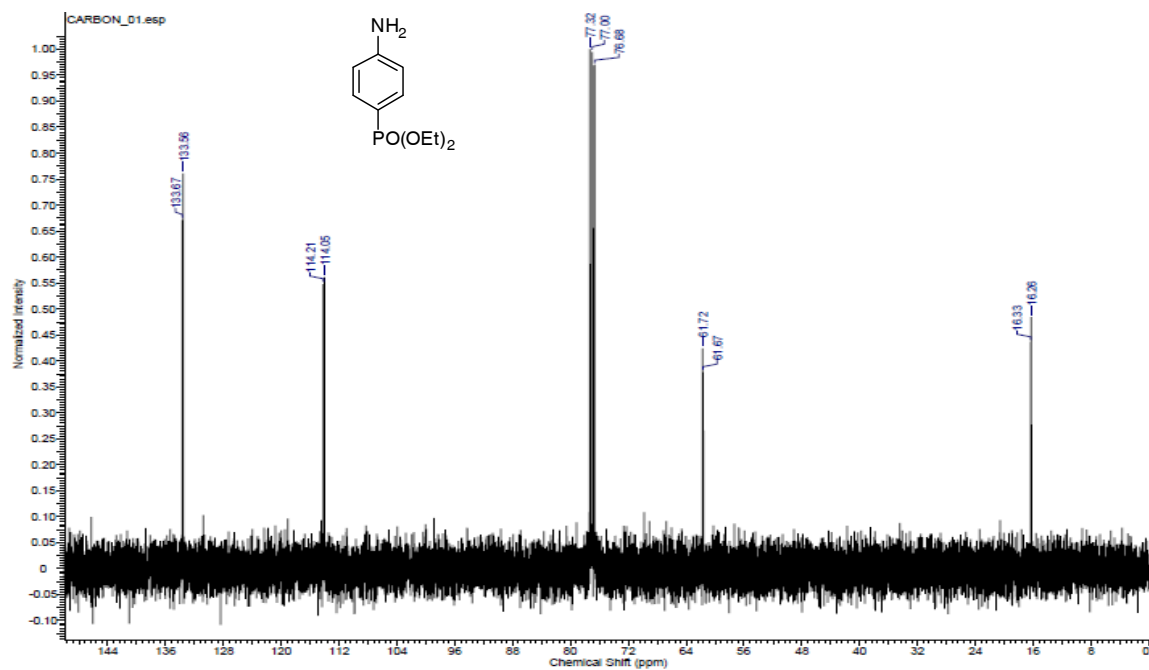
S 6.6: ^{31}P-NMR Spectrum of **6.4**
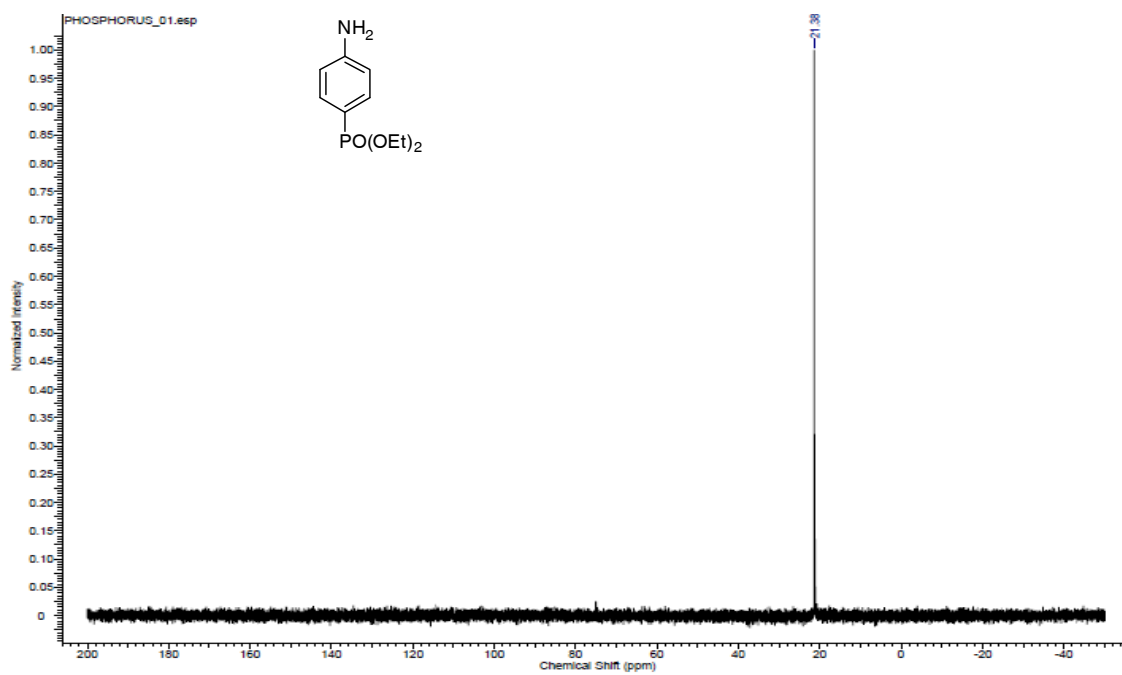
S 6.7: ^{1}H-NMR Spectrum of **6.5**
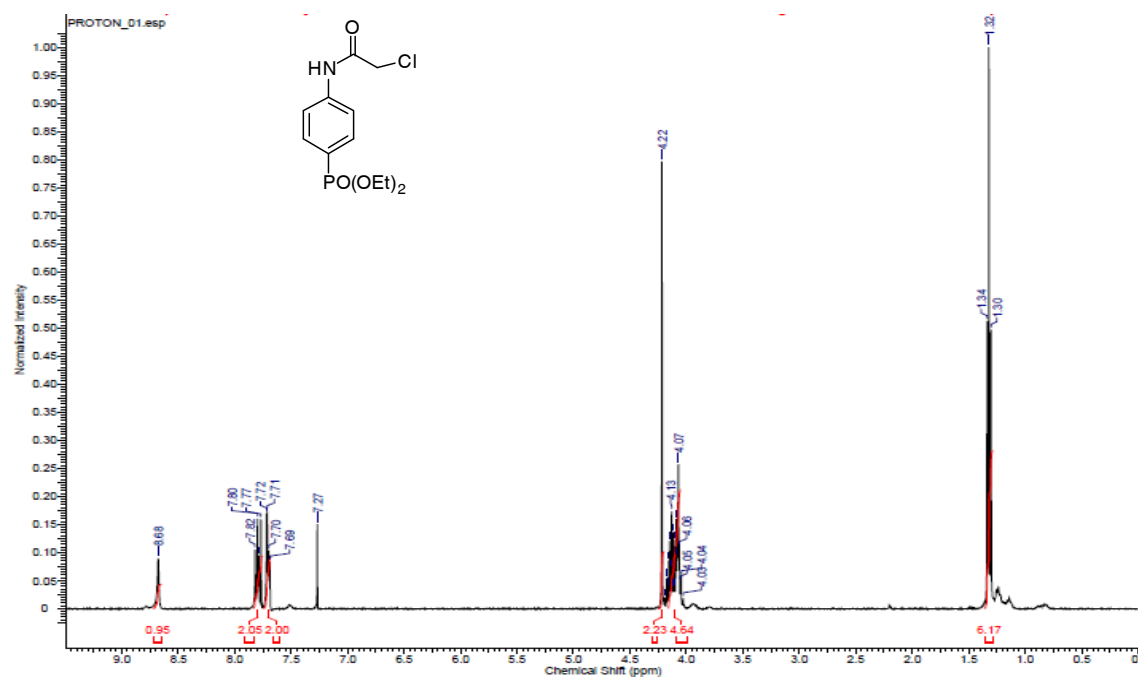
S 6.8: ^{13}C-NMR Spectrum of **6.5**
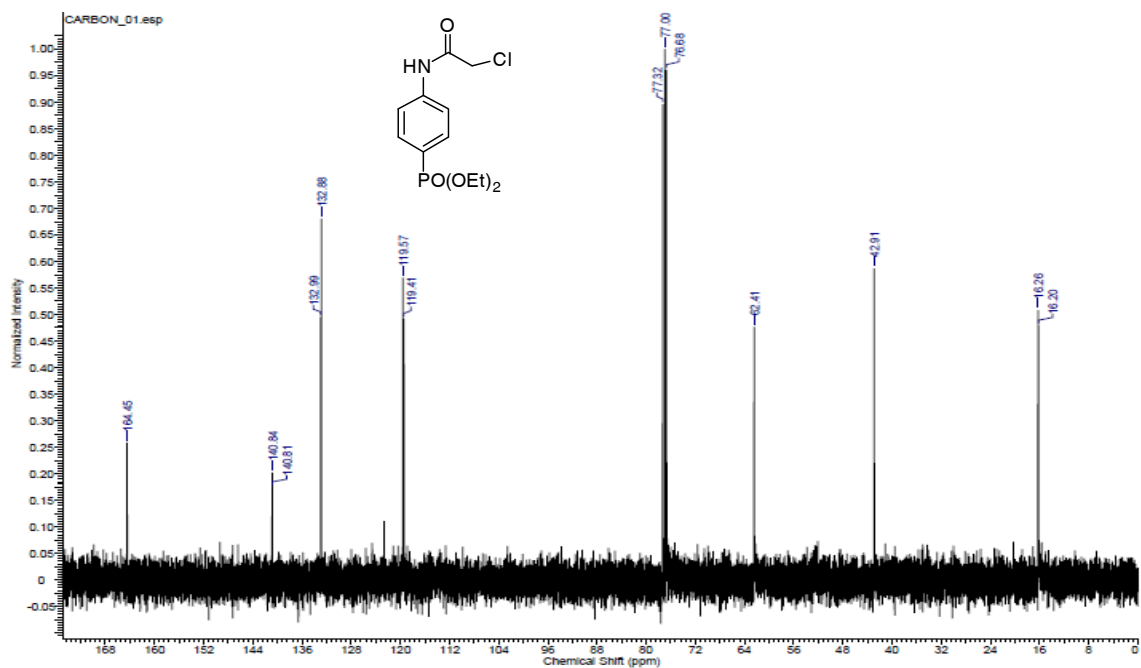
S 6.9: ^{31}P-NMR Spectrum of **6.5**
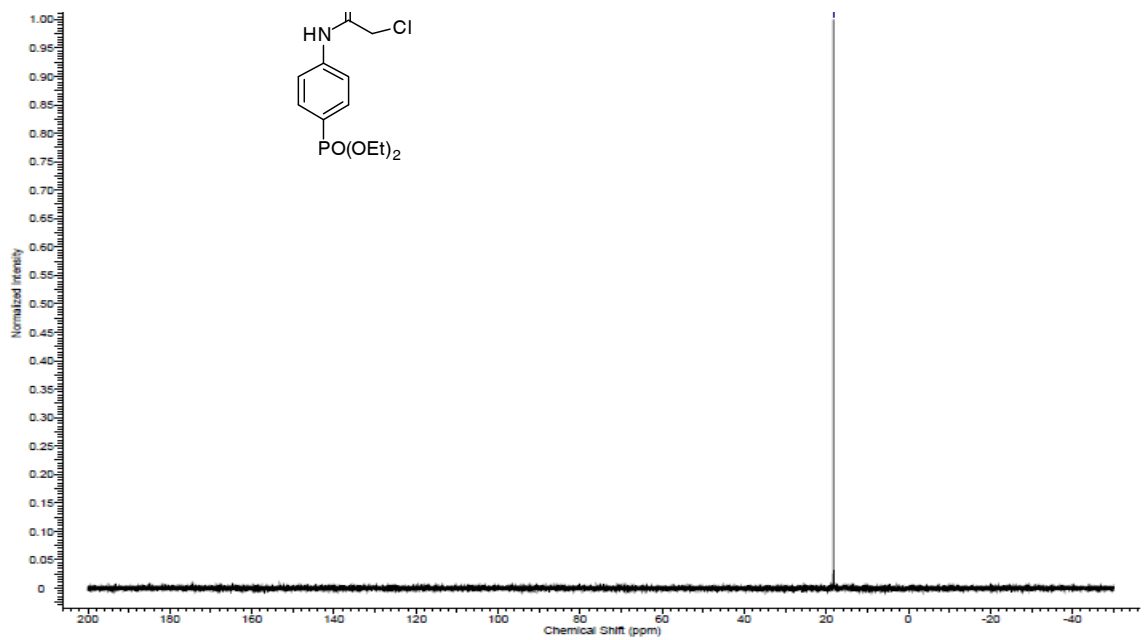
S 6.10: ^{1}H-NMR Spectrum of **6.8**
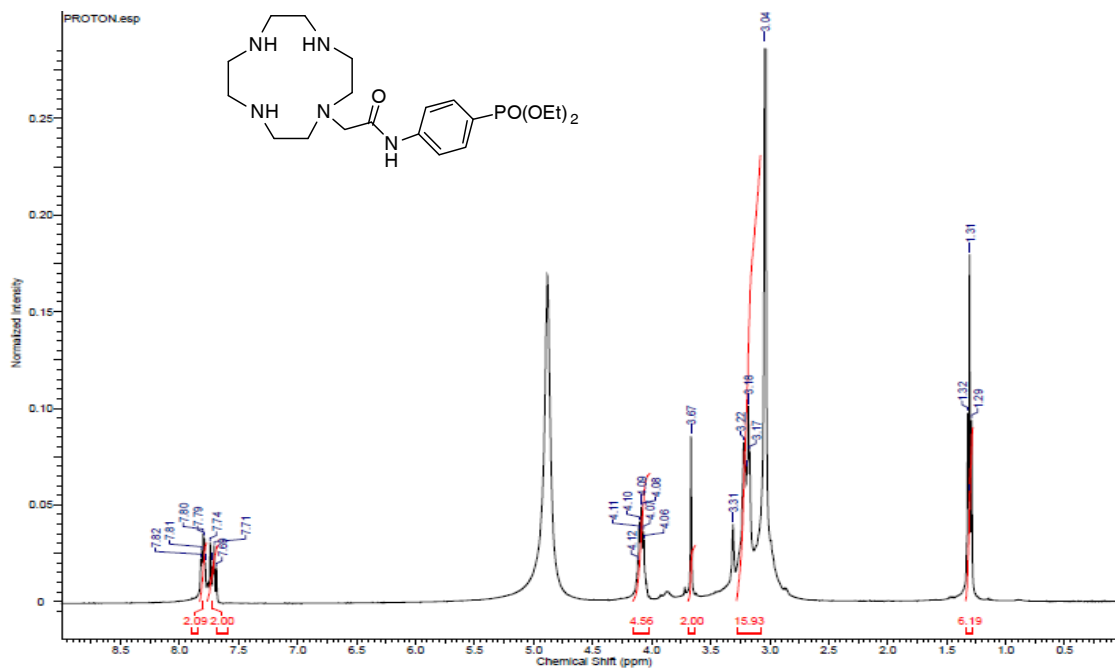
S 6.11: ^{13}C-NMR Spectrum of **6.8**
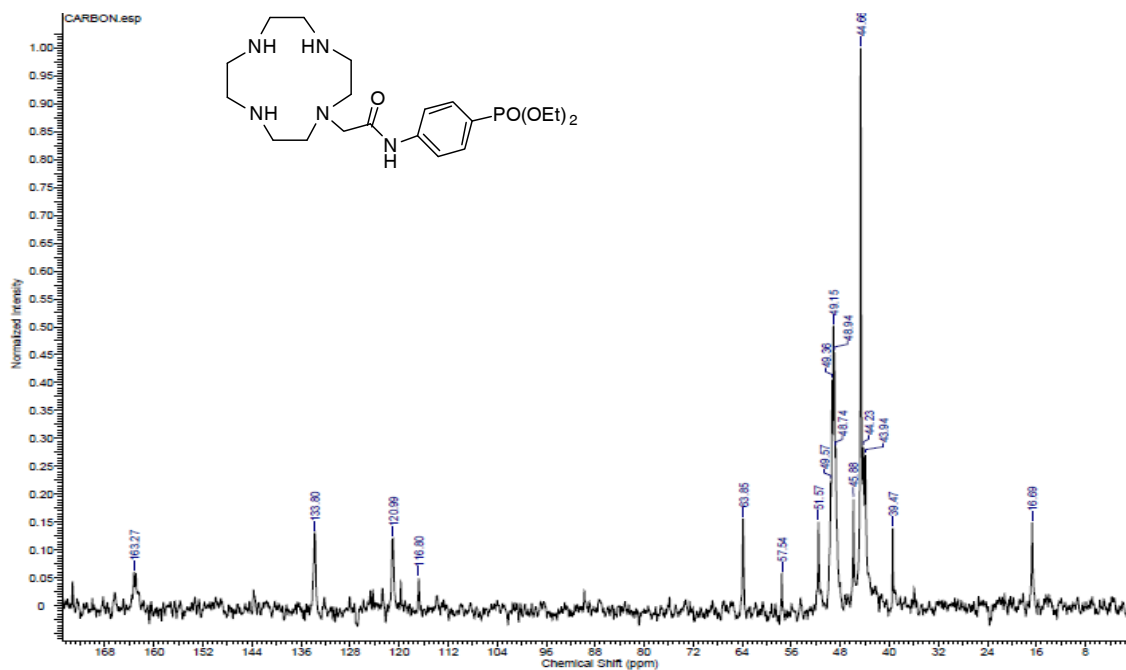
S 6.12: ^{31}P-NMR Spectrum of **6.8**
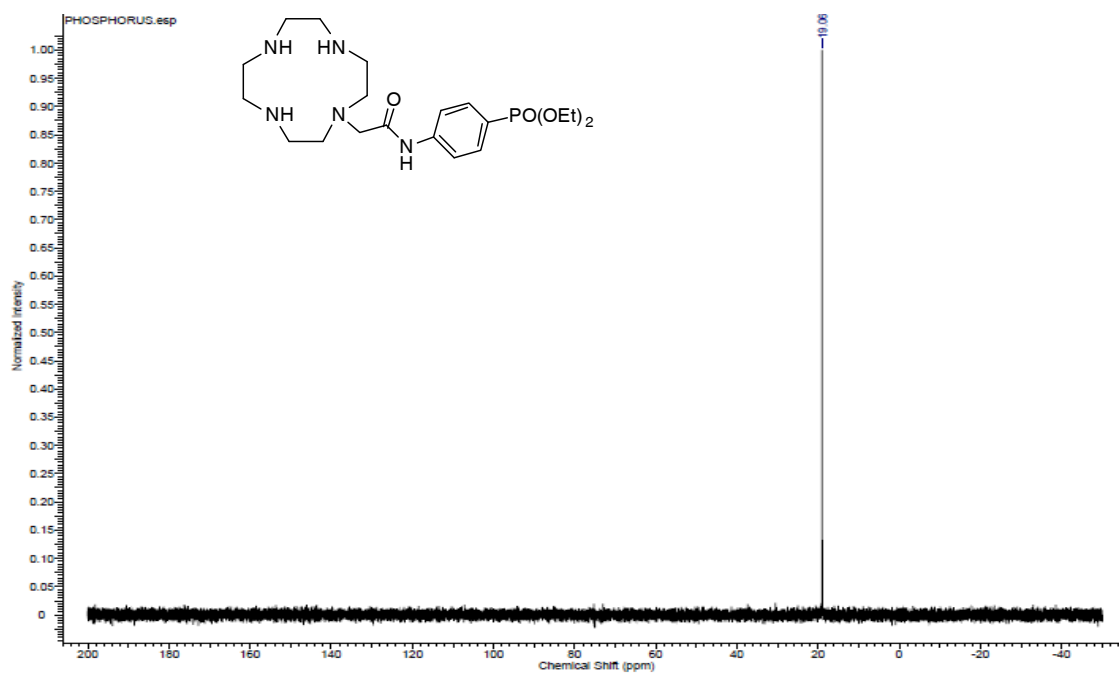
S 6.13: ^{1}H-NMR Spectrum of **6.11**
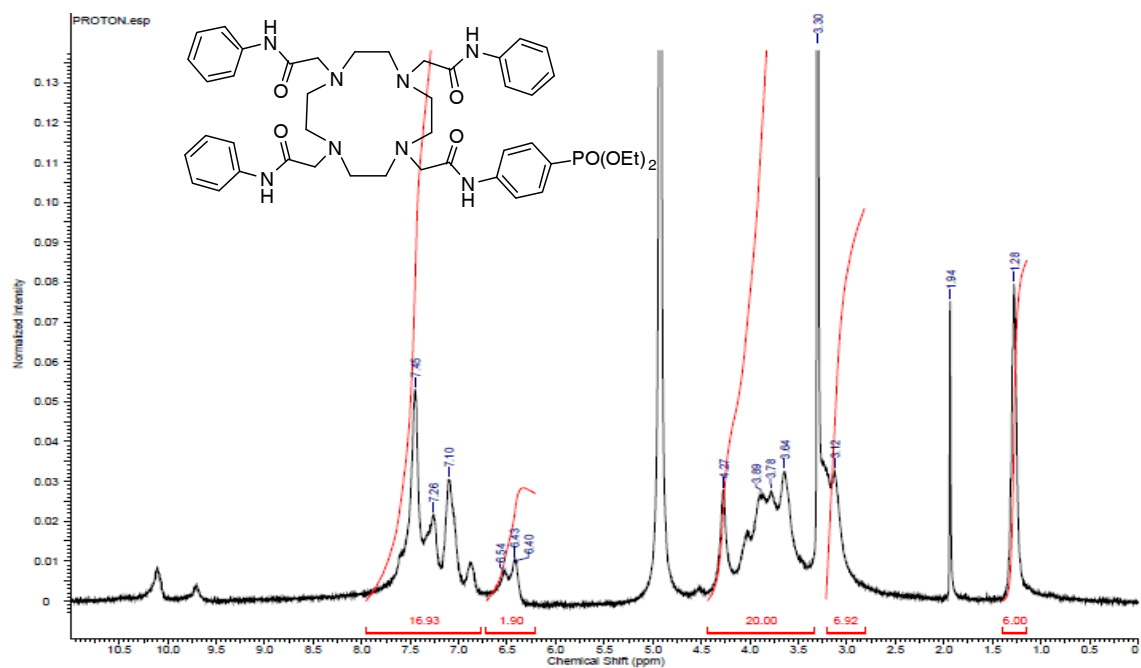
S 6.14: ^{31}P-NMR Spectrum of **6.11**
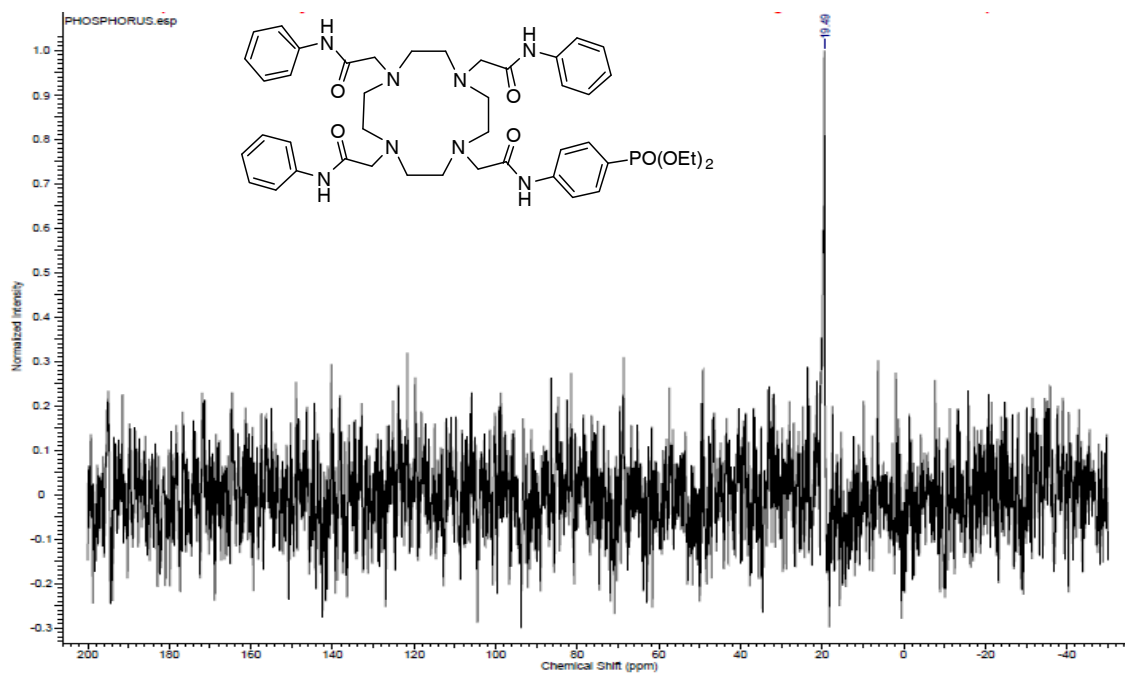
S 6.15: ^{1}H-NMR Spectrum of **6.12**
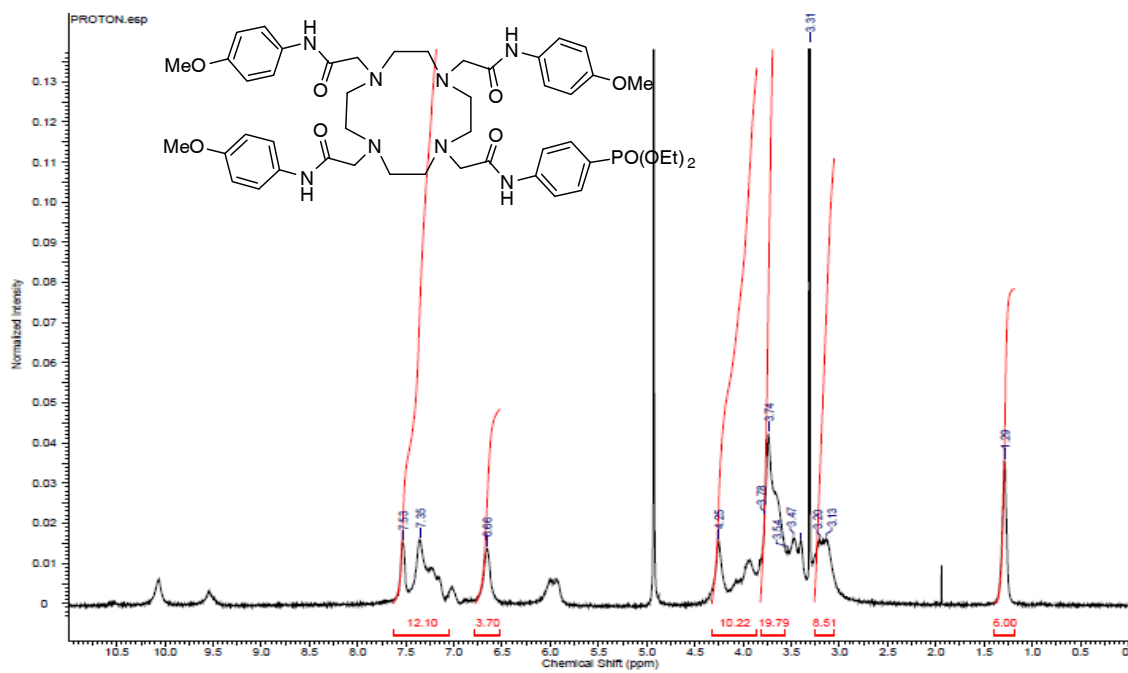
S 6.16: ^{31}P-NMR Spectrum of **6.12**
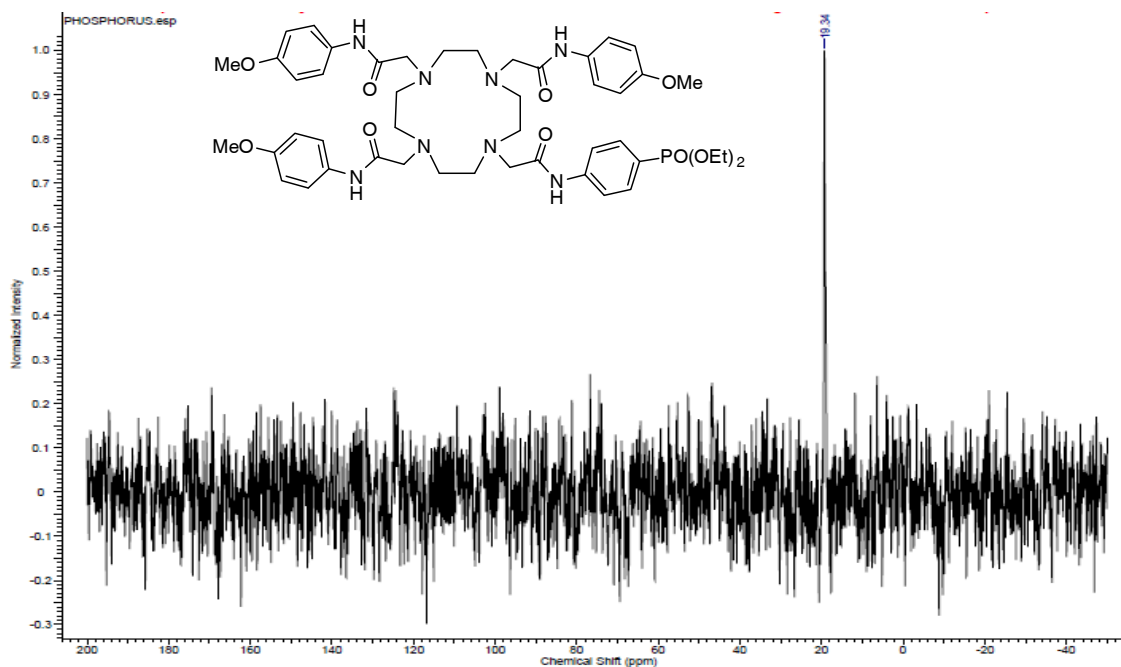
6.5   References

(1) Milne, M.; Lewis, M.; McVicar, N.; Suchý, M.; Bartha, R.; Hudson, R. H. E. *RSC Adv.* **2014,** *4*, 1666-1674.

(2) Kumar, K. *J. Alloys Compd.* **1997,** *249*, 163-172.

(3) Castelli, D. D.; Terreno, E.; Aime, S. *Angew. Chem. Int. Ed.* **2011,** *50*, 1798-1800.

(4) Pacheco-Torres, J.; Calle, D.; Lizarbe, B.; Negri, V.; Ubide, C.; Fayos, R.; Lopez Larrubia, P.; Ballesteros, P.; Cerdan, S. *Curr. Top. Med. Chem.* **2011,** *11*, 115-130.

(5) Tavs, P. *Chem. Ber.* **1970,** *103*, 2428-2436.

(6) Peng, Y.; Liu, H.; Tang, M.; Cal L.; Pike, V. *Chin. J. Chem.* **2009,** *27*, 1339-1344.

(7) Villemin, D.; Elbilali, A.; Siméon, F.; Jaffrès, P.; Maheut, G.; Mosaddak, M.; Hakiki, A. *J. Chem. Research (S)* **2003,** *2003*, 436-437.

(8) Balthazor, T. M.; Grabiak, R. C. *J. Org. Chem.* **1980,** *45*, 5425-5426.

(9) Clearfield, A.; Demadis, K. *Metal Phosphonate Chemistry: From Synthesis to Applications;* Royal Society of Chemistry: 2011; , pp 1-655.

(10) Jansa, P.; Baszczynski, O.; Prochazkova, E.; Dracinsky, M.; Janeba, Z. *Green Chem.* **2012,** *14*, 2282-2288.

(11) Rehor, I.; Kubicek, V.; Kotek, J.; Hermann, P.; Lukes, I.; Szakova, J.; Vander Elst, L.; Muller, R. N.; Peters, J. A. *J. Mater. Chem.* **2009,** *19*, 1494-1500.

(12) Keglevich, G.; Grün, A.; Bölcskei, A.; Drahos, L..; Kraszni, M.; Balogh, G. T. *Heteroatom Chem.* **2012,** *23*, 574-582.

Chapter 7

7   Conclusions and Future Work

The Gd^{3+}-based T_1 relaxation agents currently used in clinical settings are limited in the amount of anatomical information they provide during imaging. This low sensitivity has led to the need to design and synthesize MRI contrast agents that will be better at providing information regarding physiological changes such as temperature and pH. The studies described in this body of work primarily sought to improve signal generation and sensitivity, in a variety of metal complexes by PARACEST. This area of research represents a part of an ongoing theme within the Hudson laboratory, that is, the synthesis of DOTAM-based lanthanide complexes for potential clinical applications in MRI, of which I was a part of over the past four years. For thorough analysis of the complexes synthesized, the relaxometric properties of the complexes were additionally investigated. The PARACEST and relaxometric data reported here for the assortment of lanthanides and transition metals complexes studied demonstrate the progress, achievements as well as unforeseen failures on the path towards the aforementioned goals.

The studies began by synthesizing and evaluating lanthanide complexes of DOTAM analogues bearing a *para*-nitrophenol group that could undergo reversible binding to the metal center in a pH dependent manner. With the remaining three arms of the complexes being the same, this overall design made the complexes asymmetric. As seen in Chapter 2, the PARACEST results for the lone Tb^{3+} complex indicated that pH dependent reversible binding was indeed possible. The increased relaxivity of the Gd^{3+} complex at acidic pH implied a complex combination of factors. The results of this slight pH dependent modulation of PARACEST and relaxivity suggests that tuning of the labile arm is needed to produce possible contrast agents with the desired increase in physiological pH sensitivity. This tuning may be accomplished by varying the electron density of the labile arm.

The original goal of the work in Chapter 3 was the symmetric and asymmetric rigidification of the DOTAM scaffold, in order to increase the PARACEST signal generation through preferential formation of the desired SAP isomer. The desired ligands were to be tetraaza macrocycles consisting of one or two fused cyclohexane rings. However, the final complexes (consisting of bicyclic hexaaza macrocycles) were more rigidified than originally desired. Since the ligands deviated from the DOTA-based design upon which the definition of SAP and TSAP is based on, these definitions are therefore not applicable to these new macrocyclic ligands. These ligands were found to be selective for the smaller transition metals. The absence of PARACEST signals in these transition metal complexes demonstrated the negative impact that rigidity of that form (and possibly steric bulk by those cyclohexyl groups) has on the exchange rate. In order to observe a CEST signal, reduction in the level of rigidity of the structures is likely needed.

The Dy^{3+} and Tm^{3+} DOTAM tetraanilides of Chapter 4 contained varying *para*-substituents that would limit T_2 exchange and increase PARACEST pH measurements that are amide-based. This limitation of T_2 exchange was possible owing to the four aromatic rings of the acetamide pendant arms, which provided steric bulk to the complex and blocked access of water to the metal center. This absence of a metal bound water for the Tm^{3+} aniline agents increased the sensitivity of PARACEST imaging and produced appreciable amide PARACEST contrast without decreasing image signal. These results have good implications for *in vivo* PARACEST imaging which may benefit by combining the features of the highly shifted amide CEST signal (observed in the Tm^{3+}-*p*-OMe complex) and long T_2 times.

Due to the low solubilities of a majority of the complexes in Chapter 4 that prohibited them from being fully studied, *para*-substituted monoanilide Dy^{3+} and Tm^{3+} DO3A complexes were synthesized and investigated (Chapter 5). The presence of EDGs and EWGs affected the pH at which the maximum PARACEST effect is observed. This feature is an advantage for developing biologically sensitive pH PARACEST probes. To further maximize this feature, bis(amide)-bis(carboxylate) ligands complexes may be investigated, along with varying the position of EDGs and EWGs on the aniline ring.

The final chapter dealt with the endeavours made to synthesize biocompatible DOTAM tetraanilides complexes containing a *para*-phosphonate monoanilide arm. These complexes were to be based on the Dy^{3+} and Tm^{3+} complexes of -*p*-H and-*p*-OMe tetraanilides that were evaluated in Chapter 4. Such efforts involved synthesizing complexes that had one of the four aniline rings contain a phosphonate group in the *para*-position. The synthetic procedure to remove the diesters of the phosphonate group of the ligands has proved to be very challenging and as such, the synthesis is still ongoing. Once the desired complexes have been obtained, the magnetic properties of the complexes can then be evaluated and compared to the unmodified DOTAM tetraanilide complexes.

Due to the unanticipated complications faced, vital lessons were learned and highlighted regarding the significance of structural design for ligands that are to be used as metal chelates for MRI contrast agents. By suitably adapting and building on each stratagem reported here or by combining them, complexes may be generated that can be customized for different applications. It is important to ensure that these new agents will possess high kinetic and thermodynamic stabilities, have low toxicities and exhibit their desired imaging properties in the clinically relevant magnetic field strengths. This research is important because it has answered questions, compared differences and similarities in data and of course, created expectations. Current and future researchers seeking to optimize various MRI contrast agents may use the work described here as a guide in the expansion of more sensitive and specific MRI contrast agents.

Appendices

Appendix 1: General Considerations

A.1.1 General Experimental Considerations

All solvents were used as purchased unless otherwise stated, except for dioxane (dried by passing through columns of activated Al_2O_3) and water (18.2 $M\Omega\cdot cm^{-1}$ deionized). Solvents were removed under reduced pressure in a rotary evaporator. Aqueous solutions were lyophilized. Flash column chromatography (FCC) was carried out using silica gel (SiO_2; mesh size 230–400 Å). Thin-layer chromatography (TLC) was carried out on an Al backed silica gel plate with compounds visualized by 254 nm UV light. Size exclusion chromatography (SEC) was carried out on Bio-Gel P2, 45–90 μm mesh resin. Dialysis was performed against water using a cellulose membrane with molecular weight cut off at 500 Da.

NMR spectra were recorded on a 400 MHz spectrometer; for ^1H (400 MHz), chemical shift values (δ) are referenced relative to the residual proton in the deuterated solvents as follows: $CDCl_3$ (7.26 ppm), D_2O (4.75 ppm), CD_3OD (3.31 ppm), DMSO-d_6 (2.49 ppm); ^{13}C NMR (125 MHz): $CDCl_3$ (77.0 ppm), CD_3OD (49.0 ppm), DMSO-d_6 (39.5 ppm); ^{31}P NMR (161.97 MHz). Mass spectra (MS) were obtained using electrospray ionization (ESI). UV-visible absorption spectra were recorded over a range of 190 - 800 nm using a Cary 300 Bio UV-Visible Spectrophotometer. Samples were placed in a 10 mm quartz cuvette. Microwave reactions were performed in a Biotage® MW reactor using sealed glass vials. Melting point (m.p.) was recorded in capillary tubes using a Gallenkamp Variable Heater.

The effective magnetic moment (μ_{eff}) was calculated by using the Evans' method.[1, 2] Five millimolar of metal complex and 5 % t-butanol by volume was placed in a capillary tube which was then placed in an NMR tube containing 5 % by volume t-butanol in D_2O. The concentration of the metal complexes was determined by preparation of stock solutions of complex. The μ_{eff} was calculated at 298 K (T) from NMR data, using the following equations:

$$X_g = (-3\Delta f)/(4\pi fm) + X_0 + [X_0 (d_0-d_s)]/m \qquad\qquad 1$$

$$\mu_{eff} = 2.84 (X_mT)^{1/2} \qquad\qquad 2$$

The mass susceptibility of solute (X_g) was calculated by obtaining the observed frequency shift of the reference (Δf) in Hz, the spectrometer frequency (f) in Hz, the mass of the substance per cm^3 of solution (m), and the mass susceptibility of solvent D_2O (X_0= -0.6466 x 10-6 cm^3/g). The last term is neglected due to the minimal contribution to mass susceptibility of solute, in which d_o is density of the solvent and d_s is density of the solution in g/cm^3. The molar susceptibility (X_m) is the product of X_g multiplied by the molecular weight of the metal complex studied.

(1R, 2R)-cyclohexane-1,2-diamine tartrate, bromoacetyl bromide, ethylenediamine, LiBr and 1M BH_3 in THF were purchased from Sigma Aldrich. K_2CO_3 and $ZnCl_2$ were purchased from Fisher Scientific. $CoCl_2.6H_2O$ (98%) was purchased from Lancaster Chemicals. Lanthanide salts and transition metals salts were purchased from Strem Chemicals. Compounds **2.3**[3], **3.4**[4], **3.15**[4], **5.1 - 5.5**[5], **Et3DO3A**[6], **6.2**[7, 8], **6.6**[9], **6.9**[5] and **6.10**[5] were synthesized as previously. Compound ethyl (2-chloroacetyl)glycinate **3.7** was produced by a former laboratory member.

A.1.2 General Crystallographic Considerations

The sample was mounted on a Mitegen polyimide micromount with a small amount of Paratone N oil. All X-ray measurements were made on a Bruker Kappa Axis Apex2 diffractometer at a temperature of 110 K. The unit cell dimensions were determined from a symmetry constrained fit of 9608 reflections with 5.16° < 2q < 76.3°. The data collection strategy was a number of w and j scans which collected data up to 84.758° (2q). The frame integration was performed using SAINT.[10] The resulting raw data was scaled and absorption corrected using a multi-scan averaging of symmetry equivalent data using SADABS.[10]

The structure was solved by direct methods using the SIR92 program.[11] All non-hydrogen atoms were obtained from the initial solution. The organic hydrogen atoms

were introduced at idealized positions and were allowed to refine isotropically. The positions of the hydrogen atoms on the water molecule were obtained from a difference Fourier map. The O—H bond lengths and the H···H distance were restrained to chemically reasonable distances. The isotropic displacement parameters for the water bound hydrogen atoms were allowed to refine. The structural model was fit to the data using full matrix least-squares based on F^2. The calculated structure factors included corrections for anomalous dispersion from the usual tabulation. The structure was refined using the SHELXL-2013 program from the SHELXTL program package.[12] Graphic plots were produced using the NRCVAX program suite.[13] Additional information and other relevant literature references can be found in the reference section of this website (http://xray.chem.uwo.ca).

A.1.3 References

(1) Evans, D. F. *J. Chem. Soc.* **1959,** , 2003-2005.

(2) Schubert, E. M. *J. Chem. Educ.* **1992,** *69*, 62.

(3) Boldrini, V.; Giovenzana, G. B.; Pagliarin, R.; Palmisano, G.; Sisti, M. *Tetrahedron Lett.* **2000,** *41*, 6527-6530.

(4) Saburi, M.; Yoshikawa, S. *Bull. Chem. Soc. Jpn.* **1974,** *47*, 1184-1189.

(5) Milne, M.; Lewis, M.; McVicar, N.; Suchý, M.; Bartha, R.; Hudson, R. H. E. *RSC Adv.* **2014,** *4*, 1666-1674.

(6) Natrajan, L. S.; Villaraza, A. J. L.; Kenwright, A. M.; Faulkner, S. *Chem. Commun.* **2009,** 6020-6022.

(7) Peng, Y.; Liu, H.; Tang, M.; Cai, L.; Pike, V. *Chin. J. Chem.* **2009,** *27*, 1339-1344.

(8) Bian, L.; Yang, D.; Yin, L.; Zhang, J.; Tang, W. *Macromol. Chem. Phys.* **2013,** *214*, 2136-2143.

(9) Woods, M.; Kiefer, G. E.; Bott, S.; Castillo-Muzquiz, A.; Eshelbrenner, C.; Michaudet, L.; McMillan, K.; Mudigunda, S. D.; Ogrin, D.; Tircso, G.; Zhang, S.; Zhao, P.; Sherry, A. D. *J. Am. Chem. Soc.* **2004,** *126*, 9248-9256.

(10) Bruker-Nonius *SAINT* **2012,** *12*.

(11) Altomare, A.; Cascarano, G.; Giacovazzo, C.; Guagliardi, A.; Burla, M. C.; Polidori, G.; Camalli, M. *J. Appl. Cryst.* **1994,** *27*, 435.

(12) Sheldrick, G. M. *Acta Cryst. A* **2008,** *64*, 112-122.

(13) Gabe, E. J.; Le Page, Y.; Charland, J. -.; Lee, F. L.; White, P. S. *J. Appl. Cryst.* **1989,** *22*, 384-387.

Appendix 2: Copyright Permissions

A.2.1 Royal Society of Chemistry License:

1) License Number: 3416661359933

License date: Jun 26, 2014

2) License Number: 3416680351983

License date: Jun 26, 2014

3) License Number: 3416681289148

License date: Jun 26, 2014

A.2.2 Elsevier License Terms and Conditions

1) License number: 3416690176441

License date: Jun 26, 2014

A.2.3 John Wiley and Sons License Terms and Conditions

1) License Number: 3416690973940

License date: Jun 26, 2014

2) License Number: 3416691407911

License date: Jun 26, 2014

Curriculum Vitae

Name:	Melissa M. Lewis

Post-secondary Education and Degrees:

York University
Toronto, Ontario, Canada
2002-2006 B.Sc. (Hons.)

University of Toronto
Toronto, Ontario, Canada
2006-2008 M.Sc.

The University of Western Ontario
London, Ontario, Canada
2010-2014 Ph.D. Candidate

Related Work Experience

Graduate Teaching Assistant and Research Assistant
University of Toronto
2006-2008

Research Technician I Assistant
University Health Network
2008-2010

Graduate Teaching Assistant and Research Assistant
The University of Western Ontario
2010-2014

Publications:

(5) **Melissa M. Lewis**, Mark Milne, Robert Bartha and Robert H.E. Hudson, "Dysprosium(III) and Thulium(III) Complexes of DO3A-monoanilides: An Investigation of Electronic Effects on their Relaxometric and Amide-based PARACEST Properties" Accepted *Can. J. Chem.*, **2014**.

(4) Milne, M., **Lewis, M.**, McVicar, N., Suchy, M., Bartha, R. and Hudson, R. H. E., MRI ParaCEST agents that improve amide based pH measurements by eliminating inner sphere water T_2 exchange. *RSC Adv.* **2014,** 4, 1666-1674.

(3) **Lewis, M.**, Meza-Avina, M. E., Wei, L., Crandall I. E., Bello, A. M., Liu, Y., Paige, C. J., Kain, K. C., Pai, E. F., and Kotra, L. P., Novel Interactions of Fluorinated Nucleotide Derivatives Targeting Orotidine- 5'-Monophosphate Decarboxylase *J. Med. Chem.* **2011**, 54, 2891–2901.

(2) Bello, A. M., Konforte, D., Poduch, E., Furlonger, C., Wei, L., Liu, Y., **Lewis, M.**, Pai, E. F., Paige, C. J., and Kotra, L. P., Structure-Activity Relationships of Orotidine-5'-Monophosphate Decarboxylase Inhibitors as Anticancer Agents *J. Med. Chem.* **2009,** 52*, 1648–1658.

(1) **Lewis, M.**, What does it mean to be a leader? *Competitive Advantage*, **2009**, 16, 5.

Conferences:

(2) "MRI PARACEST Agents that Improve Amide-based CEST Measurements by Eliminating Inner Sphere Water T_2 Exchange" Mark Milne, <u>Melissa M. Lewis,</u> Nevin McVicar , Mojmir Suchy, Robert Bartha and Robert H E Hudson; Inorganic Discussion Weekend, Toronto, Ontario. November **2013** (Poster Presentation).

(1) "New Ligands for Lanthanides Toward MRI Contrast Agents" <u>Melissa Lewis</u> and Robert H. E. Hudson; Ontario-Québec Physical Organic Mini-Symposium, London, Ontario. November **2011** (Poster Presentation).

Awards:

Western Graduate Research Scholarship: 2011 - 2013